Coordination Chemistry Reviews 253 (2009) 2515–2587

Contents lists available at ScienceDirect

Coordination Chemistry Reviews

journal homepage: www.elsevier.com/locate/ccr

Review

Lanthanides and actinides: Annual survey of their organometallic chemistry covering the year 2007

Frank T. Edelmann*

Chemisches Institut der Otto-von-Guericke-Universität Magdeburg, D-39106 Magdeburg, Germany

Contents

* Fax: +49 391 6712933.
E-mail address: frank.edelmann@ovgu.de.

0010-8545/$ – see front matter
doi:10.1016/j.ccr.2009.06.019

ARTICLE INFO

Article history:
Received 26 June 2009
Accepted 26 June 2009
Available online 5 July 2009

Keywords:
Lanthanides
Actinides
Cyclopentadienyl complexes
Cyclooctatetraenyl complexes
Organometallic chemistry

ABSTRACT

This review summarizes the progress in organo-*f*-element chemistry during the year 2007. A continuing trend in organolanthanide research is a strong emphasis on applications of organolanthanide complexes in homogeneous catalysis and, to a lesser extent, materials science. Roughly 15% of all relevant papers published in 2007 were in the area of organoactinide chemistry, although the latter continues to produce exciting results.

1. Introduction

This review summarizes the progress in organo-*f*-element chemistry during the year 2007. This year witnessed a significant increase of publications in the field over 2006. A continuing trend in organolanthanide research is a strong emphasis on applications of organolanthanide complexes in homogeneous catalysis and, to a lesser extend, materials science. Roughly 15% of all relevant papers published in 2007 were in the area of organoactinide chemistry, although the latter continues to produce exciting results (*cf.* Section 3.4). In this review mainly regular scientific papers are covered, while patents and conference abstracts *etc.* have mostly been excluded.

2. Lanthanides

2.1. Lanthanide carbonyls

Isolable binary lanthanide carbonyls still remain elusive, but transient species continue to be subjects of experimental and theoretical investigations. The interaction of metal atoms with small molecules (*i.e.*, CO, O_2, CO_2, H_2, CH_4, *etc.*) is of considerable interest because of its importance in a great number of catalytic processes. Among these small molecules, carbon monoxide is one of the most important in transition metal chemistry from an academic or an industrial viewpoint. In this context reactions of laser-ablated lanthanide atoms with CO have been investigated. For example, Reactions of laser-ablated lanthanum and yttrium atoms with carbon monoxide molecules in solid neon have been investigated using matrix-isolation infrared spectroscopy. The $M(CO)_x$ and MCO^+ (M = La, Y; x = 1–4) molecules have been formed and identified on the basis of isotopic shifts, mixed isotopic splitting patterns, and CCl_4-doping experiments. Density functional theory calculations were performed on these lanthanum and yttrium carbonyls. The agreement between the experimental and calculated vibrational frequencies, relative absorption intensities, and isotopic shifts substantiated the identification of these carbonyls from the matrix infrared spectrum. This study revealed that the C–O stretching vibrational frequencies of MCO^+ decrease from Sc to La, which indicates an increasing in metal d orbital → CO π^* back-donation in this series [1]. In the course of a closely related investigation, reactions of laser-ablated La atoms with CO_2 molecules in solid Ar and Ne were studied using matrix-isolation infrared spectroscopy. On the basis of isotopic shifts, mixed isotopic splitting patterns, and CCl_4-doping experiments, absorptions at 1839.9 and 753.6 cm^{-1} in Ar and 1855.9 and 771.3 cm^{-1} in Ne are assigned to the C–O and La–O stretching vibrations of the OLaCO molecule, respectively. UV–vis photoinduced isomerization of OLaCO to La-(η^2-OC)O and OLa-(η^2-CO) was observed under different wavelength photolyses in the solid matrix. Density functional theory calculations were performed on these products, which support the experimental assignments of the IR spectra. The study once again revealed that the C–O stretching vibrational frequencies of OMCO decrease from Sc to La, indicating again an increase in metal d orbital → CO π^* back-donation in this series [2].

2.2. Lanthanide hydrocarbyls

2.2.1. Homoleptic compounds

A systematic computational study of the hydrogen storage capacity of model organometallic compounds consisting of Sc, Ti, and V transition metal atoms bound to C_mH_m rings (m = 4–6) was reported. For all the complexes considered, the hydrogen storage capacity was found to be limited by the 18-electron rule. The maximum retrievable H_2 uptake predicted is 9.3 wt% using ScC_4H_4, slightly better than the 9.1 wt% hydrogen using TiC_4H_4, and much larger than the ~7 wt% hydrogen with VC_4H_4, where only four H_2 molecules can be adsorbed. The kinetic stability of these hydrogen-covered organometallic complexes was reviewed in terms of the energy gap between the highest occupied and lowest unoccupied molecular orbitals and the strength and nature of successive H2 bindings [3]. The new $[Li(DME)_3]^+$ salt of the long known tetra(*t*-butyl)erbate(III) anion $[Er(Bu^t)_4]^-$ has been prepared and structurally characterized by X-ray diffraction. The erbium(III) center in the homoleptic anion is ligated by four *t*-butyl groups in an approximately tetrahedral arrangement (Fig. 1). The C–Er–C angles between the *t*-butyl groups range from 108.8(3)° to 111.2(3)° and the Er–C distances range from 2.352(6) to 2.395(6) Å. The Li cation is surrounded by three DME molecules, which form a distorted octahedral coordination sphere. Attempts to oxidize the analogous terbate complex $[Li(DME)_3][Tb(Bu^t)_4]$ and its cerium analog to electrically neutral tetra(alkyl)lanthanide(IV) compounds did not afford any isolable products [4].

2.2.2. Heteroleptic compounds

Methane activation reactions with laser-ablated Group 3 metal atoms showed that Sc, Y, and La are just as effective as other early transition metals. Two primary products, CH_3–MH and CH_2–MH_2, were identified for each metal from the matrix IR spectra. The single insertion product becomes more favorable with increasing atomic mass of the metal, opposite the general trend observed from other early transition metal systems. The C–M bond lengths for CH_3–MH and CH_2–MH_2 are comparable to each other, on the basis of electronic structure calculations, and the methylidene dihydride complex is symmetrical without agostic distortion. The number of valence electrons of the metal is evidently an important factor in the magnitude of the agostic interaction in these simple methylidene systems [5]. In a closely related study, the infrared spectra of the transient CH_3–MX and CH_2–MHX complexes formed by reactions of laser-ablated Group 3 metal atoms (Sc, Y, La) with methyl halides have been investigated. The reactions were carried out in an excess of Ar during condensation, and the matrix IR spectra were

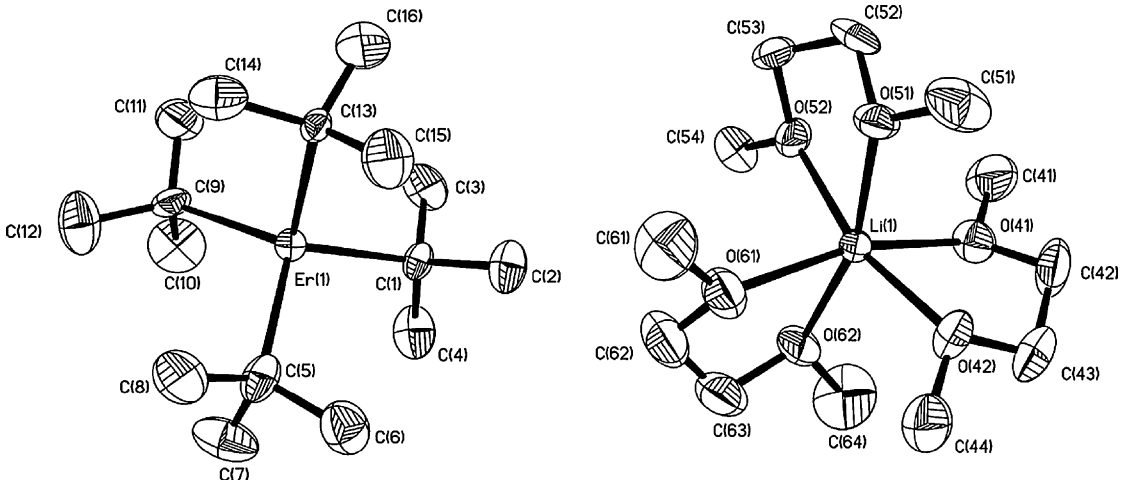

Fig. 1. Molecular structure of $[Li(DME)_3][Er(Bu^t)_4]$ [4].

studied. It was found that the metals are as effective as other early transition metals in providing insertion products (CH_3–MX) and higher oxidation state methylidene complexes (CH_2–MHX) (X = F, Cl, Br) following α-hydrogen migration [6]. A reduced multireference coupled-cluster study has been carried out to study the bonding in transition metal methylene complexes MCH_2^+, including $ScCH_2^+$ [7]. The coordination of four model amino–carbene ligands to $SmCl_3$ has been theoretically investigated using DFT calculations. Strong coordination energies were predicted for all carbenes ($\Delta G(25\,^\circ C) < -35$ kcal mol^{-1} for the monoadducts). The nature of the Sm–carbene bonds was studied by molecular orbital and natural bond orbital (NBO) analyses. No evidence for significant carbene-to-Sm π-donation or Cl-to-carbene back-donation was observed. Thus, the strong Sm–carbene bonds were essentially attributed to carbene-to-Sm σ-donation [8].

σ-Bonded organometallic derivatives of yttrium(III) and thulium(III) were synthesized with the use of donor-functionalized alkyl substituents. For example, the reaction between $LnI_3(THF)_{3.5}$ and 2 equiv. of $K[C(SiMe_3)_2(SiMe_2OMe)]$ in THF at room temperature according to Scheme 1 yielded the mono-substituted products $[(Me_3Si)_2(Me_2SiOMe)C]LnI_2(THF)_2$ (Ln Y, Tm). Both compounds were isolated as colorless or pale yellow blocks after recrystallization from cold methylcyclohexane/THF. Under more forcing reaction conditions decomposition occurred [9].

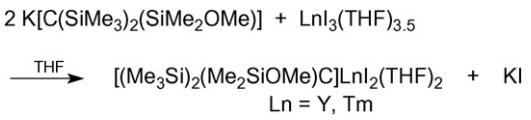

Scheme 1.

During the course of this investigation a highly unusual coupling reaction mediated by Tm(III) was discovered. As illustrated in Scheme 2, a novel separated ion-pair complex of thulium was formed in a metathesis reaction between $TmI_3(THF)_{3.5}$ and 2 equiv. of the lithium iodide-containing organopotassium reagent $[(Me_3Si)_2(Me_2SiOMe)C]K(LiI)_x$. The product was isolated in the form of pale yellow, block-like crystals. The dianionic ligand in this complex is derived from the coupling of 2 equiv. of $[(Me_3Si)_2(Me_2SiOMe)C]^-$, accompanied by the formal elimination of Me_2O. The cation and anion in the ion pair differ only in the inclusion of 2 equiv. of $Li(THF)_3$ in the former, bridged to thulium by iodide ions (Fig. 2) [9].

Closely related Ln(II) and Ln(III) dialkyls were also prepared from LnI_2 (Ln = Nd, Tm, Yb) and structurally characterized. The potassium reagents employed as starting materials in this study are shown in Scheme 3 [10].

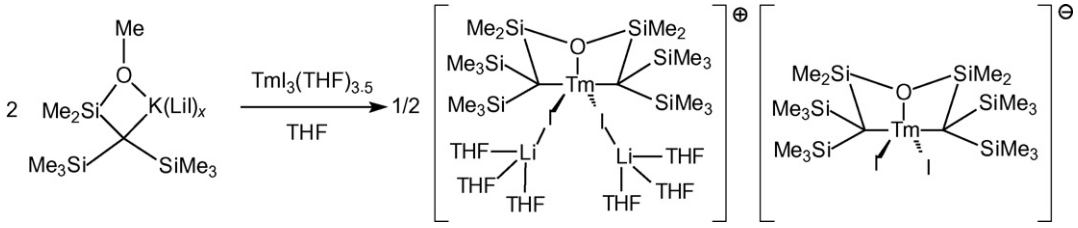

Scheme 2.

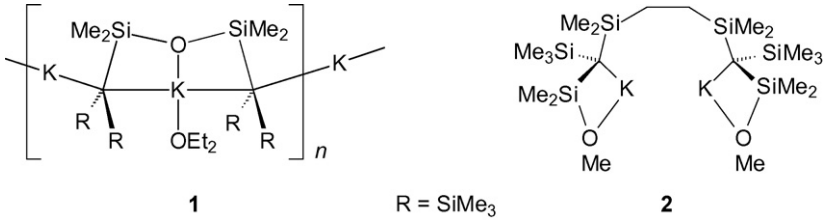

1 R = $SiMe_3$ **2**

Scheme 3.

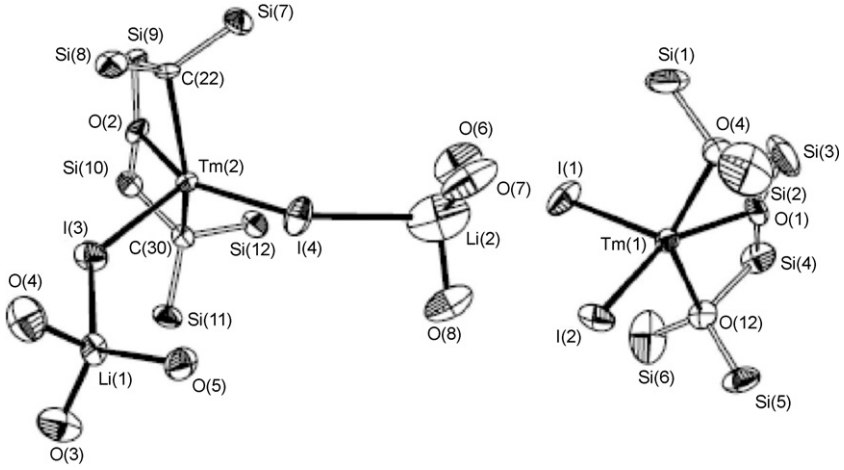

Fig. 2. Molecular structure of $[[\{(Me_3Si)_2C(SiMe_2)\}_2O]TmI_2\{Li(THF)_3\}_2]$–$[[(Me_3Si)_2C(SiMe_2)\}_2O]TmI_2]$ [9].

Whereas the reactions between either NdI_2 or TmI_2 and 1 equiv. of the dipotassium salt **1** yielded only intractable mixtures of products, reactions between LnI_2 (Ln = Tm, Nd) and 1 equiv. of **2** gave the lanthanide(III) compounds $[(Me_3Si)(Me_2MeOSi)C(SiMe_2)]_2Ln(OMe)(THF)$ *via* a ligand degradation reaction (Scheme 4). In contrast, YbI_2 reacts smoothly with either **1** or **2** to give the corresponding ytterbium(II) alkyls shown in Scheme 4. All products were structurally characterized by X-ray crystallography. The two Ln(III) methoxide complexes crystallize as structurally similar monomers with a distorted trigonal prismatic geometry about the Ln(III) ions, while in the ytterbium(II) complexes the Yb centers lie in a distorted trigonal bipyramidal geometry [10].

Alkane elimination reactions between $Ln(CH_2SiMe_3)_3(THF)_2$ precursors and the protonated forms of multidentate ligands leading to heteroleptic lanthanide alkyl complexes were reported by various research groups in 2007. This method has thus been established as a very effective route to lanthanide alkyls containing such ancillary ligands. For example, the reaction of $Ln(CH_2SiMe_3)_3(THF)_2$ (Ln = Sc, Y, Ho, Lu) with 1 equiv. of the amine ligand 2,6-^{i}Pr$_2$C$_6$H$_3$NH(SiMe$_3$) gave the corresponding amido-ligated rare-earth metal bis(alkyl) complexes [2,6-^{i}Pr$_2$C$_6$H$_3$NH(SiMe$_3$)]Ln(CH$_2$SiMe$_3$)$_2$(THF), which represent rare examples of bis(alkyl) rare earth metal complexes bearing a monodentate anionic ancillary ligand. In the case of gadolinium, a similar reaction gave the bimetallic complex $Gd_2(\mu\text{-}CH_2SiMe_2NC_6H_3{}^iPr_2\text{-}2,6)_3(THF)_3$ through intramolecular C–H activation of a methyl group of $SiMe_3$ on the amido ligand by Gd–CH_2SiMe_3 and subsequent ligand redistribution. All compounds reported in this study were structurally characterized by X-ray analyses [11].

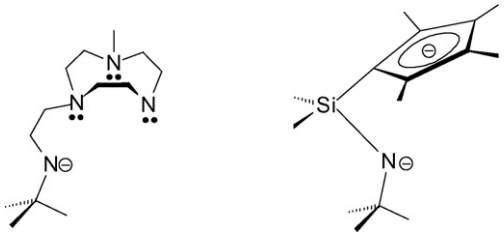

Scheme 5.

Ancillary ligand systems incorporating the 1,4,7-triazacyclononane (=TACN) *fac*-tridentate donor fragment and a pendent amide functionality (Scheme 5) are related to the well-known dianionic cyclopentadienyl-amide ligands used for cationic Group 4 metal alkyl catalysts for olefin (co-)polymerization. The TACN ligands were now employed in lanthanide chemistry as well [12].

The ligand synthesis is outlined in Scheme 6. It starts from known 1,4-dimethyl-1,4,7-triazacyclononane and yields a set of R_2TACN–amide ligands in two steps. These ligands are thermally and hydrolytically stable and can be purified by Kugelrohr distillation and/or acid–base extraction [12].

The synthesis of R_2TACN–amide metal dialkyl complexes was achieved following two different synthetic routes. For those metals for which the trialkyl complexes $M(CH_2SiMe_3)_3(THF)_2$ are available (M = Sc, Y, Sm–Lu), a convenient way to prepare the dialkyl com-

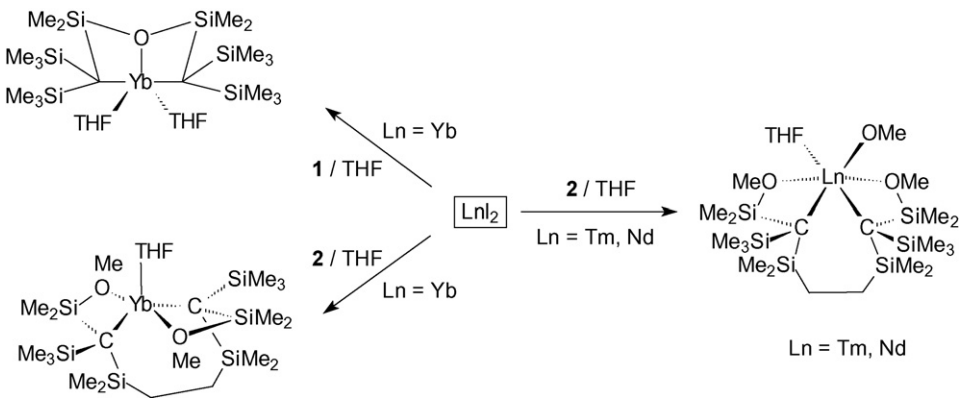

Scheme 4.

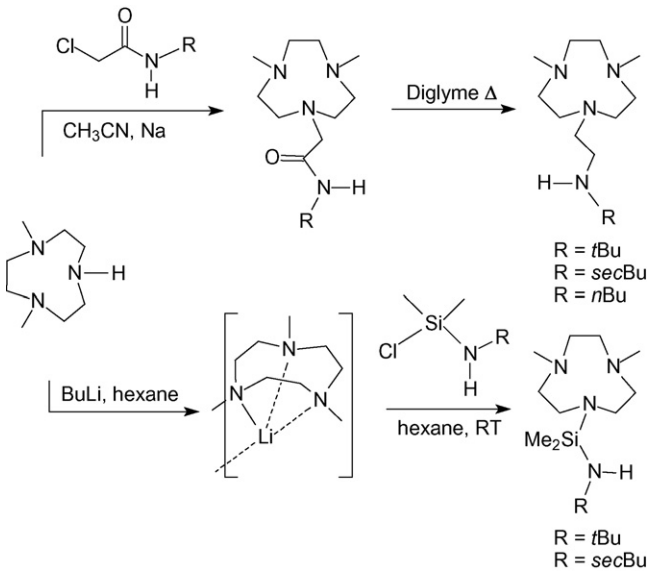

Scheme 6.

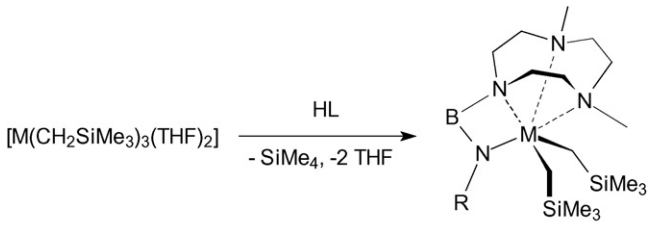

M	R	B
Sc	*t*Bu	Me_2Si
Sc	*sec*Bu	Me_2Si
Y	*t*Bu	$(CH_2)_2$
Y	*sec*Bu	$(CH_2)_2$
Y	*n*Bu	$(CH_2)_2$
Y	*t*Bu	Me_2Si
Y	*sec*Bu	Me_2Si

Scheme 7.

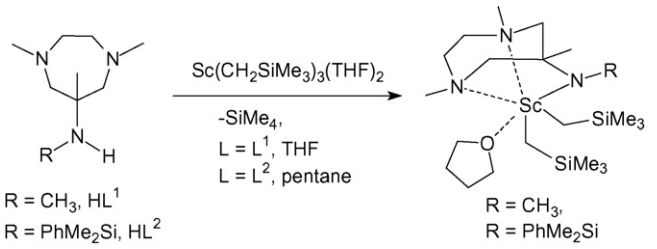

Scheme 9.

plexes is the reaction of the trialkyl with the free R_2TACN–amide ligand in pentane or THF solvent according to Scheme 7. This method affords the products as crystalline solids after crystallization from pentane in 70–80% isolated yields [12].

For the larger lanthanide metals, the neutral trialkyls $M(CH_2SiMe_3)_3(THF)_n$ are not available and thus cannot be employed as preformed starting materials. Nevertheless, it proved possible to obtain the R_2TACN–amide dialkyl complexes of lanthanum and neodymium using the *in situ* alkylation procedure shown in Scheme 8. The same procedure also allowed the synthesis of related scandium monoalkyl–monochloride complexes [12].

Closely related monoanionic *fac*-κ^3 ligands derived from 6-amino-1,4-diazepine were also successfully employed to prepare a series of scandium alkyl derivatives (Scheme 9). Reactions of the free ligands with R = Me and $PhMe_2Si$ with $Sc(CH_2SiMe_3)_3(THF)_2$ yielded the corresponding bis(alkyls) in high yields (78–83%) [13].

In toluene solvent, the compound with R = Me loses a THF molecule and decomposes cleanly *via* metalation of the methyl group of the amido functionality and elimination of 1 equiv. of $SiMe_4$ to give a single organometallic product which can be formulated as [{CH_2(μ-N)-1,4,6-trimethyl-1,4-diazepine}$Sc(CH_2SiMe_3)]_2$ (Scheme 10). In the binuclear complex the amide nitrogen bridges two scandium centers. The geometry around each Sc center is approximately octahedral [13].

In the case of R = $PhMe_2Si$ the compound upon standing in toluene solution just loses a THF molecule to form the corresponding unsolvated bis(alkyl) complex (Scheme 11) [13].

In THF solution, both scandium bis(alkyls) shown in Scheme 11 react with $[PhNMe_2H][BPh_4]$ to generate the ionic monoalkyl compounds depicted in Scheme 12. The ionic compounds were isolated as analytically pure white powders by layering their THF solutions with apolar solvents [13].

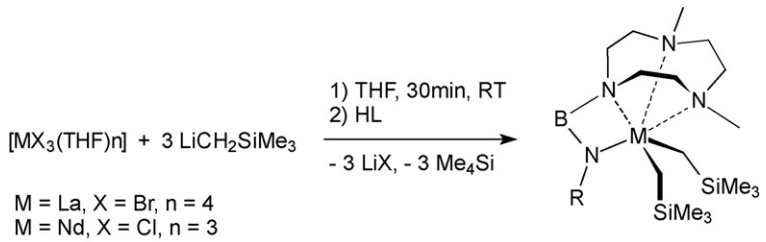

M	R	B
La	*t*Bu	$(CH_2)_2$
Nd	*t*Bu	$(CH_2)_2$
Nd	*sec*Bu	$(CH_2)_2$
Nd	*t*Bu	Me_2Si
Nd	*sec*Bu	Me_2Si

Scheme 8.

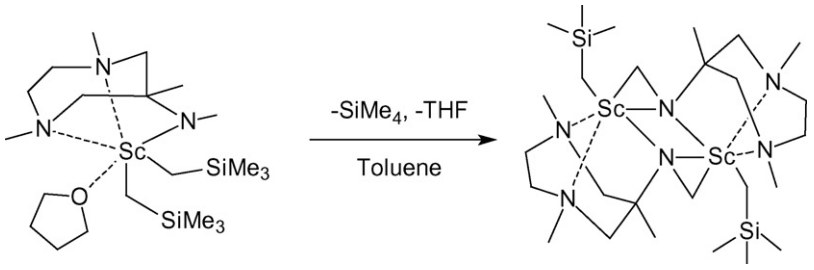

Scheme 10.

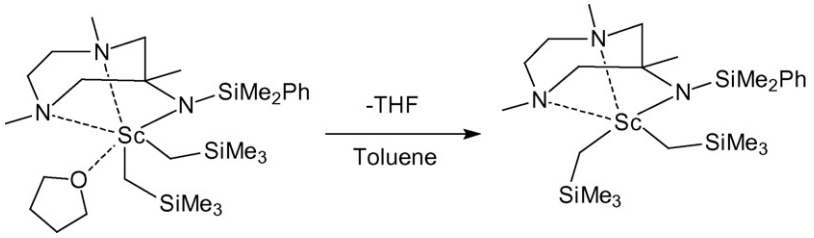

Scheme 11.

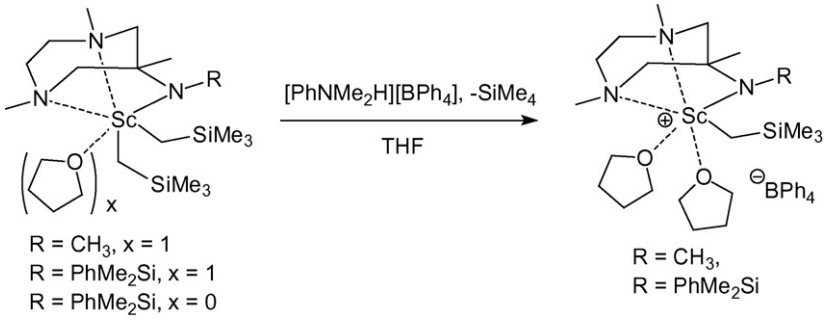

Scheme 12.

Catalytic ethylene polymerization experiments in toluene solvent did not show any activity of the cationic species generated *in situ* using $[PhNMe_2H][B(C_6F_5)_4]$. A catalytically active species could only be obtained using the THF-free precursor shown in Scheme 10 (*cf.* Section 2.11.1). It was found that the dimeric species $[\{CH_2(\mu\text{-}N)\text{-}1,4,6\text{-trimethyl-}1,4\text{-diazepine}\}Sc(CH_2SiMe_3)]_2$ (Scheme 10) reacts with ethylene *via* stoichiometric insertion into the Sc–CH_2N bond to yield $[\{CH_2CH_2CH_2(\mu\text{-}N)\text{-}1,4,6\text{-trimethyl-}1,4\text{-diazepine}\}Sc(CH_2SiMe_3)]_2$ (Scheme 13) [13].

The ligand metalation in a β-diketiminato scandium dimethyl complex activated with bis(pentafluorophenyl)borane has been investigated. Equimolar reactions of $LScMe_2$ (L = (Ar)NC(^{t}Bu)CHC(^{t}Bu)N(Ar); Ar = 2,6-^{i}Pr$_2$C$_6$H$_3$) and $HB(C_6F_5)_2$ were found to proceed through an isolable ion pair to a metalated scandium borate with loss of methane. The proposed mechanism (Scheme 14) was corroborated by multinuclear NMR experiments as well as synthesis *via* alternative routes [14].

The same reaction of $LScMe_2$ with 2 equiv. of $HB(C_6F_5)_2$ yielded the μ_2-hydridoborate complex $[LScMe][(\mu\text{-}H)_2B(C_6F_5)_2]$, while 4 equiv. of borane react to afford the bis-μ_2-hydridoborate complex $[LSc][(\mu\text{-}H)_2B(C_6F_5)_2]_2$ (Scheme 15) [14].

A series of bis(phosphinimino)methanide yttrium and lanthanide amido complexes $[CH(PPh_2NSiMe_3)_2]Ln[N(SiHMe_2)_2]_2$ (Ln = Y, La, Sm, Ho, Lu) were synthesized by three different pathways illustrated in Scheme 16. The compounds can be obtained either from $Ln[N(SiHMe_2)_2]_3(THF)_2$ and $CH_2(PPh_2NSiMe_3)_2$ or from $KN(SiHMe_2)_2$ and $[Ln\{CH(PPh_2NSiMe_3)_2\}Cl_2]_2$, while in a third approach the lanthanum compound was synthesized in a one-pot reaction starting from $K[CH(PPh_2NSiMe_3)_2]$, $LaCl_3$, and $KN(SiHMe_2)_2$. All products were structurally characterized by single-crystal X-ray diffraction [15].

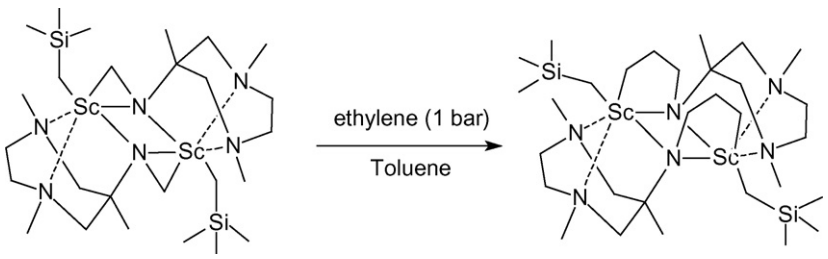

Scheme 13.

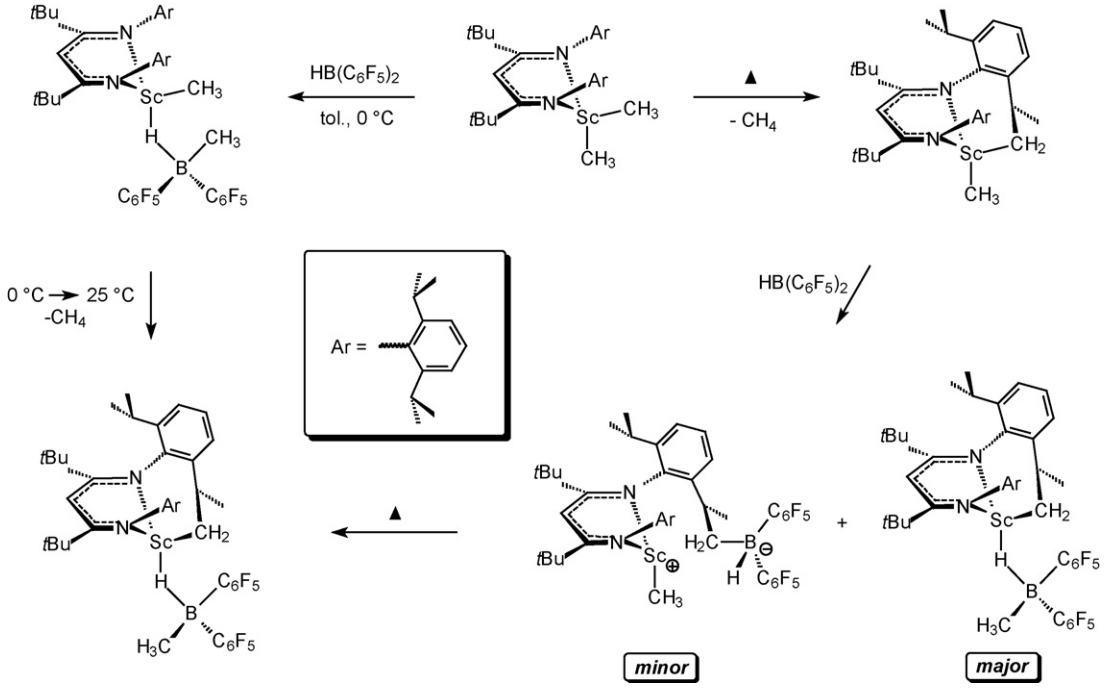

Scheme 14.

Several cationic lanthanide alkyl complexes bearing an ancillary bis(phosphinophenyl)amido (=PNP) ligand were prepared and structurally characterized. The synthetic route is outlined in Scheme 17. Analogous to the synthesis of the R_2TACN–amide metal dialkyl complexes (*cf.* Scheme 7) the acid/base reaction of the trialkyl complexes $M(CH_2SiMe_3)_3(THF)_2$ with 1 equiv. of $HN[C_6H_4(PPh_2)\text{-}2]_2$ gave the corresponding dialkyl complexes. The Y and Lu complexes contain an additional THF ligand, while the smaller Sc complex is THF-free. The cationic species could be isolated by treatment of the dialkyl precursors with $[PhMe_2NH][B(C_6F_5)_4]$ in THF. Single crystals of the Lu complex could be grown from chlorobenzene/hexane at −30 °C. An X-ray diffraction study revealed that the solid-state structure consists of separated ion pairs in which the lutetium cation adopts a distorted octahedral structure similar to that of its neutral precursor [16].

Alkane elimination was also found to be the method of choice for the synthesis of rare earth metal alkyl complexes stabilized by anilido phosphinimine and amino phosphine ligands. Scheme 18 illustrates typical reactions of yttrium and lutetium trialkyls with a bulky anilido phosphinimine ligand. In this process, deprotonation of the free ligand by one metal alkyl species was followed by intramolecular C–H activation of the phenyl group of the phosphine moiety to generate a dianion of the ligand with release of 2 equiv. of

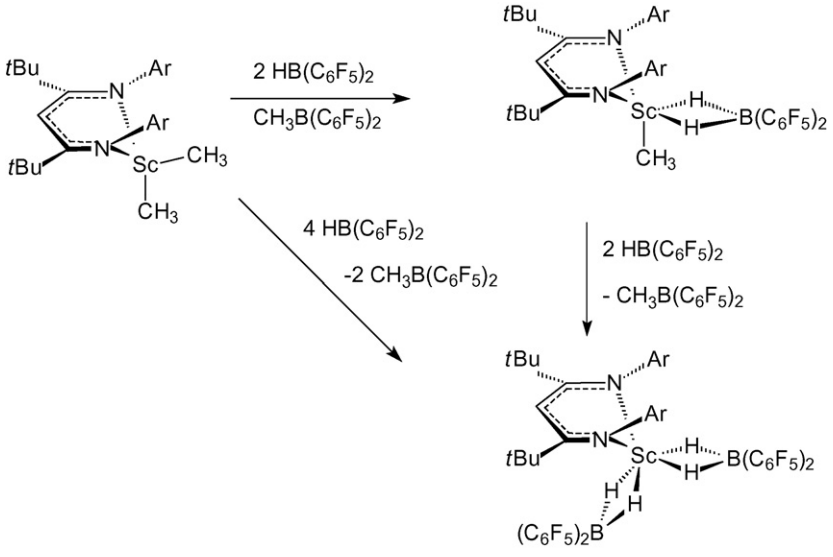

Scheme 15.

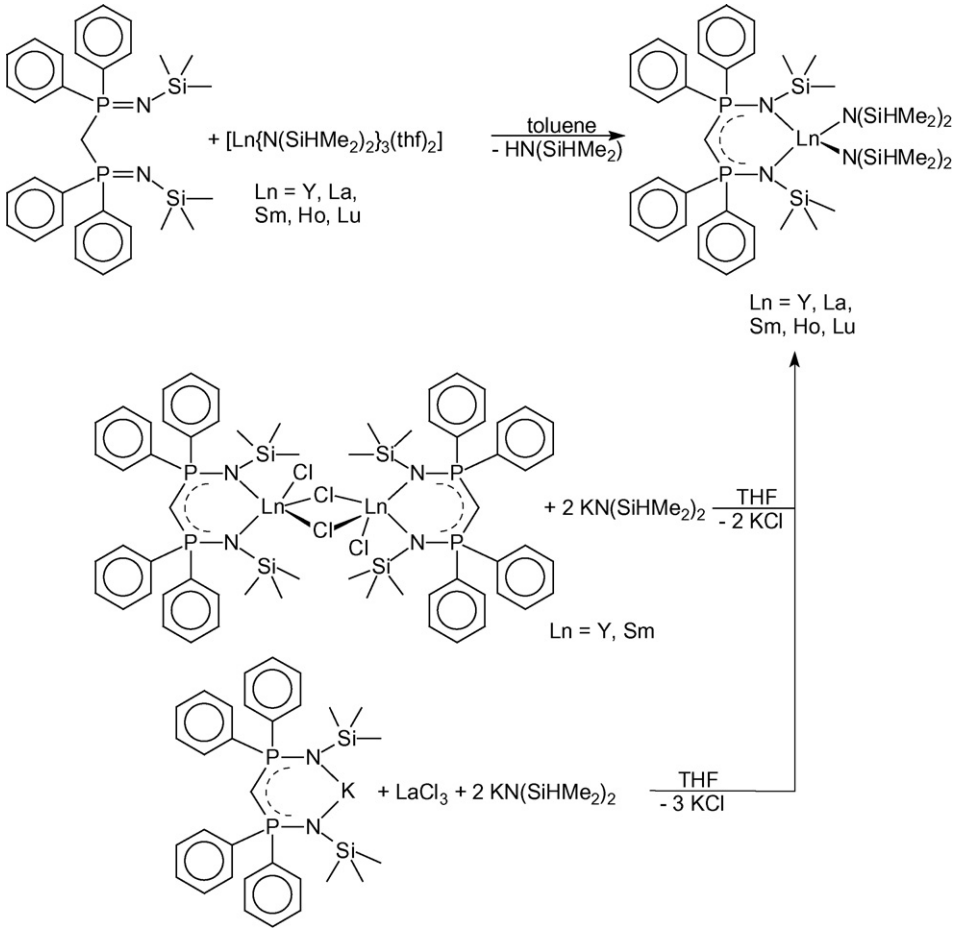

Scheme 16.

tetramethylsilane. The doubly deprotonated ligand coordinates to the Ln^{3+} ions in a rare C,N,N tridentate mode. The yttrium product reacted readily with 2 equiv. of 2,6-diisopropylaniline to give the corresponding bis-amido complex depicted in Scheme 18 selectively. This reaction shows that the C–H activation of the phenyl group is reversible. Exposure of the yttrium product to moisture afforded a hydrolyzed dimeric complex containing two OH bridging ligands (Scheme 18) [17].

Similar treatment of $Ln(CH_2SiMe_3)_3(THF)_2$ (Ln = Y, Lu) with amino phosphine ligands according to Scheme 19 gave stable rare earth metal dialkyl complexes in high yields. In this case no C-H activation of a phenyl group was observed. Subsequent amination

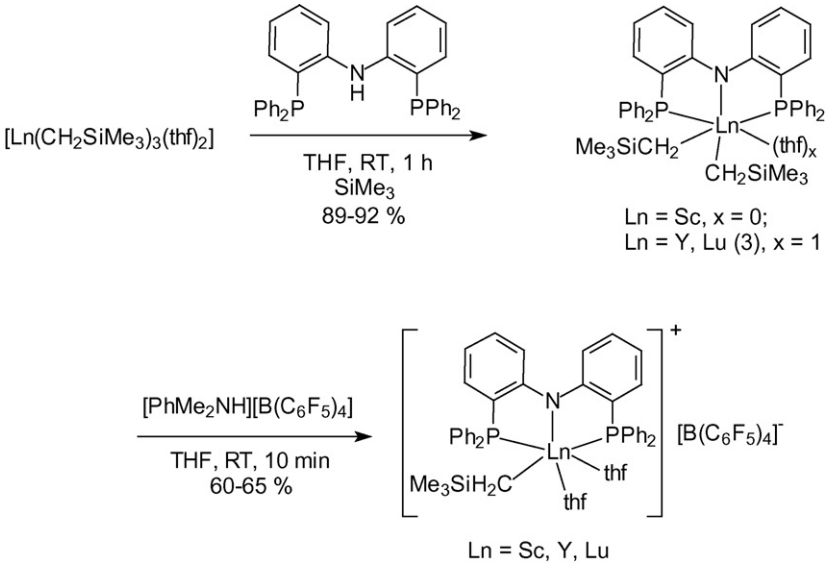

Scheme 17.

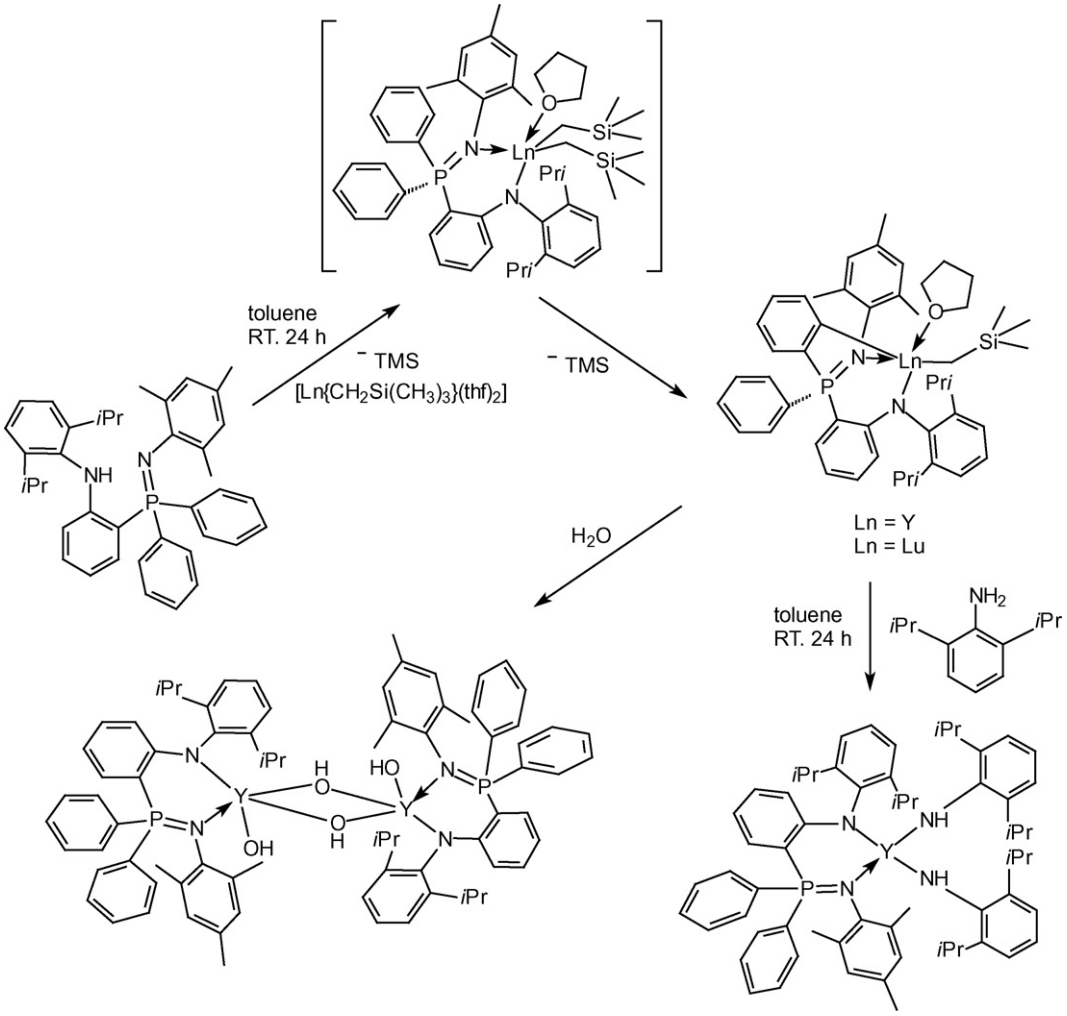

Scheme 18.

with 2,6-diisopropylaniline afforded the corresponding bis-amido derivatives [17].

In a closely related study, rare earth metal mono- and bis(alkyl) complexes bearing aminophosphine ligands were synthesized and their catalytic activity toward ethylene polymerization was investigated. As illustrated in Scheme 20, reactions of the lutetium tris(alkyl) $Lu(CH_2SiMe_3)_3(THF)_2$ with neutral aminophosphines resulted in formation of bis(ligand) mono(alkyl) complexes accompanied by alkane elimination. The product with $R = CH_2Ph$ was unstable and gradually disproportionated to a homoleptic tris(ligand) complex at room temperature within a week [18].

Using a sterically more demanding aminophosphine with a 2,6-$Me_2C_6H_3$ substituent at nitrogen, the corresponding lanthanide bis(alkyls) were cleanly obtained in high yields (Scheme 21). Fig. 3 depicts the molecular structure of the scandium derivative. When activated by $AlEt_3$ or $[Ph_3C][B(C_6F_5)_4]$ this compound was able to catalyze ethylene polymerization (*cf.* Section 2.11.1) [18].

A very similar lutetium bis(alkyl) complex stabilized by a flexible aminophosphine ligand $LLu(CH_2SiMe_3)_2(THF)$ ($L = (2,6\text{-}C_6H_3Me_2)NCH(Ph)CH_2PPh_2$) was prepared in 65% yield as shown in Scheme 22. The solid-state structure was characterized by X-ray analysis to be a monomer, adopting trigonal–bipyramidal geometry around the metal center [19].

Subsequent insertion of *N*,*N*′-diisopropylcarbodiimide led to C–H activation *via* metalation of the ligand aryl methyl followed by reduction of the C=N double bond. The synthetic pathway involving two intermediate **A** and **B** is depicted in Scheme 23 [19].

Indirect proof for the formation of intermediate **A** came from the isolation of a closely related species which was prepared as shown

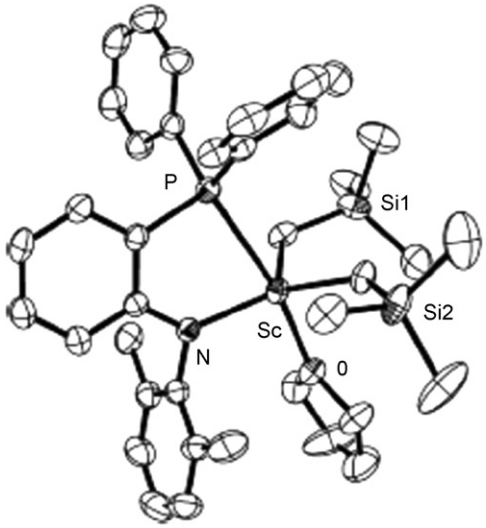

Fig. 3. Molecular structure of $[2\text{-}(2,6\text{-}Me_2C_6H_3N)C_6H_4P(Ph)_2]Sc(CH_2SiMe_3)_2(THF)$ [18].

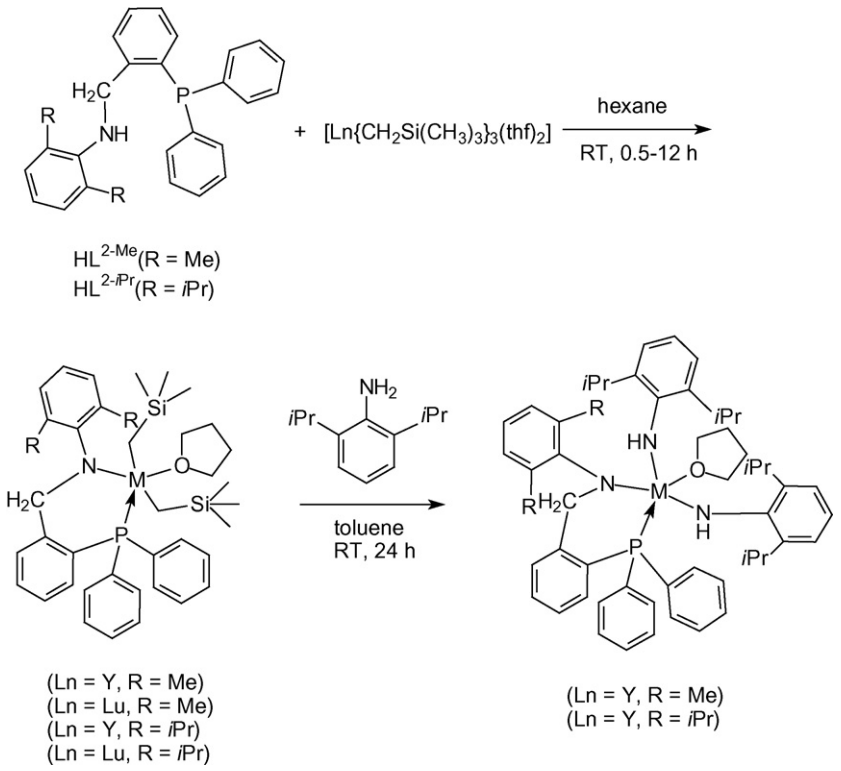

Scheme 19.

in Scheme 24 from insertion of *N*,*N*′-diisopropylcarbodiimide into a previously reported *P*,*N*-bidentate ligand stabilized lutetium bis(alkyl) complex (*cf.* Scheme 21) [19].

A similar synthetic approach, *i.e.*, alkane elimination from scandium and yttrium trialkyl complexes, was used to synthesize Group 3 metal dialkyl complexes with tetradentate monoanionic phenolate ligands (Scheme 25) [20].

As shown in Scheme 26, the dialkyl species could in principle present C_1 or C_s symmetry. X-ray crystallographic studies of three derivatives showed in all cases mononuclear structures of C_1 symmetry in the solid state [20].

The scandium dialkyl complex with R = CH_2SiMe_2Ph was found to undergo clean activation of a C–H bond of a methylene linking a pyridine to the central nitrogen donor. This process, illustrated in Scheme 27, follows first-order kinetics [20].

The yttrium dialkyl complexes react with 1 equiv. of $[PhNHMe_2][B(C_6F_5)_4]$ in chlorobenzene-d_5 to generate solutions of the corresponding monoalkyl cationic species (Scheme 28). These solutions slowly polymerize ethylene (*cf.* Section 2.11.1) [20].

Similar alkane elimination reactions of amino-amino-bis(phenols) H_2L^{1-4} (Schemes 29 and 30) and Salan H_2L^5 (Scheme 31) with the lanthanide trialkyls $Ln(CH_2SiMe_3)_3(THF)_2$

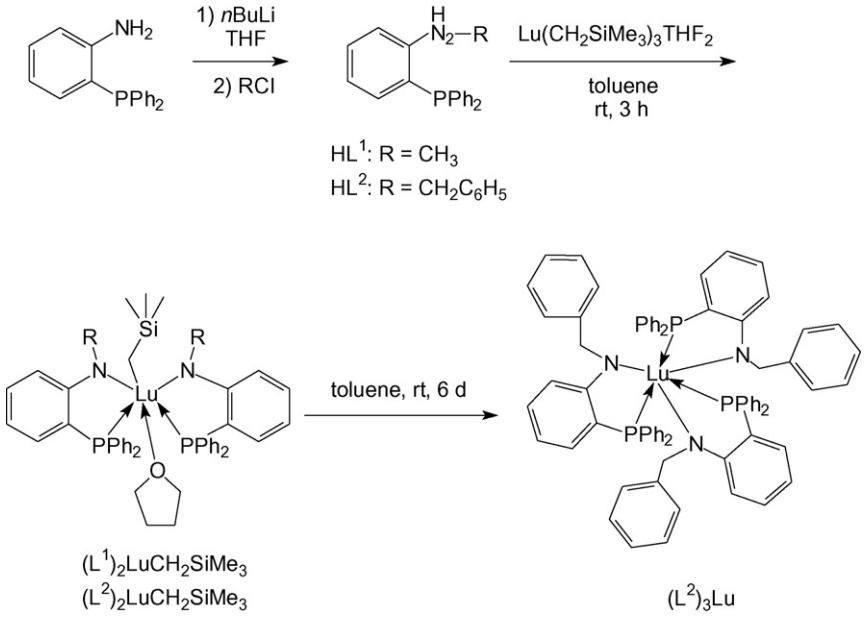

Scheme 20.

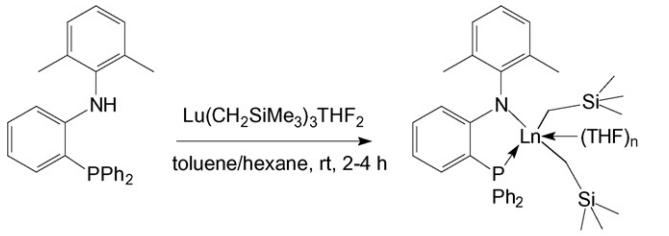

$L^3Y(CH_2SiMe_3)_2(THF)_2$, n = 2
$L^3Sc(CH_2SiMe_3)_2(THF)$, n = 1
$L^3Lu(CH_2SiMe_3)_2(THF)$, n = 1
$L^3Yb(CH_2SiMe_3)_2(THF)$, n = 1
$L^3Tm(CH_2SiMe_3)_2(THF)$, n = 1

Scheme 21.

(Ln = Y, Lu) afforded a series of lanthanide alkyl complexes with the release of tetramethylsilane. All products shown in Schemes 29–31 were found to be THF-solvated mono-alkyls stabilized by *O*,*N*,*N*,*O*-tetradentate ligands [21].

Two closely related yttrium bis(alkyl) complexes were synthesized in a similar manner by the alkane elimination route outlined in Scheme 32. Both products were shown to be solvent-free [21].

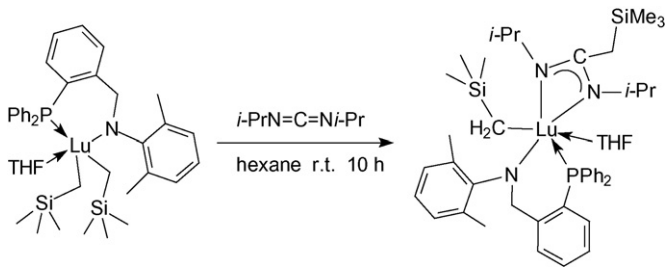

Scheme 24.

Alkane elimination reactions of lanthanide metal tris(alkyl)s, $Ln(CH_2SiMe_3)_3(THF)_2$ (Ln = Y, Lu) with the multidentate ligands HL^{1-4} afforded a series of new rare earth metal complexes. An yttrium complex supported by the flexible amino–imino phenoxide ligand HL^1 was prepared following Scheme 33 and isolated as a homoleptic product in the form of yellow crystals [22].

In the reactions of the rigid and bulky phosphino–imino phenoxide ligand HL^2 with equimolar $Ln(CH_2SiMe_3)_3(THF)_2$, HL^2 was deprotonated by the metal alkyl and its imino C=N group was reduced to C–N by intramolecular alkylation, generating THF-solvated mono-alkyl complexes (Scheme 34, Ln = Y, Lu). A bis(ligand) chelated yttrium complex without an alkyl moiety was isolated when the molar ratio of HL^2 to $Y(CH_2SiMe_3)_3(THF)_2$ increased to 2:1 [22].

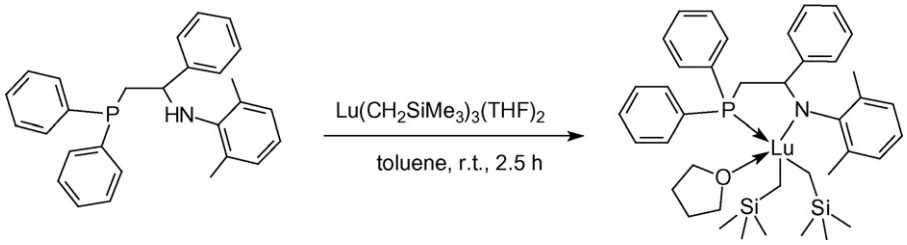

Scheme 22.

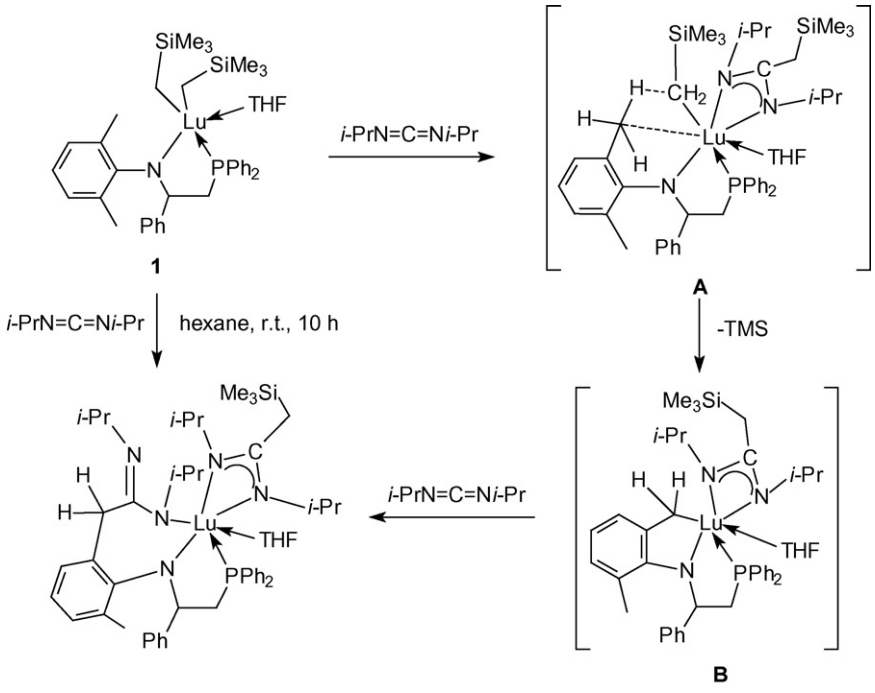

Scheme 23.

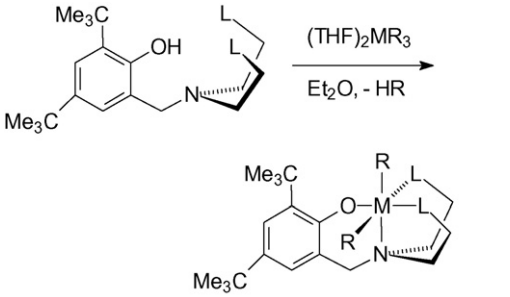

Scheme 25.

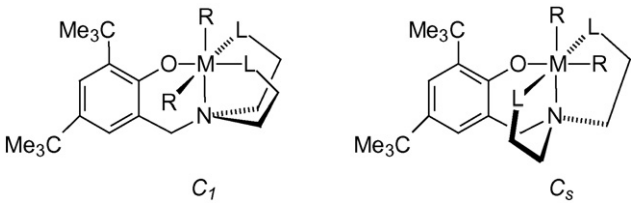

Scheme 26.

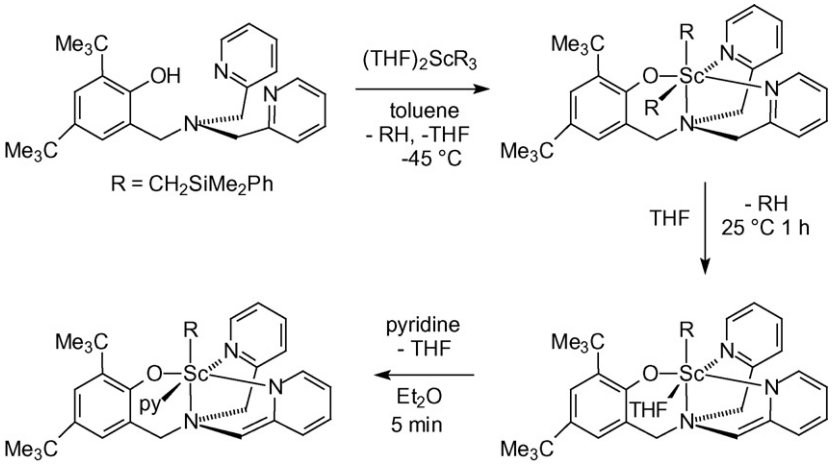

Scheme 27.

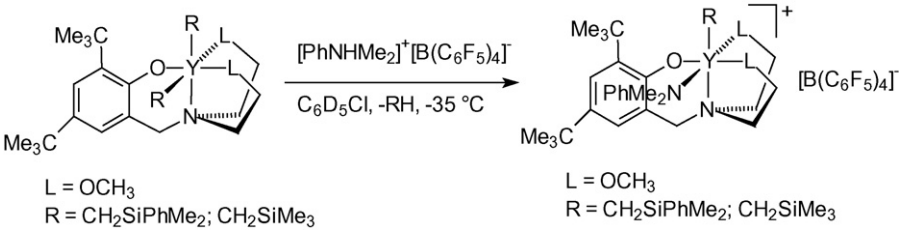

Scheme 28.

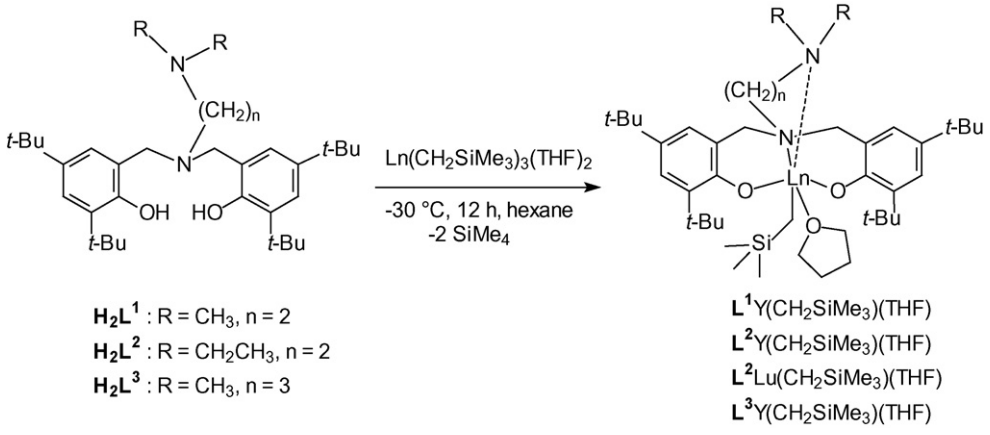

Scheme 29.

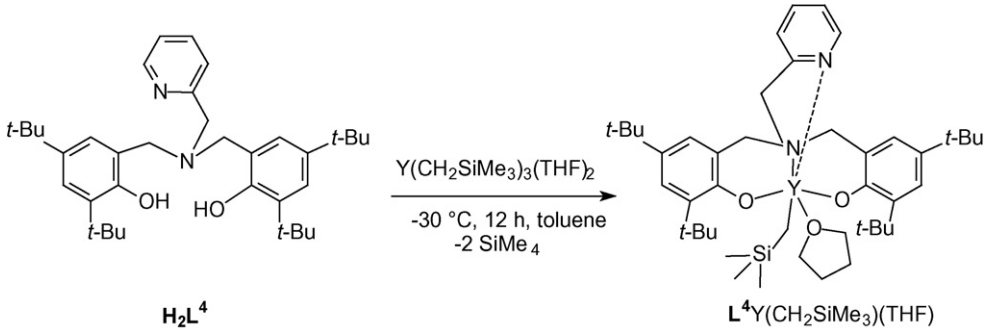

Scheme 30.

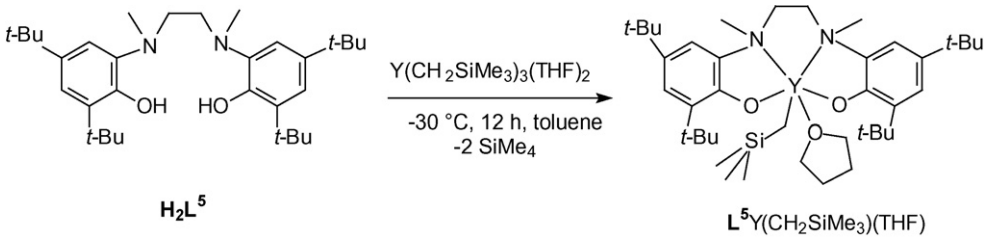

Scheme 31.

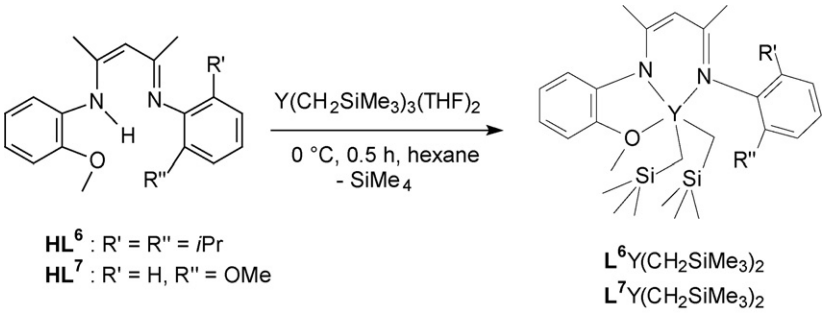

Scheme 32.

Similar reaction of the phosphino β-ketoiminato ligand HL^3 with equimolar amounts of $Ln(CH_2SiMe_3)_3(THF)_2$ (Ln = Y, Lu) afforded bis(ligated) monoalkyl complexes without occurrence of intramolecular alkylation or formation of homoleptic products (Scheme 35) [22].

Treatment of the potentially tetradentate methoxy-amino phenol HL^4 with $Y(CH_2SiMe_3)_3(THF)_2$ afforded a monomeric, THF-free yttrium bis(alkyl) complex as a colorless solid in 78% yield (Scheme 36). All complexes shown in Schemes 33–36 were characterized by IR, NMR spectra and X-ray diffraction analyses [22].

The C_3-symmetric chiral organolanthanide trialkyl complexes (*i*Pr-trisox)$Ln(CH_2SiMe_2R)_3$ (R = Me, Ln = Y, Dy, Er, Tm, Lu; R = Ph, Ln = Lu) were prepared from 1,1,1-tris[(*S*)-4-isopropyloxazolinyl]ethane (*i*Pr-trisox) and the corresponding trialkyl precursors $M(CH_2SiMe_2R)_3(THF)_n$ (Scheme 37). Their molecular structures all display a highly distorted octahedral geometry, with the angles subtended at the metal center significantly deviating from the ideal 90°, which is attributed to the steric

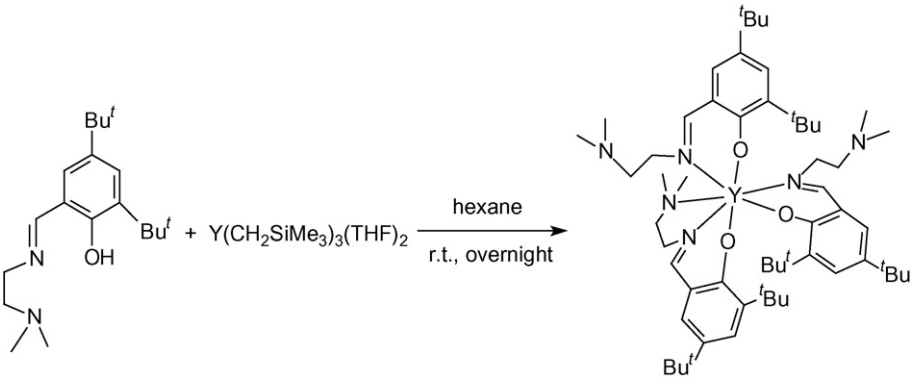

Scheme 33.

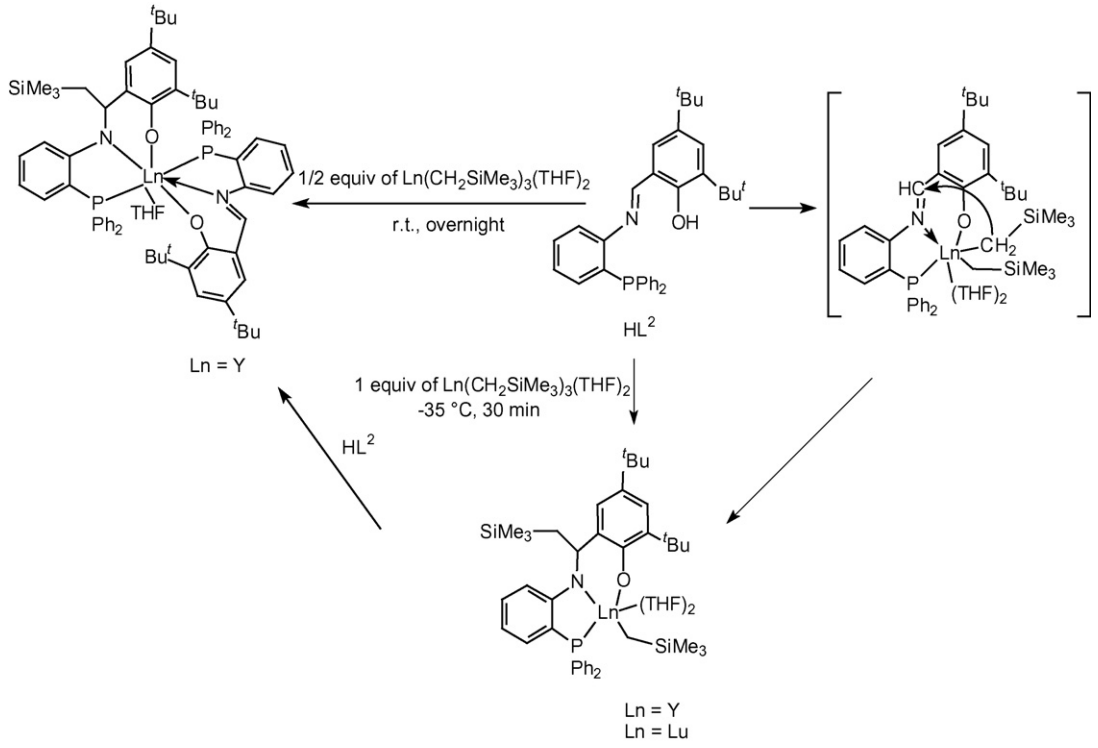

Scheme 34.

Scheme 35.

demands imposed by the large CH_2SiMe_2R ligands, both with each other and with the isopropyl groups of the *i*Pr-trisox ligand [23].

The first examples of yttrium complexes containing bis(*N*-heterocyclic carbene) ligands were reported. For example, the yttrium(III) silylamide derivative shown in Scheme 38 was obtained *via* a transamination reaction between $Y[N(SiMe_3)_2]_3$ and the lithium chloride adduct of the bis(*N*-heterocyclic carbene) ligand. According to an X-ray diffraction study, the coordination geometry around yttrium is distorted trigonal bipyramidal with the tricoordinate bis(carbene) ligand meridionally configured (Fig. 4) [24].

2.3. Lanthanide alkenyl and alkynyl compounds

The first divalent ytterbium complex supported by a diamino-bis(phenolate) ligand, $YbL(THF)_2{\cdot}0.5C_7H_8$, was synthesized in good yield by the amine elimination reaction of $Yb[N(SiMe_3)_2]_2(THF)_2$

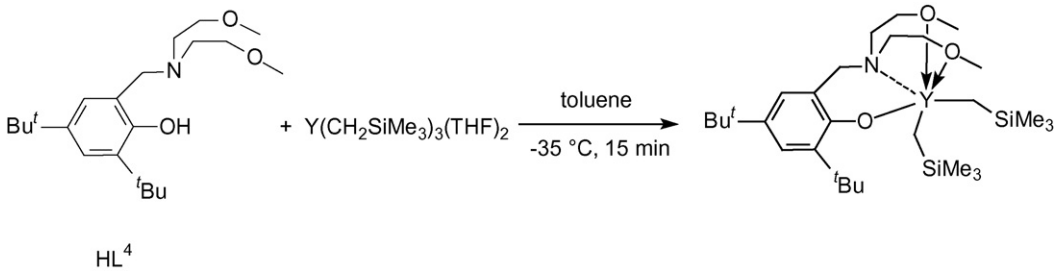

Scheme 36.

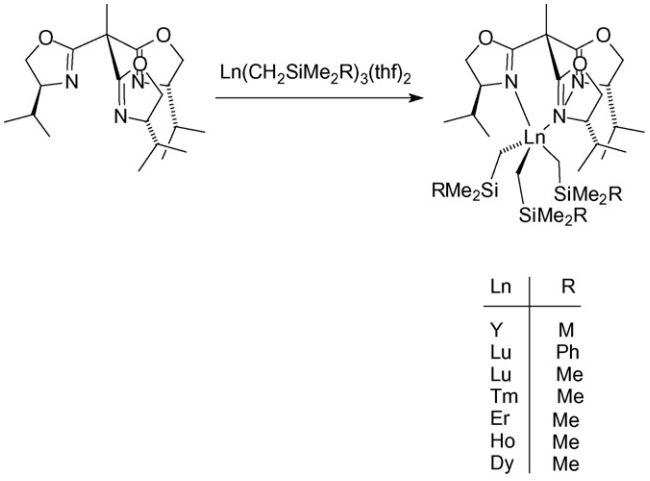

Ln	R
Y	M
Lu	Ph
Lu	Me
Tm	Me
Er	Me
Ho	Me
Dy	Me

Scheme 37.

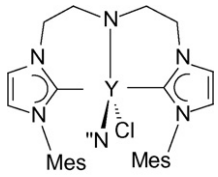

Scheme 38.

with H_2L (L = [$Me_2NCH_2CH_2N(CH_2$-2-OC_6H_2-3,5-$Bu^t_2)_2$]) in a 1:1 molar ratio (Scheme 39). X-ray structural determination showed this complex to be a THF-solvated monomer which adopts a distorted octahedral coordination geometry around the Yb atom. The compound can react with PhC≡CH, as a single electron-transfer reagent, to give the corresponding alkynide complex YbLC≡CPh(DME) (DME = 1,2-dimethoxyethane) in high yield in the form of colorless crystals. The molecular structure of this alkynide complex is monomeric (Fig. 5) with a Yb–C(terminal phenylacetylide) bond length of 2.374(3) Å [25].

2.4. Lanthanide allyls

Compositional variations in monomeric trimethylsilylated allyl lanthanide complexes have been the subject of closer inspection. Treatment of 3 equiv. of the potassium salt of the bis(1,3-trimethylsilyl)allyl anion with various late lanthanide triflates

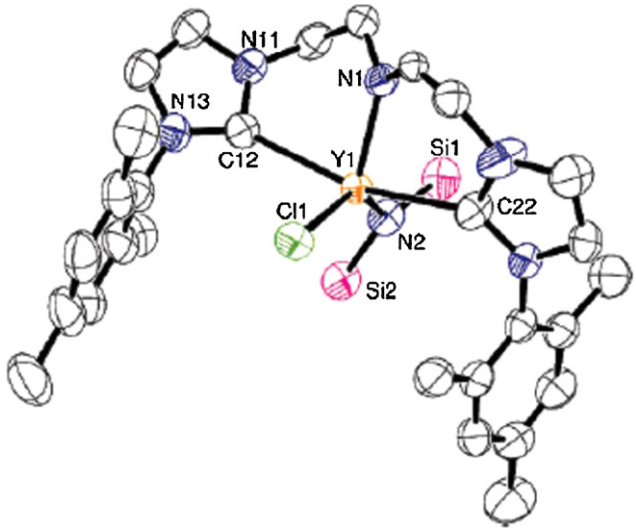

Fig. 4. Molecular structure of LYCl[$N(SiMe_3)_2$] (L = N{CH_2CH_2(1-C[NCHCHNMes])}$_2$) [24].

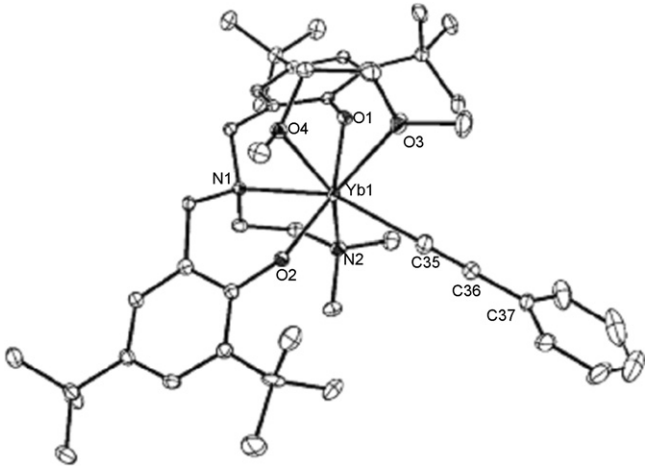

Fig. 5. Molecular structure of YbLC≡CPh(DME) [25].

(Ln = Dy, Ho, Er, Tm, Lu) produces the unsolvated triallyllanthanide complexes LnA'_3 (A′ = 1,3-$(SiMe_3)_2C_3H_3$) (Scheme 40) [26].

The use of lanthanide halides (Cl, I) with the potassium allyl also generated neutral complexes, but when lanthanide iodides and the corresponding lithium allyl were combined, the lanthanate species $[Li(thf)_4][LnA'_3I]$ were formed (Scheme 41) [26].

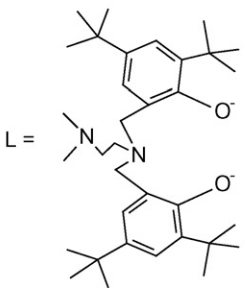

Scheme 39.

$Ln(OTf)_3 + 3KA' \xrightarrow{THF} LnA'_3(thf)$ (Ln = Ce, Nd, Tb

$Ln(OTf)_3 + 3KA' \xrightarrow{THF} LnA'_3$
(Ln = Dy, Ho, Er, Tm, Lu, Y)

Scheme 40.

$LnI_3 + nKA' \xrightarrow{THF} LnA'_3$
(Ln = Dy, n = 3; Ln = Ho, n = 2,3)

$LnCl_3 + nKA' \xrightarrow{THF} LnA'_3$ (Ln = Ho, Er, Y, n = 2,3

$LaCl_3 + nKA' \xrightarrow{THF} LaA'_2Cl(thf)$ (n = 2,3)

$LnI_3 + 3LiA' \xrightarrow{THF} [Li(thf)_4][LnA'_3I]$
(Ln = Ce, Pr, Nd, Gd, Tb, Ho, Er)

Scheme 41.

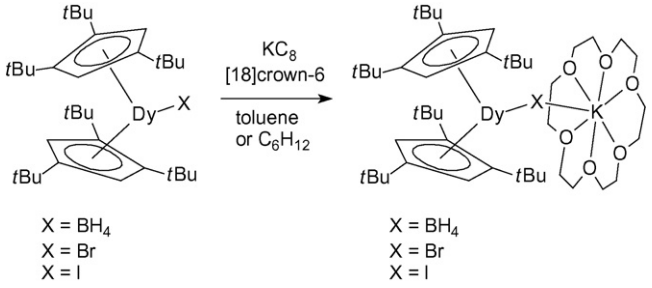

Scheme 42.

Trends in the bonding of lanthanide allyl complexes with the trimethylsilylated allyl ligand were explored and compared with those of cyclopentadienyl lanthanide complexes. It was concluded that despite the geometrically irregular shape of the substituted allyl anion, metal–ligand distances in monomeric lanthanide allyl complexes appear to be reasonably predictable based on metal radius and oxidation state. This is an expected consequence of a high degree of ionic character in the bonding [26].

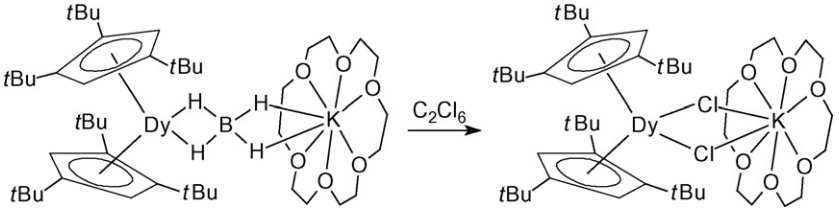

Scheme 43.

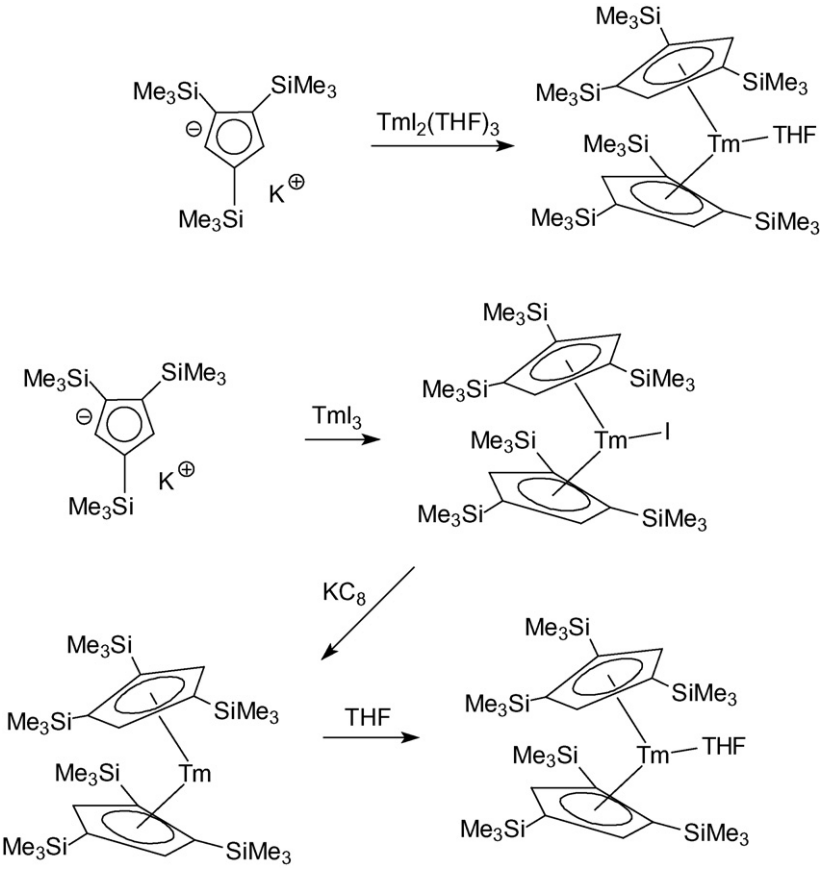

Scheme 44.

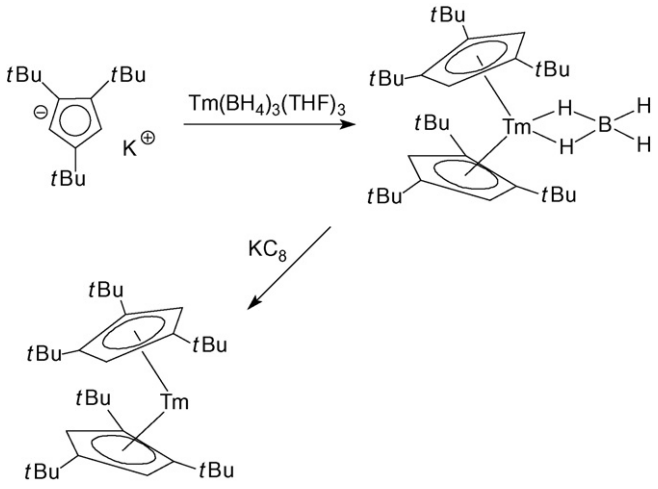

Scheme 45.

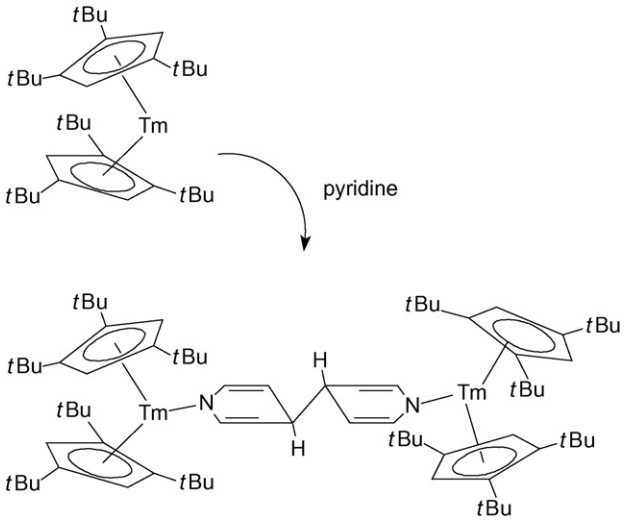

Scheme 46.

2.5. Lanthanide cyclopentadienyl complexes

2.5.1. Cp_2Ln compounds

The synthesis and characterization of "non-classical" divalent organolanthanide complexes continued to attract considerable interest. In 2007, the isolation of stable organodysprosium(II) complexes by chemical reduction of dysprosium(III) precursors was reported. Reduction of bis(tri-*tert*-butylcyclopentadienyl)dysprosium(III) complexes by potassium/graphite in the presence of a crown ether afforded structurally characterized organodysprosium(II) "ate" complexes, a new class of "non-classical" divalent organolanthanide compounds (Scheme 42), which were isolated in the form of dark red crystals [27].

The organodysprosium(II) borohydride "ate" complex was oxidized by hexachloroethane into a structurally characterized organodysprosium(III) dichloride "ate" complex (Scheme 43) and was also shown to reductively couple diphenylacetylene [27].

In a similar manner, the synthesis and reactivity of organometallic complexes of divalent thulium with bulky cyclopentadienyl ligands have been investigated. The synthetic routes are summarized in Schemes 44 and 45. Reaction of sodium 1,2,4-tris(trimethylsilyl)cyclopentadienide, Na(Cp‴), with $TmI_2(THF)_3$ afforded the divalent thulium complex $(Cp‴)_2Tm(THF)$. Its crystal structure is similar to that of the previously described $(Cp^{ttt})_2Tm(THF)$ (Cp^{ttt} = 1,2,4-tris(*tert*-butyl)cyclopentadienyl). $(Cp‴)_2TmI$ was prepared by reaction of TmI_3 with K(Cp‴) and could be reduced by KC_8 to give a new unsolvated, homoleptic complex, $(Cp‴)_2Tm$, which was characterized by NMR. $(Cp‴)_2Tm$ gave $(Cp‴)_2Tm(THF)$ by interaction with THF (Scheme 44) [28].

A convenient alternative pathway to $(Cp^{ttt})_2Tm$ by reduction of $(Cp^{ttt})_2Tm(BH_4)$ with KC_8 was found: $(Cp^{ttt})_2Tm(BH_4)$ derives from $Tm(BH_4)_3(THF)_3$, which can be prepared from the less expensive $TmCl_3$ (Scheme 45). On the other hand, the dimer $[(Cp^{tt})_2TmI]_2$ (Cp^{tt} = 1,3-bis(*tert*-butyl)cyclopentadienyl), obtained by reaction of TmI_3 with $Na(Cp^{tt})$, gave only intractable results by reaction with KC_8 [28].

A reaction of $(Cp^{ttt})_2Tm$ with pyridine resulted in immediate reduction of pyridine into 1,1′-bis(1,4-dihydropyridylamide) and formation of the structurally characterized product $(\mu\text{-}NC_5H_5\text{-}C_5H_5N)[(Cp^{ttt})_2Tm]_2$ (Scheme 46) [28].

Reaction of the photoisomerizable dimethyldihydropyrene-fused cyclopentadiene HCpDHP with the divalent ytterbium silylamide precursor $Yb[N(SiMe_3)_2]_2(THF)_2$ afforded the bent ytterbium(II) metallocene $Yb(CpDHP)_2(THF)_2$ which was isolated in the form of dark red crystals. According to the X-ray diffraction analysis the complex adopts a highly distorted *pseudo*-tetrahedral bent metallocene structure (Fig. 6) [29].

2.5.2. $CpLnX_2$ compounds

Organometallic structures comprising (cyclopentadienyl)scandium units grafted on silsesquioxanes have been theoretically investigated as possible novel hydrogen storage materials. Using density functional theory it was shown that a recently synthesized silsesquioxane (SQ) nano-complex $[RSiO_{3/2}]_n$ with $R = -C_5H_5$ provides a novel material for hydrogen storage. Grafting cyclopentadienyl rings on SQ totally changes its electronic structure and chemistry: cyclopentadienyl becomes a reactive site where a transition metal atom (*e.g.*, Sc) can be doped to serve as an effective adsorption site for hydrogen molecules [30]. The insertion of an alkene into a metal–hydrogen (M–H) bond (or hydrogen migratory insertion) is a key elementary step in many important catalytic and stoichiometric processes, such as hydrogenation, hydroformylation, isomerization, and polymerization. Thus, the insertion of ethylene into a Y–H bond of the tetranuclear yttrium polyhydride complex $(\eta^5\text{-}C_5H_4SiH_3)_4Y_4H_8$, a model of $(\eta^5\text{-}C_5Me_4SiMe_3)_4Y_4H_8$, which possesses one μ_4-H, one μ_3-H, and six μ_2-H atoms, was computationally investigated by the method of two-layer ONIOM (B3LYP:HF). It was found that the enthalpy

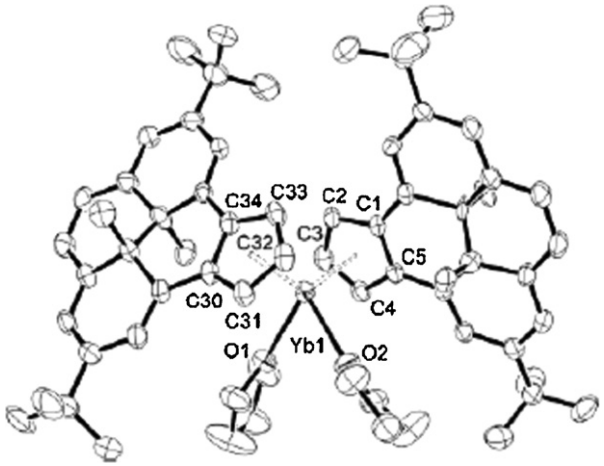

Fig. 6. Molecular structure of $Yb(CpDHP)_2(THF)_2$ [29].

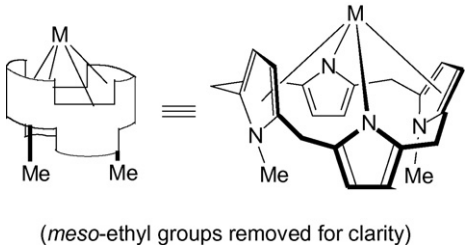

Scheme 47.

barrier for the μ_3-H migratory insertion (15.3 kcal mol^{-1}) is higher than that for μ_2-H migratory insertion (10.9 kcal mol^{-1}). Both μ_2-H and μ_3-H migratory insertion reactions lead to a structurally and hence energetically identical insertion product, in which the resulting ethyl group adopts a μ_2-bridging structure. These results suggested that the μ_2-H migratory insertion reaction pathway is kinetically preferable [31].

Reactions of $Cp_3Ln(THF)$ with 2,2′-ethylene-bis(4,6-di-*tert*-butylphenol) (=EDBP-H_2) in a 1:1 molar ratio in THF gave the mono(cyclopentadienyl) bis(phenolate) lanthanide complexes $CpLn(EDBP)(THF)_2$ (Ln = Nd, Sm, Yb) in nearly quantitative yields. The coordinated THF can be readily replaced by DME to give CpLn(EDBP)(DME). Further reaction of the $CpLn(EDBP)(THF)_2$ complexes with 1 equiv. of ^{i}PrOH afforded the neutral bis(phenolate) lanthanide isopropoxides $[(EDBP)Ln(\mu\text{-}O^iPr)(THF)_2]_2$ (Ln = Nd, Sm, Yb) in high yields [32]. A mono(cyclopentadienyl) samarium complex containing an $\eta^5{:}\eta^1{:}\eta^1{:}\eta^1$-bound modified porphyrinogen has been prepared as illustrated in Scheme 47 by treatment of the Sm(II) precursor with ^{t}BuCl, followed by reaction of the intermediate Sm(III) chloro complex with 1 equiv. of NaCp. The unique $\eta^5{:}\eta^1{:}\eta^1{:}\eta^1$ macrocyclic binding mode in this complex is a response to steric pressure which results in distortion of the macrocyclic ligand [33].

Treatment of the yttrium tris(alkyl) precursor $Y(CH_2SiMe_3)_3(THF)_2$ with equimolar $H(C_5Me_4)SiMe_3$ (=HCp′) afforded the mono(cyclopentadienyl) complex $Cp'Y(CH_2SiMe_3)_2(THF)$ *via* alkane elimination. A THF-free mono(alkyl) derivative was obtained upon subsequent treatment with a potentially tetradentate aminophenol ligand (Schemes 48 and 49) [34].

Half-sandwich dibenzyl complexes of scandium were prepared according to Scheme 50 by stepwise treatment of anhydrous scandium trichloride with lithium derivatives of silyl-functionalized tetramethylcyclopentadienes $(C_5Me_4H)SiMe_2R$ (R = Me, Ph) and benzyl magnesium chloride. The resulting complexes $(\eta^5\text{-}C_5Me_4SiMe_3)Sc(CH_2Ph)_2(THF)$ and $(\eta^5\text{-}C_5Me_4SiMe_2Ph)Sc(CH_2Ph)_2$(1,4-dioxane) show structures related to that of the corresponding bis(trimethylsilylmethyl)

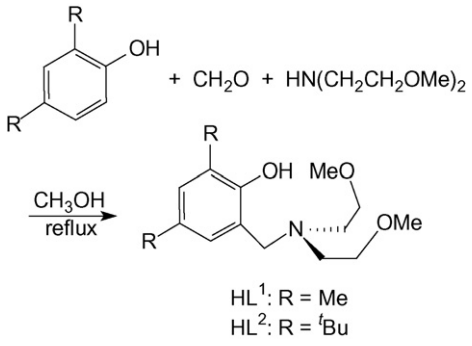

Scheme 48.

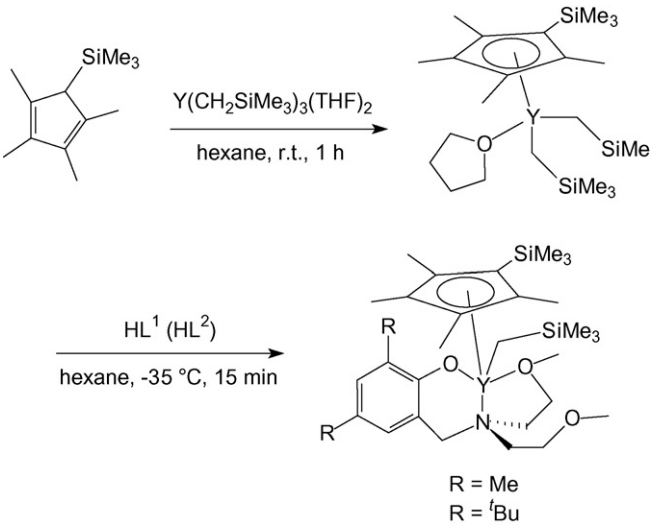

Scheme 49.

compounds $(\eta^5\text{-}C_5Me_4SiMe_2R)Sc(CH_2SiMe_3)_2(THF)$. The *pseudo*-tetrahedral complexes display η^1-coordinated benzyl ligands without significant interaction of the *ipso*-carbon of the phenyl moiety [35].

Subsequent conversion of $(\eta^5\text{-}C_5Me_4SiMe_3)Sc(CH_2Ph)_2(THF)$ into the cationic species by treatment with triphenylborane in THF led to the formation of a stable charge-separated complex $[(\eta^5\text{-}C_5Me_4SiMe_3)Sc(CH_2Ph)(THF)_x][BPh_3(CH_2Ph)]$ (Scheme 51) [35].

A series of scandium, lutetium, and yttrium complexes containing a tetramethylcyclopentadienyl ligand with a pendant furyl group, $[\eta^5\text{-}C_5Me_4SiMe_2(C_4H_2MeO\text{-}2)]Ln(CH_2SiMe_3)_2(THF)$ (Ln = Sc, Y, Lu; R = H, Me), were synthesized according to Scheme 52 and structurally characterized. Single-crystal X-ray diffraction studies of the scandium complexes $[\eta^5\text{-}C_5Me_4SiMe_2(C_4H_2MeO\text{-}2)]Sc(CH_2SiMe_3)_2(THF)$ (R = H, Me) revealed a *pseudo*-four-coordinate metal center without additional coordination of the furyl group. The previously elusive lutetium complex $[\eta^5\text{-}C_5Me_4SiMe_2(C_4H_2MeO\text{-}2)]Lu(CH_2SiMe_3)_2(THF)$ could be isolated and exhibited structural features analogous to those of the scandium compound [36].

Variable-temperature ^{1}H NMR spectroscopic studies of the entire series confirmed the labile nature of both the THF ligands and furyl donor in solution. Rates for a subsequent ring-opening reaction (Scheme 53), triggered by intramolecular C-H bond activation, were shown to depend primarily on the metal size. The ring-opening reaction resulted in the formation of the corresponding dinuclear yne-enolate complexes $[Ln\{\eta^5{:}\eta^1\text{-}C_5Me_4SiMe_2(C{\equiv}CCH{=}CRO)\}(CH_2SiMe_3)]_2$ (Ln = Sc, Y, Lu; R = H, Me). Substitution at the 5-furyl position did not markedly influence the rate of the ring-opening reaction but shifted the position of the monomer–dimer equilibrium toward the monomer. Only a large excess of THF allowed the observation of monomeric yne-enolate complexes such as $[Y\{\eta^5{:}\eta^1\text{-}C_5Me_4SiMe_2(C{\equiv}CCH{=}CHO)\}(CH_2SiMe_3)(THF)_2]$ (Scheme 53), which was characterized by X-ray crystallography [36].

In a related paper the synthesis and full characterizaion of a series of silylene-linked half-sandwich rare-earth metal complexes has been reported. Reaction of $Ln(CH_2SiMe_3)_3(THF)_2$ (Ln = Y, Yb, Lu) with 1 equiv. of $Me_2Si(C_5Me_4H)NHR'$ (R′ = Ph, 2,4,6-$Me_3C_6H_2$, ^{t}Bu) according to Scheme 54 afforded straightforwardly the corresponding half-sandwich rare-earth metal alkyl complexes $[Me_2Si(NR')]Ln(CH_2SiMe_3)(THF)_n$ (Ln = Y, R′ = Ph, n = 2; Ln = Y, R′ = $C_6H_2Me_3$-2,4,6, n = 1; Ln = Y, R′ = ^{t}Bu, n = 1; Ln = Yb, R′ = Ph, n = 2; Ln = Lu, R′ = Ph, n = 2) in high yields. These complexes, espe-

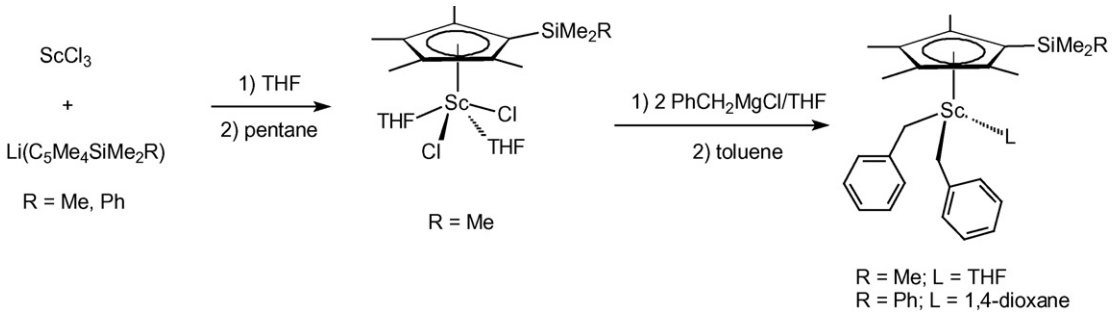

Scheme 50.

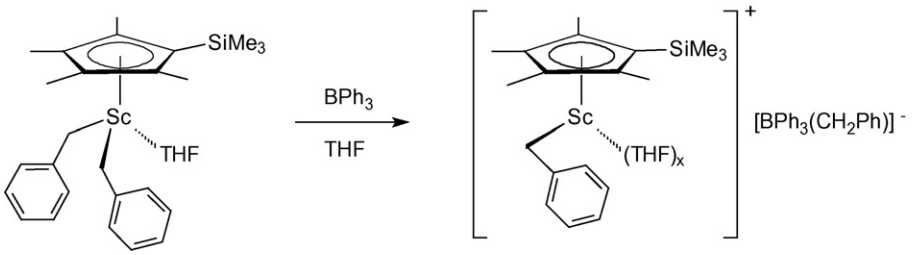

Scheme 51.

cially the yttrium complexes, were found to be excellent catalyst precursors for the catalytic addition of various primary and secondary amines to carbodiimides (*cf.* Section 2.11) [37].

A mono(cyclopentadienyl) ytterbium(III) complex containing a chiral bridged aminotroponiminate ligand was prepared according to Scheme 55 (orange crystals, 67% yield) and structurally characterized by X-ray diffraction [38].

Exciting transformations have been developed around a new class of polynuclear rare-earth polyhydrido complexes. The unique reactivity of these clusters includes the hydrogenation of carbon monoxide leading to selective formation of ethylene and structurally characterizable polyoxo and oxo/hydrido rare earth metal clusters. The reactions of yttrium and lutetium polyhydrido complexes with carbon monoxide are summarized in Scheme 56 [39].

The hydrogenation of carbon monoxide by the tetranuclear rare earth metal polyhydrido complexes resulted in unprecedented selective formation of ethylene under mild conditions. This reaction also afforded a new series of well-defined novel polymetallic rare earth metal complexes, such as a hexahydrido/oxymethylene complex, a tetrahydrido/dioxo complex, and a tetraoxo cubane complex (Scheme 56), and might shed new light on the mechanistic aspects of the Fischer–Tropsch process [39]. Unprecedented cationic hydride complexes have been prepared by treatment of the polyhydrido clusters with $[Ph_3C][B(C_6F_5)_4]$ as illustrated in Scheme 57. These cationic polyhydrido complexes not only are the first cationic rare-earth hydride complexes but also show excellent regio- and stereoselectivity for the polymerization of 1,3-cyclohexadiene (=CHD) (*cf.* Section 2.11.1) [40].

For comparison, the reaction of a neutral polyhydrido complex with CHD was also examined. It gave selectively a single CHD insertion product in a quantitative yield (Scheme 58). The overall structure of the Y_4 frame in the product is similar to that of the starting material. The resultant cyclohexenyl ligand adopts an allylic form, which bridges two Y atoms through the two terminal

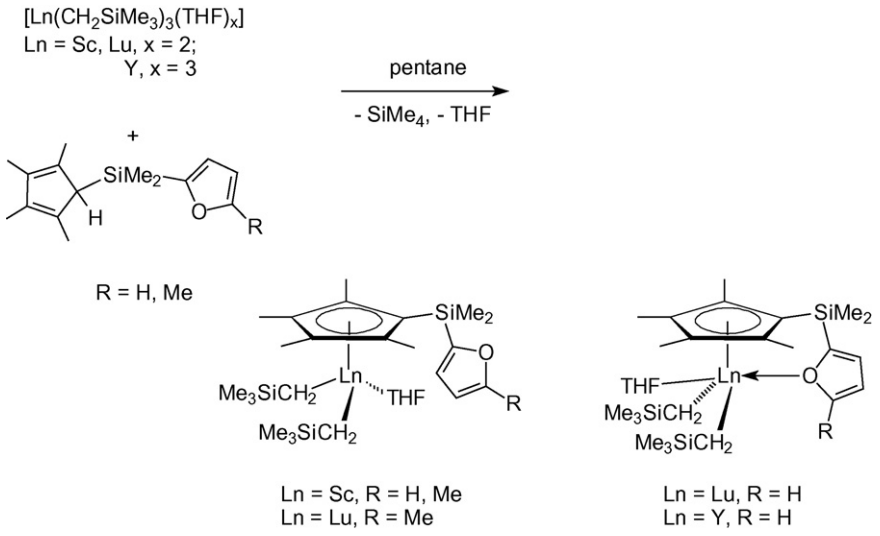

Scheme 52.

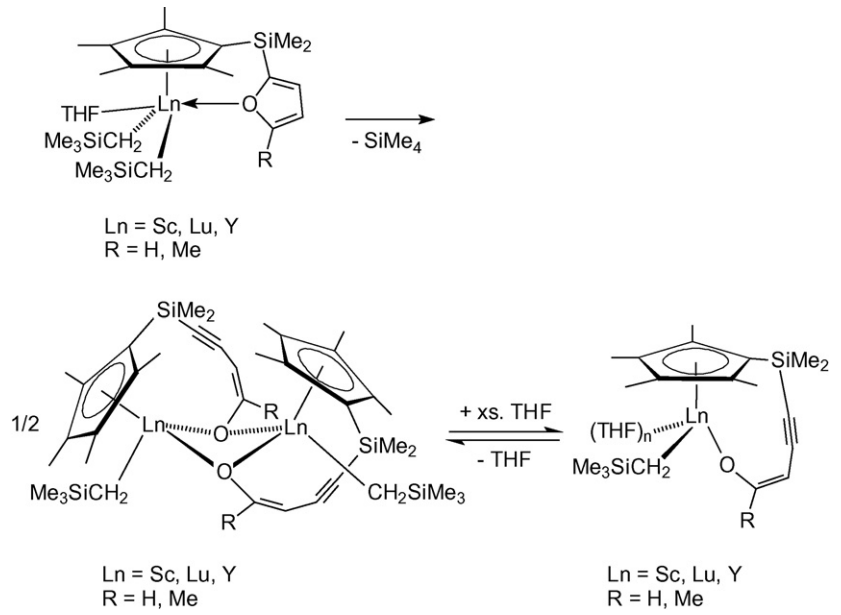

Scheme 53.

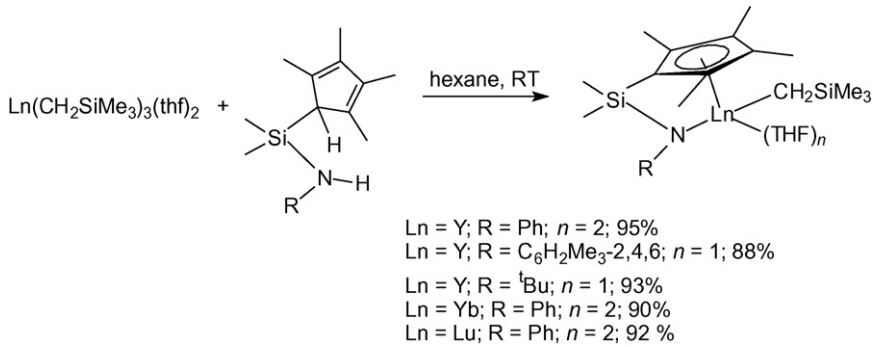

Scheme 54.

carbon atoms of the allyl moiety, each bonding to one metal center in an η^1 fashion (Fig. 7). The $\{Y_4H_7\}$ core has one μ_4-H, two μ_3-H, and four μ_2-H ligands [40].

2.5.3. Cp_2LnX compounds

The cation size dependent reactivity of lanthanide trihalides with the bulky alkylcyclopentadienyl anions tri-*tert*-butylcyclopentadienide (Cp′ = 1,2,4-^{t}Bu$_3$C$_5$H$_2$) and tetraisopropylcyclopentadienide (^{4}Cp = ^{i}Pr$_4$C$_5$H) was investigated. As illustrated in Scheme 59, reactions of $NdCl_3$ or $PrCl_3$ with 2 equiv. of NaCp′ afforded base- and salt-free Cp′$_2$NdCl and Cp′$_2$PrCl in good yields. Trimethylaluminum adds to the neodymium complex to form Cp′$_2$Nd(μ-Cl)AlMe$_3$. With $LaCl_3$ or $CeCl_3$ base-free bis(cyclopentadienyl) complexes were not obtained, but in the latter case the "ate" complex [^{4}Cp$_2$Ce(μ-Cl)$_2$Na(TMEDA)]$_\infty$ could be extracted from the product mixture with tetramethylethylenediamine (=TMEDA) and crystallized as a zigzag chain polymer. The corresponding samarium derivative ^{4}Cp$_2$Sm(μ-Cl)$_2$Na(DME)$_2$ retained the coordinated sodium chloride even when dissolved in non-polar solvents [41].

An attempted preparation of Cp′$_2$YbCl gave the mono(cyclopentadienyl) complex [Cp′YbCl(μ-OCH$_2$CH$_2$OMe)]$_2$ resulting from cleavage of the dimethoxyethane solvent, and with lutetium trichloride the hexanuclear complex (^{4}CpLu)$_5$LuCl$_{13}$(OEt$_2$)$_5$ was prepared in low yield (Scheme 60). The molecular structure of this unusual cluster is depicted in Fig. 8. Mono(cyclopentadienyl) complexes are also readily available from the trichlorides of thulium, ytterbium, and lutetium. Apart

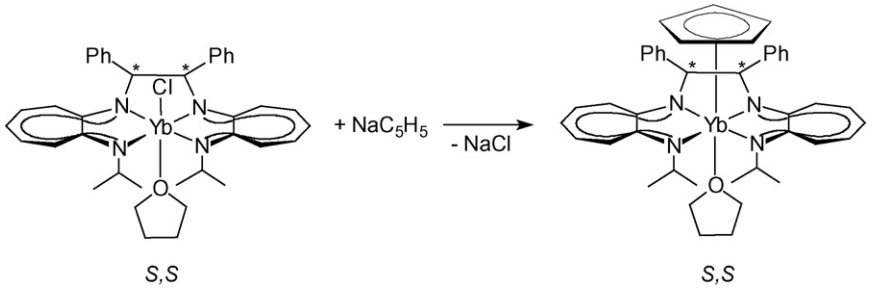

S,S S,S

Scheme 55.

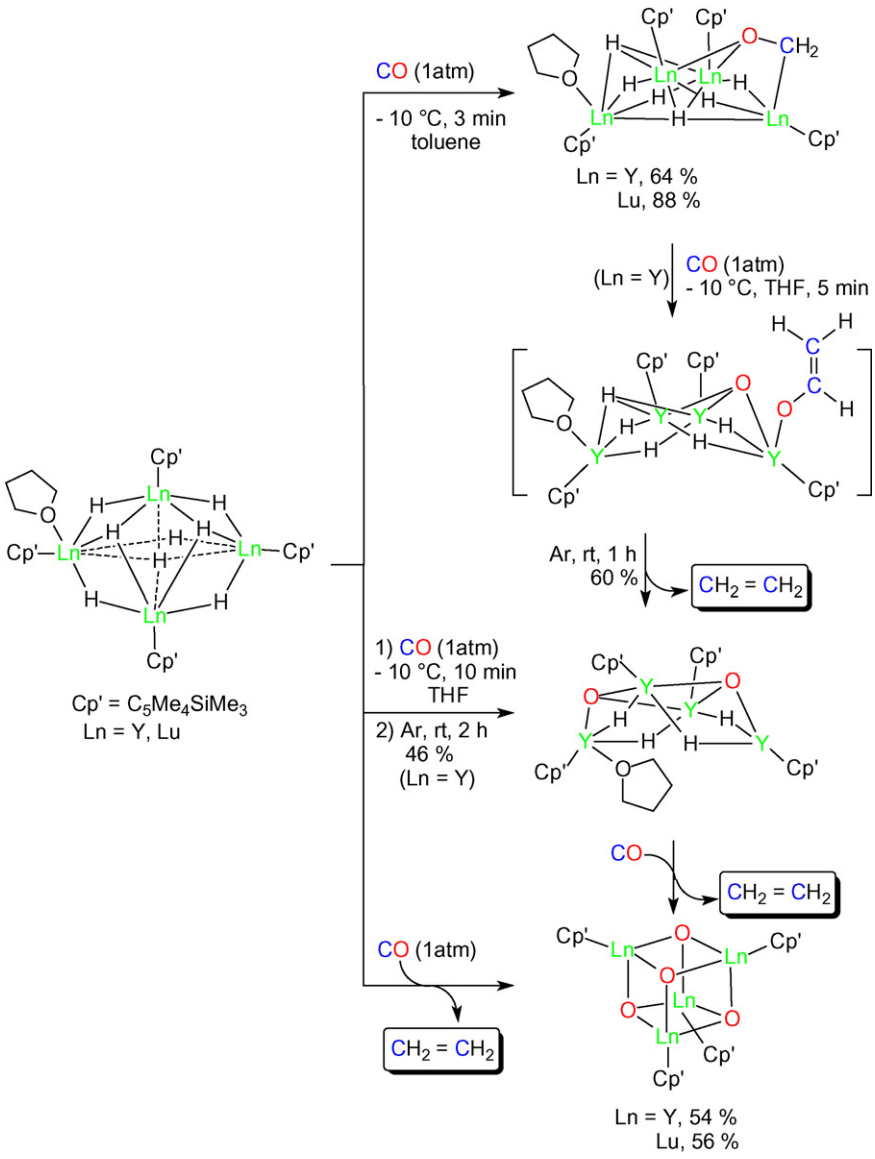

Scheme 56.

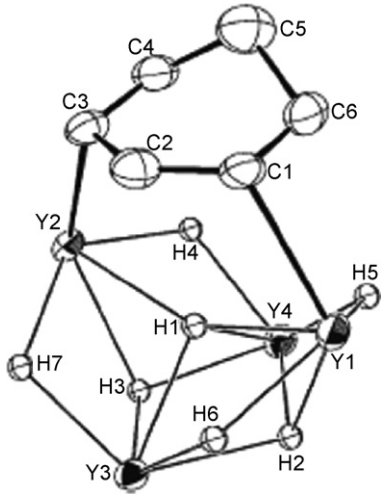

Fig. 7. ORTEP drawing of the cluster core in the CHD insertion product [40].

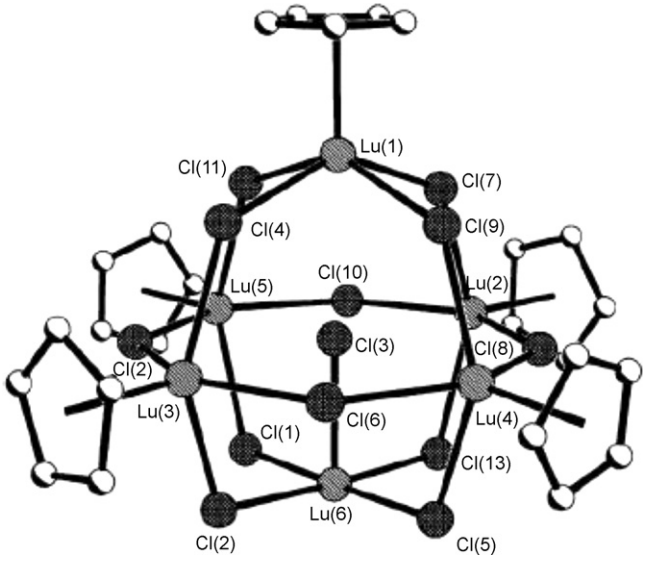

Fig. 8. Molecular structure of $(^4CpLu)_5LuCl_{13}(OEt_2)_5$ [41].

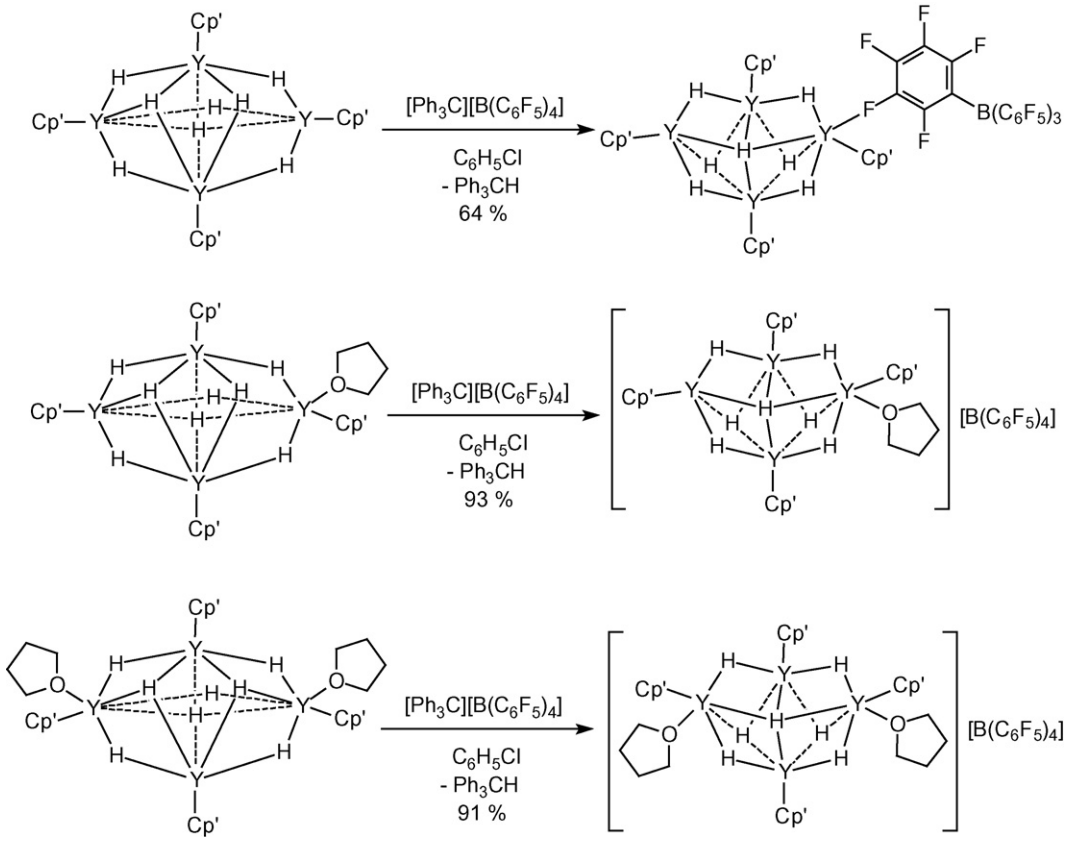

Scheme 57.

from the donor solvent adducts ^{4}CpTmCl$_2$(DME), Cp′YbCl$_2$(THF)$_2$, and ^{4}CpLuCl$_2$(DME), which were isolated from solutions in the corresponding donor solvent, the salt- and donor-free dihalides [Cp′TmCl$_2$]$_n$ and [Cp′YbCl$_2$]$_n$ were obtained as oligomers from pentane or petroleum ether extracts. The thulium compound gave Cp′Tm[N(SiMe$_3$)$_2$]$_2$ upon treatment with 2 equiv. of NaN(SiMe$_3$)$_2$, and the ytterbium complex underwent cyclopentadienyl ring exchange with lithium *tert*-butylcyclopentadienide and formation of [(^{t}BuC$_5$H$_4$)$_2$Yb(μ-Cl)]$_2$ (Scheme 60) [41].

For lanthanum and thulium use of the triiodide as a starting compound enabled synthesis of the corresponding (^{4}CpLu)$_2$LnI (Scheme 61). Cp′$_2$LaI was also prepared from LaI$_3$. (^{4}CpLu)$_2$TmI shows a unique conformation with two isopropyl neighbors rotated towards each other indicating extreme steric congestion (Fig. 9). Oxidation of Cp′$_2$Sm with copper(I) iodide gave Cp′$_2$SmI in high yield [41].

Reactions of the monomeric organocerium(III) hydride complex (1,2,4-^{t}Bu$_3$C$_5$H$_2$]$_2$CeH with CO and H$_2$ were studied by experimental and computational methods. Scheme 62 summarizes the reaction pathways discovered in this system. Addition of CO to (1,2,4-^{t}Bu$_3$C$_5$H$_2$]$_2$CeH (=Cp′CeH) in toluene yields *cis*-(μ-OCHCHO)(Cp′$_2$Ce)$_2$, in which the *cis*-enediolate group bridges the two metallocene fragments. The *cis*-enediolate quantitatively isomerizes intramolecularly to the *trans*-enediolate in C$_6$D$_6$ at 100 °C over a period of 7 months. Both the *cis*- and *trans*-enediolates react with Me$_3$SiN$_3$ to give Cp′$_2$CeN$_3$. When the solvent in the reaction of Cp′$_2$CeH with CO is pentane, Cp′$_2$Ce(OCH$_2$)CeCp′$_2$ forms, in which the oxomethylene group or the formaldehyde dianion bridges the two metallocene fragments. The bridging oxomethylene complex reacts with H$_2$, but not with CH$_4$, to give Cp′$_2$OMe, which is also the product of the reaction between Cp′$_2$CeH and a mixture of CO and H$_2$. The oxomethylene complex reacts with CO to afford the *cis*-enediolate complex. X-ray crystal structure determinations were carried out on the oxomethylene complex and the two enediolate complexes. Fig. 10 displays the molecular structures of the latter [42].

Facile insertion of CO$_2$ into tetramethylcyclopentadienyl lanthanide moieties to form (C$_5$Me$_4$HCO$_2$]$^-$ carboxylate ligands has been studied in detail. These efforts to extend the reduction chemistry of LnZ$_3$/M and LnZ$_2$Z′/M (Z = C$_5$Me$_4$H; Z′ = BPh$_4$, Cl; M = alkali metal) to substrates beyond N$_2$ have identified unexpectedly facile insertion of CO$_2$ into lanthanide cyclopentadienyl linkages

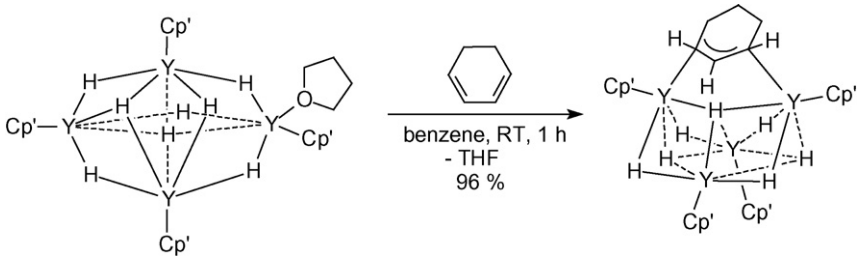

Scheme 58.

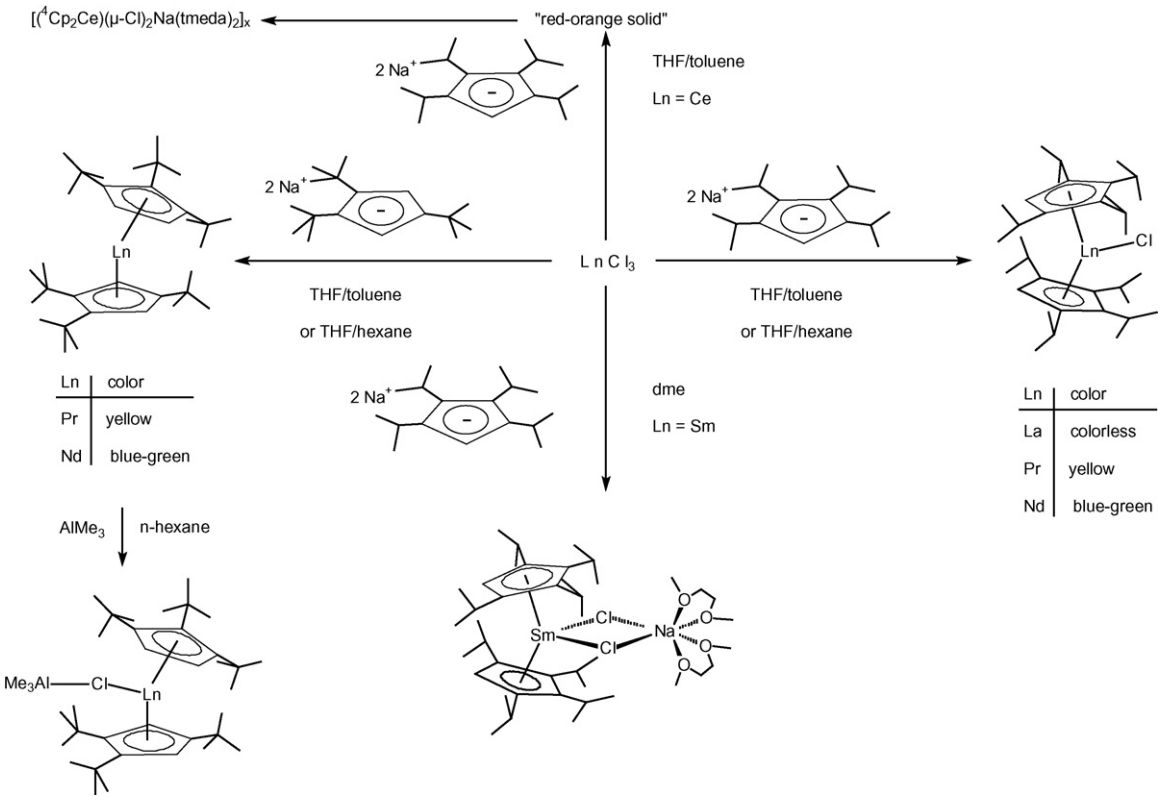

Scheme 59.

to make carboxylate ligands. The insertion was initially identified in $[(C_5Me_4H)La(THF)]_3(\mu\text{-}\eta^1\text{:}\eta^1\text{-}O_2CC_5Me_4H)_3(\mu_3\text{-}\eta^2\text{:}\eta^2\text{-}CO_3)(\mu_3\text{-}Cl)$ (Fig. 11), a product of a $(C_5Me_4H)_3La/Na/CO_2$ reaction in the presence of chloride. In this case, both insertion and reduction of CO_2 to carbonate was observed [43].

CO_2 insertion also occurs in the absence of an alkali metal when the tris(tetramethylcyclopentadienyl)lanthanides complexes were used as starting materials. Hence, the $(C_5Me_4H)_3Ln$ complexes (Ln = La, Nd, Sm, Gd) react with CO_2 to form mixtures of tetramethylcyclopentadienyl carboxylate products. In the La complex, single crystals of $[\{(C_5Me_4H)_2La\}(\mu\text{-}\eta^1\text{:}\eta^1\text{-}O_2CC_5Me_4H)]_2$, could be isolated and structurally characterized (Fig. 12) [43].

Crystallographic characterization of a rare example of a tetramethylcyclopentadienyl lanthanide "*ate*" salt, $[(\mu\text{-}C_5Me_4H)(C_5Me_4H)LaCl(\mu\text{-}Cl)K(18\text{-crown-}6)]_n$, was also obtained as part of this study and found to have a chain structure in the solid

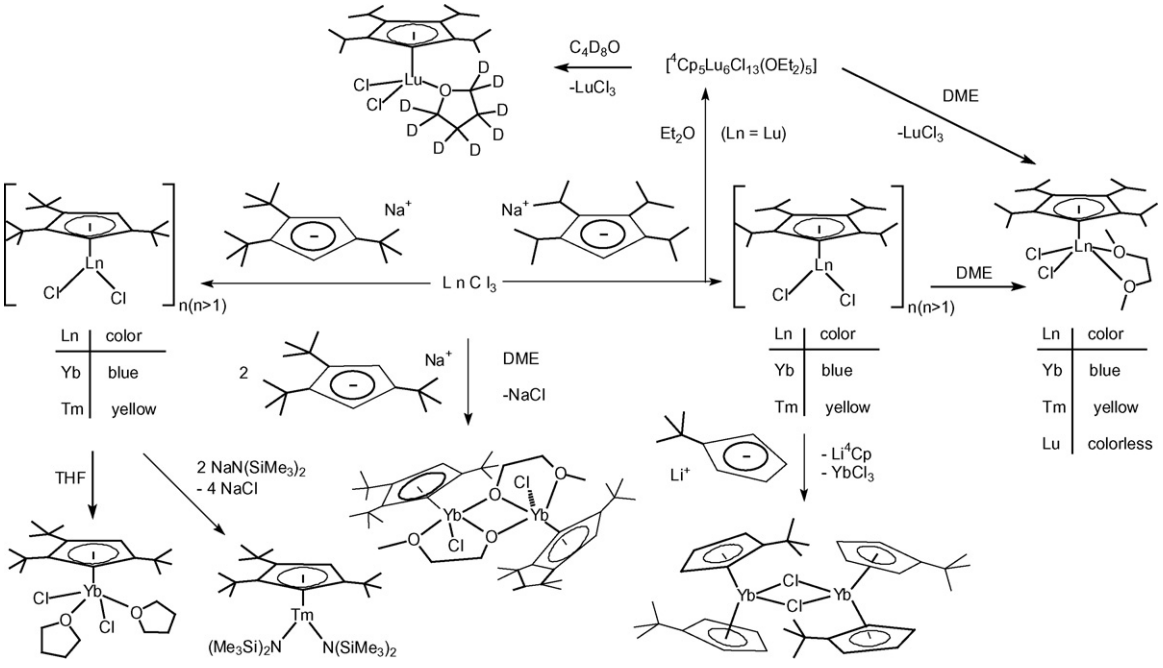

Scheme 60.

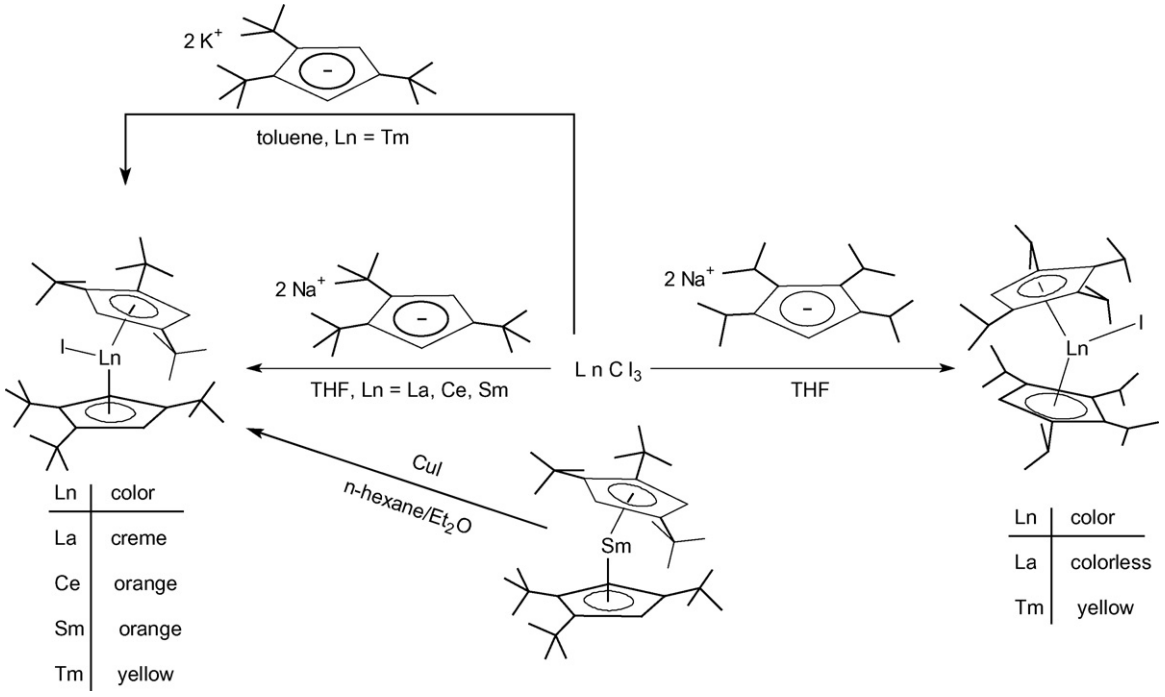

Scheme 61.

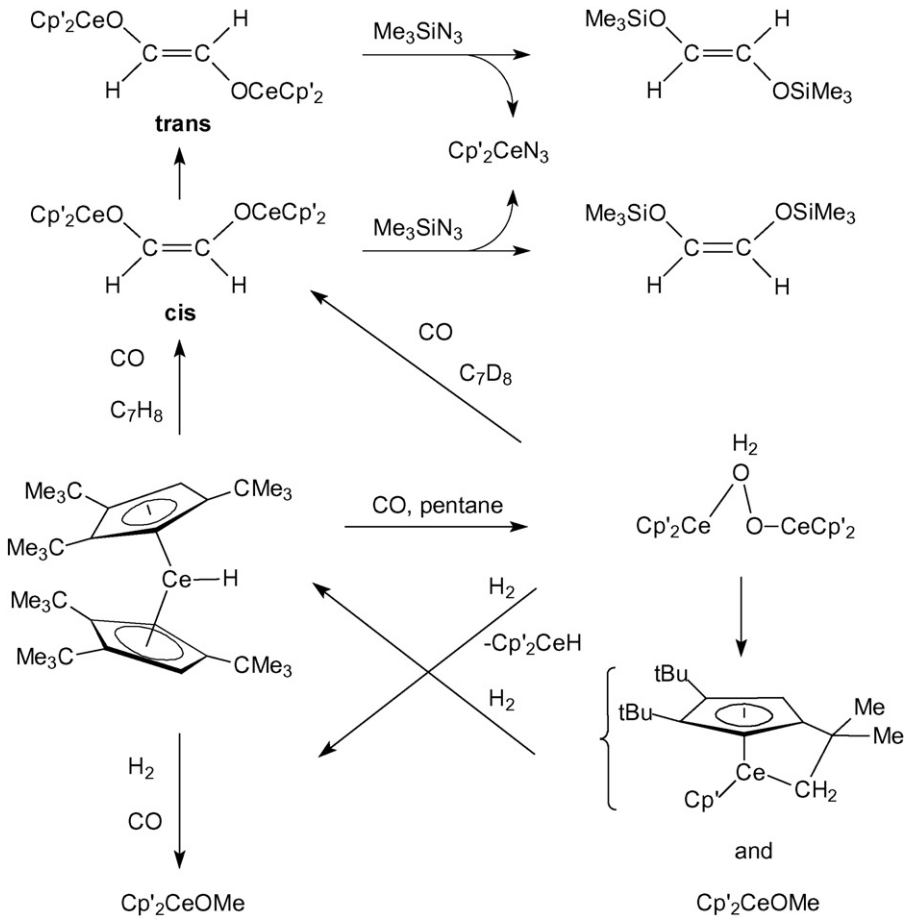

Scheme 62.

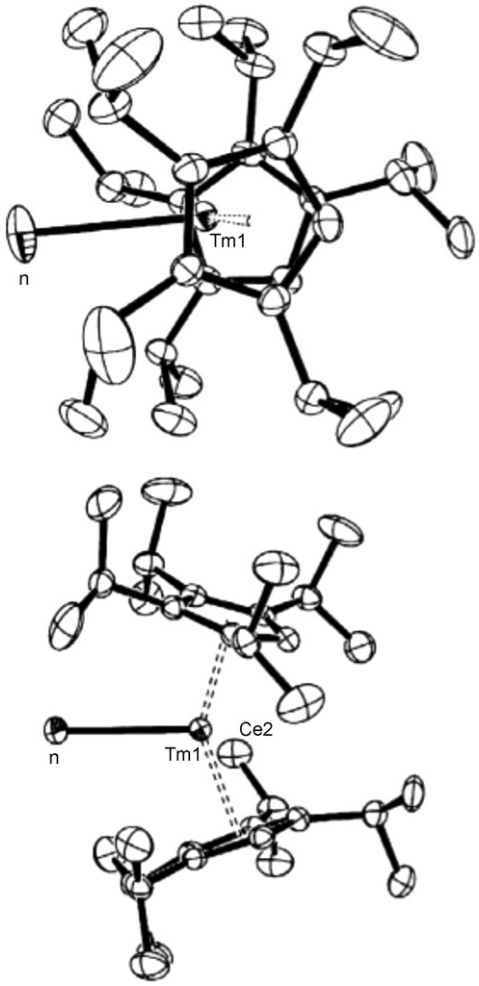

Fig. 9. Two different views of the molecular structure of $(^4CpLu)_2TmI$ [41].

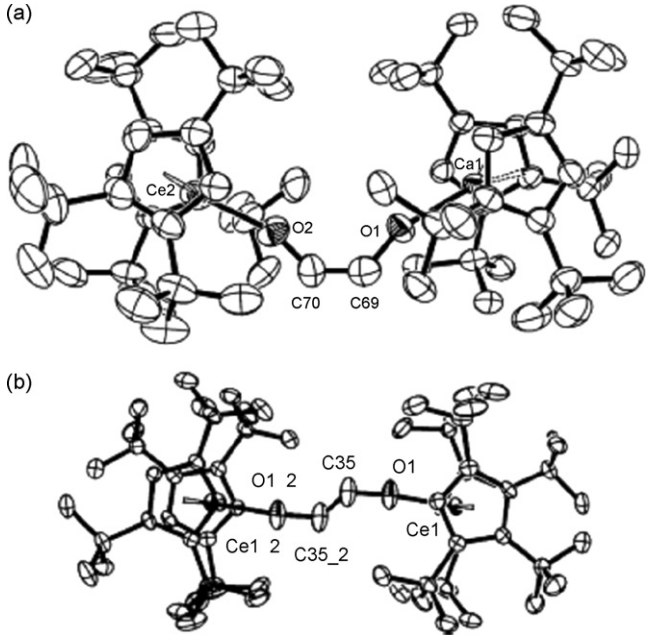

Fig. 10. Molecular structures of (a) *cis*-(μ-OCHCHO)(Cp′$_2$Ce)$_2$ and (b) *trans*-(μ-OCHCHO)(Cp′$_2$Ce)$_2$ [42].

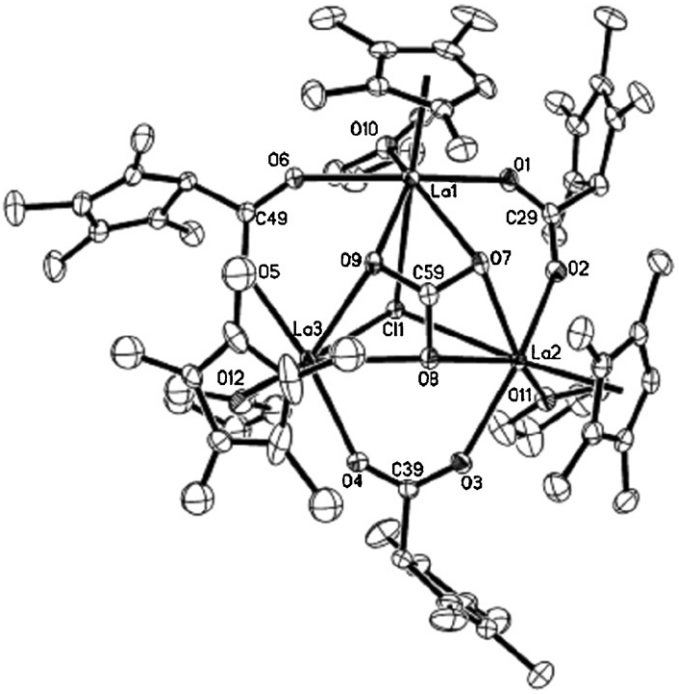

Fig. 11. Molecular structure of [(C$_5$Me$_4$H)La(THF)]$_3$(μ-η^1:η^1-O$_2$CC$_5$Me$_4$H)$_3$(μ_3-η^2:η^2:η^2-CO$_3$)(μ_3-Cl) [43].

state involving bridging methyl groups as well as bridging chloride ligands (Fig. 13) [43].

A series of (+)-neomenthyl and (−)-phenylmenthyl-substituted bis(cyclopentadienyl) lanthanide complexes was prepared and investigated as catalysts in asymmetric hydroamination/cyclization of aminoalkenes (*cf.* Section 2.11.3). As shown in Scheme 63, the chiral, terpenoid-substituted yttrocene (η^5-neomenthylCp)$_2$Y(*o*-C$_6$H$_4$CH$_2$NMe$_2$) can be prepared *via* facile arene elimination starting from Y(*o*-C$_6$H$_4$CH$_2$NMe$_2$)$_3$. The compound retains a C_1-symmetric structure in solution on the NMR time scale, due to tight binding of the amine donor [44].

The related (−)-phenylmenthyl-substituted complexes (η^5-(−)-phenylmenthylCp)$_2$Y(μ-Cl)$_2$Li(OEt$_2$)$_2$ and (η^5-(−)-phenylmenthylCp)$_2$YN(SiMe$_3$)$_2$ were prepared *via* salt metathesis reactions (Scheme 64) [44].

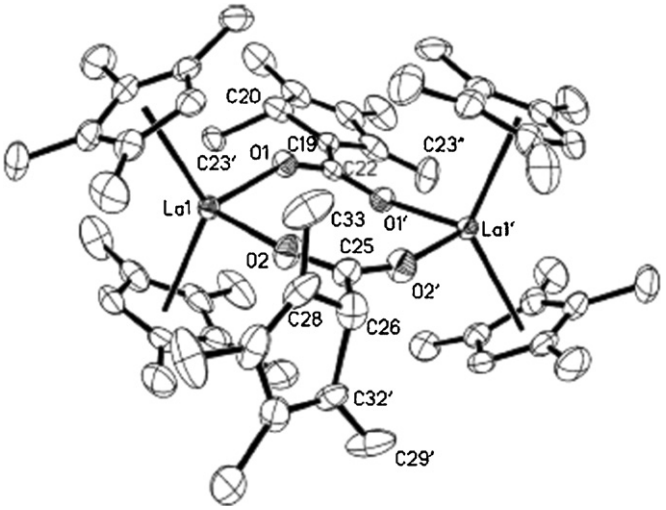

Fig. 12. Molecular structure of [{(C$_5$Me$_4$H)$_2$La}(μ-η^1:η^1-O$_2$CC$_5$Me$_4$H)]$_2$ [43].

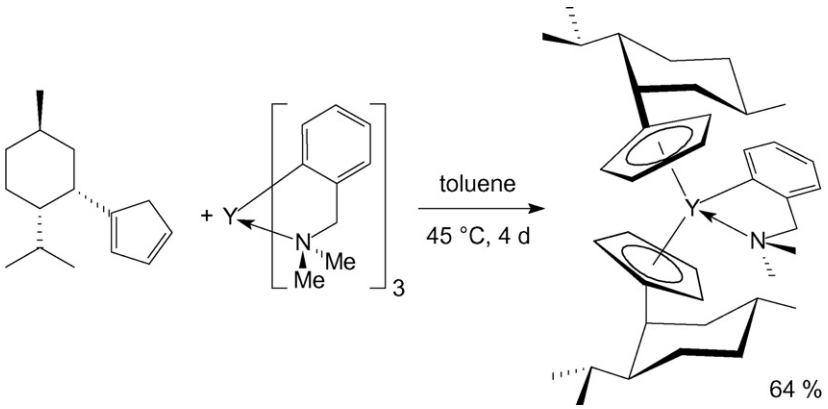

Scheme 63.

Treatment of $(C_5H_4SiMe_2{}^tBu)_2LnR$ with 1 equiv. of elemental sulfur in toluene at ambient temperature afforded the dimeric thiolate-bridged complexes $[(C_5H_4SiMe_2{}^tBu)_2Ln(\mu\text{-}SR)]_2$ (R = Me, Ln = Yb, Er, Dy, Y; R = ^{n}Bu, Ln = Yb, Dy] (Scheme 65). All these complexes were characterized by elemental analysis, IR and mass spectrometry. The structures of four complexes were also determined through single-crystal X-ray diffraction analysis, indicating that only one sulfur atom from elemental sulfur inserts into the Ln–C σ-bond [45].

The facile construction of novel organolanthanide square-planar macrocycles through addition of carbodiimide to an amino group has been achieved. In this study, the reactivity of lanthanocene derivatives containing the *p*-aminothiophenolate ligand towards carbodiimides was examined. Reaction of $Cp_2Ln(p\text{-}SC_6H_4NH_2)(THF)$ with RN=C=NR in THF at room temperature gave four novel organolanthanide guanidinate complexes $[Cp_2Ln(p\text{-}SC_6H_4N(H)C(NHR)=NR)]_4$ (R = *i*Pr, Ln = Yb, Er; R = Cy, Ln = Yb, Er), formed by the addition of the C=N double bonds of the carbodiimide molecule to the amino group in the *para*-position (Scheme 66). Their unique square-planar macrocycle structures were determined through X-ray single-crystal diffraction analyses (Fig. 14). This result provided a potentially useful method for the construction of organolanthanide macrocycles [46].

In a related study several bis(cyclopentadienyl)ytterbium(III) complexes containing di- or trianionic diguanidinate ligands were synthesized and structurally characterized. The synthetic routes are summarized in Scheme 67 [47].

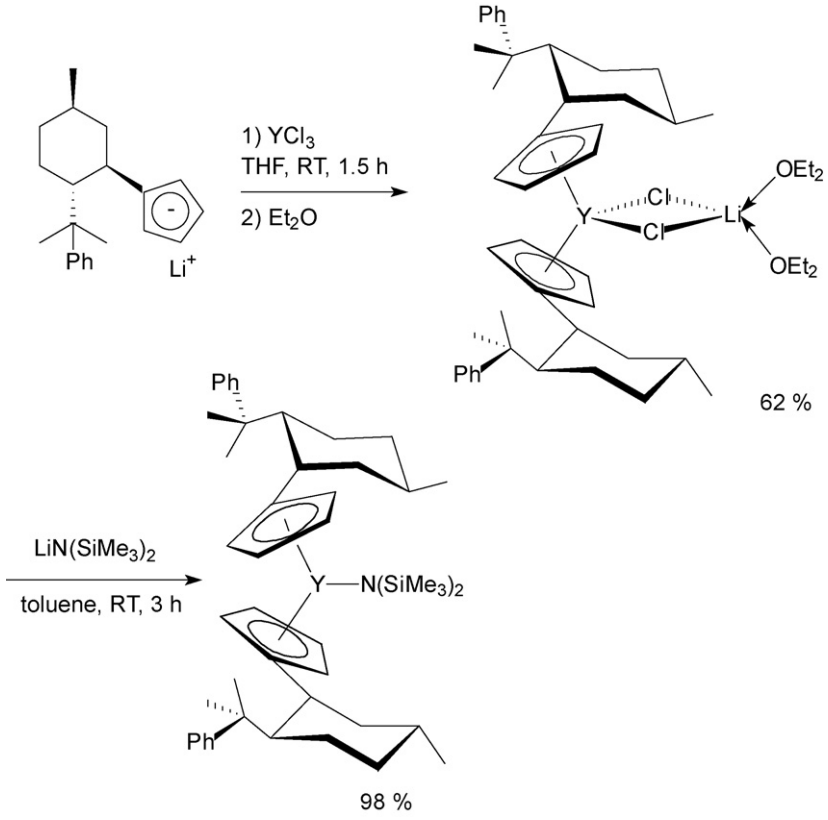

Scheme 64.

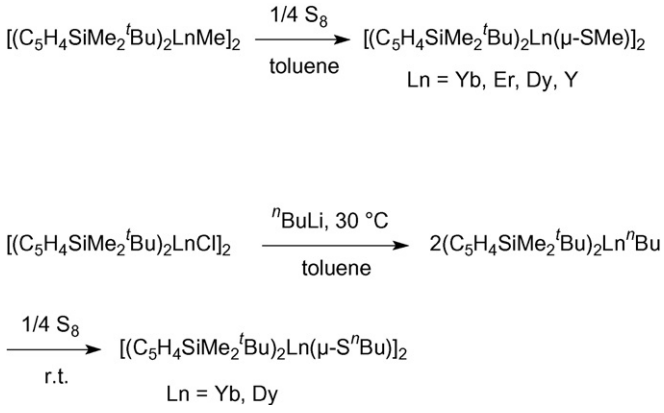

Scheme 65.

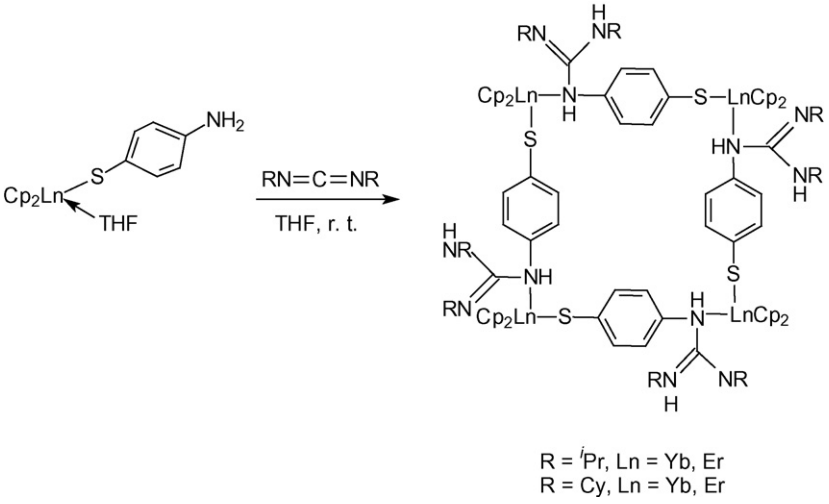

Scheme 66.

Closely related 1,3- and 1,4-diamido ytterbium complexes comprising a phenyl group as spacer unit have been prepared as illustrated in Scheme 68. In contrast to the pyridyl-bridged bis(guanidinate monoanion) complexes shown in Scheme 67, the aryl-bridged bis(guanidinate monoanion) complexes are stable even with prolonged heating at 110 °C. These results not only demonstrate that the presence of the pyridyl bridge can impart the diamido complexes with a unique reactivity and initiate unexpected reaction sequences but also indicate evidently that the number and distribution of negative charges of the diguanidinate ligand is tunable from double monoanionic units to mixed neutral/dianionic isomers [48].

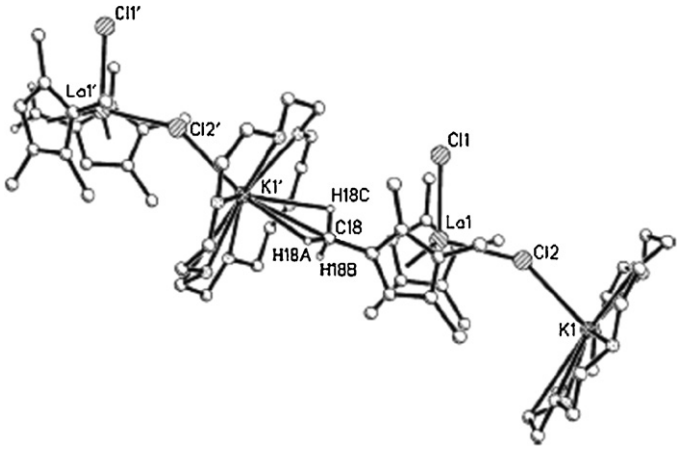

Fig. 13. Ball-and-stick representation of the polymer chain of [(μ-C_5Me_4H)(C_5Me_4H)LaCl(μ-Cl)K(18-crown-6)]$_n$ [43].

A closely related dinuclear bis(guanidinate) ytterbium complex containing a fluorenyl bridging unit was synthesized by the reaction sequence shown in Scheme 69 [48].

The same multiple N–H bond activation chemistry has also been extended to a series of new functionalized amido complexes of ytterbium, [Cp_2YbNHR]$_2$ (R = 8-quinolyl (Qu), 2-pyridyl (Py), 2-aminophenyl, 3-amino-2-pyridyl, and $Cp_2Yb[NHC_6H_4(CH_2NH_2)]$, which were synthesized by metathesis of Cp_2YbCl and the corresponding amido lithium salts (Scheme 70). All compounds shown in Scheme 70 were isolated as orange to red crystalline solids [49].

The reactivity of these amido complexes toward carbodiimides has been investigated in an analogous manner (Scheme 71) [49].

The syntheses and structures of a series of new lanthanide complexes supported by a chelating diamide ligand *N*,*N*′-bis(trimethylsilyl)-*o*-phenylenediamine have been described. As shown in Scheme 72, anhydrous $LnCl_3$ reacts with $Li_2[o\text{-}(Me_3SiN)_2C_6H_4]$, followed by treatment of NaC_5H_4Me in a 1:1:2 molar ratio to afford the corresponding anionic complexes $[Li(DME)_3][\{o\text{-}(Me_3SiN)_2C_6H_4\}Ln(MeC_5H_4)_2]$ (Ln = Nd, Sm, Yb) in high yield. The complexes were characterized by elemental analysis, IR and ^{1}H NMR. The molecular structures of the samarium and ytterbium derivatives were further determined by X-ray diffraction

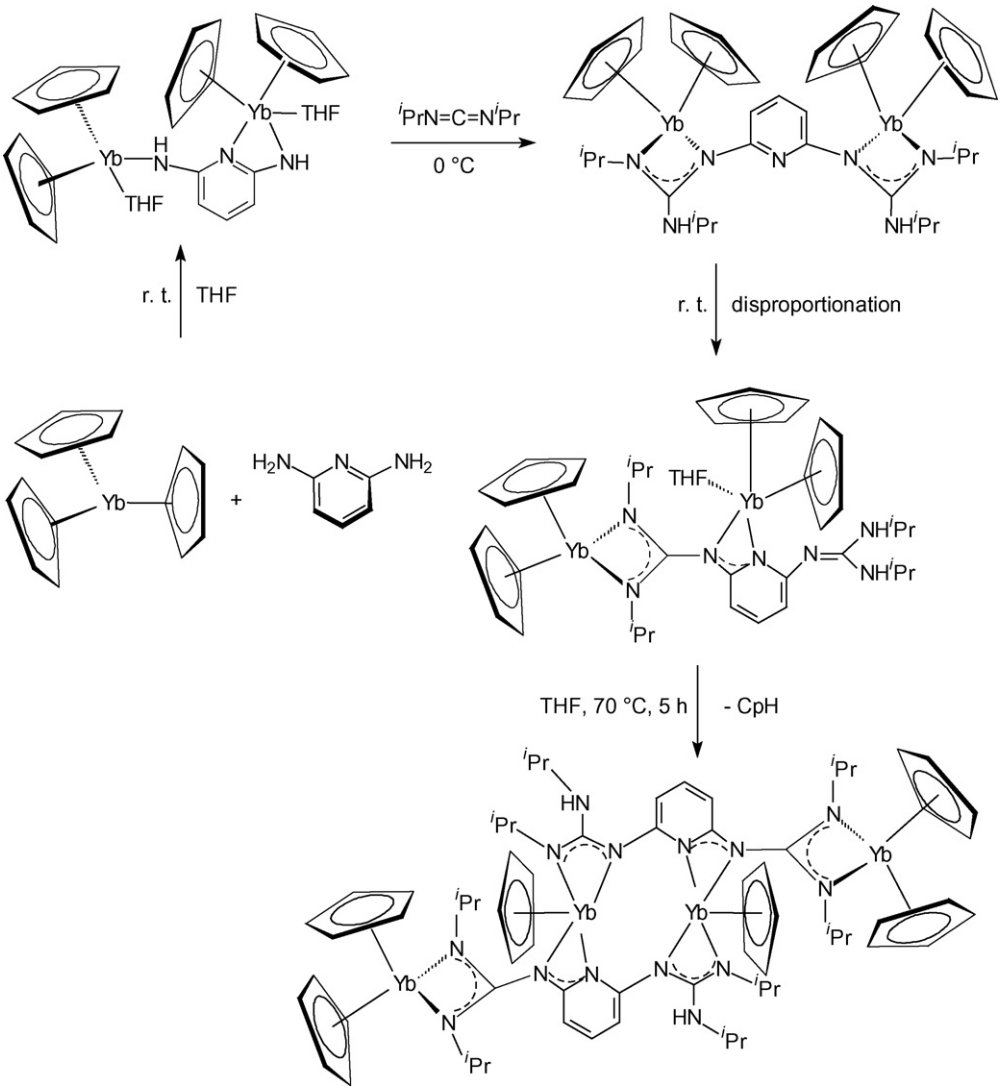

Scheme 67.

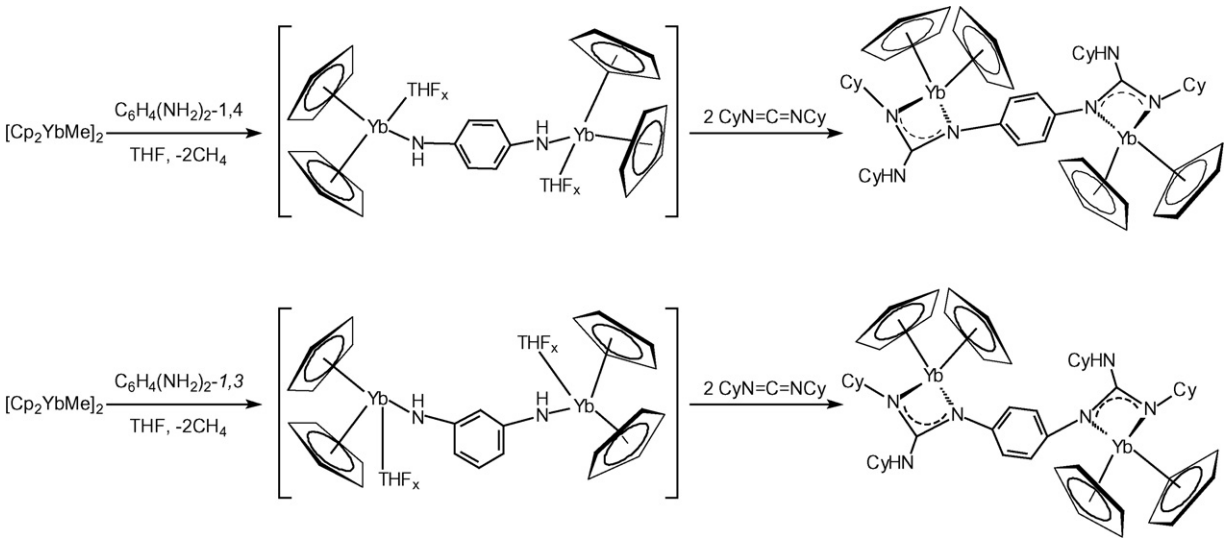

Scheme 68.

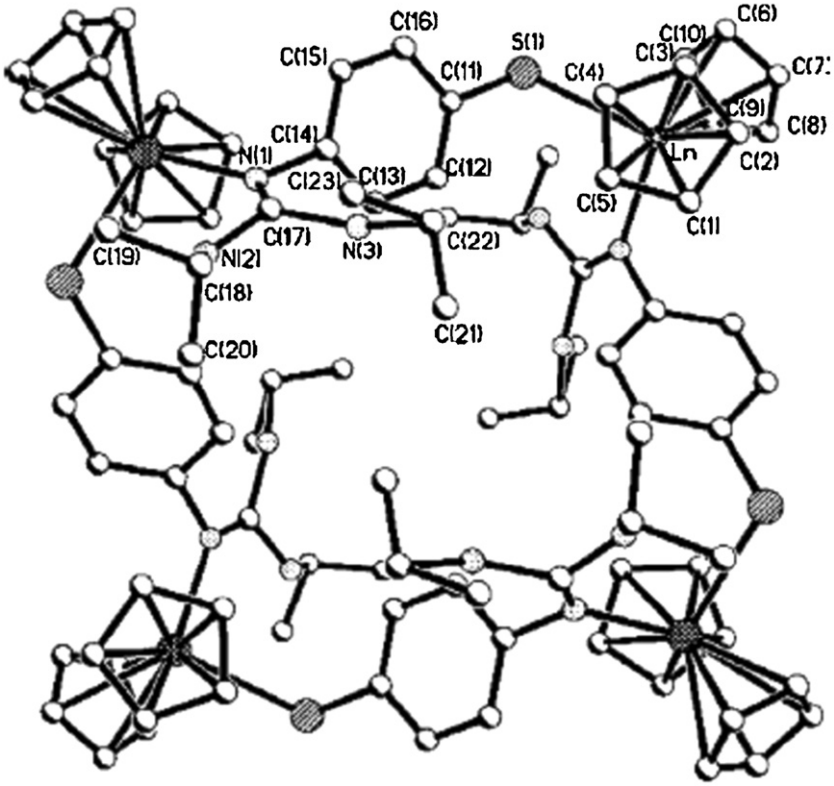

Fig. 14. Molecular structure of the macrocycles with R = Cy and Ln = Er, Yb [46].

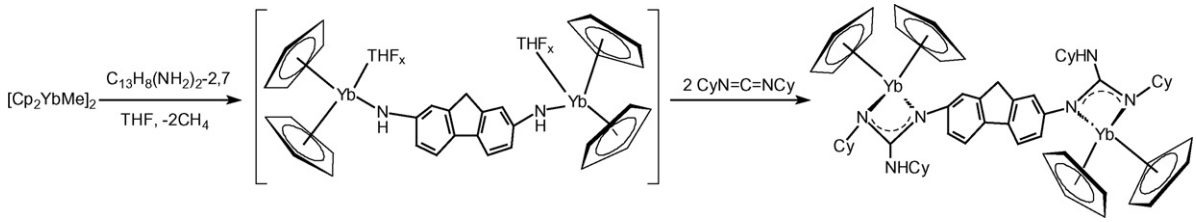

Scheme 69.

techniques to be ion-pair complexes composed of the anion [{*o*-$(Me_3SiN)_2C_6H_4$}$Ln(MeC_5H_4)_2]^-$ and the cation $[Li(DME)_3]^+$ [50].

The THF adduct of dimethylytterbocene, $(C_5H_4Me)_2Yb(THF)_2$ reacts with the diazabutadiene 2,6-$^iPr_2C_6H_3$–N=CH–CH=N–$C_6H_3{}^iPr_2$-2,6 (=DAD) as a one-electron reductant to afford a bis(cyclopentadienyl) Yb^{III} derivative containing a DAD radical anion $(C_5H_4Me)_2Yb(DAD^{\bullet -})$ (wine-red crystals, 61% yield) as illustrated in Scheme 73 [51].

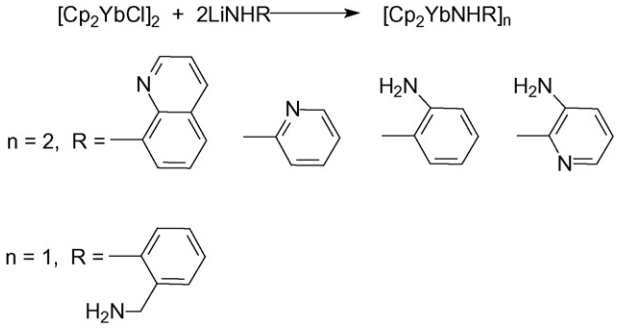

Scheme 70.

2.5.4. Cp_3Ln and Cp_3LnL compounds

For the first time, linear dichroism of a homoleptic organometallic π-complex of an *f*-element was observed. In this study, the absorption spectra of the homoleptic pseudo-trigonal planar complex $Nd(\eta^5\text{-}C_5Me_4H)_3$ were measured at room temperature and at ca. 40 K, respectively, and the linear dichroism spectra of σ- and π-type of an oriented single crystal were measured at ambient temperature and at 77 K. For these measurements large, well-formed red-brown single crystals up to a size of 6 mm × 2 mm × 2 mm were grown by very slow cooling of a solution of the complex in toluene. Neglecting the signals of the C–H combination vibrations and overtones extracted from the absorption spectrum of $La(\eta^5\text{-}C_5Me_4H)_3$, the observed polarization properties of the remaining *f*–*f* transitions allowed the derivation of a truncated crystal field splitting pattern [52]. In a closely related study, the absorption spectra of pseudo (ψ) trigonal planar $Sm(\eta^5\text{-}C_5Me_4H)_3$ and $La(\eta^5\text{-}C_5Me_4H)_3$ in KBr pellets have been measured at room temperature and 77 K, respectively. Additionally, the linear dichroism spectra of σ and π type of an oriented single crystal of $Sm(\eta^5\text{-}C_5Me_4H)_3$ have been recorded at ambient temperature. The observed polarization properties of the *f*–*f* transitions allowed the assignment of the transitions. The free parameters of a phenomenological Hamiltonian were fitted to the energies of the assigned terminal levels, lead-

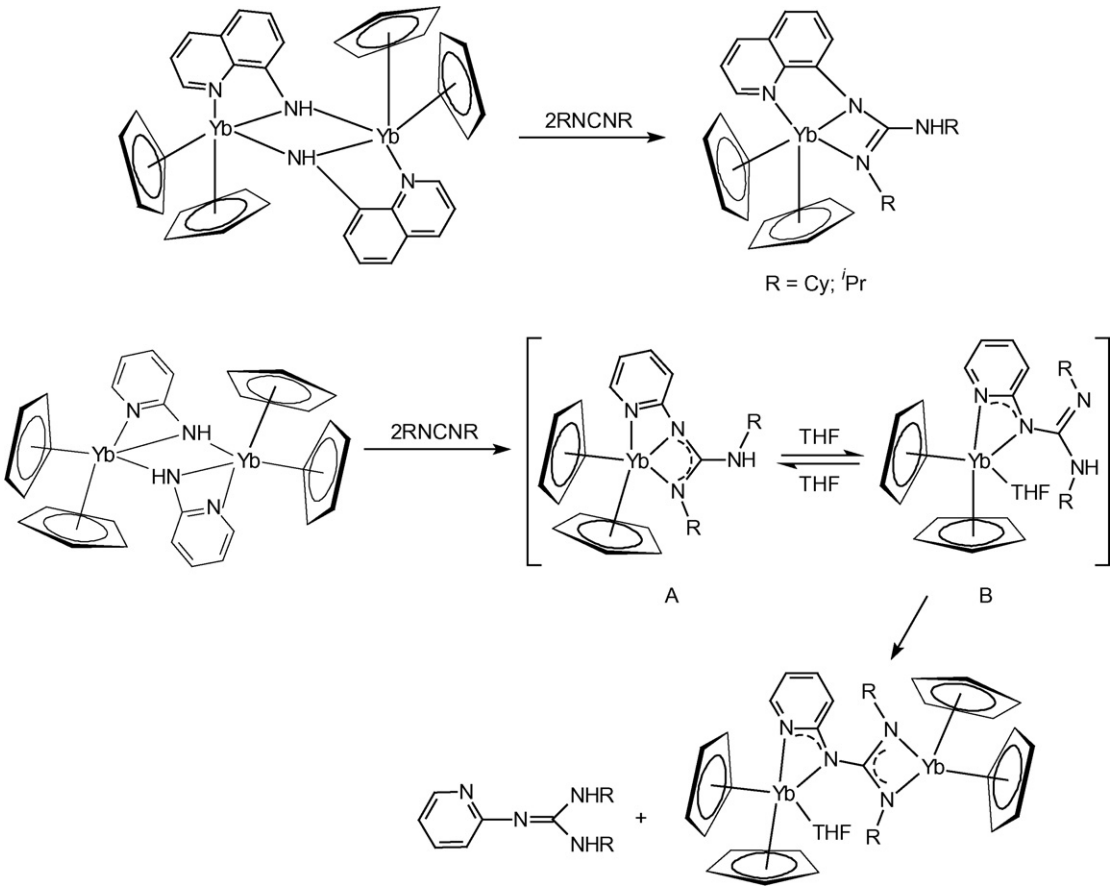

Scheme 71.

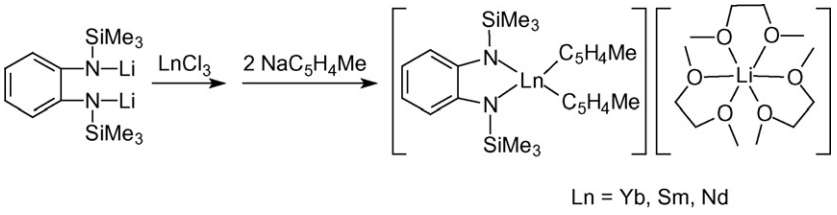

Scheme 72.

ing to a reduced r.m.s. deviation of 19.1 cm^{-1} for 19 assignments. On the basis of these phenomenological CF parameters, the global CF strength experienced by the Sm^{3+} central ion was estimated, and seems to be the largest one ever encountered in samarium(III) chemistry. The obtained Slater parameter F^2 and the spin–orbit coupling parameter f_{4f} allowed the insertion of Sm(η^5-$C_5Me_4H)_3$ into empirical nephelauxetic and relativistic nephelauxetic series, respectively. On the basis of these models, Sm(η^5-$C_5Me_4H)_3$ turns out to be the most covalent Sm^{III} compound found to date. The experimentally based non-relativistic molecular orbital scheme (in

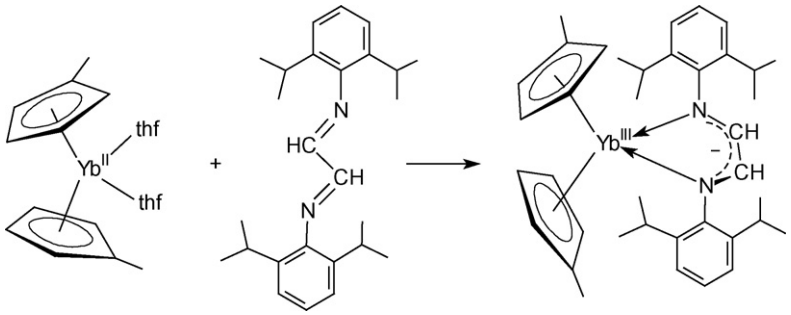

Scheme 73.

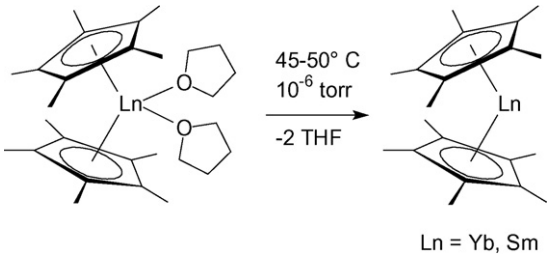

Scheme 74.

the *f* range) of Sm(η^5-$C_5Me_4H)_3$ was determined and compared with the results of a previous Xa-SW calculation on the ψ trigonal planar model compound Sm(η^5-$C_5Me_4H)_3$ [53].

2.5.5. Pentamethylcyclopentadienyl compounds

2.5.5.1. Cp^*_2M compounds. More facile synthetic routes leading to the unsolvated decamethylmetallocenes Cp^*_2Ln (Ln = Sm, Yb) were reported. Green Cp^*_2Yb and Cp^*_2Sm were obtained in nearly quantitative yields by desolvation of the THF-adducts $Cp^*_2Ln(THF)_2$ under high vacuum (Scheme 74) [54].

In the course of a study on the reactivity of the divalent organosamarium complex $Cp^*_2Sm(THF)_2$ with nitriles, the divalent nitrile adducts $Cp^*_2Sm(NC^tBu)(THF)_n$, $Cp^*_2Sm(NC^tBu)_2(THF)$, and $Cp^*_2Sm(NC^tBu)_2$ were isolated and structurally characterized by X-ray crystallography. Dark brown $Cp^*_2Sm(NC^tBu)_2(THF)$ was obtained by treatment of $Cp^*_2Sm(THF)_2$ with ^{t}BuCN in THF solution at −35 °C (Scheme 75) [55].

2.5.5.2. Mono(pentamethylcyclopentadienyl)lanthanide(III) compounds. The synthesis of unsolvated $Cp^*Ln(BPh_4)$ complexes (Ln = Sm, Yb) has been investigated to determine if

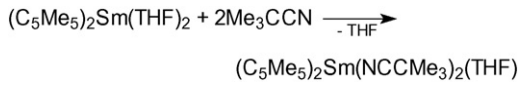

Scheme 75.

the productive chemistry of the metallocene tetraphenylborate complexes, $Cp^*_2Ln(\mu\text{-}Ph)_2BPh_2$, can be expanded to mono(pentamethylcyclopentadienyl) systems. The unsolvated Ln(II) precursors Cp^*_2Ln (Ln = Sm, Yb) react with $[Et_3NH][BPh_4]$ to form $Cp^*Ln(\mu\text{-}\eta^6\text{:}\eta^1\text{-}Ph)_2BPh_2$ complexes with yields over 80% (Scheme 76) in which two of the phenyl rings of the tetraphenylborate counteranion coordinate η^6 to the lanthanide to generate a three-ring coordination geometry involving cyclopentadienyl and arene coordination (Fig. 15) [54].

In contrast to the expected trigonal plane defined by the three-ring centroids in $Cp^*Yb(\mu\text{-}\eta^6\text{:}\eta^1\text{-}Ph)_2BPh_2$, the structure of $Cp^*Sm(\mu\text{-}\eta^6\text{:}\eta^1\text{-}Ph)_2BPh_2$ is pyramidal with Sm 0.41 Å out of the plane of the three-ring centroids (Fig. 16) [54].

The ytterbium derivative $Cp^*Yb(\mu\text{-}\eta^6\text{:}\eta^1\text{-}Ph)_2BPh_2$ could also be synthesized in high yield according to Scheme 77 from Cp^*_2Yb and $AgBPh_4$. In contrast, the analogous reaction with the more strongly reducing Cp^*_2Sm produced the trivalent complex $Cp^*Sm(\mu\text{-}Ph)_2BPh_2$ and Ag metal [54].

The reactivity of the readily available tris(ring) precursors towards various reagents was also studied. For example, $Cp^*Yb(\mu\text{-}\eta^6\text{:}\eta^1\text{-}Ph)_2BPh_2$ reacts with THF to make the polysolvated complex $[Cp^*Yb(THF)_4][BPh_4]$ (Scheme 78) which is the first example of a mono(pentamethylcyclopentadienyl) lanthanide cation containing only THF as other ligands. The same compound could also be obtained from $Cp^*_2Yb(THF)_2$ and $[Et_3NH][BPh_4]$ [54].

The samarium complex $Cp^*Sm(\mu\text{-}\eta^6\text{:}\eta^1\text{-}Ph)_2BPh_2$ reacts with THF under formation of the monosolvated complex $Cp^*Sm[(\mu\text{-}$

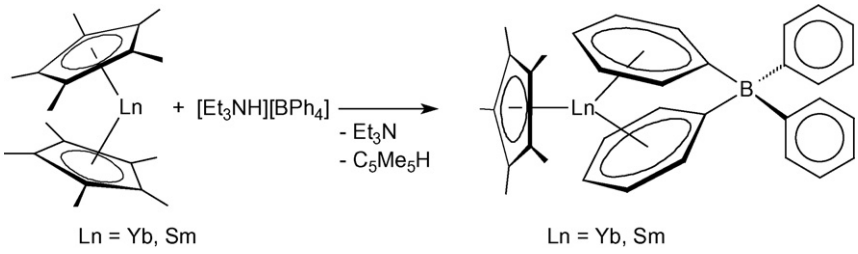

Scheme 76.

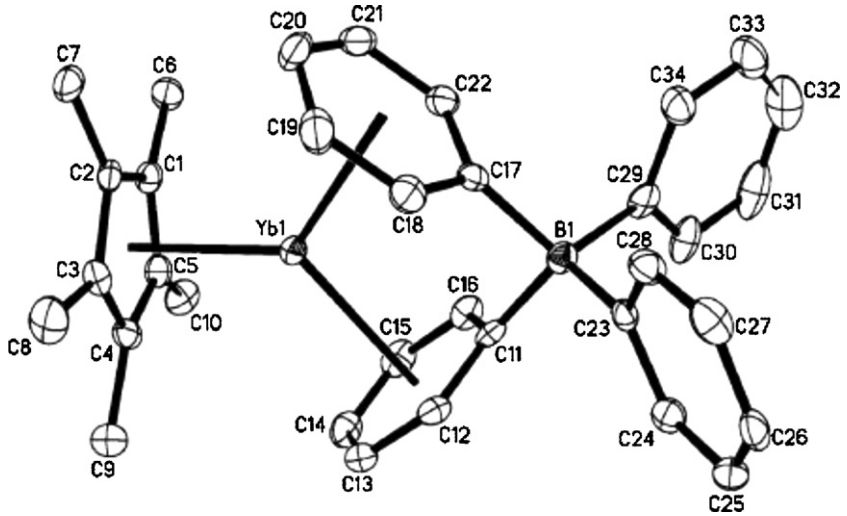

Fig. 15. Molecular structure of $Cp^*Yb(\mu\text{-}\eta^6\text{:}\eta^1\text{-}Ph)_2BPh_2$ [54].

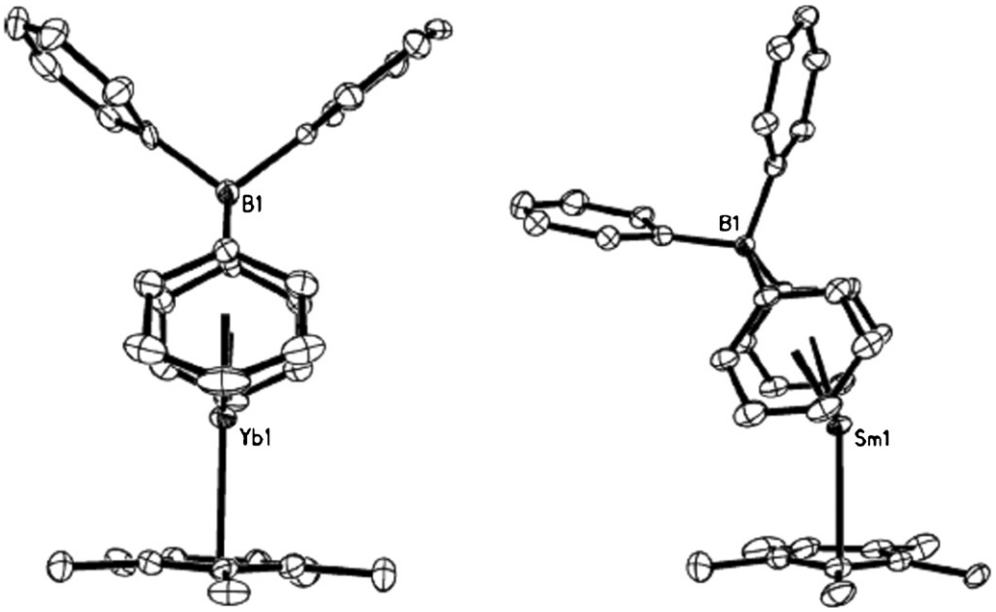

Fig. 16. Side-on view of Cp*Yb(μ-η^6:η^1-Ph)$_2$BPh$_2$ and Cp*YSm(μ-η^6:η^1-Ph)$_2$BPh$_2$ [54].

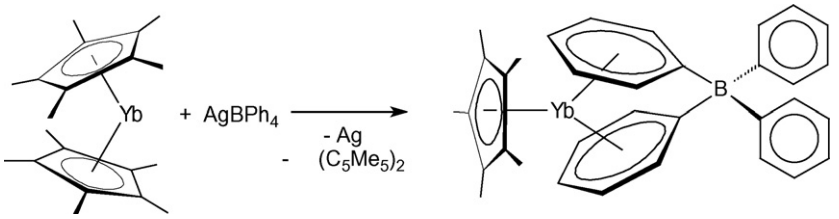

Scheme 77.

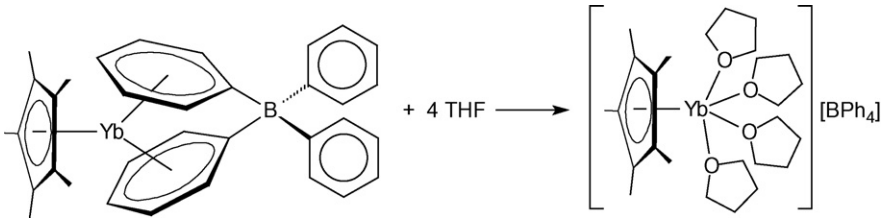

Scheme 78.

η^6:η^1-Ph)(μ-η^2:η^1-Ph)BPh$_2$](THF) (Scheme 79, dark green solid, 97% yield) which retains η^6 coordination by one phenyl ring and displays η^2 coordination with the other phenyl ring [54].

Reactions of Cp*Ln(μ-η^6:η^1-Ph)$_2$BPh$_2$ (Ln = Sm, Yb) were found to be accompanied by ligand redistribution to form the trivalent bis(pentamethylcyclopentadienyl) products, (μ-η^3:η^3-C$_{12}$H$_8$N$_2$)[Cp*$_2$Ln]$_2$ (Ln = Sm, Yb) (Scheme 80) [54].

Reduction of azobenzene by Cp*Sm(μ-η^6:η^1-Ph)$_2$ BPh$_2$ generates a dark blue mono(pentamethylcyclopentadienyl) tetraphenylborate complex, Cp*Sm[(μ-η^6:η^1-Ph)BPh$_3$](N$_2$Ph$_2$),

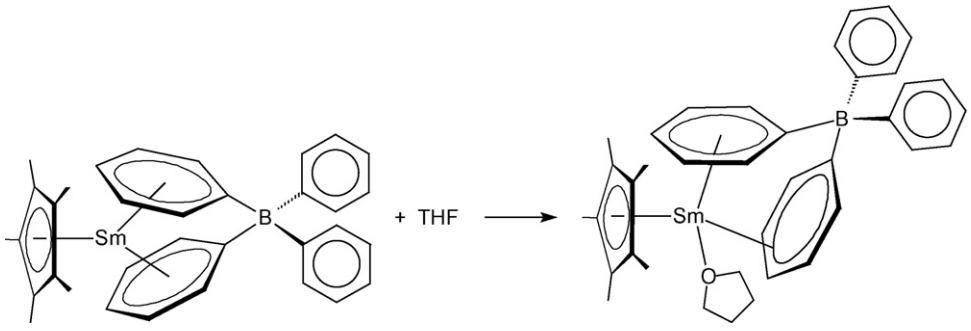

Scheme 79.

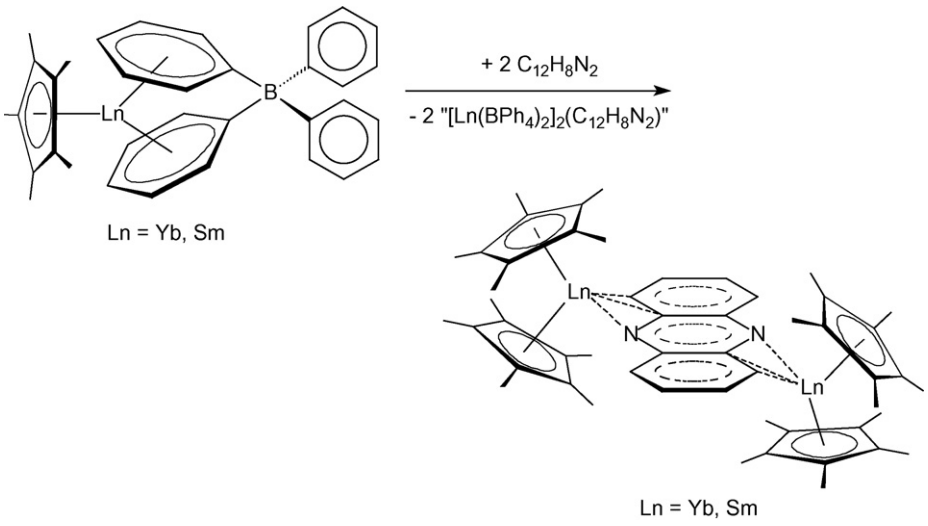

Scheme 80.

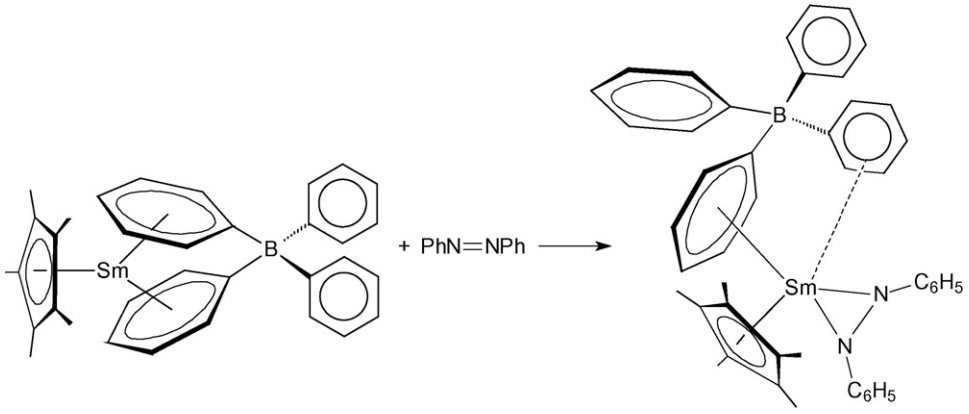

Scheme 81.

that contains an η^6 coordinated phenyl ring and an azobenzene radical anion (Scheme 81) [54].

A $[Cp^*_2La][(\mu\text{-}Ph)_2BPh_2]/KC_8/CO_2$ reaction provided a CO_2 insertion product, $[Cp^*La(\mu\text{-}\eta^1\text{:}\eta^1\text{-}O_2CC_5Me_5)(\mu\text{-}\eta^1\text{:}\eta^2\text{-}O_2CC_5Me_5)]_2$ (Fig. 17), while a CO_2 reduction product was not identified [43].

A series of mono(pentamethylcyclopentadienyl) bis(phosphinimino)methanide complexes of yttrium and lanthanides (Sm, Yb) were prepared by two different approaches. As illustrated in Scheme 82, the compounds can be obtained either from dimeric $[\{CH(PPh_2NSiMe_3)_2\}LnCl_2]_2$ (Ln = Y, Sm, Yb) and KCp* or in a one-pot reaction in which $K[CH(PPh_2NSiMe_3)_2]$ is caused to react with anhydrous rare-earth trichlorides in the presence of KCp* [56].

Ytterbocenes $Cp^*_2Yb(THF)_2$ (Cp * = C_5Me_5, C_5Me_4H) coordinated by sterically demanding cyclopentadienyl ligands act as two-electron reductants in their reactions with diazadienes (=DAD). These reactions occur by abstraction of one Cp* ring and result in the formation of novel Yb^{III} mixed-ligand bent sandwich complexes of the type Cp*Yb(DAD)(THF) (Scheme 83), in which the dianion of the DAD has an uncommon terminal η^4-coordination to the ytterbium atom. Variable-temperature magnetic measurements of the complex Cp*Yb(DAD)(THF)] suggest the existence of redox tautomerism for this compound [51].

The synthesis and structural characterization of an η^2-(*N*,*C*)-pyridyl (mono)pentamethylcyclopentadienyl lutetium(III) complex have been reported. Reaction of $Cp^*Lu(CH_2SiMe_3)_2(THF)$ with pyridine according to Scheme 84 resulted in the activation of an *ortho*-C–H bond to form the corresponding η^2-(*N*,*C*)-pyridyl complex (orange, block-shaped crystals) with elimination of $SiMe_4$. This is a rare example of pyridine metalation at a lanthanide

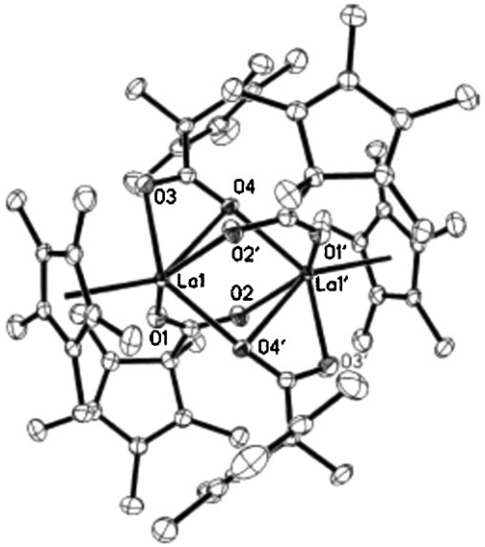

Fig. 17. Molecular structure of $[Cp^*La(\mu\text{-}\eta^1\text{:}\eta^1\text{-}O_2CC_5Me_5)(\mu\text{-}\eta^1\text{:}\eta^2\text{-}O_2CC_5Me_5)]_2$ [43].

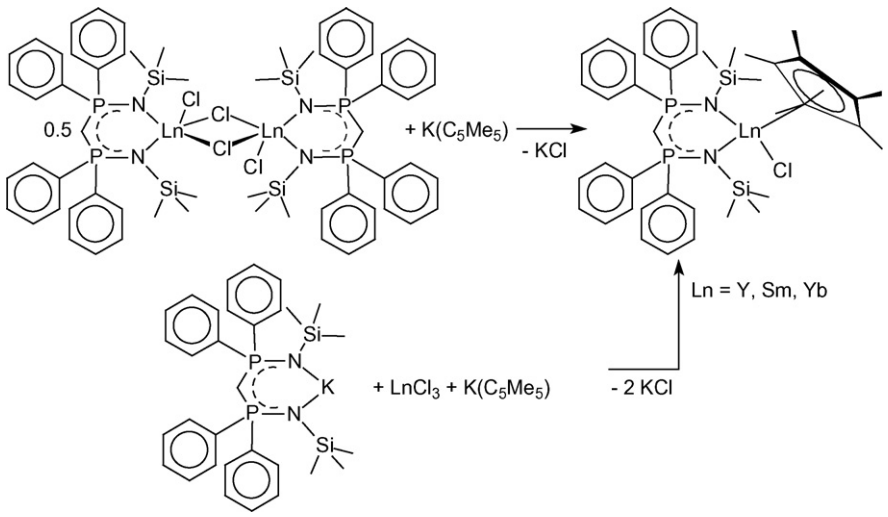

Scheme 82.

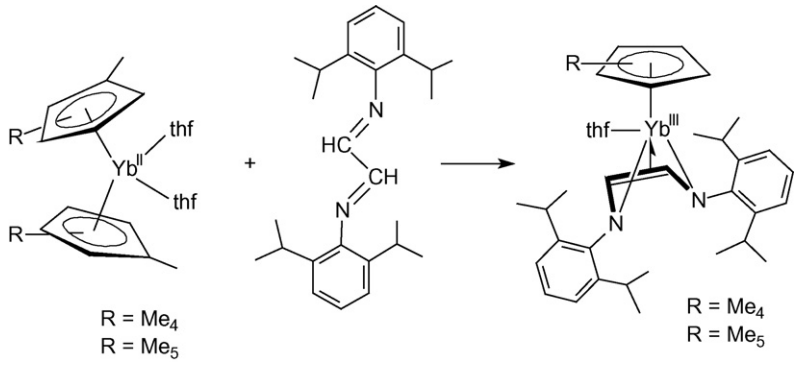

Scheme 83.

metal center in the absence of a bent metallocene framework. The η^2-(*N*,*C*)-pyridyl coordination mode was confirmed by X-ray crystallographic analysis. The pyridyl complex adopts a distorted square-pyramid geometry with the Cp* unit residing in the apical position and the pyridyl ligand and remaining ligands residing in the basal plane. Isotopic labeling studies suggested that C–H bond activation is consistent with a σ-bond metathesis mechanism [57].

2.5.5.3. Bis(pentamethylcyclopentadienyl)lanthanide(III) compounds. The divalent samarocene complex $Cp^*_2Sm(THF)_2$ reacts in toluene solution with ^{t}BuCN to form the insoluble trivalent cyanide complex $[Cp^*_2SmCN]_n$. This reaction was found to proceed through divalent $Cp^*_2Sm(^t BuCN)(THF)$. The latter transforms *via* C–C bond cleavage to form the cyanide complex and $Cp^*_2Sm(N{=}CH^tBu)(THF)$, which is the product of insertion of ^{t}BuCN into a Sm–H bond presumably formed by β-hydrogen elimination of a ^{t}Bu intermediate. Complex $Cp^*_2Sm(N{=}CH^tBu)(THF)$ can be synthesized directly from the reaction of $[Cp^*_2Sm(\mu\text{-}H)]_2$ with ^{t}BuCN and THF. Scheme 85 summarizes the reaction pathways in this system [55].

Novel cyanide metallocenes have also been reported for trivalent cerium. Addition of N^nBu_4CN to Cp^*_2CeI or $(Cp^*_2Ce(OTf)$ in acetonitrile led to the precipitation of the neutral monocyanide species $[Cp^*_2Ce(\mu\text{-}CN)]_n$, which likely has an oligomeric structure, as shown by the trimeric cyanide-bridged complex $[Cp^*_2Ce(\mu\text{-}CN)(CN^tBu)]_3$ obtained by addition of excess ^{t}BuNC into a suspension of $[Cp^*_2Ce(\mu\text{-}CN)]_n$ in acetonitrile (Scheme 86). The anionic polycyanide $[Cp^*_2Ce(CN)_3][N^nBu_4]_2$ was synthesized by treatment of $[Cp^*_2Ce(\mu\text{-}CN)]_n$ with 2 equiv. or an excess of N^nBu_4CN in acetonitrile. The same compound was also prepared in a one-pot procedure by stepwise addition of 1 equiv. of KCN and 2 equiv. of N^nBu_4CN to the parent iodide in acetonitrile. The bent metallocene $[Cp^*_2Ce(\mu\text{-}CN)]_n$ is a unique example of a molecular polycyanide compounds of a lanthanide element that has been structurally identified [58].

Various adducts of decamethylytterbocene with 1,4-diazadienes and 2,2′-bipyridyl-type ligands have been synthesized and stud-

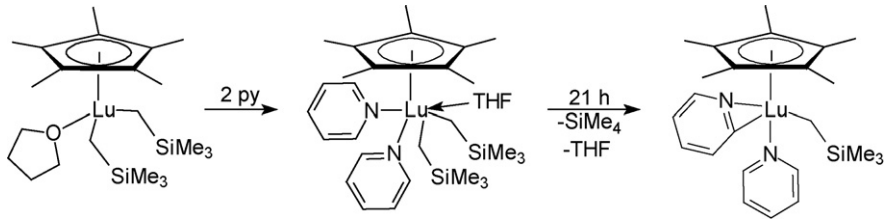

Scheme 84.

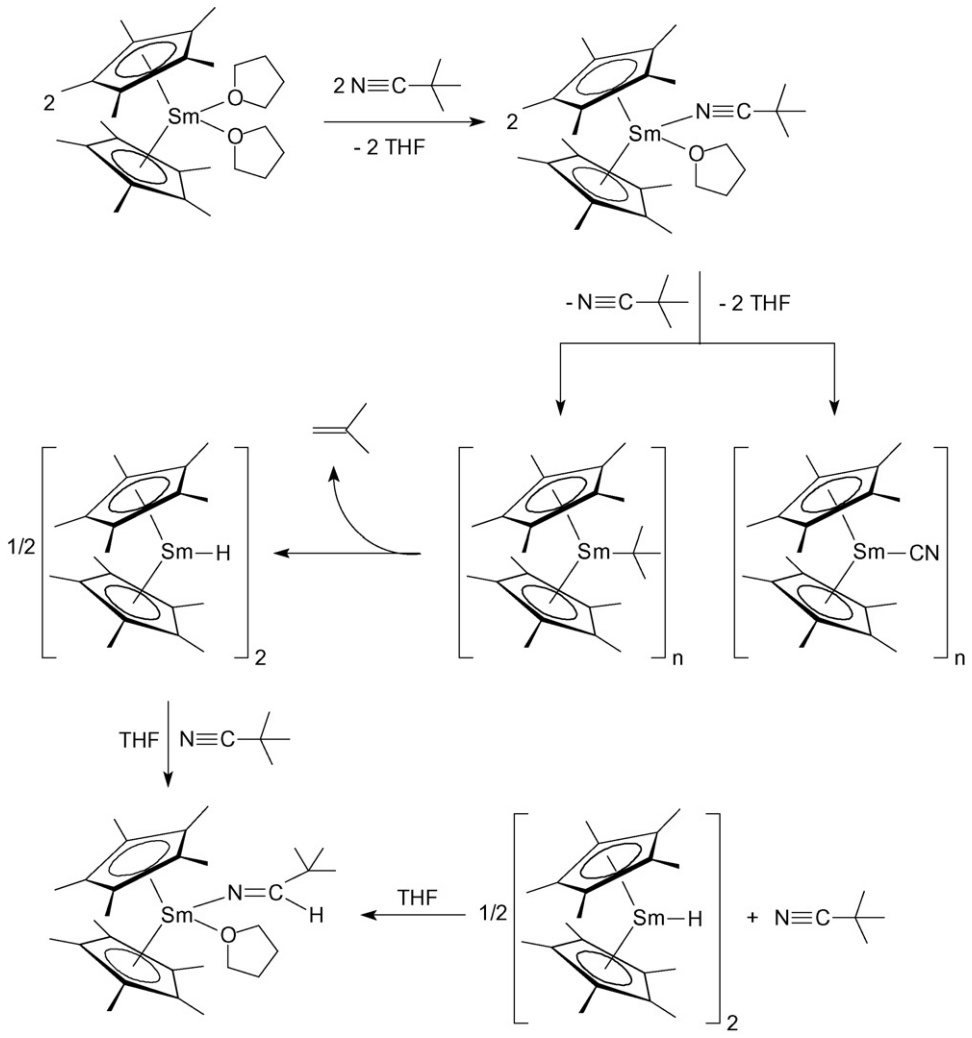

Scheme 85.

ied in detail. For example, the paramagnetic 1:1 coordination complexes of Cp^*_2Yb with a series of diazadiene ligands, RN=C(R′)C(R′)=NR, where R = ^{i}Pr, ^{t}Bu, adamantyl, *p*-tolyl, *p*-anisyl, mesityl when R′ = H and R = *p*-anisyl when R′ = Me, were prepared. The complexes are paramagnetic, but their magnetic moments are less than expected for the two uncoupled spin carriers, $Cp^*_2Yb^{III}(4f^{13})$ and the diazadiene radical anions (S = 1/2), which implies exchange coupling between the spins. The variable-temperature ^{1}H NMR spectra showed that rotation about the R–N bond is hindered and these barriers were estimated. The barriers are largely determined by steric effects, but electronic effects are not unimportant [59]. Two new bimetallic complexes, (μ-1,3-(2,2′-bipyridyl)-5-Bu^{t}C$_6$H$_3$)[Cp^*_2Yb]$_2$ and (μ-1,4-(2,2′-bipyridyl)-C$_6$H$_4$[Cp^*_2Yb]$_2$) (Scheme 87), and their corresponding two-electron oxidation products were synthesized with the aim of determining the impact of the bridging ligand geometry on the electronic and magnetic properties of these materials. Electrochemistry, optical spectroscopy, and bulk susceptibility measurements all supported a ground-state electronic configuration of the type [$(f)^{13}$-$(\pi_a{}^*)^1$-$(\pi_b{}^*)^1$-$(f)^{13}$]. Density functional theory calculations on the uncomplexed bridging ligands as doubly reduced species also indicated that the diradical electronic configuration is the lowest lying for both *meta*- and *para*-bis(bipyridyl) systems. The electrochemical and optical spectroscopic data indicated that the electronic coupling between the metal centers mediated by the diradical bridges is weak, as evidenced by the small separation of the metal-based redox couples and the similarity of the *f*–*f* transitions of the associated dicationic complexes relative to those of the monometallic [Cp^*_2Yb(bpy)]$^+$ analogue. The magnetic susceptibility data showed no evidence for exchange coupling between the paramagnetic metal centers in the neutral complexes, but did indicate weak exchange coupling between Yb^{III} and ligand radical spins on each of the effectively independent halves of the bimetallic complexes [60].

In a related study, the ligand 1-methyl-3,5-bis(2,2′:6′,2″-terpyridin-4′-yl)benzene has been employed in the synthesis of a new bimetallic ytterbocene complex [Cp^*_2Yb](1-methyl-3,5-bis(2,2′:6′,2″-terpyridin-4′-yl)benzene)[$YbCp^*_2$] (**1**) and the doubly oxidized congener [**1**]$^{2+}$ in an attempt to determine the impact of the bridging ligand geometry on the magnetic/electronic properties

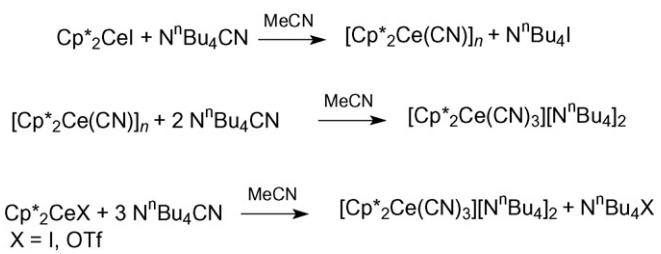

Scheme 86.

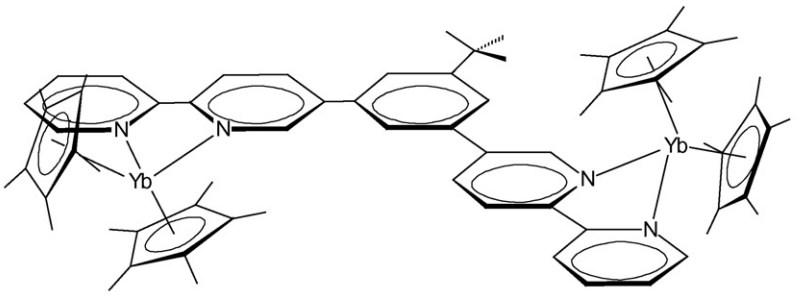

$[Cp^*_2Yb]_2$(*m*-bbb)

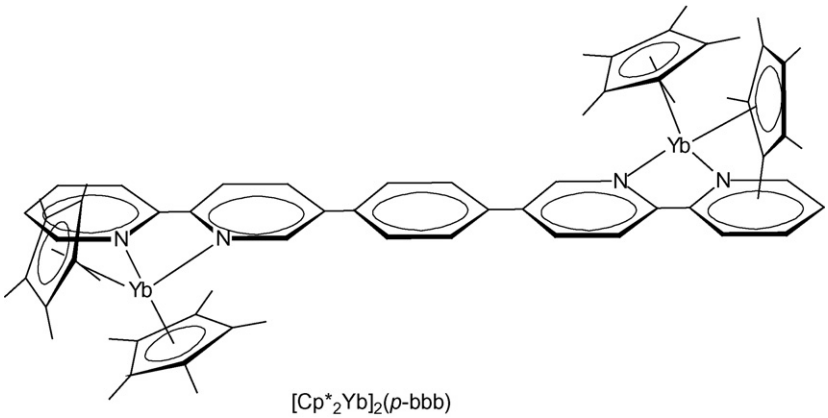

$[Cp^*_2Yb]_2$(*p*-bbb)

Scheme 87.

as compared to the previously reported 1,4-analog [Cp^*_2Yb](1,4-di(terpyridyl)benzene)[$YbCp^*_2$] (**2**). Electrochemical, electronic, and magnetic data provided compelling evidence that the 1,3-geometry associated with the bridging ligand of **1** does an effective job of inhibiting electronic communication between metal centers and magnetic coupling of spin carriers at room temperature as compared to **2** [61].

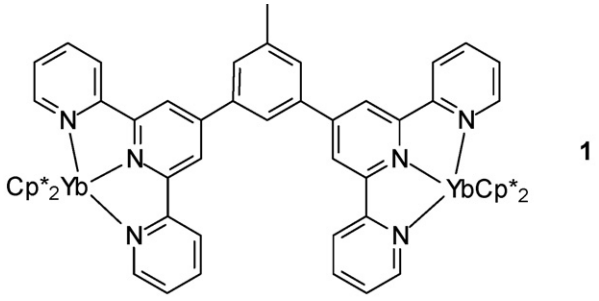

1

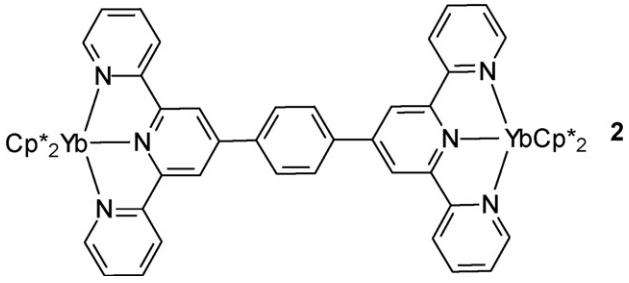

2

In a related study the synthesis and structures of 1,2-bis(imino)acenaphthene (BIAN) lanthanide complexes that involve the transfer of zero, one, or two electrons were investigated. The isolated compounds, all obtained by treatment of $Cp^*_2Ln(OEt_2)$ (Ln = Sm, Eu) with the appropriate R-BIAN ligands, are depicted in Scheme 88. In a result it was demonstrated that the lanthanide metal → BIAN charge transfer process can be controlled by (a) the choice of metal, (b) tuning of the BIAN ligand substituents, or (c) use of a bulky BIAN ligand [62].

2.5.6. Pentalenyl, indenyl and fluorenyl compounds

Bis(permethylpentalene)cerium, Ce(η^8-C_8Me_6)$_2$ was prepared and its molecular structure determined. The reaction of $Li_2C_8Me_6(TMEDA)_x$ and $CeCl_3$ (2:1 ratio) in THF led to a brown solution, presumably containing solvated Li[Ce(η^8-C_8Me_6)$_2$]. Attempted oxidation of this extremely air-sensitive solution with oxidants commonly used to synthesize Ce(COT)$_2$ (*e.g.*, allyl bromide or AgI) failed. However, it was found that the use of excess 1,2-dichloroethane resulted in smooth conversion to a vividly purple product. High vacuum sublimation afforded Ce(η^8-C_8Me_6)$_2$ as an air-sensitive purple–black solid in moderate yield. An X-ray crystal structure determination confirmed the presence of neutral bis(permethylpentalene)cerium. As can bee seen from Fig. 18, the pentalene moieties are appreciably non-planar, with a fold-angle of 24.7°. The average Ce–C bond length of 2.682 Å is similar to that found in Ce(COT)$_2$ (2.671 Å) [63].

In addition to the X-ray crystal structure analysis, Ce(η^8-C_8Me_6)$_2$ was also studied using a variety of techniques including XANES spectroscopy and DFT calculations. The former gave strong evidence for a formal valency close to Ce(III) in this molecule which thus provides an example of the self-contained Kondo effect in a discrete molecule [63].

Cerium(III) and cerium(IV) bis(η^8-pentalene) sandwich complexes containing the $[C_8H_4(Si^iPr_3\text{-}1,4)_2]^{2-}$ ligand have also been investigated in detail. The anionic Ce(III) bis(pentalene) sandwich complex K[Ce{$C_8H_4(Si^iPr_3\text{-}1,4)_2$}$_2$] was prepared by treatment of

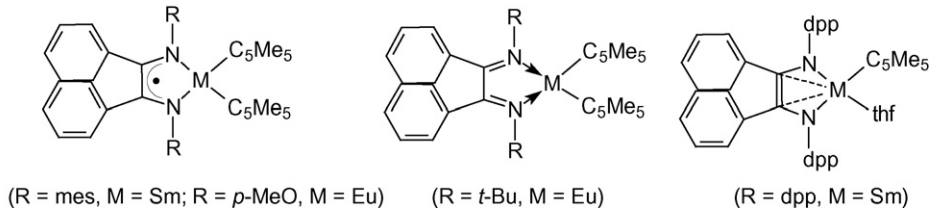

Scheme 88.

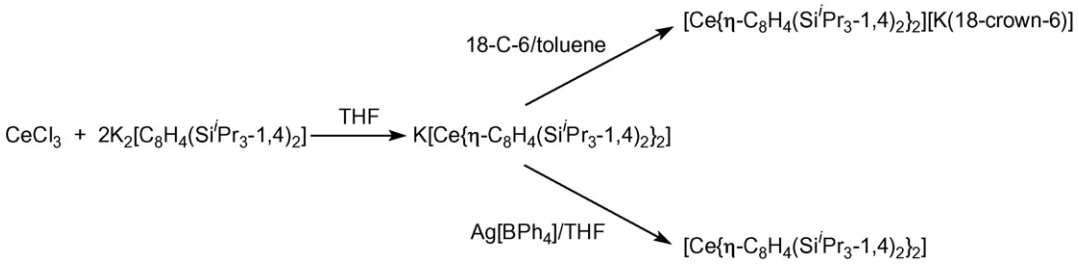

Scheme 89.

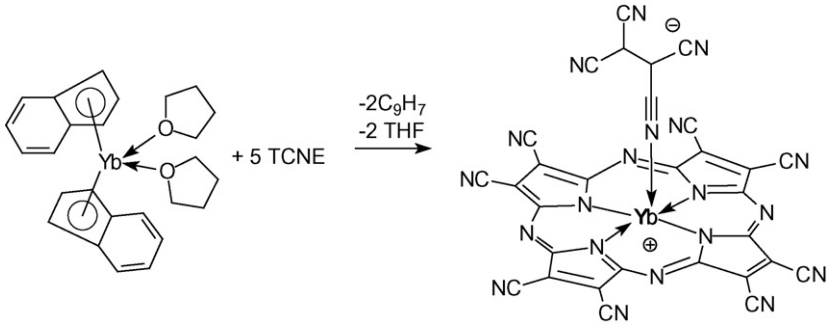

Scheme 90.

$CeCl_3$ with $K_2[C_8H_4(Si^iPr_3\text{-}1,4)_2]$ (Scheme 89) and crystallographically characterized as its 18-crown-6 complex. Oxidation of the anionic precursor with $Ag[BPh_4]$ afforded the neutral, formally Ce(IV) sandwich complex $Ce[C_8H_4(Si^iPr_3\text{-}1,4)_2]_2$, whose molecular structure was also determined. Its electronic structure has been investigated in detail by a combination of magnetic studies, K-edge XANES measurements, gas-phase photoelectron spectroscopy, and density functional calculations [64].

The divalent ytterbium bis(indenyl) complex $(Ind)_2Yb(THF)_2$ was found to undergo an unusual metal template assisted formation of a highly functionalized octacyanoporphyrazine framework upon treatment with tetracyanoethylene (=TCNE). The reaction of bis(indenyl)ytterbium(II) with TCNE proceeds at room temperature in dry THF under vacuum and is accompanied by the destruction of the ytterbium π-complex and formation of porphyrazine complex as a green–black solid (Scheme 90) [65].

Treatment of the yttrium tris(alkyl) precursor $Y(CH_2SiMe_3)_3(THF)_2$ with an equimolar amount of indene afforded the mono(indenyl) complex $(Ind)Y(CH_2SiMe_3)_2(THF)$ *via* alkane elimination (Scheme 91). A THF-free mono(alkyl) derivative was obtained upon subsequent treatment with the potentially tetradentate aminophenol ligand HL^2 shown

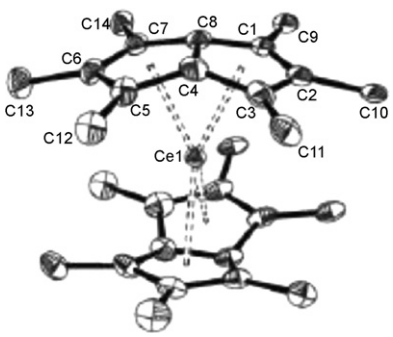

Fig. 18. Molecular structure of $Ce(\eta^8\text{-}C_8Me_6)_2$ [63].

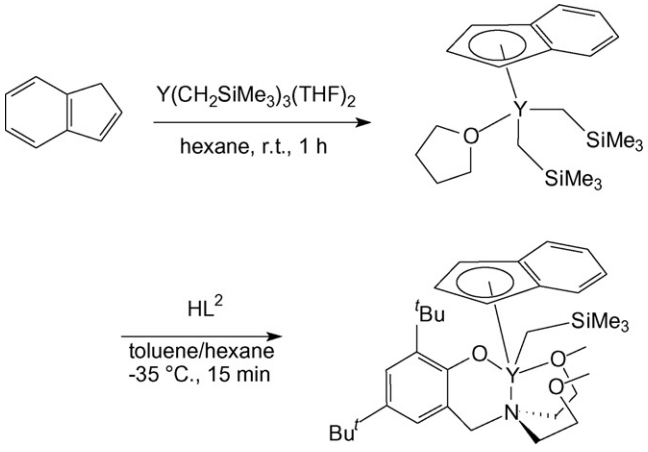

Scheme 91.

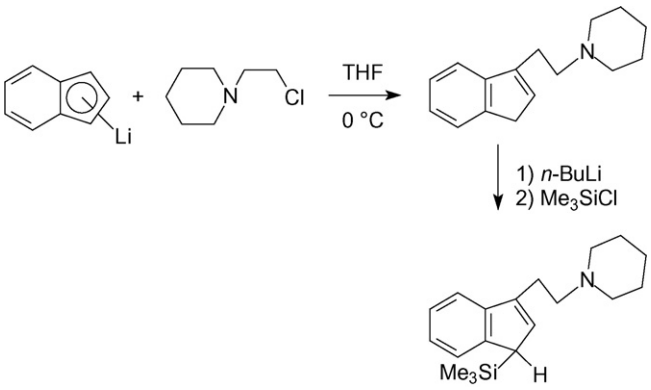

Scheme 92.

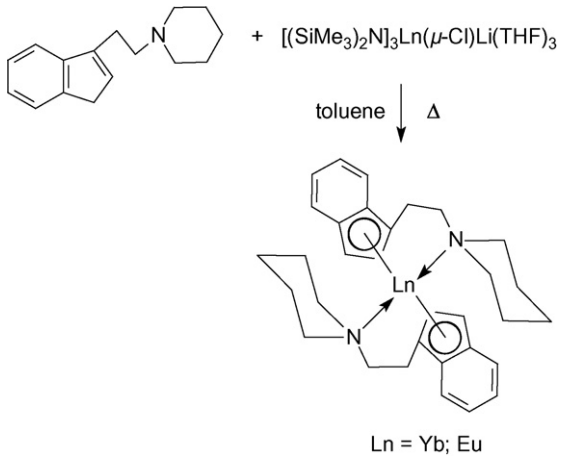

Scheme 93.

in Scheme 91. The yellow solid was isolated in 78% yield [34].

The coordination and reactivity diversity of *N*-piperidineethyl-functionalized indene compounds with the lanthanide(III) amides $[(Me_3Si)_2N]_3Ln(\mu\text{-}Cl)Li(THF)_3$ (Ln = Yb, Eu, Sm, Nd) were studied. The ligand was obtained according to Scheme 92 by the reaction of freshly prepared indenyl lithium with *N*-piperidineethyl chloride in THF. Subsequent lithiation with *n*-butyllithium, followed by treatment with excess chlorotrimethylsilane gave the corresponding trimethylsilyl-substituted precursor [66].

Reactions of the lanthanide(III) amides $[(Me_3Si)_2N]_3Ln(\mu\text{-}Cl)Li(THF)_3$ (Ln = Eu, Yb) with 2 equiv. of these new indenyl ligands produced lanthanide(II) in all cases. The reactions are illustrated in Schemes 93 and 94 [66].

In the case of Ln = Eu, an unexpected highly π-conjugated bis(*N*-piperidineethyl)dibenzofulvalene, $(C_5H_{10}NCH_2CH_2C_9H_5)_2$ was isolated as a by-product. As expected, reduction did not take place in the case of Ln = Nd and Sm. Instead, treatment of $[(Me_3Si)_2N]_3Ln(\mu\text{-}Cl)Li(THF)_3$ (Ln = Nd, Sm) with 2 equiv. of $C_5H_{10}NCH_2CH_2C_9H_7$ as shown in Scheme 95 afforded new tris(indenyl) lanthanide(III) complexes. The metal atom in these molecules is located at the center of a *pseudo*-tetrahedron formed by three indenyl five-membered rings and one nitrogen atom of a piperidine substituent [66].

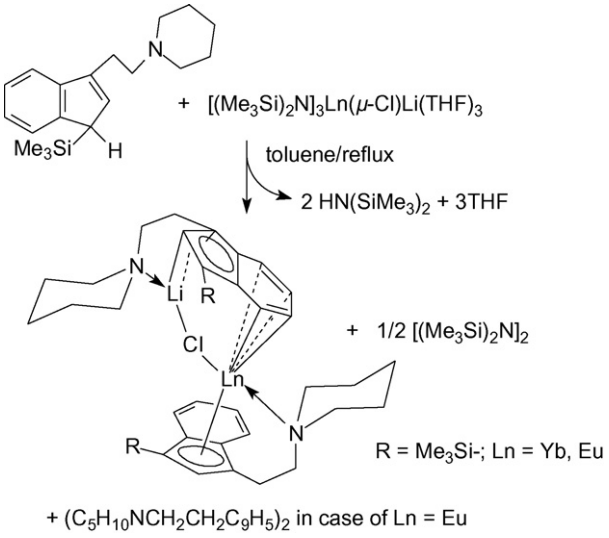

Scheme 94.

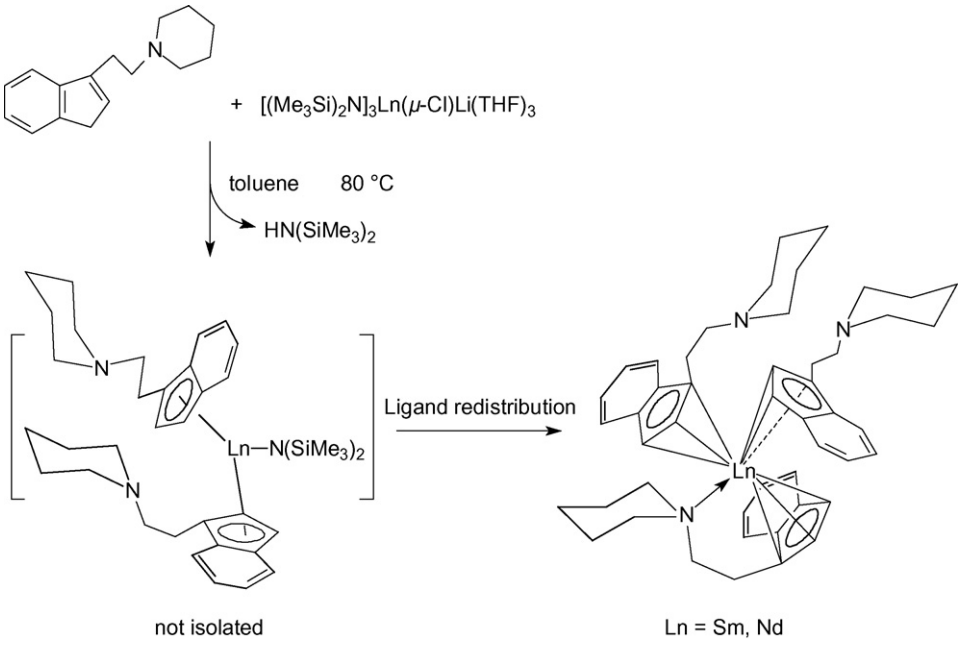

Scheme 95.

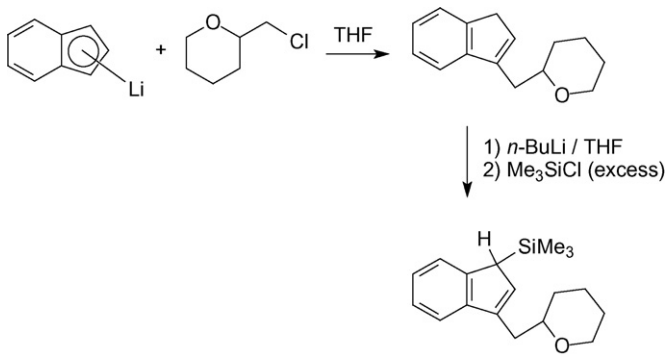

Scheme 96.

In a closely related study, two series of divalent organolanthanide complexes with new tetrahydro-2*H*-pyranyl-functionalized indenyl ligands were reported. The straightforward synthesis of the ligands is outlined in Scheme 96 [67].

Treatment of the lanthanide(III) amide precursors $[(Me_3Si)_2N]_3Ln(\mu\text{-}Cl)Li(THF)_3$ (Ln = Yb, Eu) with 2 equiv. of the tetrahydro-2*H*-pyranyl-functionalized indenyl ligands in hot toluene gave, after workup, the corresponding lanthanide(II) complexes in good yield (Scheme 97). X-ray analyses of the products revealed that the central lanthanide atoms are coordinated by two indenyl ligands through the five-membered ring in η^5-fashion, and two oxygen atoms of the tetrahydropyranyl ring in η^1-mode, resulting in a distorted pseudo-tetrahedral coordination geometry around the lanthanide. The catalytic activity of these complexes in methylmethacrylate and ε-caprolactone polymerization was also studied (*cf.* Section 2.11.1) [67].

The synthesis of the first rare earth metal bis(alkyls) bearing an indenyl-functionalized *N*-heterocyclic carbene (=NHC) ligand has been reported. Treatment of a specially designed indenyl-modified imidazolium bromide (Scheme 98) with either the heterobimetallic lanthanide tetra(alkyl) complexes $Ln(CH_2SiMe_3)_4Li(THF)_2$ or alternatively with $LiCH_2SiMe_3$ followed by the lanthanide tris(alkyls) $Ln(CH_2SiMe_3)_3(THF)_2$ afforded the first NHC-stabilized monomeric rare earth metal bis(alkyl) complexes $(IndNHC)Ln(CH_2SiMe_3)_2$ (Ln = Sc, Y, Lu) *via* double-deprotonation reactions. The compounds were isolated as THF-free isostructural monomers. The

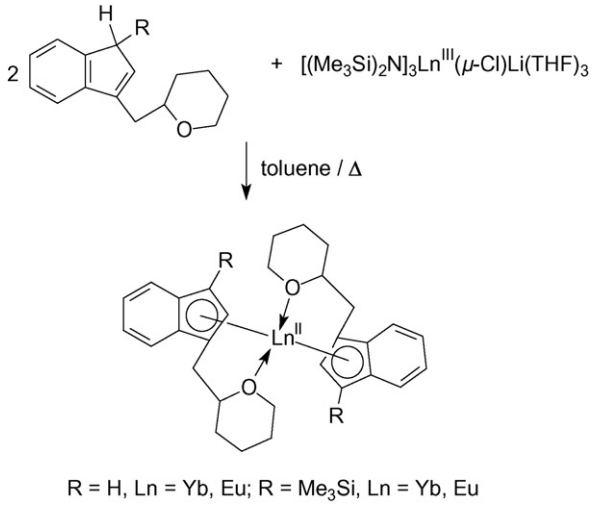

R = H, Ln = Yb, Eu; R = Me_3Si, Ln = Yb, Eu

Scheme 97.

monoanionic Ind-NHC ligands are coordinated to the central metal ion in an $\eta^5{:}\kappa^1$ constrained geometry configuration (CGC) mode and together with the two *cis*-located alkyl moieties form a *pseudo*-tetrahedral ligand environment, leading to chirality of the complexes. The Lu derivative was found to exhibit catalytic activity in isoprene polymerization (*cf.* Section 2.11.1) [68].

A series of (+)-neomenthyl-substituted bis(indenyl) lanthanide complexes was prepared and tested as catalysts for the asymmetric hydroamination/cyclization of aminoalkenes. The synthetic procedures are outlined in Scheme 99. Reaction of YCl_3 with the planar chiral (1-neomenthylindenyl)lithium predominantly produced a single, C_2-symmetric, racemic-like diastereomer [44].

X-ray crystal structure analysis confirmed that of the three possible isomers shown in Scheme 100 $(\eta^5\text{-neomenthylCp})_2Y(\mu\text{-}Cl)_2Li(Et_2O)_2$ represent the p-S,p-S metallocene diastereomer. As shown in Scheme 99, the heterobimetallic "ate"-complex intermediate reacts with $LiN(SiMe_3)_2$ to form $(\eta^5\text{-neomenthylCp})_2YN(SiMe_3)_2$ with retention of configuration. Some of these complexes were found to show moderate to good catalytic activity in asymmetric hydroamination/cyclizations of aminoalkenes (*cf.* Section 2.11.2) [44].

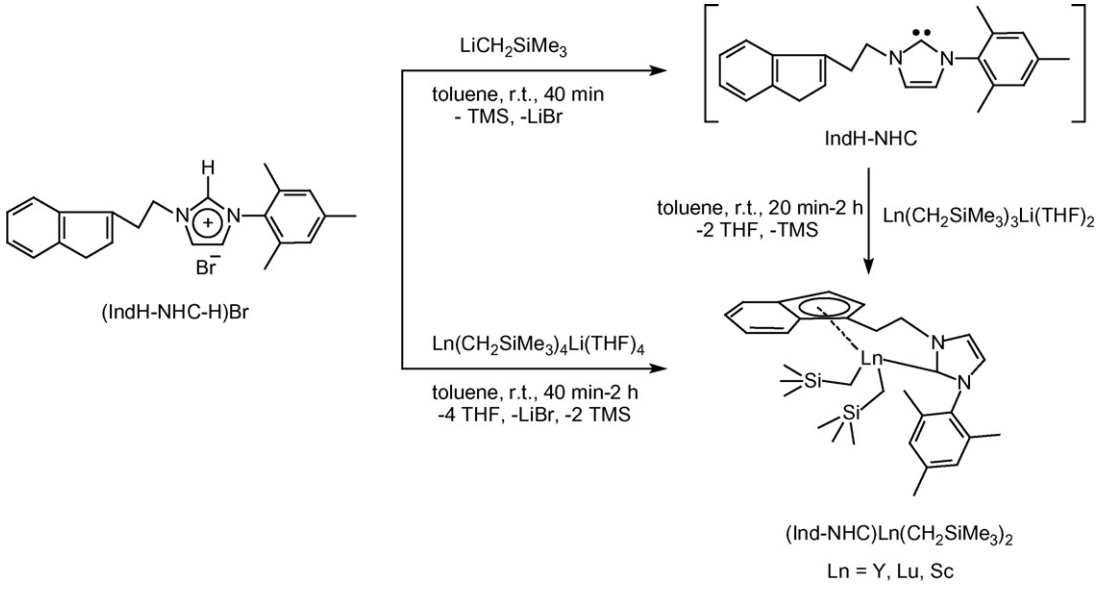

Scheme 98.

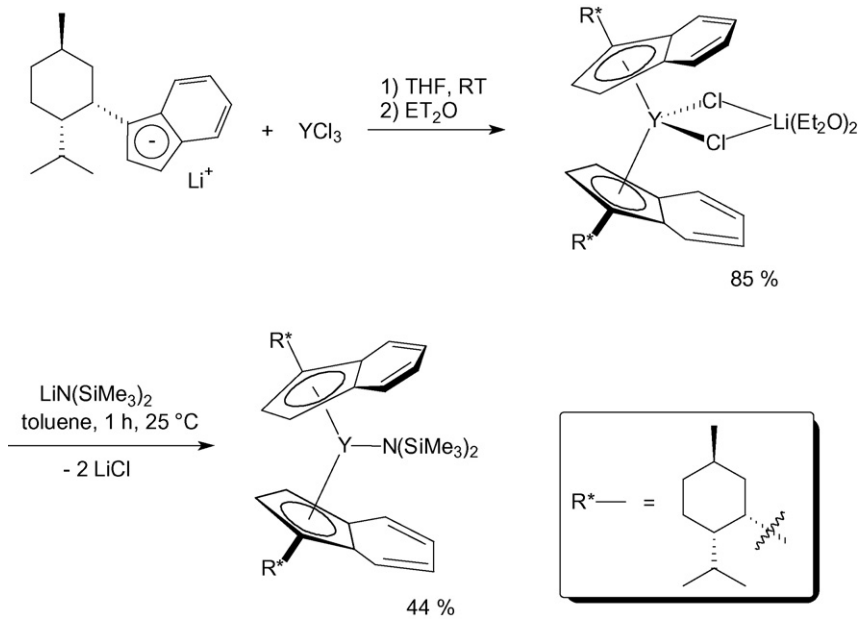

Scheme 99.

A series of new neutral lanthanide allyl complexes bearing *ansa*-bridged fluorenyl/cyclopentadienyl ligands [Flu-EMe$_2$-(3-R-Cp)]Ln(η^3-C$_3$H$_5$)(THF) (E = C, R = H, Ln = Y, La, Nd, Sm; R = Bu^t, Ln = Y, Nd; E = Si, R = H, Ln = Y, Nd) were synthesized as illustrated in Scheme 101 in good yields *via* salt metathesis protocols. The complexes were characterized by elemental analysis, NMR spectroscopy for diamagnetic complexes, and single-crystal X-ray diffraction studies for three representative derivatives [69].

Simple silylamine elimination reactions of ethylene-bis(indene) with the lanthanide amides [(Me$_3$Si)$_2$N]$_3$Ln(μ-Cl)Li(THF)$_3$ produced the [ethylene-bis(η^5-indenyl)][bis(trimethylsilyl)amido]lanthanide(III) complexes (EBI)LnN(SiMe$_3$)$_2$ (Ln = Y, Sm, Yb) (Scheme 102), which exhibited diverse catalytic activities on the addition of the N–H bond of amines and the C–H bond of terminal alkynes to the carbodiimides and on the ring-opening polymerization of ε-caprolactone as well (*cf.* Section 2.11). The new complexes were fully characterized by spectroscopic methods, elemental analyses, and X-ray crystallographic analyses. This work offers a straightforward, highly atom efficient route for the syntheses of substituted guanidines and propiolamidines, and it represents the first application of readily accessible lanthanocene amides to these reactions [70].

Unprecedented N=C bond insertion into the η^5-Yb-indenyl bond occurred in the reaction of 2-(((2,6-diisopropylphenyl)imino)methyl)pyridine with (C$_9$H$_7$)$_2$Yb(THF)$_2$ and afforded the Yb(III) derivative (η^5-C$_9$H$_7$)Yb[N(2,6-^{i}Pr$_2$C$_6$H$_3$)CH(C$_9$H$_7$)(C$_5$H$_4$N)]{2,6-^{i}Pr$_2$C$_6$H$_3$NCH(C$_5$H$_4$N)$^{\bullet-}$] (Scheme 103). The compound was isolated in 61% yield in the form of deep green crystals [71].

For the complexes Cp$_2$Yb(THF)$_2$ (Cp = C$_{13}$H$_9$, Cp*) coordinated by bulkier η^5 ligands the same reaction results in an oxidative cleavage of the η^5 Yb–Cp bond and formation of homoleptic Yb[(2,6-^{i}Pr$_2$C$_6$H$_5$NCH(C$_5$H$_4$N)$^{\bullet-}$]$_3$ and Cp*Yb[(2,6-^{i}Pr$_2$C$_6$H$_3$NCH(C$_5$H$_4$N)$^{\bullet-}$]$_2$, respectively (Scheme 104) [71].

2.6. Organolanthanide complexes with cyclopentadienyl-like ligands

2.6.1. Compounds with heteroatom five-membered ring ligands

A series of pyrrolide-ligated organoyttrium complexes were prepared and structurally characterized, some of which involve η^5-azacyclopentadienyl-type coordination of pyrrolyl rings. The compounds were made by alkane elimination reactions between the parent protonated ligands and Y(CH$_2$SiMe$_3$)$_3$(THF)$_2$. Reactions starting from the *N*,*N*-bidentate ligand 2-[(*N*-2,6-diisopropylphenyl)iminomethyl]pyrrole (L^1) are summarized in Scheme 105. Treatment of Y(CH$_2$SiMe$_3$)$_3$(THF)$_2$ with 1 equiv. of L^1 (i) generated a THF-solvated bimetallic (pyrrolylaldiminato)yttrium monoalkyl complex of central symmetry. In this process, L^1 is deprotonated by the yttrium trialkyl and its imino

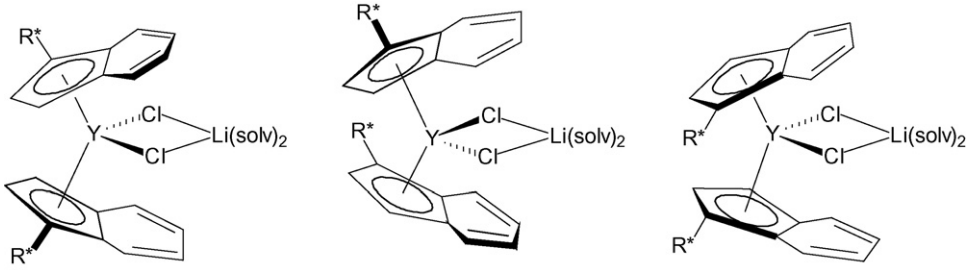

Scheme 100.

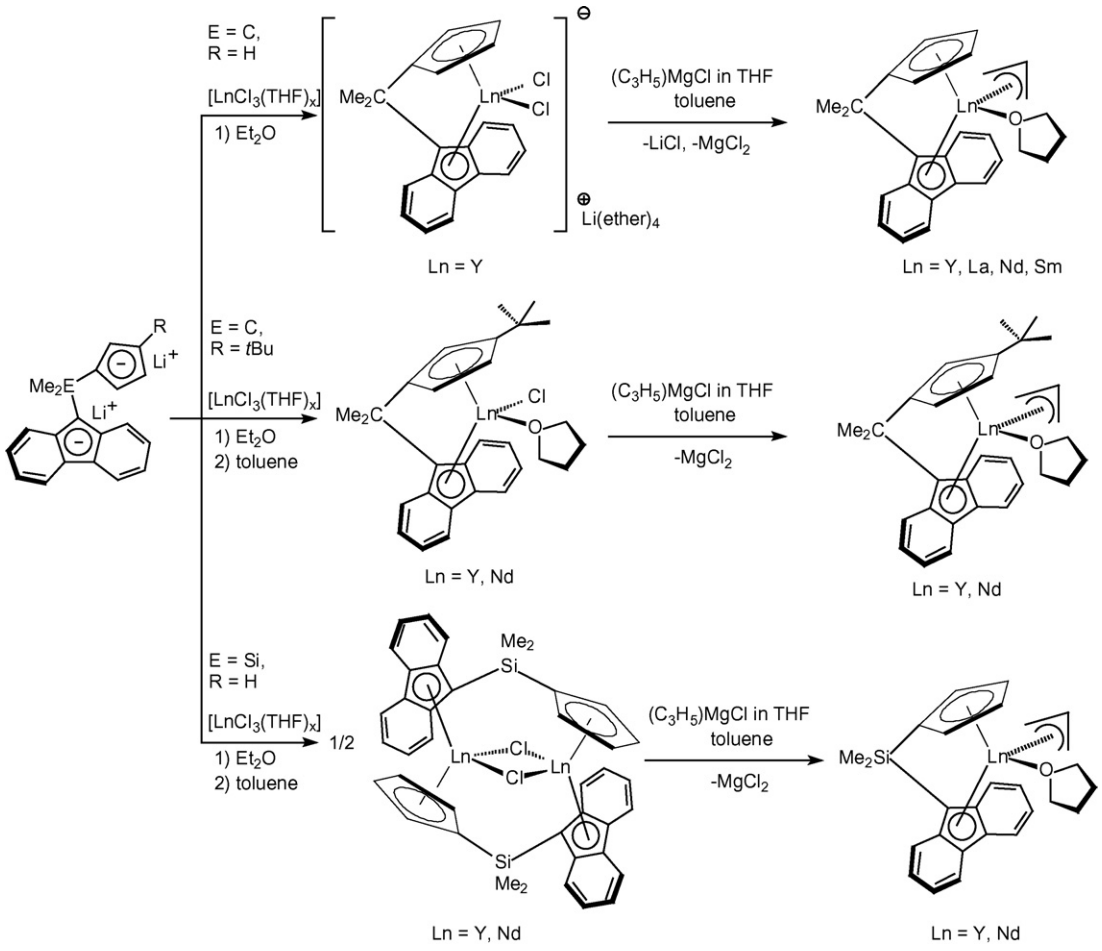

Scheme 101.

C=N group is reduced to C–N by intramolecular alkylation, generating dianionic species that bridge two yttrium alkyl units in a unique $\eta^5/\eta^1{:}\kappa^1$ coordination mode. In this complex the pyrrolyl rings behave like azacyclopentadienyl ligands. Similar treatment of $Y(CH_2SiMe_3)_3(THF)_2$ with 2 equiv. of L^1 selectively afforded a monomeric bis(pyrrolylaldiminato)yttrium monoalkyl complex. Subsequent amination with 2,6-diisopropylaniline gave the corresponding yttrium amido complex. In this compound the pyrrolide ligands are monoanionic and bind to the central yttrium atom in an $\eta^1{:}\kappa^1$ coordination mode. Finally, the homoleptic tris($\eta^1{:}\kappa^1$-pyrrolylaldiminato)yttrium complex was isolated when the molar ratio of L^1 to $Y(CH_2SiMe_3)_3(THF)_2$ was increased to 3:1. All products shown in Scheme 105 were structurally characterized by X-ray diffraction. As an example, the molecular structure of the unusual binuclear complex is shown in Fig. 19 [72].

Closely related pyrrolide-supported lanthanide alkyl complexes were also reported for scandium and lutetium [73]. The ligand HL^1 reacted readily with 1 equiv. of the lanthanide tris(alkyls) $Ln(CH_2SiMe_3)_3(THF)_2$, affording lanthanide bis(alkyl) complexes $L^1Ln(CH_2SiMe_3)_2(THF)_n$ (Ln = Lu, $n = 2$; Ln = Sc, $n = 1$) *via* alkane elimination. Surprisingly, the bulkier ligand HL^2 reacts with $Ln(CH_2SiMe_3)_3(THF)_2$ to give the bis(pyrrolylaldiminato) lanthanide mono(alkyl) complexes $L^2{}_2Ln(CH_2SiMe_3)(THF)$ (Ln = Lu, Sc), selectively (Scheme 106) [73].

In a similar manner, the *N*,*N*-bidentate ligand HL^3, 2-dimethylaminomethylpyrrole, reacted with $Ln(CH_2SiMe_3)_3(THF)_2$ under formation of bimetallic bis(alkyl) complexes of central symmetry (Scheme 107). The reaction presumably proceeds *via* a monomeric bis(alkyl) intermediate A. All three compounds (Ln = Sc, Y, Lu) were isolated as colorless crystals in moderate yields [73].

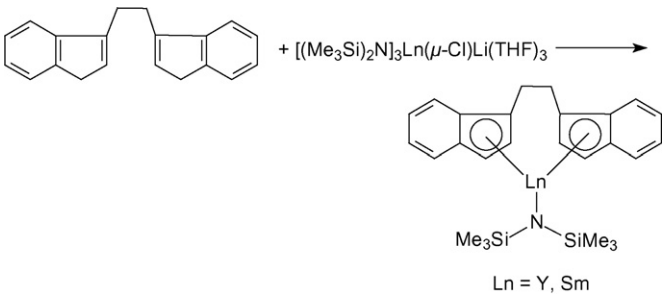

Scheme 102.

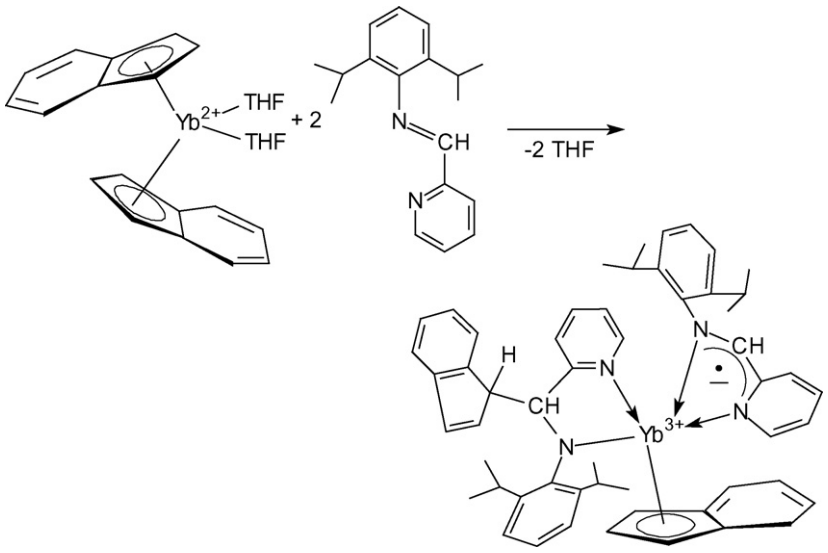

Scheme 103.

Treatment of the *N*,*N*,*N*,*N*-tetradentate ligand HL^4, 2,2′-bis(dimethylpropyldiimino)methylpyrrole, with equimolar amounts of $Ln(CH_2SiMe_3)_3(THF)_2$ afforded a C_2-symmetric binuclear complex as illustrated in Scheme 108. A plausible reaction pathway proceeds *via* the intermediates B and C. The compounds shown in Schemes 107 and 108 represent rare examples of THF-free binuclear lanthanide bis(alkyl) complexes supported by non-cyclopentadienyl ligands [73].

The reactivity of the related *N*,*N*,*P*-tridentate ligand 2-[(*N*-2-diphenylphosphinophenyl)iminomethyl)]pyrrole (L^2) toward $Y(CH_2SiMe_3)_3(THF)_2$ was also investigated. As shown in Scheme 109, reaction of L^2 with equimolar $Y(CH_2SiMe_3)_3(THF)_2$ afforded an asymmetric binuclear complex *via* two probable intermediates. The dianionic *N*,*N*,*P*-tridentate moieties derived from L^2 coordinate to the yttrium atoms in $\eta^5/\eta^1{:}\kappa^2$ modes, generating tetrahedral and trigonal/pyramidal geometry around the two metal centers, respectively. In these molecules, both alkylation of the imino C=N group of ligand L^2 and the pyrrole's ability to act similar to a heterocyclopentadienyl moiety were also found (Fig. 20) [72].

Pyrrolyl π-coordination was also found in a dinuclear ytterbium complex of the novel chiral (*R*)-bis(pyrrol-2-ylmethyleneamino)-1,1′-binaphthyl ligand. The synthetic routes leading to this complex are summarized in Scheme 110 [74].

In the course of extending the metallocene chemistry of "non-classical" divalent lanthanides, the synthesis and reactivity of organometallic complexes of divalent thulium with bulky phospholyl ligands have been investigated. The previously described Tm^{II} complex $(Dtp)_2Tm$ (Dtp = 2,5-di-*tert*-butyl-3,4-dimethylphospholyl) and the new, homoleptic, structurally charac-

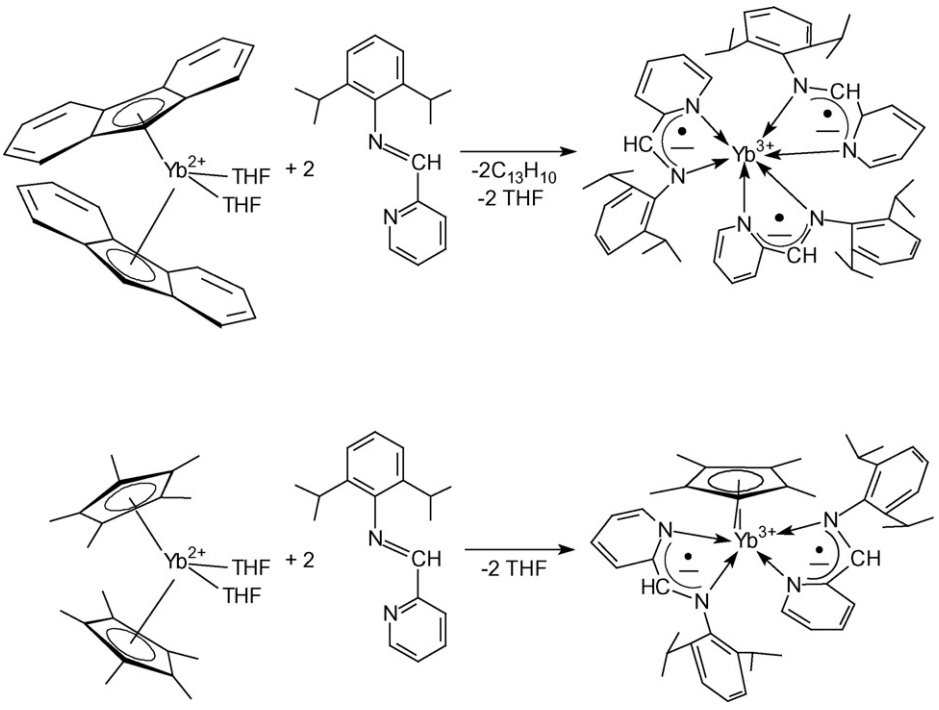

Scheme 104.

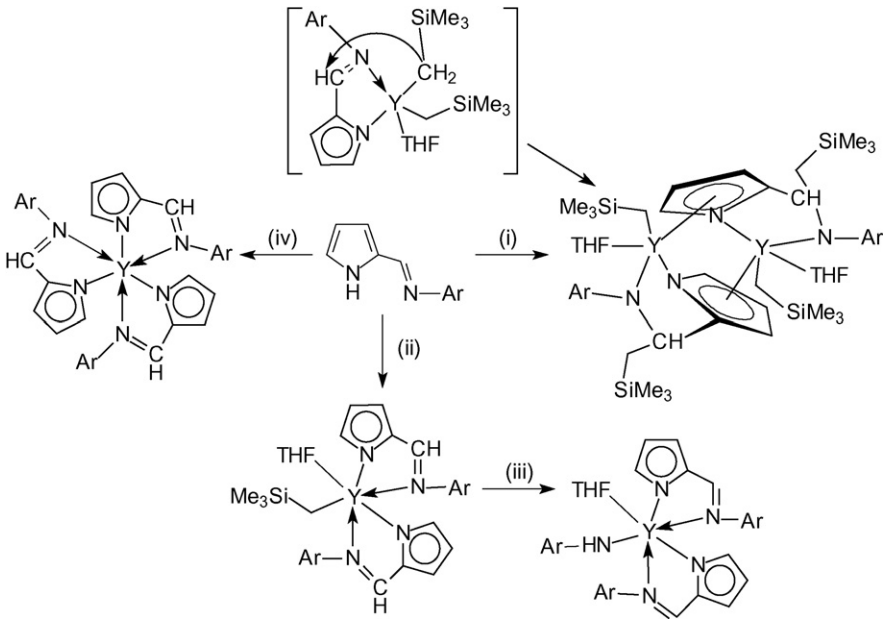

Scheme 105. Reagents and conditions: Ar = $C_6H_3{}^iPr_2$-2,6, toluene, r.t., 24 h; (i) 1 equiv. of $Y(CH_2SiMe_3)_3(THF)_2$; (ii) 1/2 equiv. of $Y(CH_2SiMe_3)_3(THF)_2$; (iii) 2,6-$^iPr_2C_6H_3NH_2$, 6 h; (iv) 1/3 equiv. of $Y(CH_2SiMe_3)_3(THF)_2$.

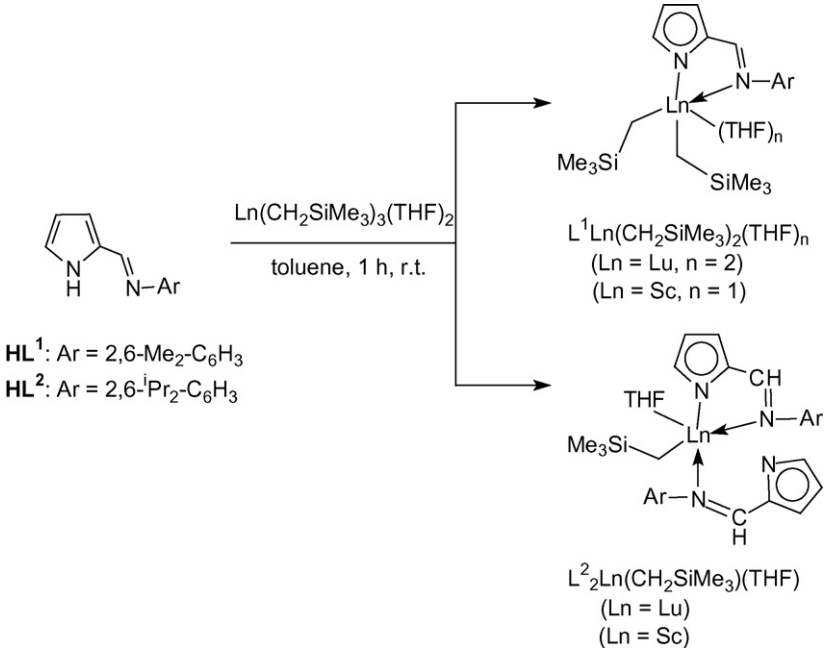

Scheme 106.

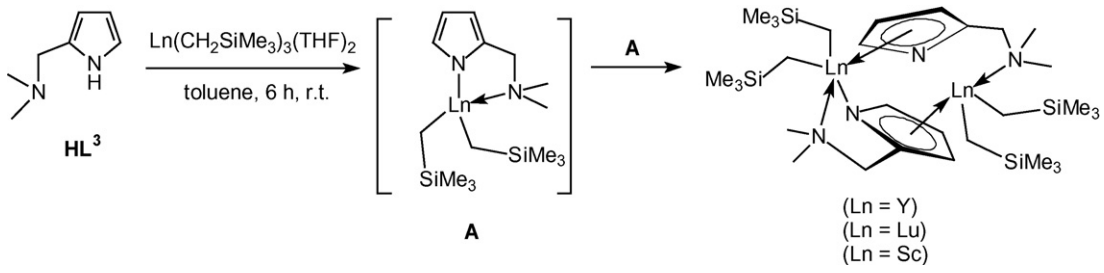

Scheme 107.

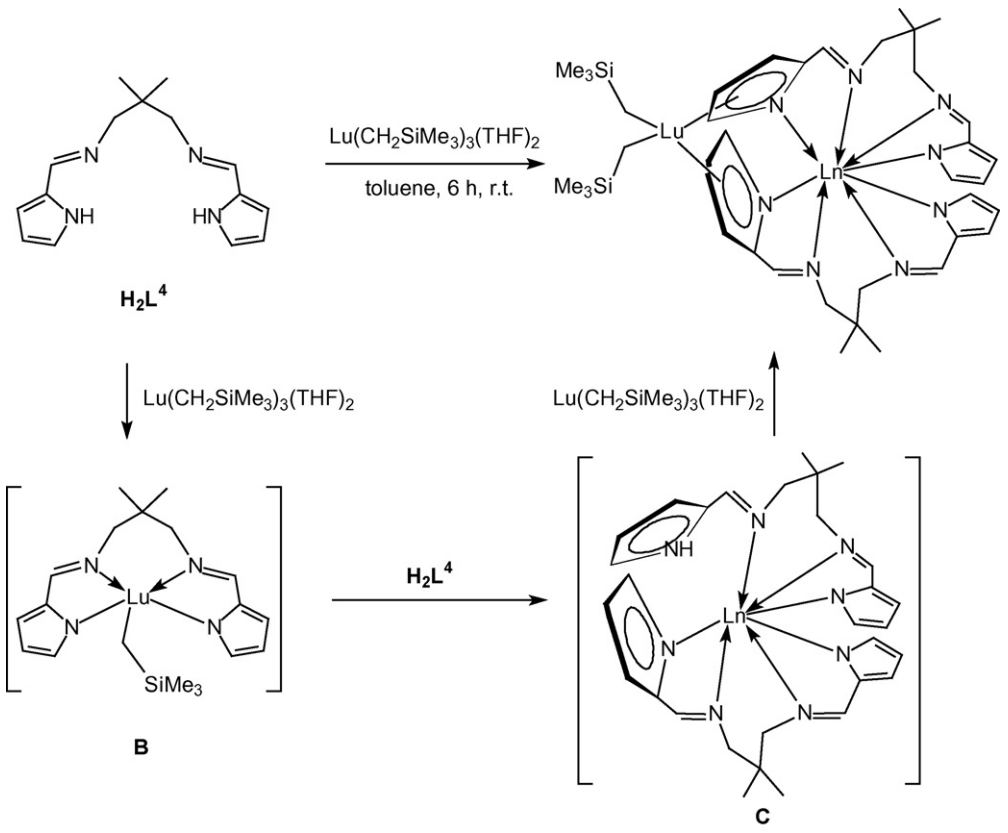

Scheme 108.

terized Tm^{II} dimer $[(Htp)_2Tm]_2$ (Htp = 2,5-di-*tert*-butylphospholyl) were prepared by KC_8 reduction of $(Dtp)_2TmI$ and $[(Htp)_2TmI]_2$, respectively (Scheme 111). A subsequent reaction of $(Dtp)_2Tm$ with pyridine gave no isolable complexes. An NMR study suggested that initially a simple Tm^{II} adduct such as $(Dtp)_2Tm$(pyridine) is formed in this reaction [28].

The chemistry of organolanthanide complexes containing bulky phospholyl ligands has been expanded by a study of the synthesis, characterization, and reactivity of mono(phospholyl)lanthanide(III) bis(dimethylaminobenzyl) complexes. Reaction of potassium 2,5-di-*tert*-butyl-3,4-dimethylphospholide, K(Dtp) with YCl_3 or $SmI_3(THF)_{3.5}$ in THF followed by reaction with *o*-

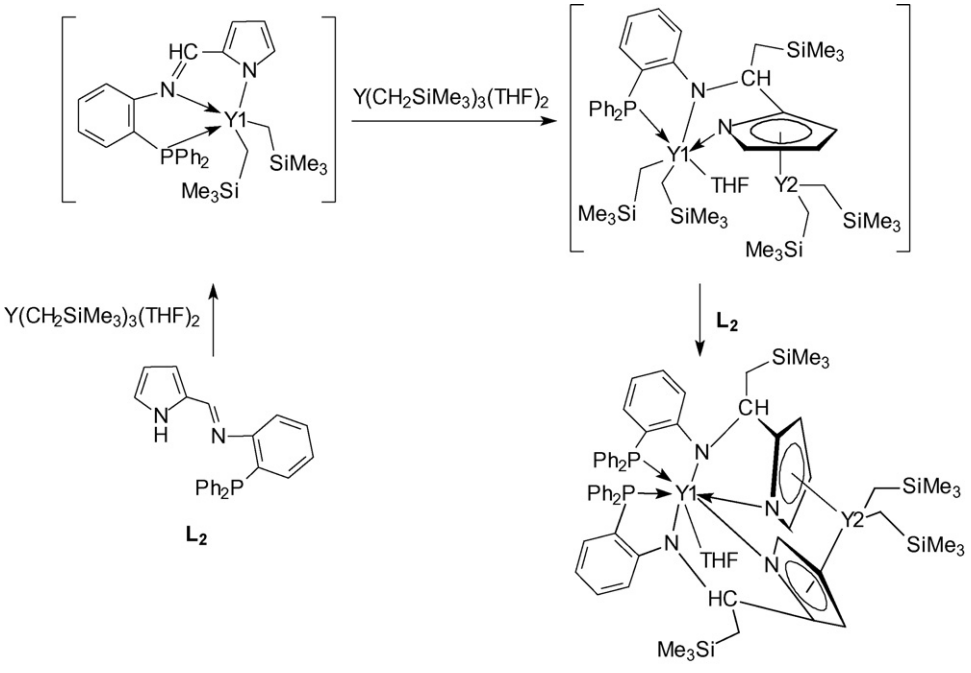

Scheme 109.

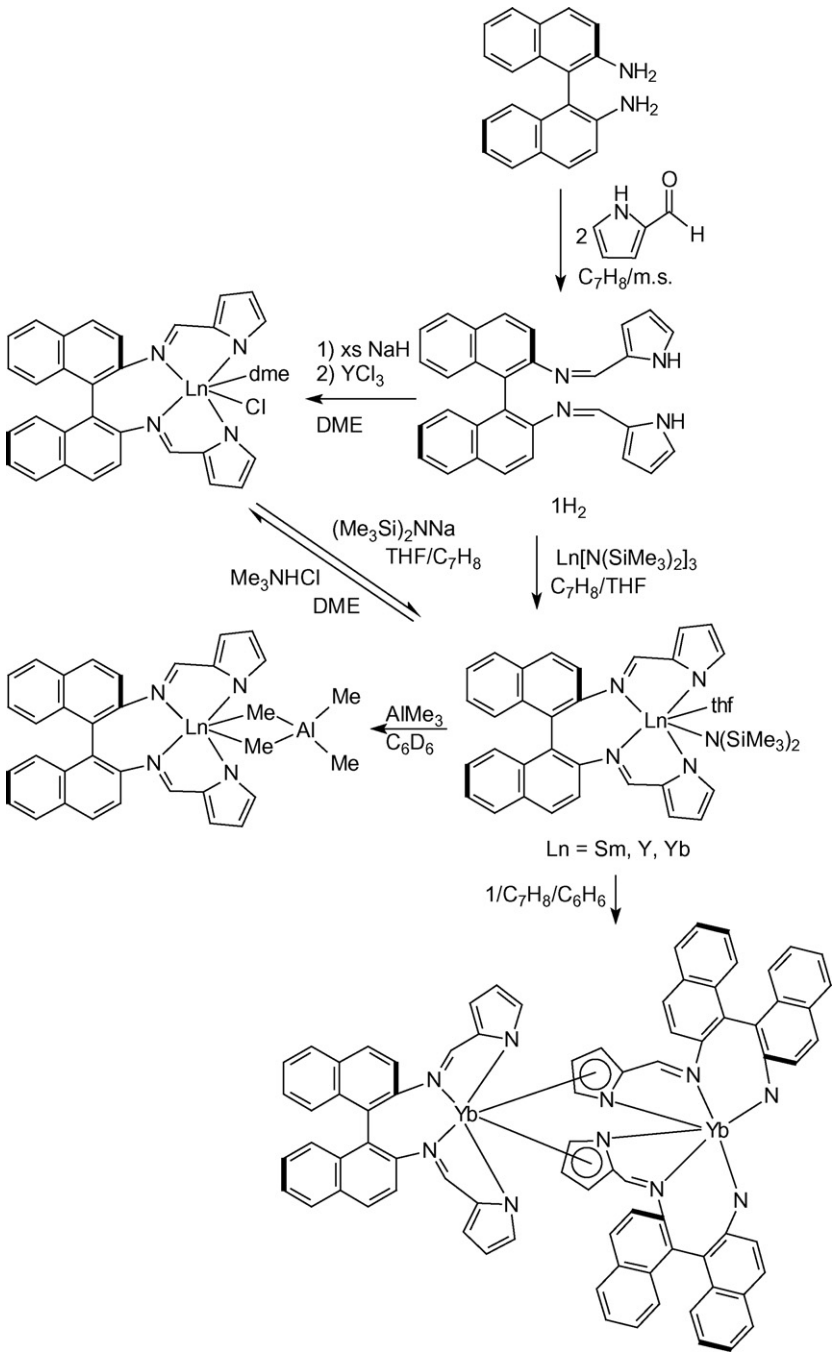

Scheme 110.

dimethylaminobenzylpotassium, $K(CH_2C_6H_4NMe_2\text{-}o)$, afforded the solvent-free mono(phospholyl)lanthanide bis(benzyl) complexes $(Dtp)Ln(CH_2C_6H_4NMe_2\text{-}o)$ (Scheme 112, Ln = Y, Sm) [75].

The Sc analogue could not be obtained under the same conditions, as the reaction between K(Dtp) and $ScCl_3$ in THF led to the THF-ring-opened product $[Sc\{\mu\text{-}O(CH_2)_4(Dtp)\}Cl_2(THF)_2]_2$. Replacement of THF by a mixture of toluene and pyridine gave $(Dtp)ScCl_2$(pyridine), which on further reaction with $K(CH_2C_6H_4NMe_2\text{-}o)$ in toluene afforded $(Dtp)Sc(CH_2C_6H_4NMe_2\text{-}o)_2$ (Scheme 113) [75].

The same scandium bis(benzyl) complex, $(Dtp)Sc(CH_2C_6H_4NMe_2\text{-}o)_2$, could also be isolated by an alternative route shown in Scheme 114. In this case, protonation of K(Dtp) with p-toluenesulfonic acid first gave the 1H-phosphole Dtp-H, which could not be isolated pure, but is stable in solution at room temperature. A subsequent reaction between *in situ*-prepared Dtp-H and $Sc(CH_2C_6H_4NMe_2\text{-}o)_3$ in toluene produced $(Dtp)Sc(CH_2C_6H_4NMe_2\text{-}o)_2$ [75].

2.6.2. Compounds with carboranyl ligands

A large series of mixed-ligand complexes containing both pentadienyl (="open cyclopentadienyl") and carborane ligands were synthesized by a two-step procedure illustrated in Scheme 115. All products were isolated as crystalline solids in 75–88% yield and fully characterized by spectroscopic methods and X-ray diffraction analyses [76].

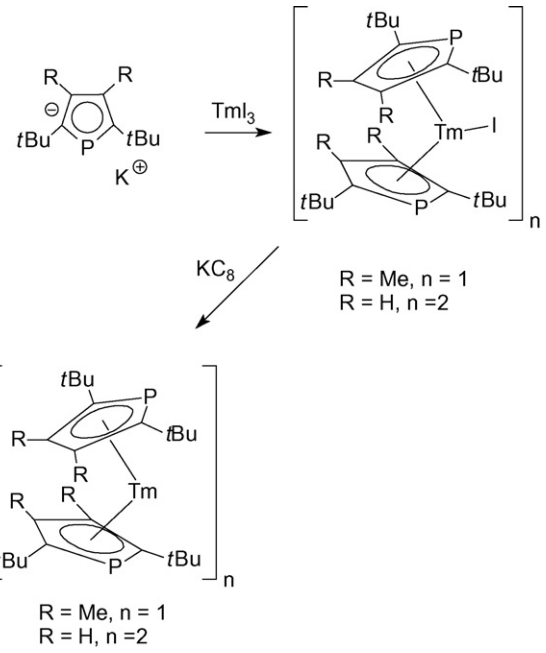

Scheme 111.

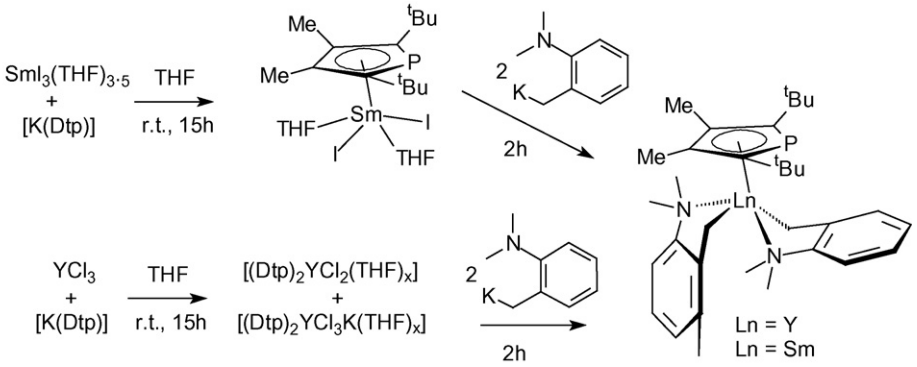

Scheme 112.

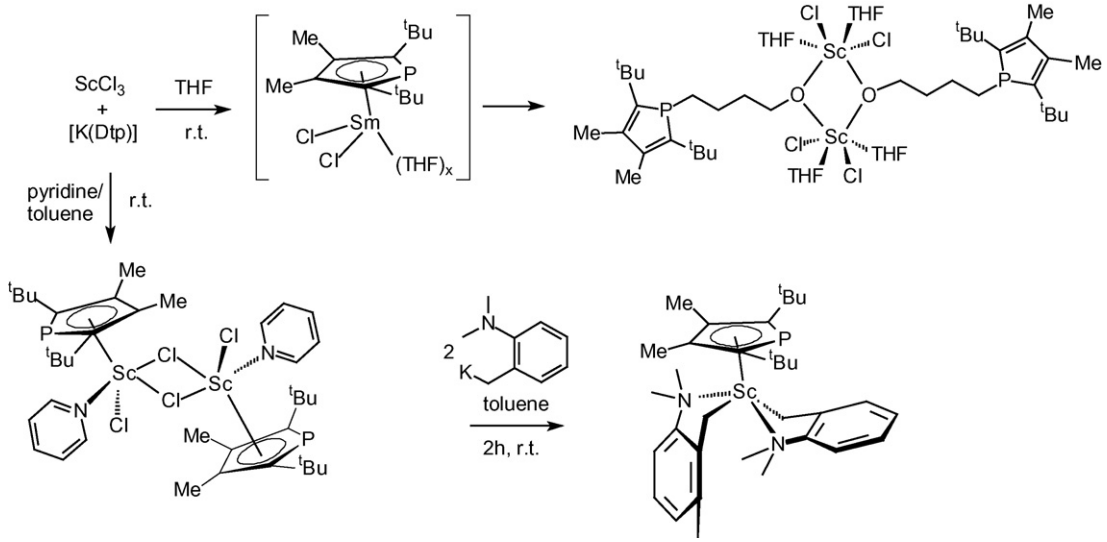

Scheme 113.

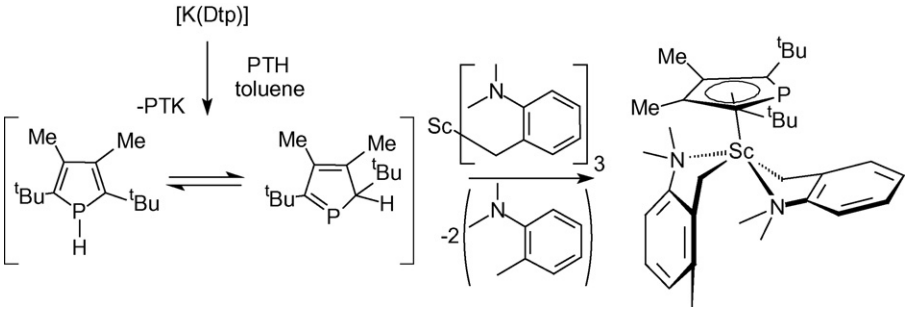

Scheme 114.

2.7. Lanthanide arene complexes

Stern–Gerlach experiments of the one-dimensional metal-benzene sandwich clusters $M_n(C_6H_6)_m$ (M = Al, Sc, Ti, V) have been reported. A molecular beam of the multilayer scandium-benzene organometallic clusters $Sc_n(C_6H_6)_m$ was produced by a laser vaporization method, and their magnetic deflections were measured. The multidecker sandwich clusters $Sc_n(C_6H_6)_{n+1}$ (n = 1, 2) possess magnetic moments that increase monotonously with n. These sandwich species represent a new class of one-dimensional molecular magnets in which the scandium atoms are formally zero-valent [77].

A family of novel isolable solvent-separated organoscandium methyl cations stabilized by β-diketiminato ligands, ArNC(Me)CHC(Me)NAr (=L^{Me}, Ar = $C_6H_3{}^iPr_2$-2,6) was prepared as illustrated in Scheme 116 by reaction of $L^{Me}ScR_2$ with $[Ph_3C][B(C_6F_5)_4]$ in the presence of an arene solvent. Arenes such as bromobenzene, benzene, toluene, *para*-xylene and mesitylene bind the scandium center in an η^6-bonding mode, yielding the cations shown in Scheme 116. Their solution and solid-state structures were explored using multinuclear NMR spectroscopy and X-ray crystallography. As a typical example, the cationic part of the η^6-mesitylene complex is shown in Fig. 21 [78].

Quantitative kinetic experiments for arene exchange from the η^6-mesitylene complex to the η^6-toluene derivative were performed. The results imply a partially dissociative mechanism as illustrated in Scheme 117 whereby the rate limiting step involves dissociation to lower hapticity [78].

The mechanism for arene displacement was further investigated upon exploring the reactivity of these solvent-separated ion-pairs with diphenylacetylene (Scheme 118). It was determined that rate limiting coordination of the alkyne to the metal center had a slightly higher barrier than arene ring slipping. On a preparative scale, the alkyne insertion product could be isolated in 61% yield [78].

DFT and hybrid HF-DFT studies were carried out to elucidate structure and bonding in the hypothetical triple-decker sandwich complexes $CpM(P_6)MCp$ with a P_6 middle ring ranging from 18 to 28 valence electrons. The scandium complexes $CpSc(P_6)ScCp$, $(C_2P_3H_2)Sc(C_3P_3H_3)Sc(C_2P_3H_2)$, $[CpSc(C_3B_3H_6)ScCp]^+$, and $CpSc(P_3B_3H_3)ScCp]^-$ were also investigated in this study [79].

Lanthanide π-arene interactions were also detected in several other rare-earth metal coordination compounds which are

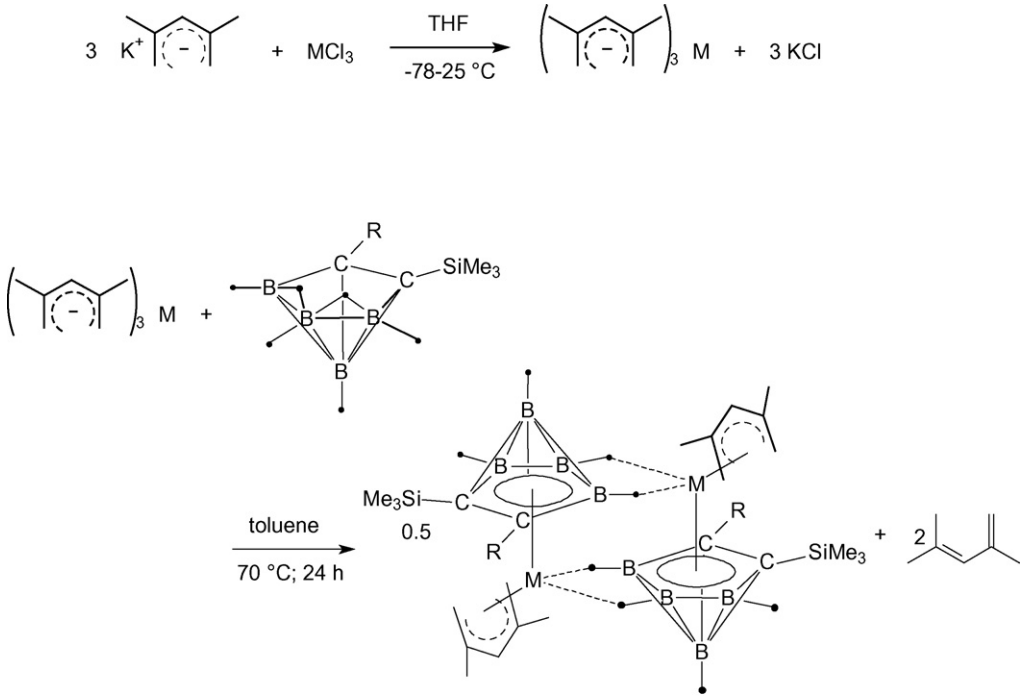

Scheme 115.

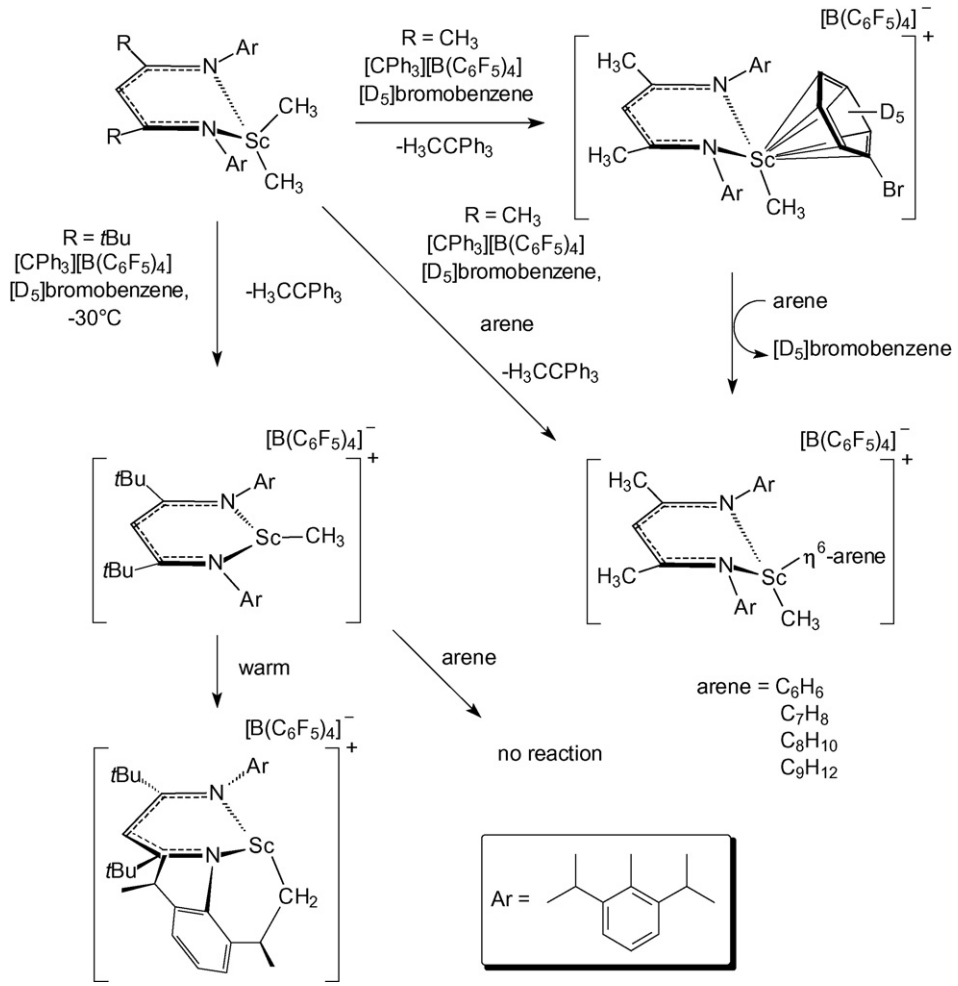

Scheme 116.

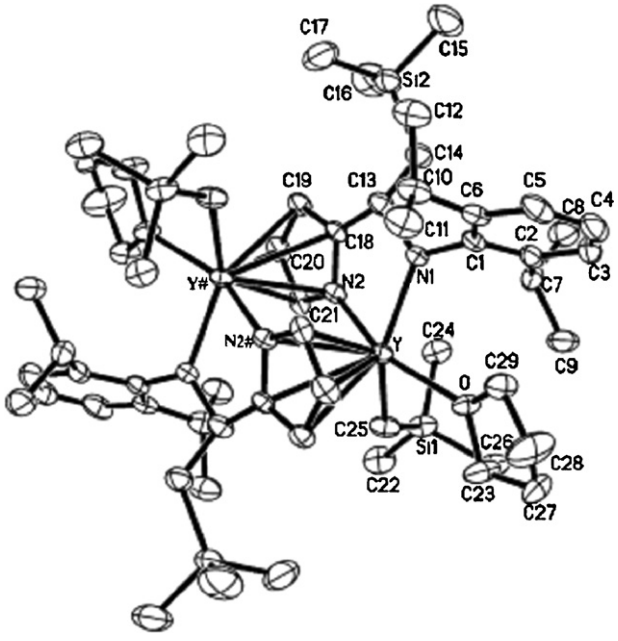

Fig. 19. Molecular structure of [{2-(2,6-^{i}Pr$_2$C$_6$H$_3$NC(H)(CH$_2$SiMe$_3$))C$_4$H$_3$N}-Y(CH$_2$SiMe$_3$)(THF)]$_2$ [72].

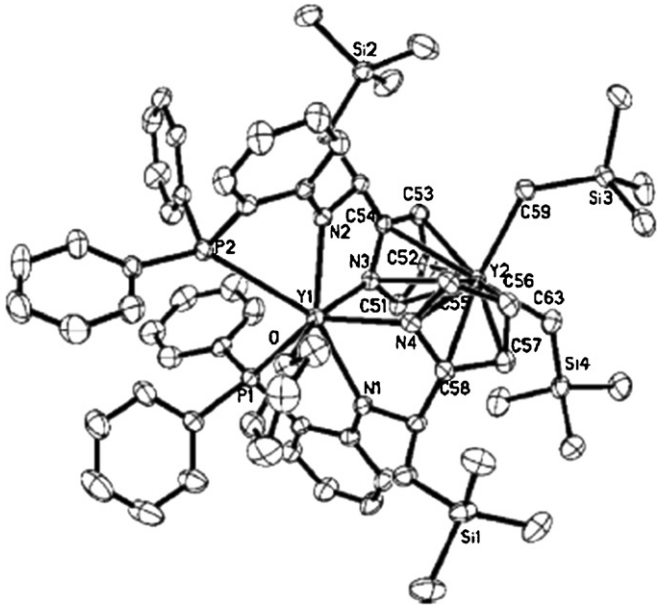

Fig. 20. Molecular structure of [2-(2-Ph$_2$PC$_6$H$_3$NC(H)(CH$_2$SiMe$_3$))C$_4$H$_3$N]$_2$Y$_2$-(CH$_2$SiMe$_3$)$_2$(THF) [72].

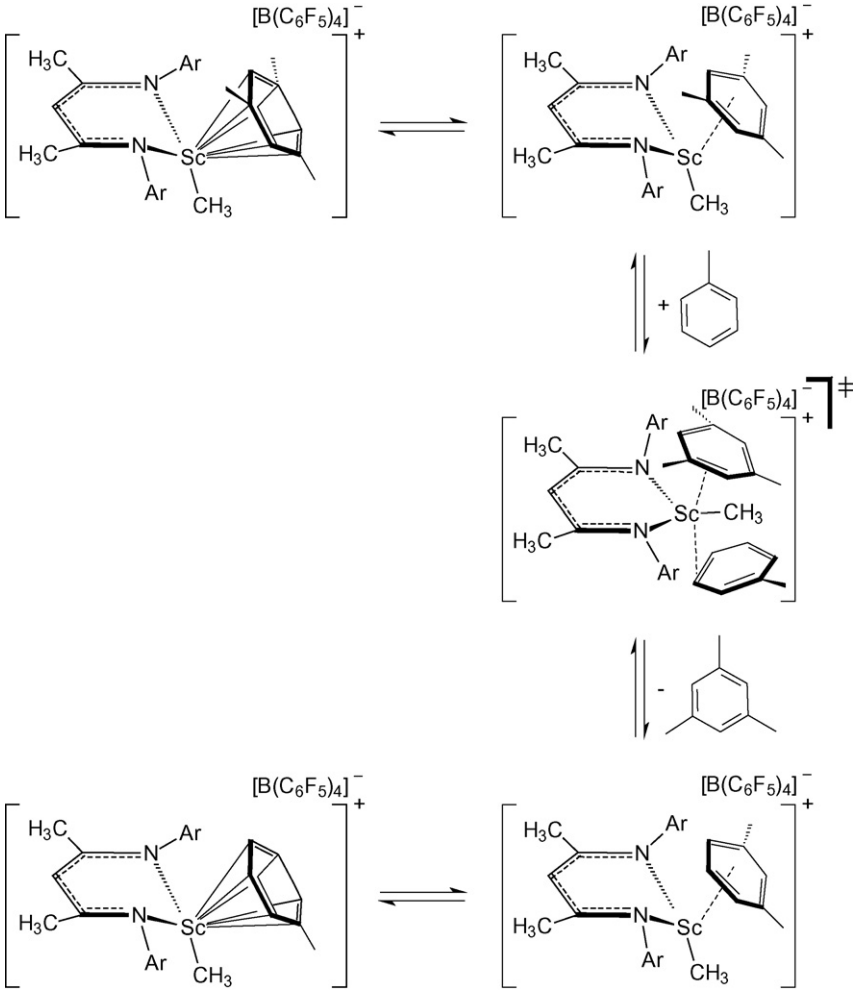

Scheme 117.

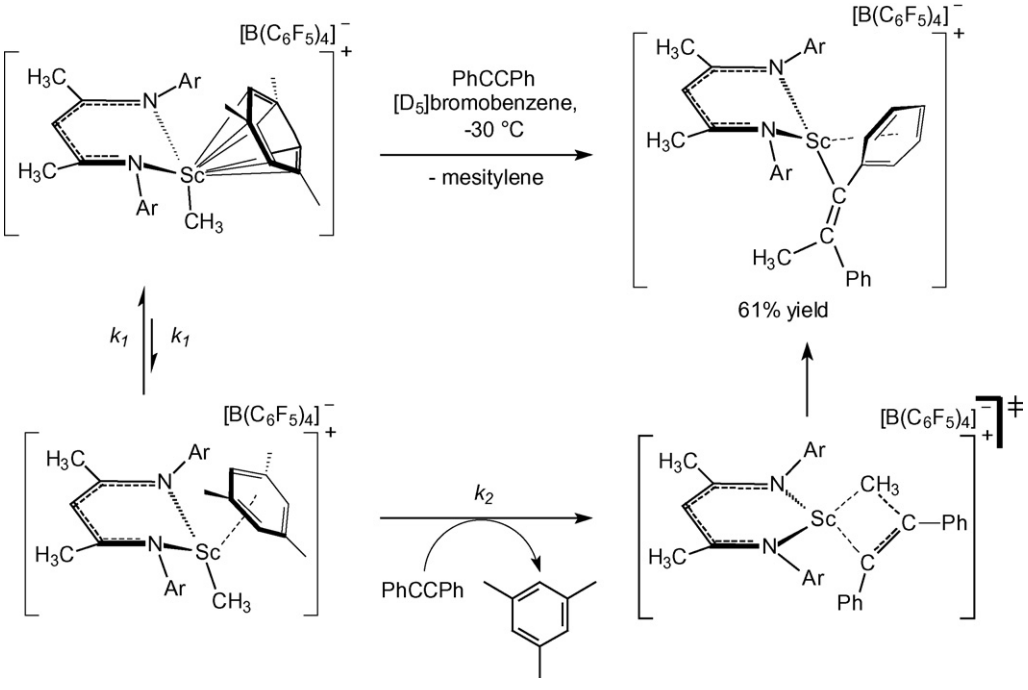

Scheme 118.

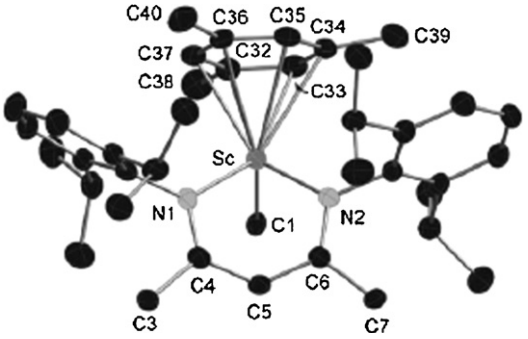

Fig. 21. Molecular structure of the cation in $[L^{Me}ScMe(\eta^6\text{-mesitylene})][B(C_6F_5)_4]$ [78].

not organometallic compounds in the strict sense. For example, the amine-elimination reaction of a tripodal triamine ligand with $Sm[N(SiMe_3)_2]_3$ according to Scheme 119 produced the tripodal triamido Sm complex $\{MeSi[SiMe_2N(4\text{-}MeC_6H_4)]_3Sm\}_2$ involving coordination of the samarium centers to two aryl rings in an η^6-fashion (Fig. 22) [80].

Yet another lanthanide coordination compound in which π-arene was found is a member of a series of lanthanide(II) guanidinate complexes containing the very bulky Giso ligand (Giso = $[(ArN)_2CN(C_6H_{11})]^-$, Ar = $C_6H_3Pr^i_2$-2,6). The synthetic routes leading to such compounds are summarized in Scheme 120 [81].

Desolvation of the THF-coordinated dimeric ytterbium(II) iodide derivative affords an iodide-bridged dimer in which the Giso$^-$ ligands have arranged upon THF desolvation to "chelate" the ytterbium centers *via* η^1-amide and η^6-arene interactions (Fig. 23) [81].

2.8. Lanthanide cyclooctatetraenyl complexes

The synthesis and structural characterization of mononuclear lutetium imido complexes with very short Lu–N bonds was achieved using a novel imidazolin-2-iminato ligand in a half-sandwich cyclooctatetraenyl lanthanide coordination environment. The starting material 1,3-bis(2,6-diisopropylphenyl)imidazolin-2-imine (=$Im^{Dipp}NH$) was synthesized according to a published procedure from the corresponding Arduengo-carbene 1,3-bis(2,6-diisopropylphenyl)imidazolin-2-ylidene by reaction with trimethylsilyl azide, followed by desilylation of the $Im^{Dipp}N$–$SiMe_3$ intermediate in methanol (Scheme 121). Reaction of the resulting imine $Im^{Dipp}NH$ with trimethylsilylmethyllithium and anhydrous $LuCl_3$ in THF solution afforded the lutetium complex $LuCl_2(NIm^{Dipp})(THF)_3$ as a colorless crystalline solid in 69% yield after extraction with pentane (Scheme 121). Subsequent treatment of the dichloride with a THF solution of the dipotassium cyclooctatetraenide salt $K_2(C_8H_8)$ lead to formation of the COT lutetium complex $(COT)Lu(NIm^{Dipp})(THF)_2$ [82].

An unusual η^2-bound cyclooctatetraenyl lanthanide complex of an $\eta^5{:}\eta^1{:}\eta^1{:}\eta^5$-bound modified porphyrinogen has been prepared according to Scheme 122. The low hapticity of the bridging COT ligand as compared to the preferred η^8 binding mode is a result of steric pressure displayed by the macrocyclic ligand. In contrast, when the auxiliary ligand is the smaller cyclopentadienyl ligand, η^5-coordination is achieved through distortion of the macrocycle, leading to a reduction in its hapticity to $\eta^5{:}\eta^1{:}\eta^1{:}\eta^1$ binding (*cf.* Section 2.5.2) [33].

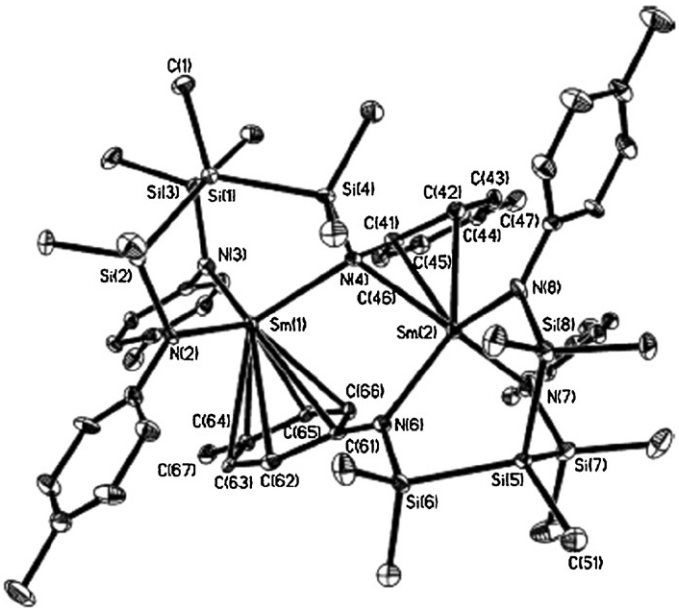

Fig. 22. Molecular structure of $\{MeSi[SiMe_2N(4\text{-}MeC_6H_4)]_3Sm\}_2$ [80].

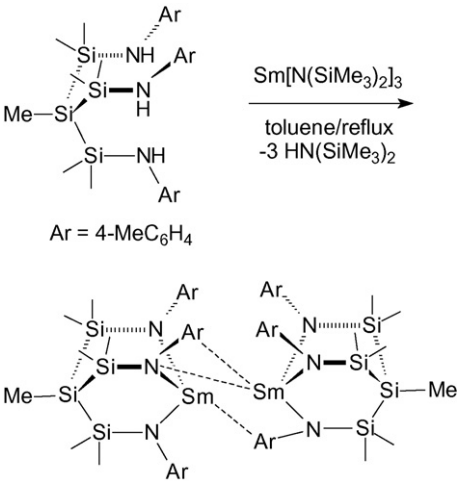

Scheme 119.

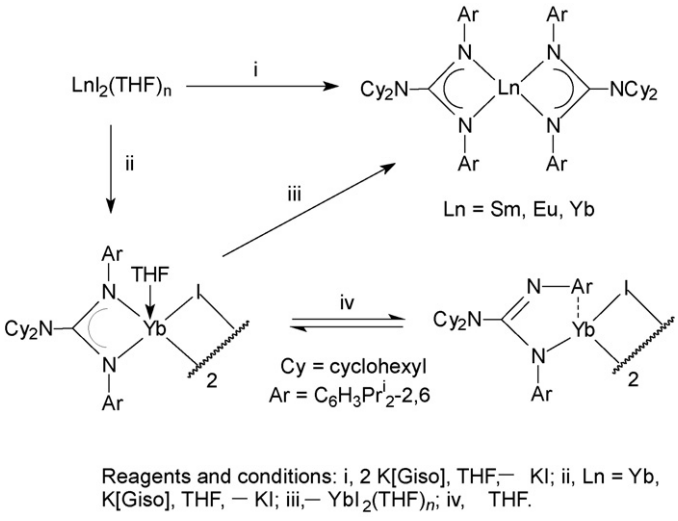

Scheme 120.

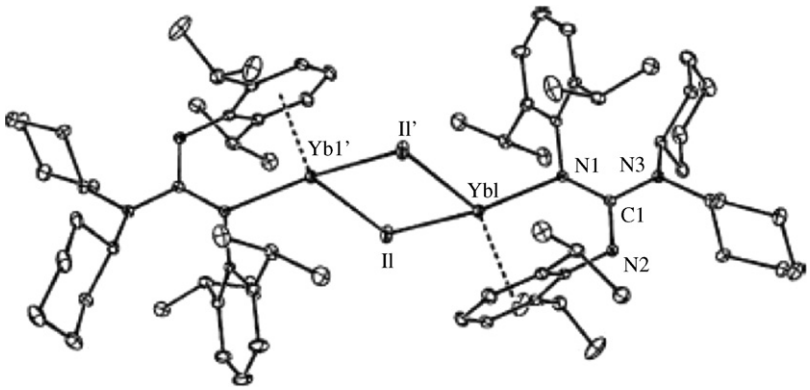

Fig. 23. Molecular structure of $[(Giso)Yb(\mu\text{-}I)]_2$ [81].

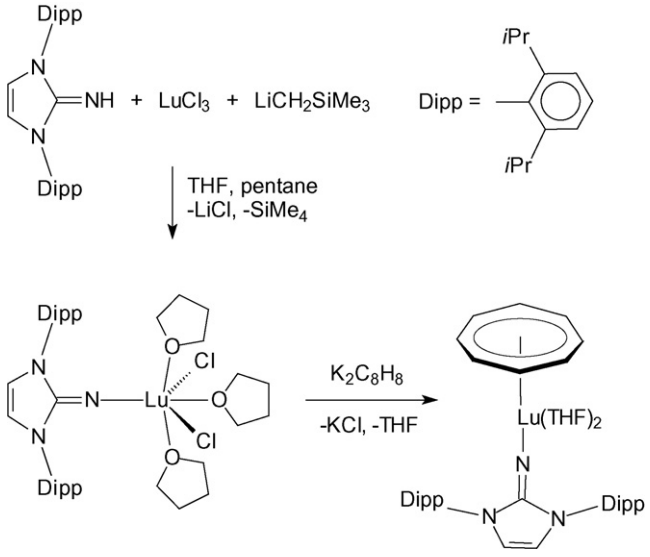

Scheme 121.

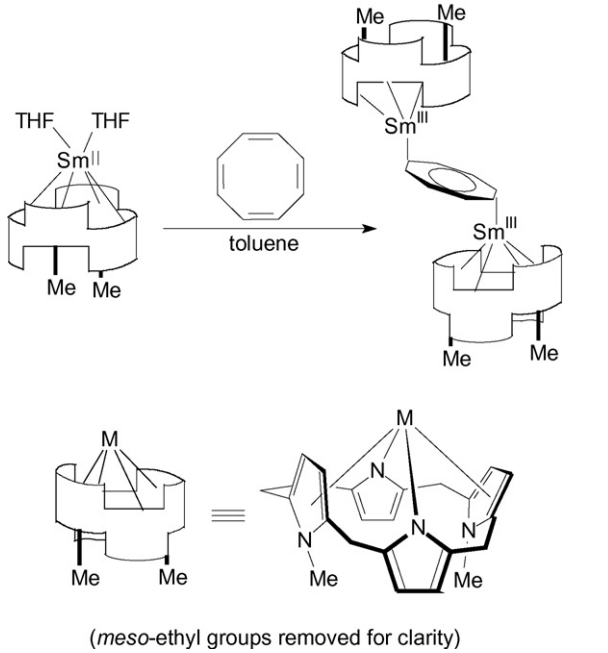

Scheme 122.

Use of the bulky 1,4-bis(trimethylsilyl)cyclooctatetraenyl ligand (=COT″) allowed the synthesis of a unique organolanthanide cluster. The reaction of anhydrous $PrCl_3$ with $Li_2(COT'')$ in THF solution as illustrated in Scheme 123 afforded the unprecedented cluster-centered Pr/Li multidecker sandwich complex of composition $[Pr(COT'')]_2[Pr_2(COT'')_2]_2Li_2(THF)_2Cl_8$ which was isolated as orange-yellow, needle-like crystals in 83% yield. According to the X-ray structural analysis (Fig. 24), a central cube of eight Cl atoms is capped by two $[Pr(COT'')]^+$ half-sandwich and two $[Pr_2(COT'')_2]^{2+}$ sandwich units as well as two $[Li(THF)]^+$ moieties [83].

The unprecedented ytterbium(II) tetra-decker complex $Cp^*Yb(\mu\text{-}\eta^8,\eta^8\text{-}COT''')Yb(\mu\text{-}\eta^8,\eta^8\text{-}COT''')YbCp^*$ was synthesized according to Scheme 124 (forest-green crystals, 64% yield) and fully characterized by X-ray diffraction and spectroscopic methods, including ^{171}Yb NMR spectroscopy [84].

The X-ray study (Fig. 25) clearly established the presence of the first neutral tetra-decker sandwich complex of an *f*-element in which a central $[Yb(COT''')_2]^{2-}$ unit is extended on both sides by a $[YbCp^*]^+$ fragment. For the first time this molecule also offered the unique opportunity to directly observe two chemically nonequivalent ^{171}Yb nuclei in a single compound. The ^{171}Yb NMR spectrum of the tetra-decker sandwich complex in a THF-d_8 solution displayed two signals at δ 595 and 364 ppm in an intensity ratio of approximately 2:1, thereby allowing a clear assignment to the two different ^{171}Yb nuclei [84].

2.9. Lanthanide metallofullerenes

Endohedral metallofullerenes containing Group 3 and lanthanide metals continued to attract special attention as new spherical molecules with unique properties that are unexpected for empty fullerenes. Among these, scandium carbide endohedral metallofullerenes such as $Sc_2C_2@C_{84}$ and $Sc_3C_2@C_{80}$ are particularly interesting because of the encapsulation of the C_2 unit together with several metal atoms. For the metallofullerene Sc_2C_{84} three isomers (I, II, and III) have been isolated. The structure of the most abundant isomer of Sc_2C_{84}(III) was recently revised by a detailed ^{13}C NMR analysis to be in fact the scandium carbide metallofullerene $Sc_2C_2@C_{82}$. This was now further confirmed by a single-crystal X-ray analysis (Fig. 26) and density functional calculations. The latter confirmed that the structure is most stable when the encapsulated Sc_2C_2 moiety has a bent structure and the two Sc atoms are not equivalent. The electronic structure can be described as $(Sc_2C_2)^{4+}C_{82}^{4-}$ as a result of four-electron transfer from Sc_2C_2 to C_{82} [85].

To restrain the disorder of $Sc_2C_2@C_{82}$(III) in the crystal lattice, chemical functionalization was performed by the irradiation of an o-dichlorobenzene/toluene solution of $Sc_2C_2@C_{82}$(III) and an excess molar amount of 2-adamantane-2,3-[3*H*]-diazirine in a

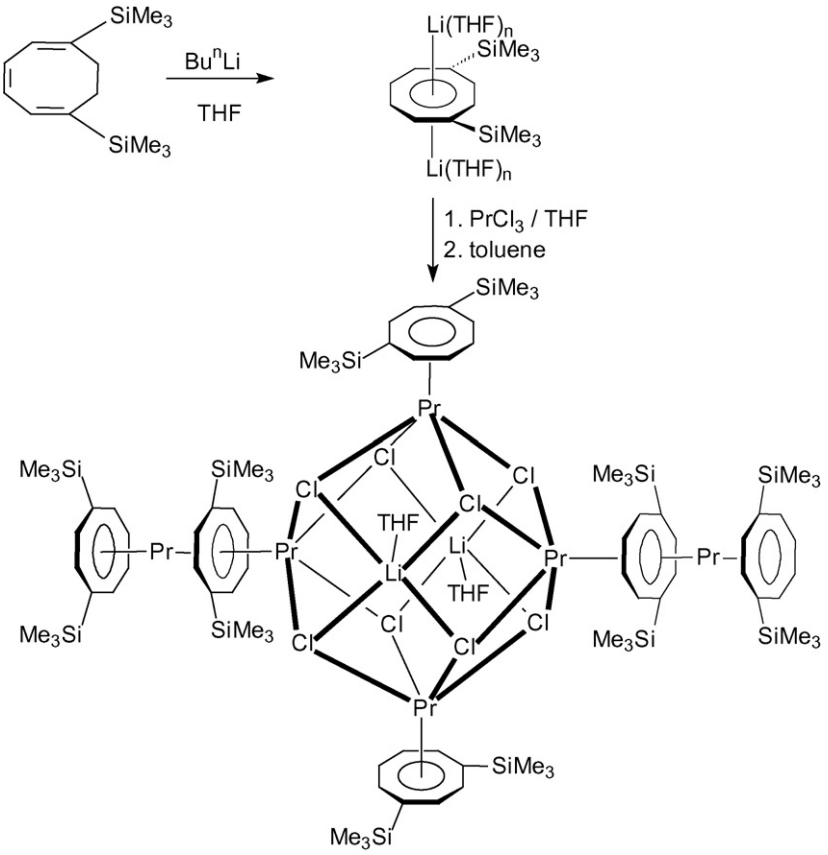

Scheme 123.

degassed sealed tube at room temperature using a high-pressure mercury-arc lamp. The resultant cycloadduct of $Sc_2C_2@C_{82}$(III) and adamantylidene carbene (Ad), $Sc_2C_2@C_{82}$(Ad), was purified by preparative HPLC and isolated as black crystals. MALDI-TOF mass analysis of the purified sample exhibited a single molecular ion peak. The structure of $Sc_2C_2@C_{82}$(Ad), determined by single-crystal X-ray analysis, is shown in Fig. 27. The adduct results from the 5,6-addition of Ad and has an opened structure with the carbon cage clearly originating from the C_{3v} isomer of C_{82} and not C_{84} [85].

The C_{80} fullerene cage can be used to realize confinement with the highest possible icosahedral (I_h) symmetry. As examples, $La_2@C_{80}$ and $Sc_3C_2@C_{80}$ are molecules in which metal dimers and trimers are encapsulated within the C_{80} cage. They have been purified in substantial amounts by using high performance liquid

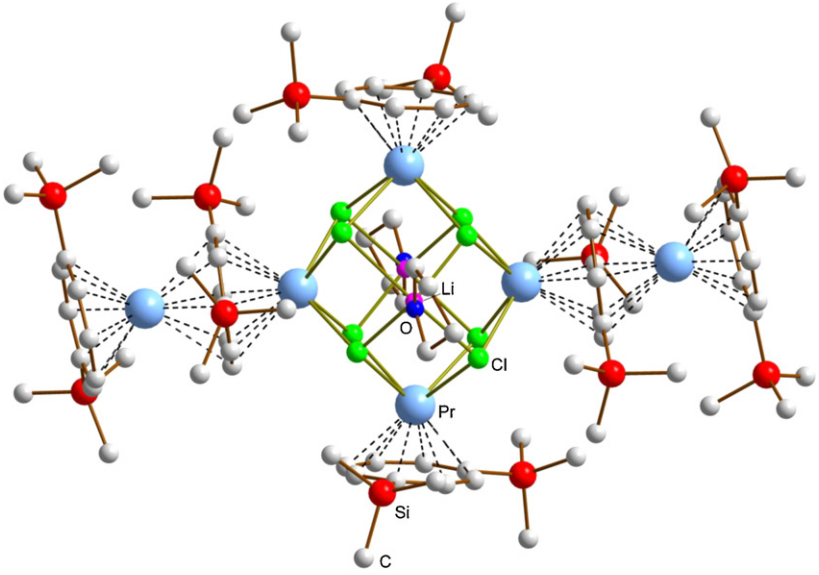

Fig. 24. Molecular structure of $[Pr(COT'')]_2[Pr_2(COT'')_2]_2Li_2(THF)_2Cl_8$ [83].

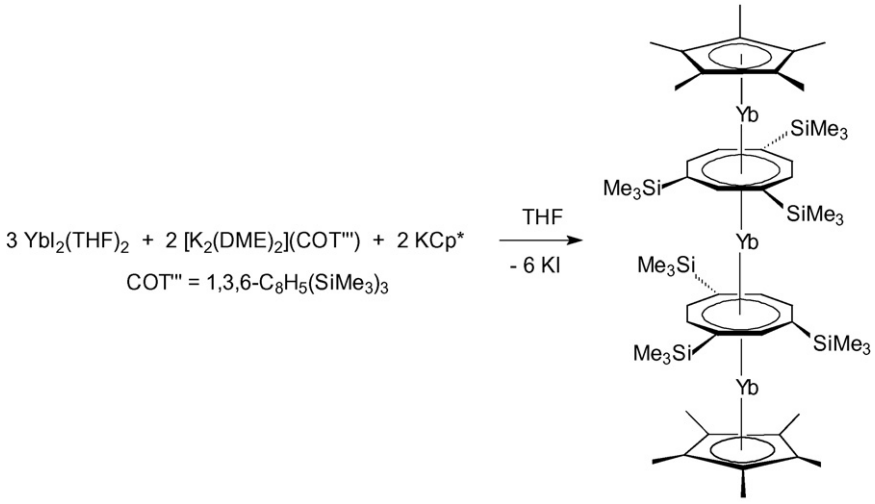

Scheme 124.

chromatography (HPLC), and studied by spectroscopy and X-ray diffraction. The confinement of the metal cluster within the high symmetry (I_h) cage is reflected in their specific potential of the intra-molecular rotation for the cluster. The results of electron spin resonance (ESR) measurements indicated that the intra-molecular potential is modified by the chemical modification of the C_{80} cage as well as by the injection of an excess electron [86].

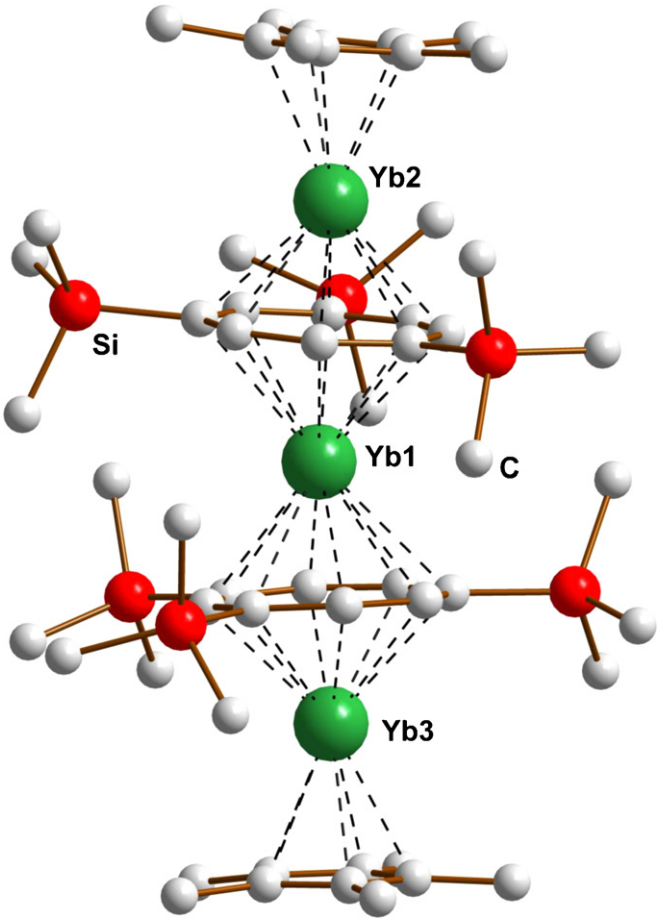

Fig. 25. Molecular structure of Cp*Yb(μ-η^8,η^8-COT'''')Yb(μ-η^8,η^8-COT'''')YbCp* [84].

2.10. Heterobimetallic organolanthanide complexes

Reactions of heterobimetallic Ln($AlMe_4$)$_3$ complexes (Ln = Y, La, Nd) with iminoamidopyridine ligands were found to afford novel heterobimetallic Ln/Al species. The ligand system HL^2 employed in this study is shown in Scheme 125 [87].

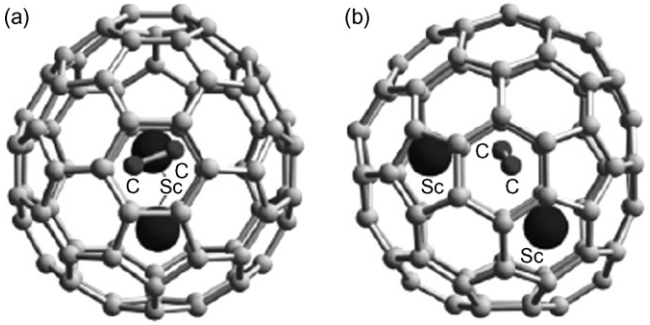

Fig. 26. The optimized structure of Sc_2C_2@C_{82}(III): (a) front view and (b) side view [85].

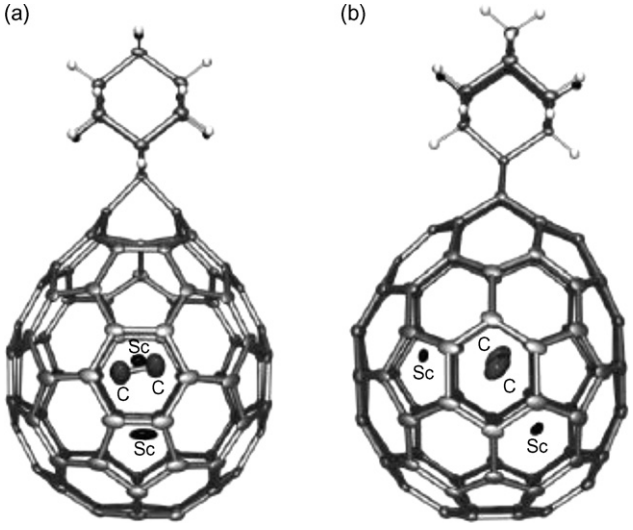

Fig. 27. ORTEP drawing of Sc_2C_2@C_{82}(Ad) with thermal ellipsoids shown at 50% probability level: (a) front view and (b) side view [85].

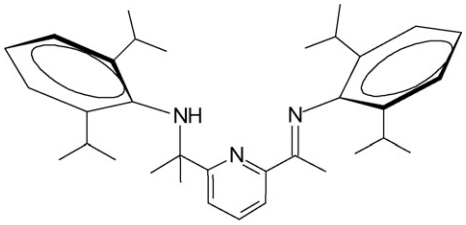

HL^2

Scheme 125.

Treatment of $Ln(AlMe_4)_3$ with pale yellow HL^2 according to Scheme 126 led to immediate reaction under gas evolution (CH_4) and formation of red solutions from which the wine-red heterometallic $LnAl_2$ products could be isolated in 49% (Y), 62% (La), and 52% (Nd) yield, respectively. A closer examination of the supernatant solutions enabled the isolation of two interesting aluminum by-products resulting from alkylation of the imino carbon atom (Scheme 126) [87].

Addition of THF to a suspension of the La/Al complex in hexane caused spontaneous dissolution of the wine-red solid and formation of a clear solution from which the binuclear La/Al complex shown in Scheme 127 could be isolated in 90% yield [87].

Unexpectedly, one intact tetramethylaluminate unit remained in the product. An X-ray structure determination revealed the presence of a novel (μ-Me)($AlMe_3$) coordination mode (Fig. 28). This was the first example of a structurally verified η^1-coordinated $AlMe_4$ ligand. The remaining THF ligand could be removed upon addition of $AlMe_3$ to afford the unsolvated tetramethylaluminate complex involving bidentate coordination of the $AlMe_4$ ligand [87].

Among the highlights of organolanthanide chemistry published in 2007 was the preparation and structural characterization of a highly unusual neodymium–gallium complex stabilized by an *N*-heterocyclic carbene group. The synthetic route is illustrated in Scheme 128. The reaction of the neodymium carbene precursor with the anionic gallium diyl reagent in cold THF proceeded smoothly with concomitant elimination of KI, to give a dark red

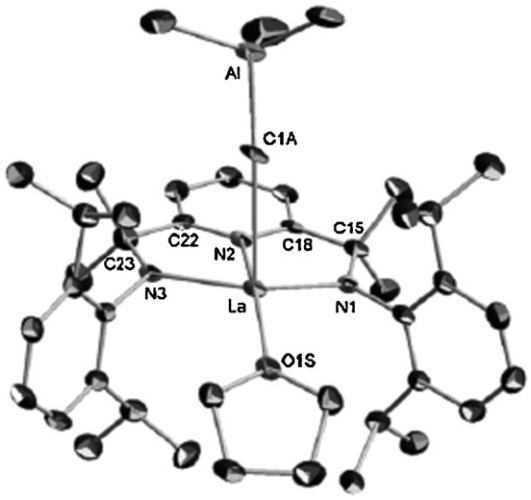

Fig. 28. Molecular structure oh (L^2)La[(μ-Me)($AlMe_3$)](THF) [87].

solution. Workup and recrystallization from toluene afforded the heterobimetallic Nd/Ga complex as large red blocks in moderate yield [88].

Surprisingly, the product is stable in solution and does not decompose when heated in toluene to 100 °C. A single-crystal X-ray diffraction study revealed a monomeric structure with a distorted trigonal bipyramidal coordination geometry around the central neodymium atom (Fig. 29). The bond length of the unsupported (and unprecedented) Nd–Ga bond is 3.2199(3) Å [88].

Also in 2007 novel metallocene-type compounds containing gallium(I)–lanthanide(II) donor–acceptor bonds were reported. Scheme 129 highlights the synthetic routes leading to $Cp^*_2Eu(GaCp^*)_2$ (dark red-purple crystals, 71% yield) and $Cp^*_2(THF)Yb(GaCp^*)$ (dark red crystals, 40% yield), both of which contain unsupported gallium–lanthanide metal-to-metal bonds according to the X-ray diffraction analyses. Fig. 30 depicts the molecular structure of the ytterbium derivative [89].

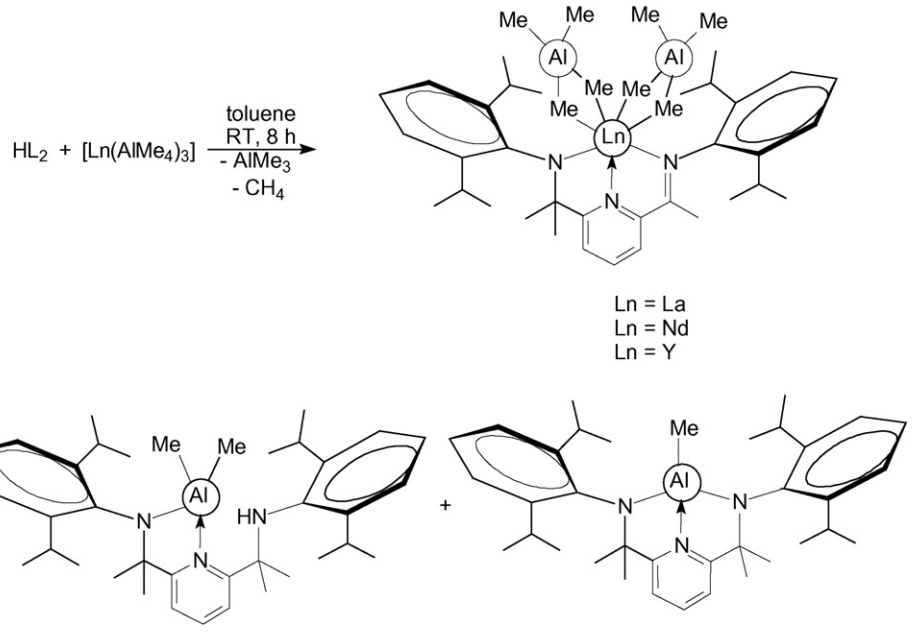

Scheme 126.

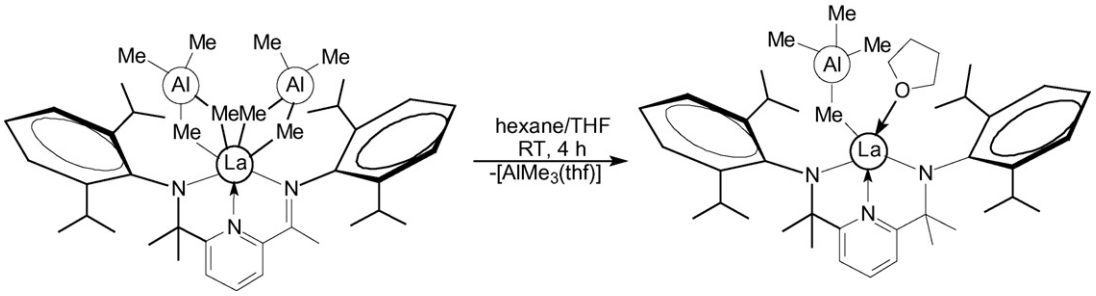

Scheme 127.

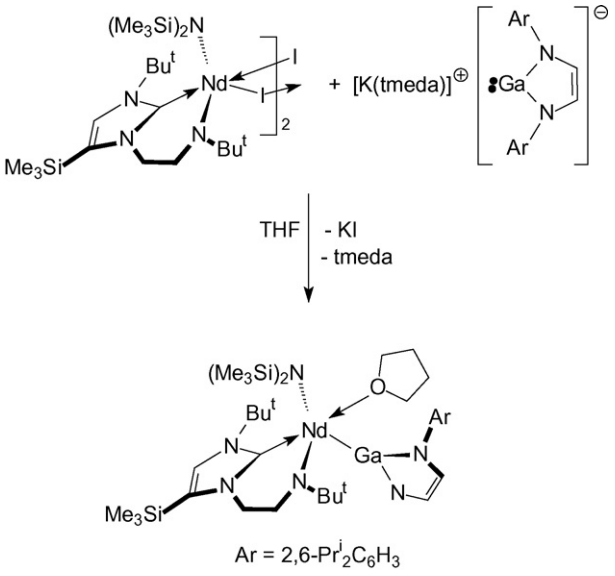

Scheme 128.

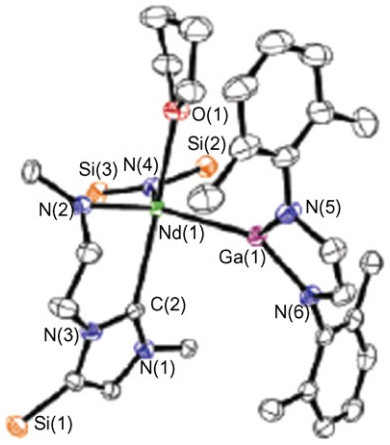

Fig. 29. Molecular structure of the first complex containing a direct Nd–Ga bond [88].

2.11. Organolanthanide catalysis

2.11.1. Organolanthanide-catalyzed polymerization reactions

2.11.1.1. Monoolefins (ethylene, propene, styrene, etc.). A series of rare earth metal alkyl complexes with methyl-substituted triazacyclononane-amide ligands (*cf.* Schemes 7 and 8) were investigated as ethylene polymerization catalysts. Comparative testing in

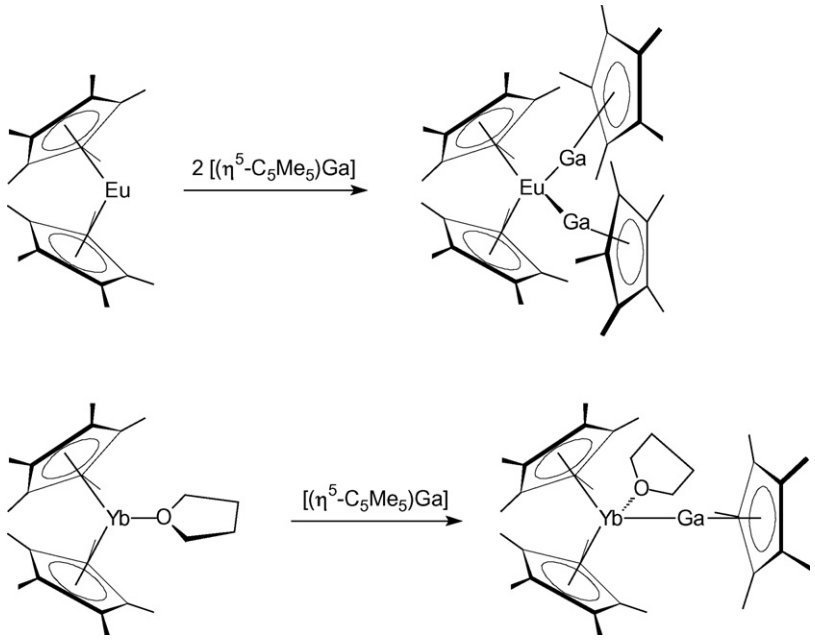

Scheme 129.

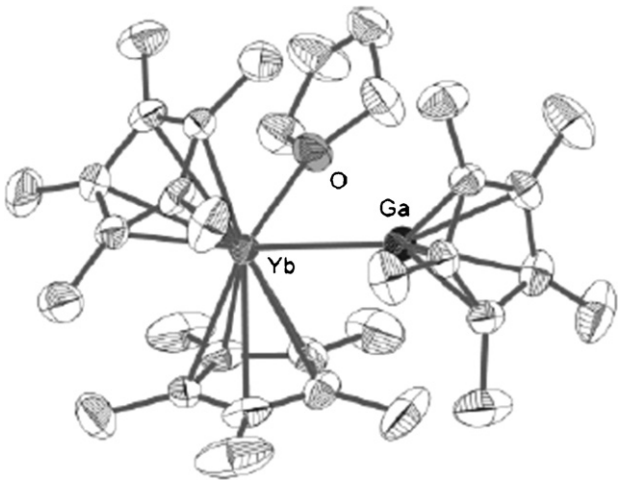

Fig. 30. Molecular structure of $Cp^*_2(THF)Yb(GaCp^*)$ [89].

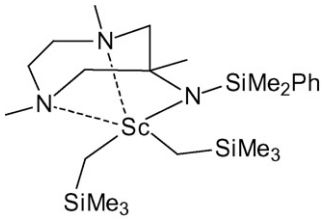

Scheme 130.

catalytic ethylene polymerization showed that the catalyst activity is most strongly influenced by the metal ionic radius, but that variations in the ligand backbone and substitution pattern do influence other factors, such as polymer molecular weight and catalyst stability. Catalysts with the intermediately sized rare earth metal yttrium generally showed the highest activity, but some of these catalysts produced polyethylene with broad molecular weight distributions, suggesting multisite behavior [12]. Likewise, several Group 3 metal alkyl complexes with tetradentate monoanionic phenolate ligands (*cf.* Scheme 25) were found to polymerize ethylene with low activity upon activation with MAO [20]. Testing was also performed with cationic scandium complexes derived from monoanionic *fac*-κ^3 ligands derived from 6-amino-1,4-diazepine. Catalytic ethylene polymerization experiments in toluene using the THF solvates shown in Scheme 10 in conjunction with $[PhNMe_2H][B(C_6F_5)_4]$ did not show any activity, presumably due to the presence of THF. In contrast, the combination of the THF-free dialkyl complex depicted in Scheme 130 with $[PhNMe_2H][B(C_6F_5)_4]$ afforded an active single-site ethylene polymerization catalyst, with a productivity of 548 kg (PE)(mol Sc)$^{-1}$ h^{-1} bar^{-1} (toluene solvent, 5 bar, 50 °C, 10 min run time), producing PE with $M_w = 1.2 \times 10^6$, $M_w/M_n = 1.9$. Thus it appears that even a single THF molecule can completely shut down the catalytic activity, suggesting that the actual active species in these systems is a THF-free (6-amido-1,4,6-trimethyl-1,4-diazepine)Sc(alkyl)-cation [13].

The rare-earth metallocene chloride complexes $Cp^*_2Ln(\mu\text{-}Cl)_2Li(OEt_2)_2$ (Ln = Y, Nd, Sm) combined with an excess of dialkylmagnesium compounds (*e.g.* butylethylmagnesium) were found to afford active species for the polymerization of ethylene in alkanes or aromatic solvents at atmospheric pressure. A dynamic equilibrium between dormant species and a low concentration of catalytically active species was suggested to explain the living character of the polymerization process observed at temperatures ≤80 °C. The resulting mixtures contain mainly di(polyethylenyl)magnesium compounds and can be directly used either for block copolymerizations with polar monomers or for any classical Grignard-like reaction for the synthesis of functionalized polyethylenes [90]. Active catalysts for the polymerization of R-alkenes (*n*-hexene, *n*-heptene, and *n*-octene) were generated *in situ* by reaction of the trialkyl precatalysts (*i*Pr-trisox)$Ln(CH_2SiMe_2R)_3$ shown in Scheme 37 with 2 equiv. of trityl tetrakis(pentafluorophenyl)borate. In all cases polyolefins with M_w/M_n values of between 1.58 and 2.08 and isotacticities of 80–95% T_m and then subsequently decrease with increasing ionic radius of the lanthanide metal due to a combination of activation with increasing ionic radius and decreasing catalyst stability [23].

The mono(phospholyl)lanthanide bis(benzyl) complexes (Dtp)$Ln(CH_2C_6H_4NMe_2\text{-}o)$ (Ln = Y, Sm) shown in Schemes 112 and 113 were activated with $[Ph_3C][B(C_6F_5)_4]$ and tested in the syndiotactic polymerization of styrene. Whereas the Sm derivative did not show any activity at all, the compounds with Ln = Sc and Y were found to give good to excellent results. Overall, the polymerization results in this study were comparable with the most active titanium catalysts reported for syndiospecific styrene polymerization [75]. A 2007 patent application claimed the use of a catalyst system based on allyl complexes of Group 3 metals incorporating bridged cyclopentadienyl-fluorenyl ligands in the copolymerization of styrene and conjugated dienes [91]. In another patent the manufacture of bimetallic Ti-rare earth metallocene catalysts for olefin polymerization was described [92]. On treatment with 1 equiv. of $[Ph_3C][B(C_6F_5)_4]$ the rare-earth metal bis(alkyl) amido complexes $[2,6\text{-}^iPr_2C_6H_3NH(SiMe_3)]Ln(CH_2SiMe_3)_2(THF)$ (Ln = Sc, Y, Ho, Lu) showed high activity for the polymerization of 1-hexene and styrene [11]. When activated by $AlEt_3$ or $[Ph_3C][B(C_6F_5)_4]$ the scandium phosphinoamide bis(alkyl) complex depicted in Scheme 21 was able to catalyze ethylene polymerization [18]. In a similar manner, half-sandwich dibenzyl complexes of scandium were used as precursors for cationic species which were tested in styrene polymerization. For example, the benzyl cation formed from $(\eta^5\text{-}C_5Me_4SiMe_3)Sc(CH_2Ph)_2(THF)$ using $[Ph_3C][B(C_6F_5)_4]$ in toluene (Scheme 131) resulted in a moderately active syndiospecific styrene polymerization catalyst [35].

Some of the allyl *ansa*-lanthanidocenes shown in Scheme 101 were reported to be effective single-component catalysts

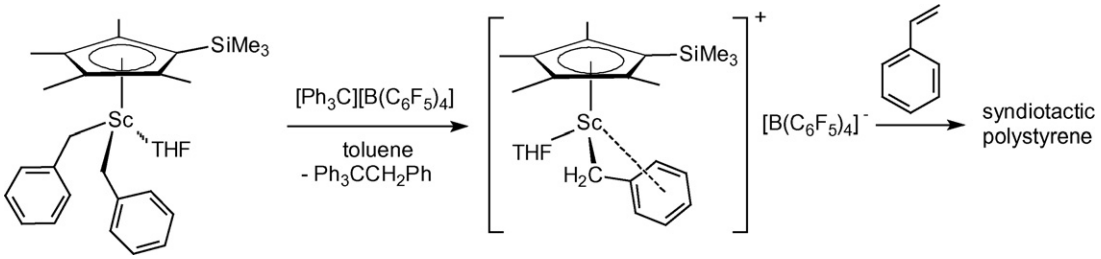

Scheme 131.

for the polymerization of styrene, giving pure syndiotactic polystyrenes (*rrrr* > 99%) with low to high molecular weights (M_n = 6000–135 000 g mol^{-1}) and narrow polydispersities (M_w/M_n = 1.2–2.6). These catalyst systems are remarkably stable and capable of polymerizing styrene up to 120 °C with high activities, while maintaining high syndiotacticity *via* chain-end control as established by a Bernoullian analysis. Highly effective copolymerization of styrene with ethylene was also achieved using a neodymium complex of this series (activity up to 2530 kg PS-PE mol^{-1} h^{-1}) to give true copolymers void of homopolymers with M_n = 9000–152 000 g mol^{-1} and again narrow polydispersities (M_w/M_n = 1.2–2.5). The nature of the resultant P(S-*co*-E) copolymers was ascertained by NMR, size-exclusion chromatography/refractive index/UV, temperature rising elusion fractionation, as well as differential scanning calorimetry. It was shown that, regardless of the amount of ethylene incorporated (1–50 mol%), the P(S-*co*-E) copolymers had a microstructure predominantly made of long, highly syndiotactic PS sequences separated by single or few ethylene units. Co-monomers feed and polymerization temperature could be used straightforwardly to manipulate the physical and mechanical characteristics of the P(S-*co*-E) copolymers (molecular weights and distributions, co-monomer content, microstructure, T_m, T_g, T_c) [69]. Other neutral *ansa*-bis(indenyl) allyl lanthanide complexes have been claimed in a

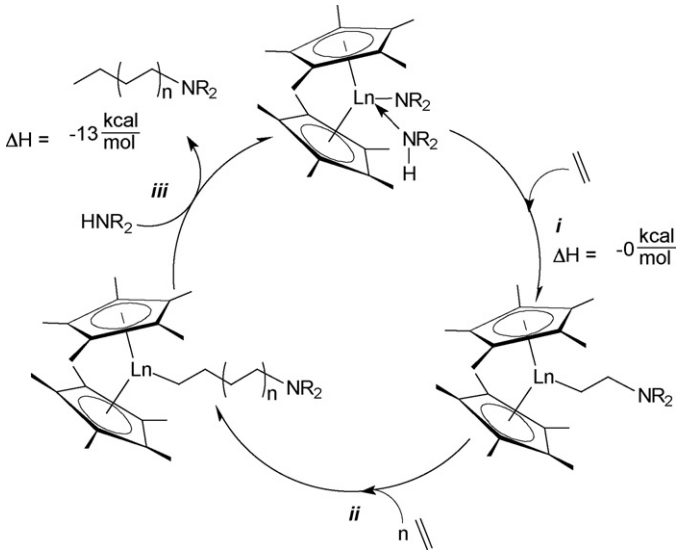

Scheme 132.

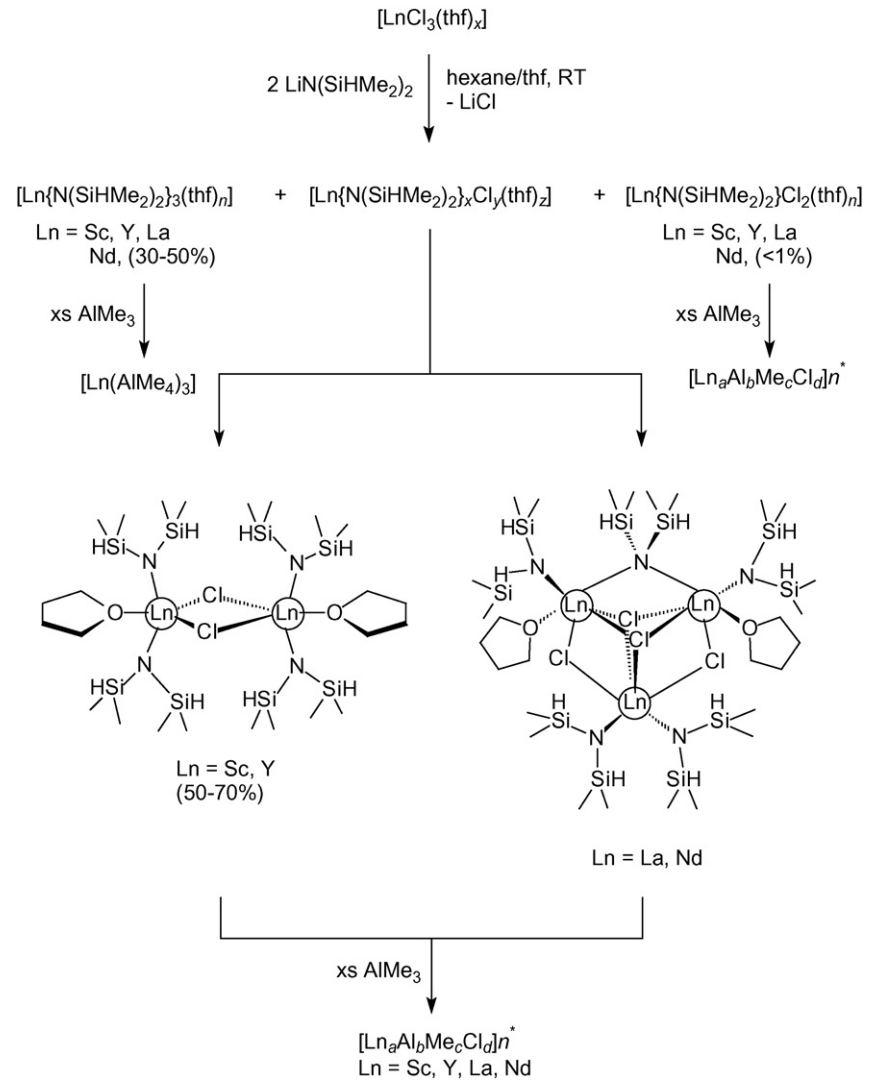

Scheme 133.

patent to be useful for the stereospecific polymerization of styrene [93].

An interesting novel aspect published in 2007 was the organolanthanide-catalyzed synthesis of amine-capped polyethylenes. A schematic catalytic cycle for the organolanthanide-mediated ethylene polymerization in the presence of amines is illustrated in Scheme 132. It was found that, despite kinetic disadvantages with respect to Ln–C protonolysis by amines, careful amine chain transfer agent selection allows the efficient, catalytic synthesis of dialkylamine-capped polyethylenes. This reaction is a flexible and efficient method for incorporating electron-rich functional groups into polyolefins [94].

2.11.1.2. Dienes (butadiene, isoprene, etc.). The nature of the active rare-earth-metal species of Ziegler mixed catalysts has been a matter of dispute since the early discoveries of their superior performance in the stereospecific polymerization of 1,3-dienes. The synthesis and isolation of the putative active species $[Me_2LnCl]_n$ and $[MeLnCl_2]_n$ utilizing lanthanide precursors with preformed Ln–Cl moieties (*i.e.* a chlorination–alkylation sequence) as well as their successful application in highly *cis*-stereoregular isoprene polymerization was the subject of a study published in 2007. Scheme 133 illustrates the synthetic pathways leading to mixed-metal Ln/Al Ziegler-type catalysts which are highly active in 1,3-diene polymerization. Transient $[Me_2LnCl]_n$ and $[MeLnCl_2]_n$ are formed as active species in the polymerization reactions [95].

Cationic lanthanide alkyl complexes bearing an ancillary bis(phosphinophenyl)amido ligand (*cf.* Scheme 17) were found to be a new catalytic system for living *cis*-1,4-polymerization and copolymerization of isoprene and butadiene. This catalyst system provides extremely high *cis*-1,4-selectivity (99%) and excellent livingness (M_w/M_n = 1.05–1.13) with no need for an aluminum additive to show high activity and high selectivity for the polymerization of isoprene and butadiene, and can also be applied to the copolymerization of isoprene and butadiene in a living *cis*-1,4-fashion [16]. The production of ethylene/butadiene copolymers was achieved with the use of fluorenyl-based lanthanide metallocenes containing additional borohydride ligands [96,97]. In another patent application, allyl-lanthanide complexes incorporating bridged cyclopentadienyl-fluorenyl ligands were claimed to efficiently catalyze the copolymerization of styrene and conjugated dienes such as isoprene as well as the terpolymerization of styrene, isoprene, and ethylene [91] 1,3-Butadiene was polymerized in the presence of $Cp^*_2GdN(SiMe_3)_2$ and an aluminoxane co-catalyst (MMAO) to give poly(1,3-butadiene) in 100% yield showing *cis*-1,4 content of 97.52 mol% and M_w/M_n = 2.05 [98]. Closely related bis(indenyl)lanthanide silylamides such as $(C_9H_7)_2GdN(SiMe_3)_2$ were claimed in a patent application to be effective polymerization catalysts for the production of polybutadiene (93% yield) having *cis*-content of 98.9%, M_n = 120 000, and M_w/M_n = 1.26 [99]. The pyrrolide-supported lanthanide alkyl complexes shown in Schemes 106–108 were tested as initiators for the polymerization of isoprene in the presence of $AlEt_3$ and $[Ph_3C][B(C_6F_5)_4]$. Only the complexes $L^1Ln(CH_2SiMe_3)_2(THF)_n$ (Ln = Lu, n = 2; Ln = Sc, n = 1) (Scheme 106) and the bimetallic bis(alkyl) complex with Ln = Y (Scheme 107) showed activity, while all other complexes were inert. The microstructure of the resultant polyisoprene had a *cis*-1,4- or *trans*-1,4 configuration depending on the initiator applied [73]. Similar observations were made with lanthanide bis(alkyls) bearing an indenyl-functionalized *N*-heterocyclic carbene ligand (*cf.* Scheme 98). In the presence of activators like $AlEt_3$ and $[Ph_3C][B(C_6F_5)_4]$ only the Y derivative showed catalytic activity toward the polymerization of isoprene to afford 3,4-regulated polyisoprene (91%) [68]. On treatment with 1 equiv. of $[Ph_3C][B(C_6F_5)_4]$ the amido-ligated rare-earth metal bis(alkyl) complexes $[2,6\text{-}^iPr_2C_6H_3NH(SiMe_3)]Ln(CH_2SiMe_3)_2(THF)$ (Ln = Sc, Y, Ho, Lu) showed high activity for the living polymerization of isoprene [11]. Selectivity, block copolymerization and chain transfer of *in situ* generated half-lanthanidocene based catalysts for the controlled oligomerization of styrene have been investigated. The combination $Cp^*Nd(BH_4)_2(THF)_2$/*n*-butylethylmagnesium afforded a controlled and syndioselective oligomerization of styrene. Living oligostyrenes could be used as macromonomers for block copolymerization, leading to the unprecedented synthesis of a (polystyrene)-*block*-(1,4-*trans* polyisoprene) copolymer. Reversible transmetallation between Nd and the magnesium atom was further established with a transfer efficiency close to 100% [100]. The insertion of single styrene units into polyisoprene was demonstrated using borohydrido rare earth/dialkylmagnesium systems. This yielded a new family of styrene/diene copolymers (SBR rubbers). The resulting poly[(1,4-*trans*-isoprene)-*co*-styrene] exhibited quite narrow molecular weight distributions, up to 30% inserted styrene, and a 96–98% 1,4-*trans*-microstructure. The presence of a bulky and electron-rich ligand in the coordination sphere of the metal lead to an increase of the amount of styrene inserted and narrower chemical composition and molecular weight distributions. The presence of significant quantities of styrene in the medium did not alter the selectivity of the reaction, in contrast to *cis*-specific polymerizations [101].

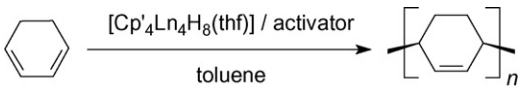

Scheme 134.

Most remarkably, cationic rare-earth polyhydride complexes were found to show excellent regio- and stereoselectivity for the polymerization of 1,3-cyclohexadiene (CHD), which afforded, for the first time, soluble crystalline *cis*-1,4-linked poly(CHD) (1,4 selectivity: 100%; *cis* selectivity: 99%) (Scheme 134). Interestingly, a significant influence of the ionic radius of the rare-earth metal centers on the catalytic activity was observed, that is, an increase of the ionic radius led to an almost linear increase in the catalytic activity among the metals examined [40].

2.11.1.3. Cyclic esters and amides (ε-caprolactone, δ-valerolactone, lactide, etc.). Polylactides (PLAs) are the most promising biodegradable and biocompatible synthetic macromolecules, possessing versatile physical properties and being widely used in medicine, pharmaceutics, and tissue engineering such as media for the controlled release of drugs, scaffolds, and the delivery of antibodies and genes. Ring-opening polymerization (ROP) of lactide (LA) by single-site catalysts presents the most efficient manner to obtain PLAs with predicted molecular weight and narrow molecular weight distribution and, significantly, tacticity. Scheme 135 illustrates the polymerization of racemic lactide (*rac*-LA) to give heterotactic PLA [21].

In 2007, several papers dealing with the use of lanthanide complexes as catalysts for the ring-opening polymerization of lactide were published. For example, the lanthanide alkyl complexes bearing *N*,*O*-multidentate ligands shown in Schemes 29–31 were successfully tested. It was found that the combination of amino-amine-modified bis(phenolate) ligands with lanthanide alkyl units generated unprecedented stereoselective initiators for the ROP of *rac*-LA to give heterotactic polylactide with P_r up to 0.99 (P_r = probability of racemic enchainment of monomer units calculated according to the methine region of the homonuclear decoupled ^1H NMR spectrum) [21]. The rare earth complexes shown in Scheme 136 (R = H, Me, ^{t}Bu; R′ = Me, Et, pyridyl; R″ = alkyl, amino, phenoxy; Ln = Sc, Y, Lu) were also found to catalyze the stereoselective ring-opening polymerization of racemic lactide. Bulk polymerizations were carried out at 70–120 °C for 0.1–5 h with a

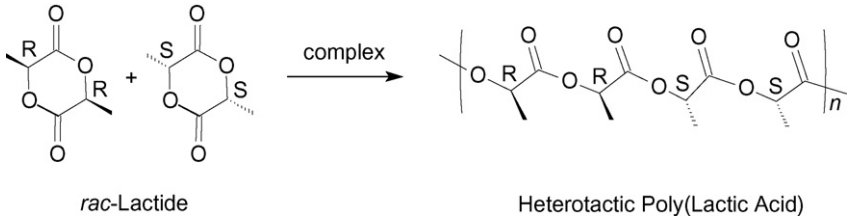

Scheme 135.

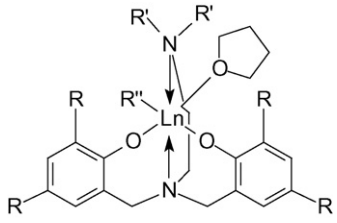

Scheme 136.

conversion ratio of 100%. THF, dichloromethane, or toluene can be employed as solvents in the polymerization reactions. The content of heterotactic polymer in the obtained polylactide reached 0.99, which is higher than the highest previously reported value (0.96) [22].

The aminophenolate-supported lanthanide mono(alkyl) complexes shown in Schemes 48 and 49 were found to be highly active initiators for the ring-opening polymerization of *L*-lactide to give isotactic polylactide with high molecular weight and narrow to moderate polydispersity [34]. Rare earth metal alkyl complexes stabilized by anilido phosphinimine and amino phosphine ligands (*cf.* Schemes 18 and 19) were reported to initiate the ring-opening polymerization of *D*,*L*-lactide with high activity to give atactic polylactides. A probable mechanism for the polymerization of lactide is illustrated in Scheme 137 [17]. Atactic polylactides were also obtained from *D*,*L*-lactide using the pyrrolide-ligated organoyttrium complexes shown in Schemes 105 and 109 [72].

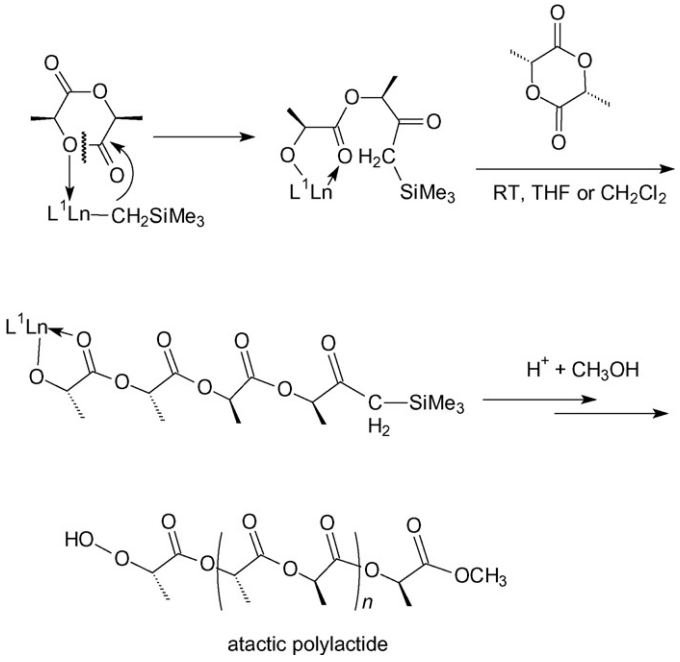

Scheme 137.

When the mono(pentamethylcyclopentadienyl) bis(phosphinimino)methanide complexes of yttrium and lanthanides (Sm, Yb) shown in Scheme 82 were combined *in situ* with 1 equiv. of 2-propanol, an active [Ln]-OiPr initiator was formed that enabled the pseudo-living ring-opening polymerization of ε-caprolactone to polymers with controlled molecular features (end groups, M_n) and very narrow molar mass distributions (Scheme 138) [56].

Lanthanide(II) complexes containing tetrahydro-2*H*-pyranyl-functionalized indenyl ligands (*cf.* Scheme 97) were reported to exhibit high catalytic activity in the polymerization of ε-caprolactone. The effects of temperature, substituents on the indenyl ring, and solvents on the catalytic activity of the complexes were examined [67]. Ring-opening polymerization of ε-caprolactone was also achieved using [ethylene-bis(η^5-indenyl)][bis(trimethylsilyl)amido]lanthanide(III) complexes (EBI)LnN(SiMe$_3$)$_2$ (Ln = Y, Sm, Yb) (*cf.* Scheme 102) [70].

2.11.1.4. Acrylic monomers (methyl methacrylate (MMA), acrylonitrile, etc.). Termination and transfer reactions in the group transfer polymerizations of acrylates catalyzed by mononuclear lanthanide metallocenes were investigated by a DFT study [102]. The catalytic activity of lanthanide complexes containing *N*-piperidineethyl-functionalized indenyl ligands on MMA polymerization has been examined. It was found that the π-bound tris(*N*-piperidineethylindenyl)lanthanide complexes shown in Scheme 95 exhibit unexpectedly good catalytic activity on MMA polymerization, and the Sm derivative also showed an unexpected high catalytic activity on ε-caprolactone polymerization. It was found that the catalytic activity of the complexes depended on the polymerization conditions. The solvents, temperatures, substituted groups, and lanthanide ionic radii effects on the catalytic activity of the complexes were examined [66]. Similarly, several lanthanide(II) complexes containing tetrahydro-2*H*-pyranyl-functionalized indenyl ligands (*cf.* Scheme 97) were found to exhibit high catalytic activity in MMA polymerization [67]. The anionic complexes [Li(DME)$_3$][{*o*-(Me$_3$SiN)$_2$C$_6$H$_4$}Ln(MeC$_5$H$_4$)$_2$] (Ln = Nd, Sm, Yb) (Scheme 72) also showed high catalytic activity for the polymerization of MMA at r.t., giving the syndiotactic-rich polymers with relatively narrow molecular weight distributions (M_w/M_n = 1.64–1.82). For this particular Ln-catalyzed MMA-polymerization reaction an anionic polymerization mechanism was proposed (Scheme 139) which was supported by various experimental results [50].

2.11.2. Organolanthanide-catalyzed hydrosilylation, hydroamination and hydrophosphination reactions

σ-Bond metathesis reactions of lanthanocene complexes Cp$_2$LnR (R = H, Me, SiH$_3$) with SiH$_4$ and MeSiH$_3$ were studied using DFT(B3PW91) calculations. It was shown that the nature of the lanthanide atom has essentially no influence on the free enthalpy profile. Therefore all reactions that could occur between MeSiH$_3$, formed from the reaction between the initial reagents (Cp$_2$LnMe and SiH$_4$), and the lanthanocene complexes (Cp$_2$LnH or Cp$_2$LnSiH$_3$),

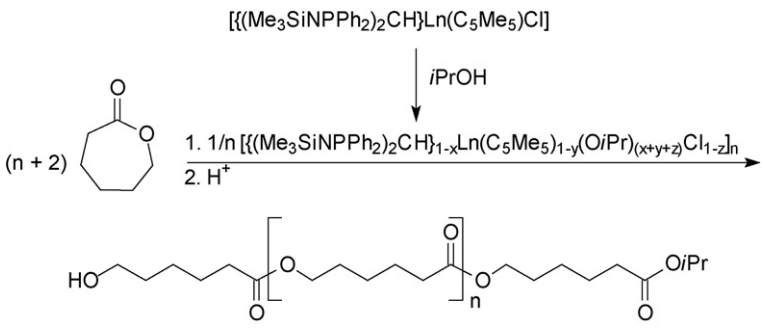

Scheme 138.

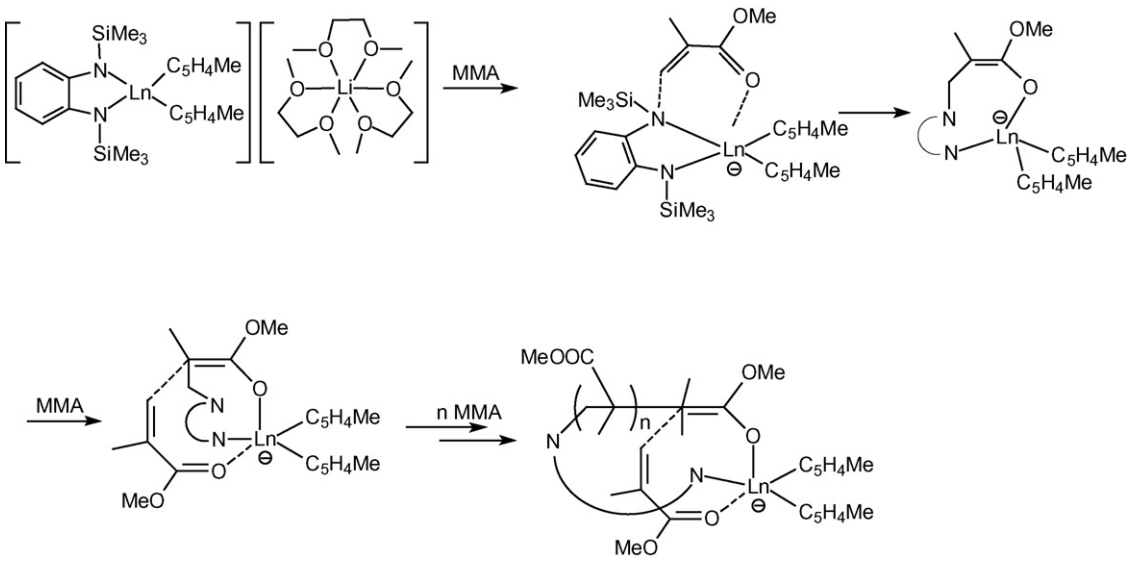

Scheme 139.

were then studied for La only. It was found that the activation of the Si-H bond is preferred over that of Si–C or C–H bonds [103].

The bis(phosphinimino)methanide yttrium and lanthanide amido complexes $[CH(PPh_2NSiMe_3)_2]Ln[N(SiHMe_2)_2]_2$ (Ln = Y, La, Sm, Ho, Lu) shown in Scheme 16 were used as catalysts for hydroamination/cyclization with different non-activated aminoalkenes and terminal aminoalkenes (Scheme 140) as well as for hydrosilylation reactions. A clear dependence of the reaction rate on the ionic radius of the central metal was observed, showing the lanthanum compound to be the most active one in both reactions. Also investigated was a combination of both reactions, *i.e.* a sequential hydroamination/hydrosilylation reaction [15].

Several chiral yttrocenes containing (+)-neomenthyl- and (−)-phenylmenthyl-substituted cyclopentadienyl (Schemes 99 and 100) were found to show moderate to good catalytic activity in asymmetric hydroamination/cyclizations of aminoalkenes, but enantioselectivities were limited to a maximum of 38% ee for the sterically most hindered catalyst [44].

2.11.3. Other organolanthanide-catalyzed reactions

[Ethylene-bis(η^5-indenyl)][bis(trimethylsilyl)amido]lanthanide (III) complexes of the type (EBI)LnN$(SiMe_3)_2$ (Ln = Y, Sm, Yb) were found to catalyze the addition of the N–H bonds of amines and the C–H bond of terminal alkynes to carbodiimides. The former reaction results in guanylation of the carbodiimides as shown in Scheme 141 [70].

The half-sandwich rare-earth metal alkyl complexes $[Me_2Si(NR')]Ln(CH_2SiMe_3)(THF)_n$ (Ln = Y, Yb, Lu; *cf.* Scheme 54), especially the yttrium derivatives, were also found to be excellent catalyst precursors for the catalytic addition of various primary and secondary amines to carbodiimides, efficiently

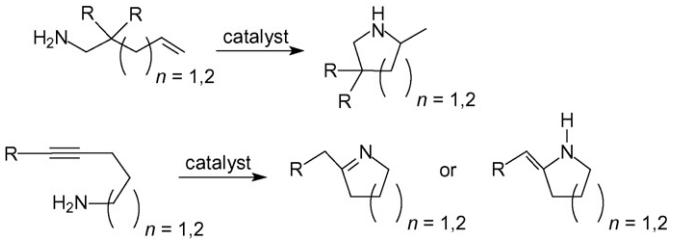

Scheme 140.

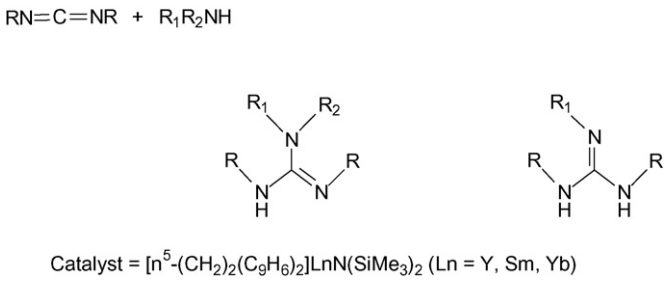

Scheme 141.

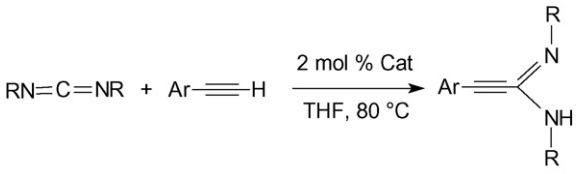

Catalyst = $[n^5\text{-}(CH_2)_2(C_9H_6)_2]LnN(SiMe_3)_2$ (Ln = Y, Sm, Yb)

Scheme 142.

yielding a series of guanidine derivatives with a wide range of substituents on the nitrogen atoms. Functional groups such as C≡N, C≡CH, and aromatic C–X (X = F, Cl, Br, I) bonds can survive the catalytic reaction conditions. A primary amino group can be distinguished from a secondary one by the catalyst system. Some key reaction intermediates or true catalyst species, such as the amido complexes $[Me_2Si(C_5Me_4)(NPh)]Y(NEt_2)(THF)_2$ and $[Me_2Si(C_5Me_4)(NPh)]Y(NHC_6H_4Br\text{-}4)(THF)_2$, and the guanidinate complexes $[Me_2Si(C_5Me_4)(NPh)]Y\{^iPrNC(NEt_2)(N^iPr)\}(THF)$ and $[Me_2Si(C_5Me_4)(NPh)]Y\{^iPrN\}C(NC_6H_4Br\text{-}4)(NH^iPr)\}(THF)$ were isolated and structurally characterized. Reactivity studies on these complexes suggested that the catalytic formation of a guanidine compound proceeds mechanistically through nucleophilic addition of an amido species, formed by acid–base reaction between a rare earth metal alkyl bond and an amine N–H bond, to a carbodiimide, followed by amine protonolysis of the resultant guanidinate species [37].

The organolanthanide-catalyzed addition of terminal alkynes to carbodiimides provides a straightforward route to propiolamidines, a reaction which had hardly been explored before. Here too the [ethylene-bis(η^5-indenyl)][bis(trimethylsilyl)amido]lanthanide(III) complexes of the type (EBI)LnN(SiMe$_3$)$_2$ (Ln = Y, Sm, Yb) were found to highly efficient catalysts giving rise to the desired propiolamidines in excellent yields (81–95%) (Scheme 142) [70].

The reaction mechanism for both organolanthanide-catalyzed addition reaction was proposed as follows (Scheme 143): interaction of the amines or the terminal alkynes with lanthanocene amides produces the new amido (or alkynyl) intermediate **A** (or **A**′) through an acid–base exchange reaction, and then the intermediate **A** (or **A**′) reacts with carbodiimide, producing a metal guanidinate or amidinate species **B** (or **B**′) through an insertion reaction. Transfer of a proton then releases the product with concomitant regeneration of the catalytically active species. A 1,3-H shift produces the final guanylation products when amines were the aromatic species [70].

2.12. Organolanthanides in organic synthesis

The levels of diastereoselection attainable by addition of vinylmagnesium bromide to a selection of bicyclo[2.2.2]octenone derivatives in the presence of various Lewis acids such as LiBr, $CeCl_3$, $TiCl_4$, $ZnBr_2$, $MgBr_2$, and Et_2AlCl have been determined (Scheme 144). The use of a preformed vinylmagnesium bromide-$CeCl_3$ reagent for the addition reactions provided almost exclusively *syn*-isomers. The substituents and reaction conditions can influence facial selectivity in the nucleophilic additions to the bicyclo[2.2.2]oct-5-en-2-one derivatives [104].

Full details of *syn*-selective catalytic asymmetric direct Mannich-type reactions of aromatic and heteroaromatic hydroxy ketones promoted by Y[N(SiMe$_3$)$_2$]$_3$/linked-BINOL complexes have been described. From a screening of various rare-earth metals and linked-BINOL derivatives, a Y[N(SiMe$_3$)$_2$]$_3$/TMS-linked-BINOL complex was determined to be the most effective. Mannich-type reactions of aromatic and heteroaromatic hydroxy ketones with aryl and alkenyl *N*-diphenylphosphinoylimines, catalyzed by 0.1 molar amount of Y[N(SiMe$_3$)$_2$]$_3$ and 0.059 molar amount of TMS-linked-BINOL, afforded *syn*-β-amino-α-hydroxy ketones in good yields (78–98%), high diastereoselectivity (*syn*/*anti* = 81/19–96/4), and high enantioselectivity (86–98% ee) [105].

2.13. Organolanthanides in materials science

The year 2007 witnessed continued interest in the production of lanthanide oxide (Ln_2O_3) thin films through MOCVD or ALD techniques using liquid organolanthanide precursors. A good overview of this rapidly expanding field can be gained from three excellent review articles which were published in 2007: "Atomic Layer Deposition of Rare Earth Oxides" by Niinistö et al. [106], "Requirements of Precursors for MOCVD and ALD of Rare Earth Oxides" by Aspinall

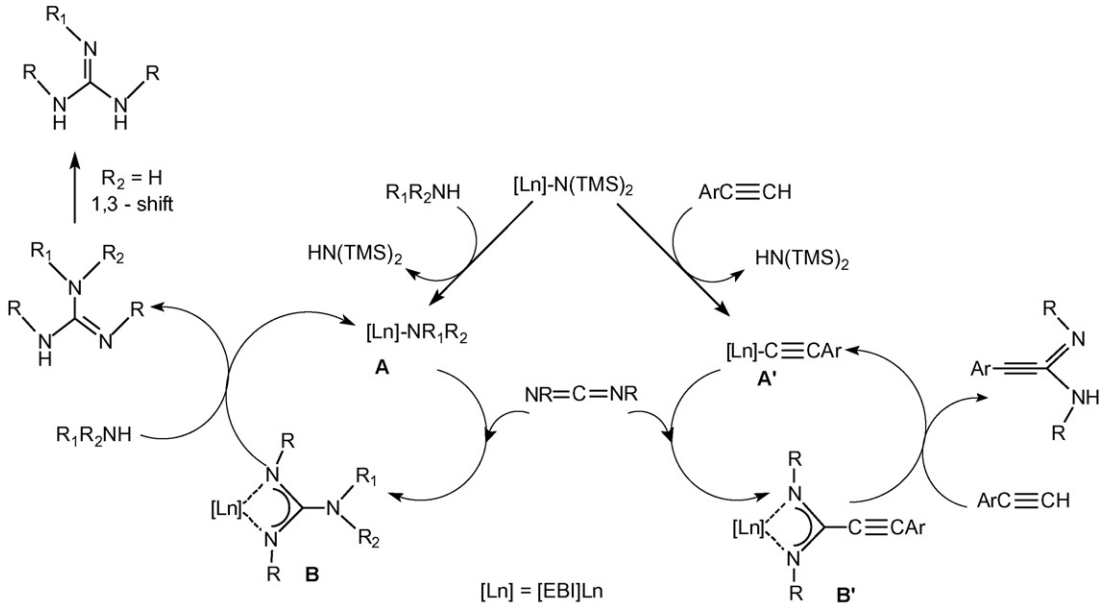

Scheme 143.

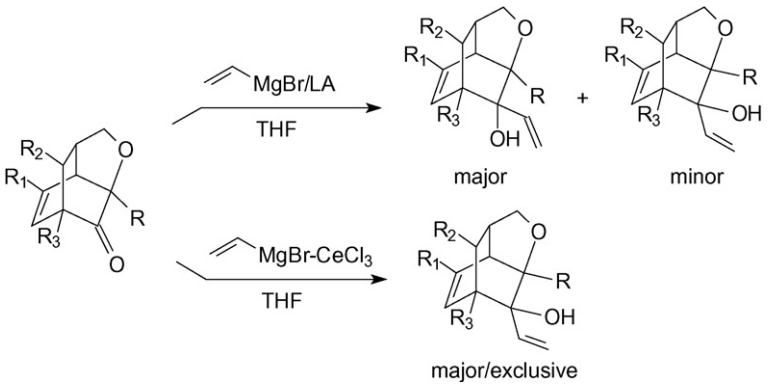

Scheme 144.

[107], and "Electrical Characterization of Rare Earth Oxides Grown by Atomic Layer Deposition" by Spiga et al. [108].

Lanthanum oxide thin films were deposited using alternate injections of La(^{i}PrC$_5$H$_4$)$_3$ and H_2O at various substrate temperatures. The proper substrate temperature, at which La_2O_3 thin films with a low equivalent oxide thickness and low leakage current were deposited, was 300 °C. During post-deposition annealing in an N_2 atmosphere, a remarkable amount of Si diffusion occurred. However, annealing in an NH_3 atmosphere (prenitridation) improved the thermal stability and dielectric constant of the La_2O_3 thin films [109]. In a similar manner erbium oxide (Er_2O_3) films have been deposited by MOCVD on Si(0 0 1) using tris(isopropylcyclopentadienyl)erbium, Er(^{i}PrC$_5$H$_4$)$_3$. The impact of Si surface passivation by the metal organic prior growth initiation was also part of this investigation. The correlation between the Er_2O_3 films structure, the optical response, the static dielectric constant (K), and density of interface traps was discussed. An Er-silicate interfacial layer with a thickness of 1.5 nm, a static dielectric constant of 10–12.4, and a density of interface traps of 4.2×10^{10} cm^2 eV^{-1} measured for a film with a physical thickness of 8.2 nm render Er_2O_3 an interesting candidate as a high-K dielectric [110]. An O_2 remote plasma metal organic chemical vapor deposition (RP-MOCVD) route was presented for tailoring the structural, morphological, and optical properties of Er_2O_3 thin films grown on Si(1 0 0) using the same precursor, tris(isopropylcyclopentadienyl)erbium, Er(^{i}PrC$_5$H$_4$)$_3$. The RP-MOCVD approach produced highly (1 0 0)-oriented, dense, and mechanically stable Er_2O_3 films with columnar structure [111].

The atomic layer deposition (ALD) growth of $Er_xGa_{2-x}O_3$ ($0 \le x \le 2$) thin films was demonstrated using two precursor systems: Er(thd)$_3$, Ga(acac)$_3$, and ozone and Er(C$_5$H$_4$Me)$_3$, Ga$_2$(NMe$_2$)$_6$, and water at substrate temperatures of 350 and 250 °C, respectively. Both processes provided uniform films and exhibited surface-limited ALD growth. The value of x in $Er_xGa_{2-x}O_3$ was easily varied by selecting a pulse sequence with an appropriate erbium to gallium precursor ratio. The organometallic Er(C$_5$H$_4$Me)$_3$, Ga$_2$(NMe$_2$)$_6$, and water precursor system provided stoichiometric $Er_xGa_{2-x}O_3$ films with carbon, hydrogen, nitrogen, and fluorine levels of 2.0–6.1, 5.0–10.3, <0.3–0.7, and ≤0.1 atom%, respectively, as determined by RBS and TOF-ERDA. The film growth rate was between 1.0 and 1.5 Å cycle^{-1} and varied as a function of the Er(C$_5$H$_4$Me)$_3$ to Ga$_2$(NMe$_2$)$_6$ pulse ratio. The effective permittivity of representative samples was between 9.2 and 10.4. The as-deposited films of both precursor systems were amorphous, but crystallized either to $Er_3Ga_5O_{12}$ or to a mixture of β-Ga_2O_3 and $Er_3Ga_5O_{12}$ upon annealing between 900 and 1000 °C under a nitrogen atmosphere. Atomic force microscopy showed root mean square surface roughnesses of <1.0 nm for typical films regardless of precursor system or film composition [112].

3. Actinides

3.1. Actinide hydrocarbyls

Multiconfigurational quantum chemical methods (complete active space self-consistent field (CASSCF)/second order perturbation theory (CASPT2)) were used to study the agostic interaction between the metal atom and H(C) in the methylidene metal dihydride complexes CH_2=MH_2, where M is a second row transition metal or the actinide atoms Th or U. The geometry of some of these complexes was found to be highly irregular due to the formation of a three center bond CH···M, where the electrons in the CH bond are delocalized onto empty or half empty orbitals of d- or f-type on the metal. No agostic interaction is expected when M = Y, where only a single bond with methylene can be formed, or when M = Ru, because of the lack of empty electron accepting metal valence orbitals. The largest agostic interaction is found in the Zr and U complexes [113]. In a closely related study the infrared spectrum and bonding in uranium methylidene dihydride, CH_2=UH_2, were investigated. Uranium atoms activate methane upon ultraviolet excitation to form the methyl uranium hydride CH_3–UH, which undergoes α-H transfer to produce uranium methylidene dihydride, CH_2=UH_2. This rearrangement most likely occurs on an excited-quintet potential-energy surface and was followed by relaxation in the argon matrix. These simple U + CH_4 reaction products were identified through isotopic substitution ($^{13}CH_4$, CD_4, CH_2D_2) and density functional theory frequency and structure calculations for the strong U–H stretching modes. Relativistic multiconfiguration (CASSCF/CASPT2) calculations substantiate the agostic distorted C1 ground-state structure for the triplet CH_2=UH_2 molecule. It was found that uranium atoms are less reactive in methane activation than thorium atoms. Our calculations show that the CH_2=UH_2 complex is distorted more than CH_2=ThH_2. A favorable interaction between the low energy open-shell U(5f) σ orbital and the agostic hydrogen contributes to the distortion in the uranium methylidene complexes [114]. Quantum chemical calculations published in 2006 had predicted the hypothetical diphenyl diuranium compound PhUUPh to have a stable ^1A_g ground state. A more recent theoretical investigation came to the conclusion that in PhUUPh a quintuple bond could be formed between the two U^I units, but that the effective bond order (=EBO) is only 3.7 [115].

Extremely stable thorium(IV) dialkyl complexes supported by new rigid tridentate 4,5-bis(anilido)xanthene and 2,6-bis(anilidomethyl)pyridine ligands have been prepared as exemplified by Scheme 145 and fully characterized. An X-ray structural analysis of the product with E = O suggested the presence of α-agostic C–H–Th interactions for both alkyl groups. In solution, both compounds exhibit temperature-dependent $^1J_{C,H}$

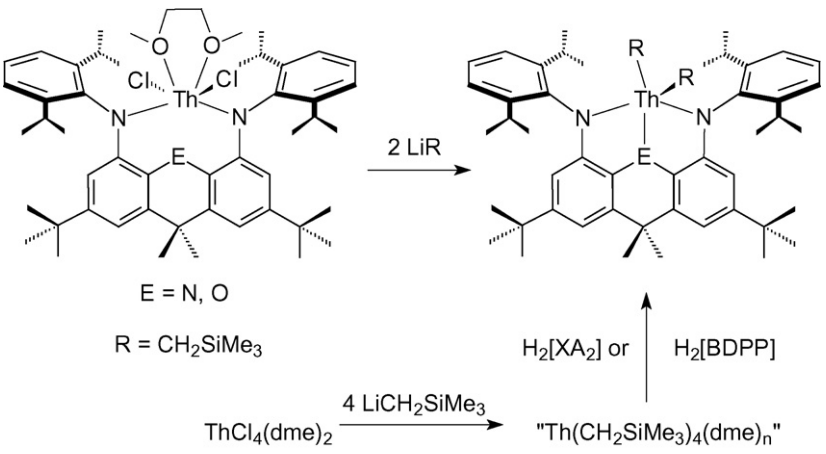

Scheme 145.

coupling constants for ThCH_2, demonstrating the presence of α-agostic interactions which become increasingly favored at lower temperature [116].

3.2. Actinide cyclopentadienyl compounds

3.2.1. $CpAnX_3$, Cp_2AnX_2 and Cp_3AnX compounds

The free energies of reaction and the activation energies were calculated, with DFT (B3PW91) and small RECP (relativistic core potential) for uranium, for the reaction of Cp_2UNMe and Cp_2UO with MeC≡CMe and H_3SiCl to give the corresponding addition products. CAS(2,7) and DFT calculations on Cp_2UO and Cp_2UNMe gave similar results, which validates the use of DFT calculations in these cases. The calculated results mirrored the experimental reaction of $[1,2,4\text{-}Bu^t{}_3C_5H_2]_2UNMe$ with dimethylacetylene and $[1,2,4\text{-}Bu^t{}_3C_5H_2]_2UO$ with Me_3SiCl. The net reactions are controlled by the change in free energy between the products and reactants, not by the activation energies, and therefore by the nature of the UO and UNMe bonds in the initial and final states. A NBO analysis indicated that the U–O interaction in Cp_2UO is composed of a single U–O σ bond with three lone pairs of electrons localized on oxygen, leading to a polarized U–O fragment. In contrast, the U–NMe interaction in Cp_2UNMe is composed of a σ and π component and a lone pair of electrons localized on the nitrogen, resulting in a less polarized UNMe fragment, in accord with the lower electronegativity of NMe relative to O. The strongly polarized $U^{(+)}$–$O^{(-)}$ bond is calculated to be about 70 kcal mol^{-1} stronger than the less polarized U=NMe bond [117].

3.2.2. Pentamethylcyclopentadienyl compounds

3.2.2.1. Cp^*AnX_2 and $Cp^*{}_2AnX$ compounds. Atmospheric pressure chemical ionization mass spectrometry (APCI-MS) has been used to characterize the air-sensitive paramagnetic organouranium azide and nitride complexes $[Cp^*{}_2UN_3(\mu\text{-}N_3)]_3$ and $[Cp^*U(\mu\text{-}I)_2]_3N$, respectively. The synthetic routes are highlighted in Schemes 146 and 147. $Cp^*{}_2UCl_2$ reacts readily with NaN_3 to give a dark red complex (> 90% isolated yield) with a single resonance in the ^{1}H NMR spectrum. The complex was identified by X-ray crystallography as the trimetallic azide (Scheme 146) [118].

In contrast to Scheme 146, the reaction of NaN_3 with trivalent $Cp^*UI_2(THF)_3$ did not generate the ionic metathesis product (dark red crystals, 33% yield) in which the halides were replaced by azide (Scheme 147) [118].

The trimetallic complex $[Cp^*U(\mu\text{-}I)_2]_3E$ had been identified by X-ray crystallography, but the data did not definitively identify E as N^{3-} *versus* O^{2-} or $(OH)^-$, a common problem in heavy-element nitride complexes involving metals with variable oxidation states.

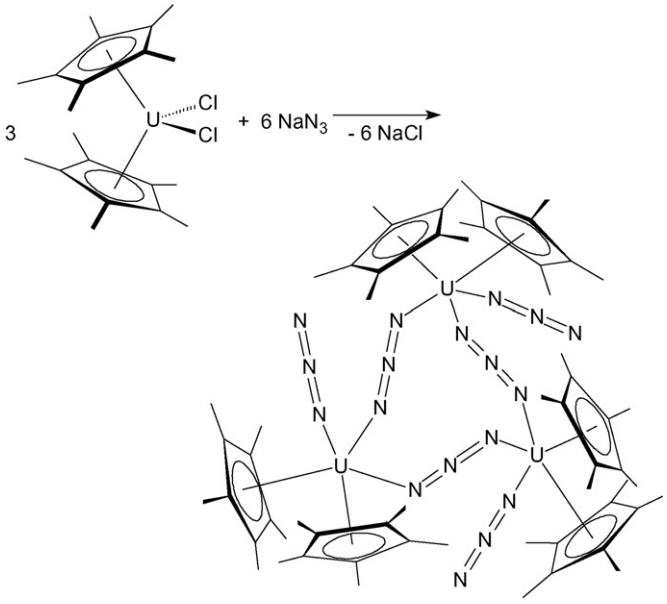

Scheme 146.

A comparison of the 250 °C APCI-MS spectra of products made from NaN_3 and $Na^{15}NNN$ showed mixed $[M]^+$ and $[M+H]^+$ envelopes at expected ion intensities for the ^{14}N and ^{15}N isotopomers. A compilation of U–C(Cp*) and U–I bond distance data for U^{3+} and U^{4+} was

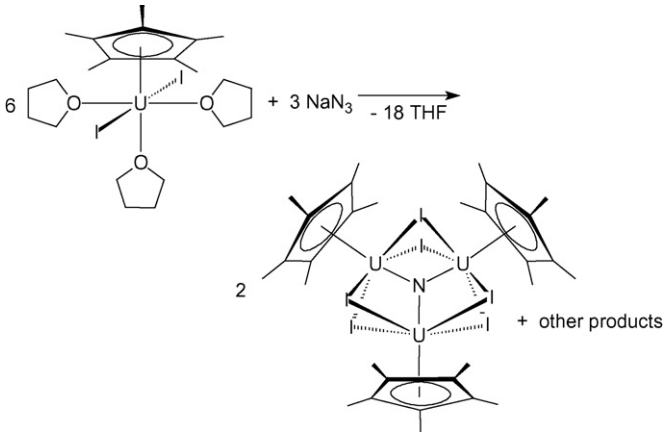

Scheme 147.

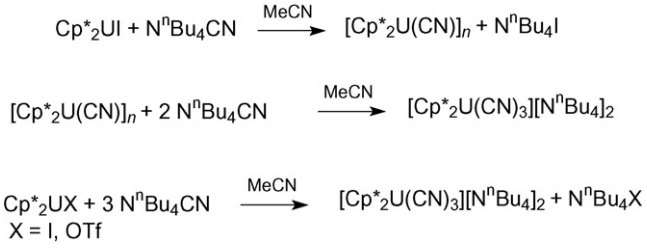

Scheme 148.

also reported that showed that the ranges for the two oxidation states have significant overlap [118].

Interesting cyanide metallocenes of trivalent uranium have been investigated in detail. For example, addition of N^nBu_4CN to $Cp^*_2UI(py)$ or $Cp^*_2U(OTf)$ (M = U, Ce) in acetonitrile led to the precipitation of the neutral monocyanide species $[Cp^*_2U(\mu\text{-}CN)]_n$, which likely have an oligomeric structure (Scheme 148). The structure of the U(III,IV) mixed valence compound $[\{Cp^*_2U\}_2(\mu\text{-}CN)\{(\mu\text{-}CN)_2Na(THF)\}_2]_\infty$, which crystallized from a THF solution of $Cp^*_2UI(py)$ in the presence of excess NaCN, revealed a unique example of an *f*-element-(μ-CN)-M interaction (M = main group or *d* transition metal) (Fig. 31). The anionic polycyanide $[Cp^*_2U(CN)_3][N^nBu_4]_2$ was synthesized by treatment of $[Cp^*_2U(\mu\text{-}CN)]_n$ with 2 equiv. or an excess of N^nBu_4CN in acetonitrile. It was also prepared in a one-pot procedure by stepwise addition of 1 equiv. of KCN and 2 equiv. of $NnBu_4CN$ to the parent iodide in acetonitrile. The bent metallocene $[Cp^*_2U(\mu\text{-}CN)]_n$ is the first fully characterized actinide(III) cyanide [58].

3.2.2.2. Pentamethylcyclopentadienyl actinide(IV)-, (V)-, and (VI)-compounds. The formation of $Cp^*_2U(EPh)Me$, $Cp^*_2U(EPh)_2$, and $Cp^*_2U(\eta^2\text{-}TeC_6H_4)$ from $Cp^*_2UMe_2$ and PhEEPh (E = S, Se, Te) has been investigated. $Cp^*_2UMe_2$ reacts with 1 and 2 equiv. of PhEEPh (E = S, Se) as shown in Scheme 149 to form $Cp^*_2U(EPh)Me$ (E = S, Se) and $Cp^*_2U(EPh)_2$ (E = S, Se), respectively, with concomitant formation of MeEPh [119].

Likewise, addition of 2 equiv. of PhTeTePh to 1 equiv. of $Cp^*_2UMe_2$ generated the tellurium analogue $Cp^*_2U(TePh)_2$, but when $Cp^*_2UMe_2$ was allowed to react with 1 equiv. of PhTeTePh, C–H activation of the aryl ring occurred to form $Cp^*_2U(\eta^2\text{-}TeC_6H_4)$ along with MeTePh and CH_4 (Scheme 150) [119].

In a related study, the reductive reactivity of the $[BPh_4]^-$ ligand in the pentamethylcyclopentadienyl complex $[Cp^*_2U][(\mu\text{-}\eta^2\text{:}\eta^1\text{-}Ph)_2BPh_2]$ was compared with that of the tetramethyl analog, $[(C_5Me_4H)_2U][(\mu\text{-}\eta^6\text{:}\eta^1\text{-}Ph)(\mu\text{-}\eta^1\text{:}\eta^1\text{-}Ph)BPh_2]$ using PhSSPh as a probe to determine if the mode of $[BPh_4]^-$ bonding affected the reduction. Both complexes act as two-electron reductants to form $(C_5Me_4R)_2U(SPh)_2$ (Scheme 151, R = Me, H), but only in the R = H case could the product be crystallographically characterized [120].

In a similar manner, actinide metallocene hydride complexes have been employed as multielectron reductants. In the course of this study, methods to separate the components of the equilibrium mixture of $[Cp^*_2U(\mu\text{-}H)]_2$ and $[Cp^*_2U(\mu\text{-}H)H]_2$ have been developed that allow their reductive chemistry to be studied. These uranium hydrides can act as four-, six-, and eight-electron reductants depending on the substrate, with H_2 as the by-product of a $H^- \rightarrow e^- + 1/2\ H_2$ redox couple. This hydride reduction chemistry even allows complexes of the redox-inactive actinide cation Th^{4+} such as $[Cp^*_2ThH_2]_2$ to be four- and six-electron reductants. $[Cp^*_2U(\mu\text{-}H)]_2$ and $[Cp^*_2U(\mu\text{-}H)H]_2$ cleanly reduce 2 equiv. of PhEEPh (E) S, Se) to form 2 equiv. of $Cp^*_2U(SPh)_2$ and $Cp^*_2U(SePh)_2$ in an overall four-electron reduction in each case (Scheme 152) [121].

An improved synthesis of $[Cp^*_2U][(\mu\text{-}\eta^2\text{:}\eta^1\text{-}Ph)_2BPh_2]$ from $[Cp^*_2U(\mu\text{-}H]_2$ and $[Et_3NH][BPh_4]$ as shown in Scheme 153 was also reported. Using this new route, $[Cp^*_2U][(\mu\text{-}\eta^2\text{:}\eta^1\text{-}Ph)_2BPh_2]$ was formed in high yield (94%) and purity on the basis of ^1H NMR spectroscopy [120].

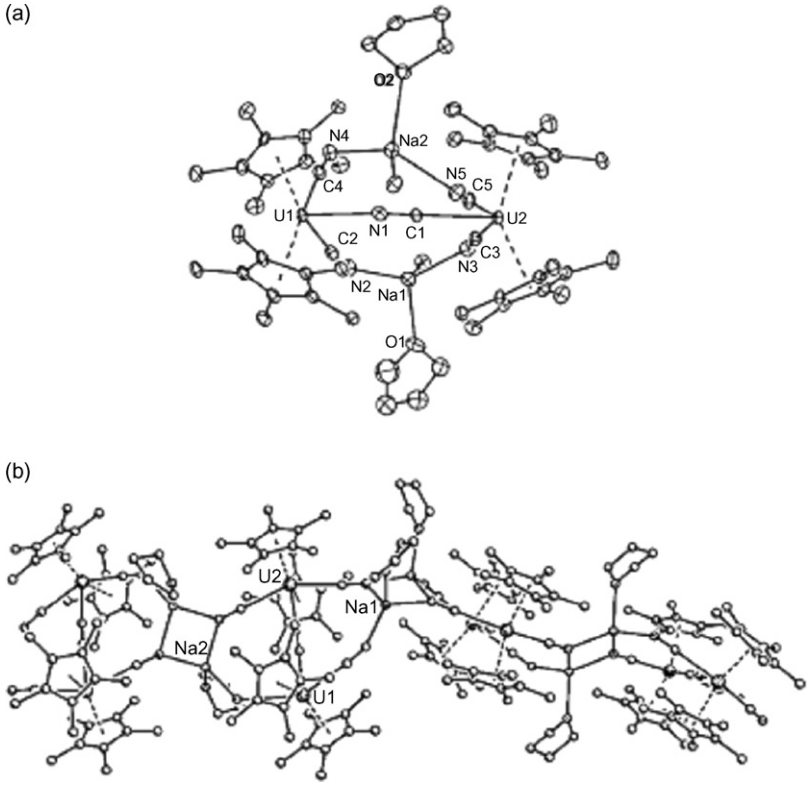

Fig. 31. (a) View of the U(III,IV) mixed valence compound $[\{Cp^*_2U\}_2(\mu\text{-}CN)\{(\mu\text{-}CN)_2Na(THF)\}_2]_\infty$. (b) View of the 1D chain.

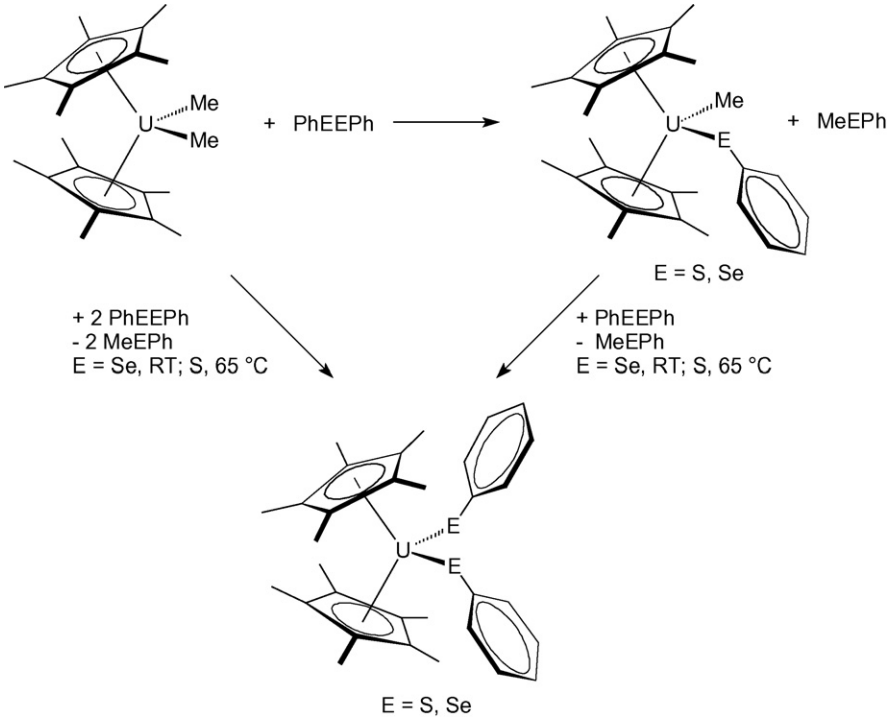

Scheme 149.

The reaction of $[Cp^*_2U][(\mu\text{-}\eta^2\text{:}\eta^1\text{-}Ph)_2BPh_2]$ with MeCN provided another route to the unusual, parallel-ring, uranium metallocene $[Cp^*_2U(NCMe)_5][BPh_4]_2$ (Scheme 154) [120].

A systematic study of bis(pentamethylcyclopentadienyl)-thorium(IV) fluoroketimides has been carried out. As shown in Scheme 155, reaction of $Cp^*_2Th(CH_3)_2$ with 2 equiv. of N≡C–Ar_F gave the corresponding fluorinated thorium(IV) bis(ketimide) complexes $Cp^*_2Th[-N{=}C(CH_3)(Ar_F)]_2$ (where Ar_F = 3-FC_6H_4, 4-FC_6H_4, 2-FC_6H_4, 3,5-$F_2C_6H_3$, 3,4,5-$F_3C_6H_2$, 2,6-$F_2C_6H_3$, 2,4,6-$F_3C_6H_2$, and C_6F_5). The complexes were characterized by a combination of single-crystal X-ray diffraction, cyclic voltammetry and NMR, and UV–vis absorption and low-temperature luminescence spectroscopies. Density functional theory (DFT) and time-dependent DFT (TD-DFT) results were reported for selected complexes and $Cp^*_2Th[-N{=}C(Ph)_2]_2$ for comparison with experimental data and to guide in the interpretation of the spectroscopic results. The most significant structural perturbation imparted by the fluorine substitution in these complexes is a rotation of the fluorophenyl group (Ar_F) out of the plane defined by the $N{=}C(C_{Me})(C_{ipso})$ fragment in the fluorinated complexes when the Ar_F group possesses two ortho fluorine atoms [122].

In the course of this work, a unique eight-membered thorium(IV) tetraazamacrocycle was discovered which is produced by the sequential, metal-mediated coupling of 4 equiv. of 4-

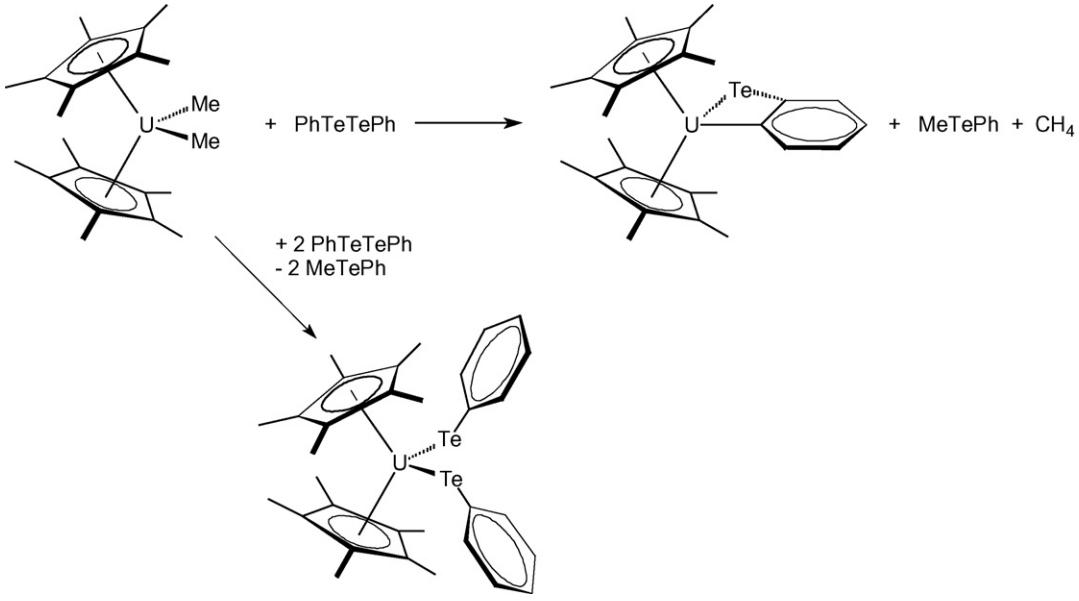

Scheme 150.

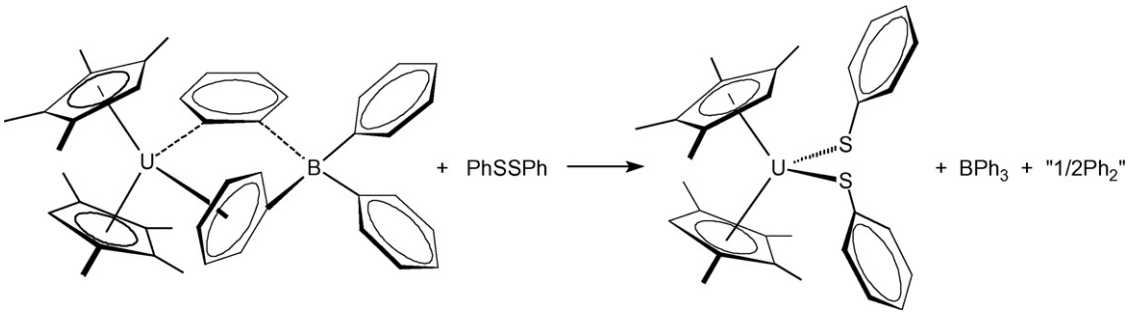

Scheme 151.

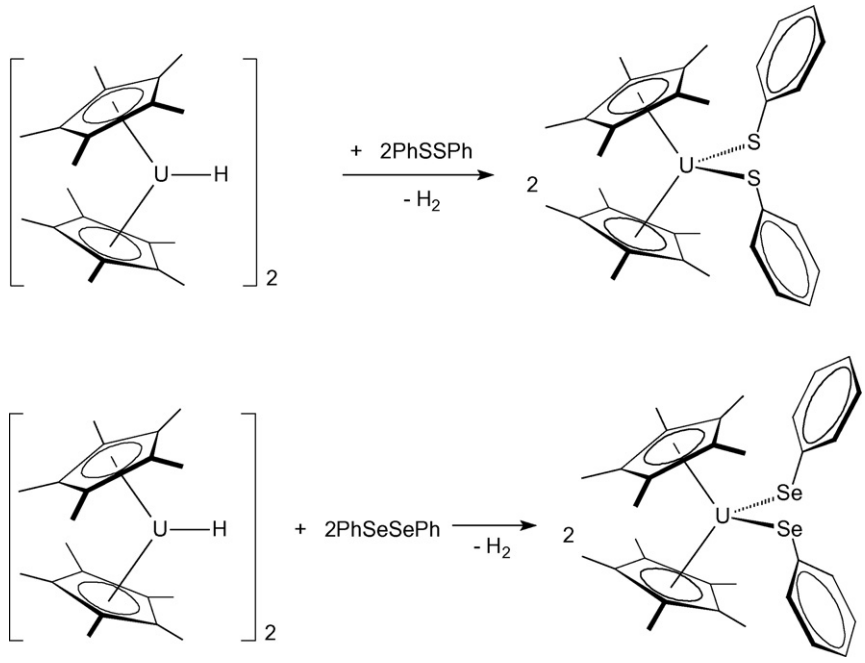

Scheme 152.

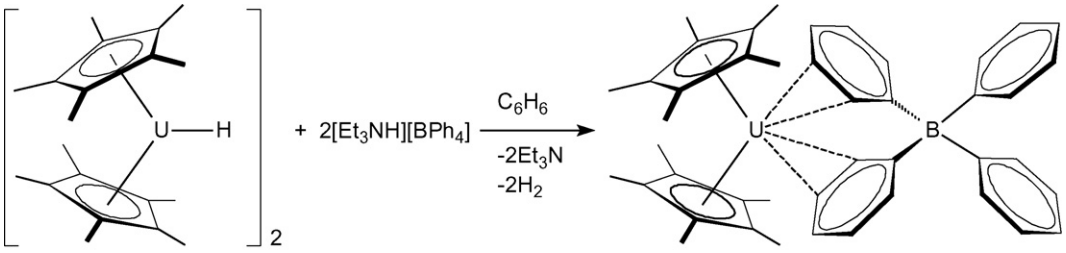

Scheme 153.

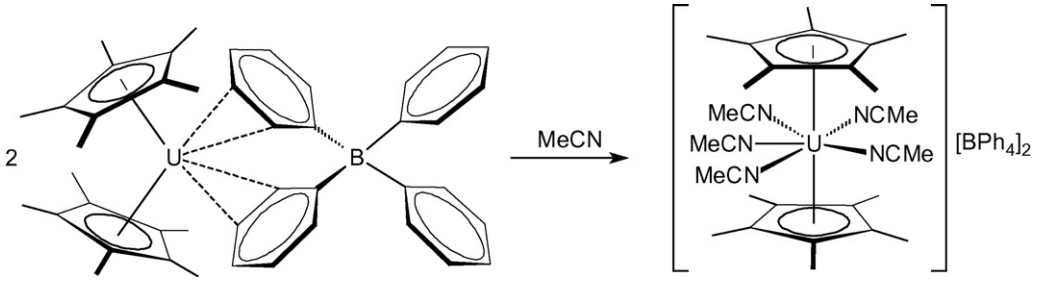

Scheme 154.

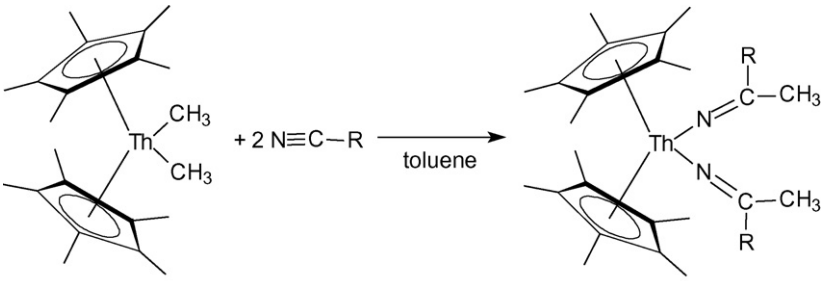

R = 3-F-C_6H_4, 44%, orange
4-F-C_6H_4, 48%, yellow
2-F-C_6H_4, 81%, yellow
3,5-F_2-C_6H_3, 70%, orange
3,4,5-F_3-C_6H_2, 48%, orange
2,6-F_2C_6-H_3, 69%, yellow
2,4,6-F_3-C_6H_2, 53%, orange
C_6F_5, 95%, orange

Scheme 155.

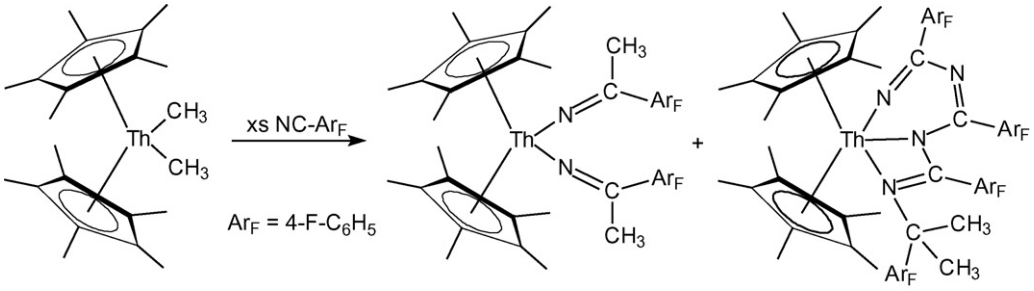

Scheme 156.

fluorobenzonitrile. As illustrated in Scheme 156, treatment of $Cp^*_2ThMe_2$ with excess 4-fluorobenzonitrile yielded the expected bright yellow bis(ketimide) complex $Cp^*_2Th[-N{=}C(Me)(C_6H_4F\text{-}4)]_2$ as the major product (48% isolated yield), in addition to a novel orange-red Th(IV) tetraazamacrocycle $Cp^*_2Th[-N{=}C(4\text{-}FC_6H_4)-N{=}C(4\text{-}FC_6H_4)-N-C(4\text{-}FC_6H_4){=}N-C(4\text{-}FC_6H_4)Me_2]$ (3% isolated yield). Following work-up and crystallization from cold pentane solution, both complexes were reproducibly isolated in an analytically pure form, and were characterized by a combination of $^1H/^{13}C/^{19}F$ NMR and UV–vis/NIR spectroscopy, electrochemistry, elemental analysis and X-ray crystallography [123].

Confirmation that the Th(IV) metal center had coupled together 4 equiv. of 4-fluorobenzonitrile and formed the eight-membered tetraazametallacycle was obtained by a single-crystal X-ray crystallography study (Fig. 32). The molecular structure reveals that the thorium atom is 9-coordinate, adopting a characteristic bent-metallocene geometry, with Th–Cp* bond lengths of 2.598(5) and 2.577(5) Å and a Cp*(centroid)-Th-Cp*(centroid) bond angle of 133.7(5)°. These values are well within the range typically found for $Cp^*_2Th(IV)$ complexes. The dianionic tetraaza ligand is contained within the metallocene wedge and consists of alternating C–N units, originating from the four 4-fluorobenzonitrile molecules. The ligand is bound to the Th metal center in an η^3-(*N*,*N*′,*N*″)-fashion through two Th–N s-bonds (Th(1)–N(2) and Th(1)–N(4)) and one Th–N dative interaction (Th(1)–N(1)) [123].

Formation of the thorium(IV) tetraazametallacycle is consistent with the involvement of an imido intermediate, generated from a thorium ketimide complex as illustrated in Scheme 157. Attempts to increase the yield of the metallacycle by using deficient or excess nitrile and a large dilution of reagents did not change the observed ratio of products [123].

In a closely related study the analoguos uranium(IV) fluoroketimides have been investigated in detail. Reactions of

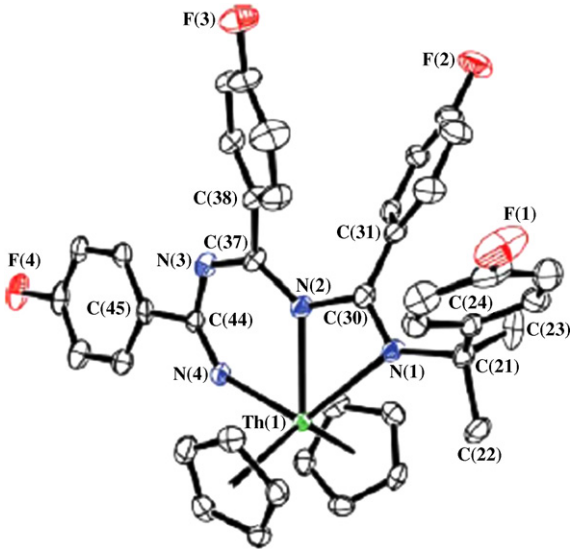

Fig. 32. Molecular structure of $Cp^*_2Th[-N{=}C(4\text{-}FC_6H_4)-N{=}C(4\text{-}FC_6H_4)-N-C(4\text{-}FC_6H_4){=}N-C(4\text{-}FC_6H_4)Me_2]$ (methyl groups of the Cp* ligands omitted for clarity) [123].

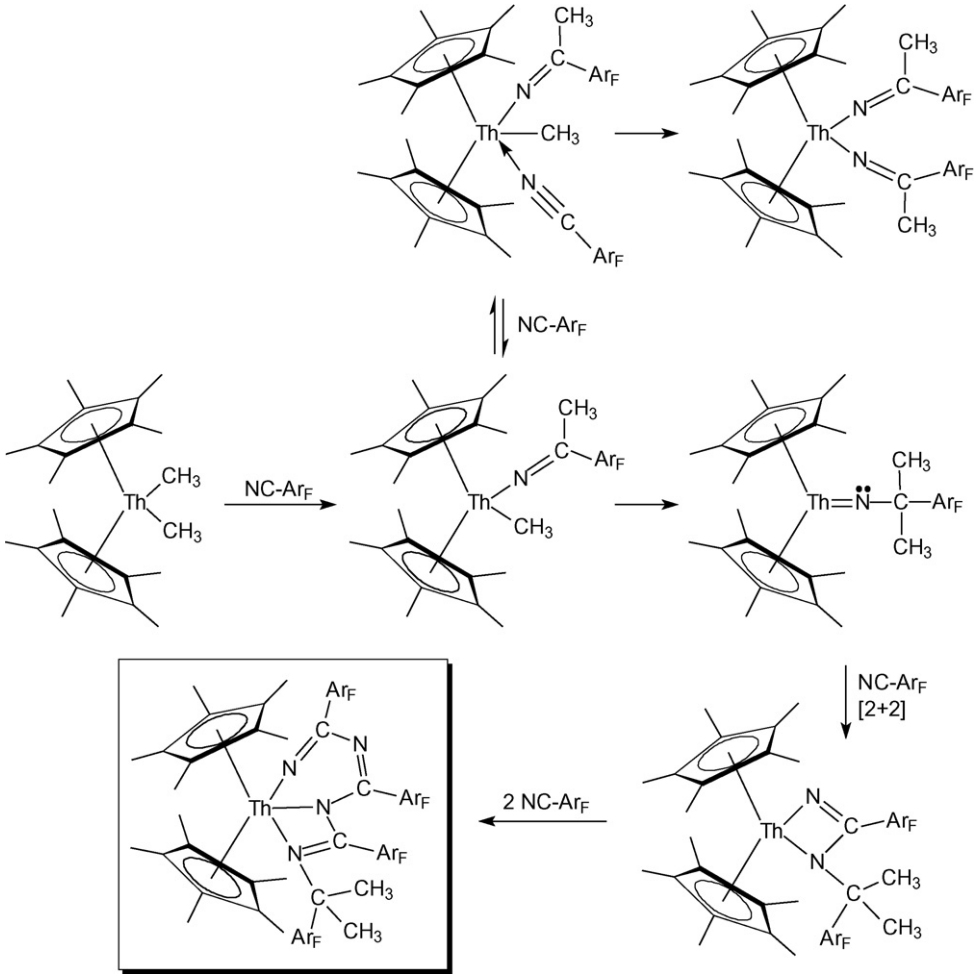

Scheme 157.

$Cp^*_2UMe_2$ with 2 equiv. of N≡C-Ar$_F$ as illustrated in Scheme 158 afforded the fluorinated uranium(IV) bis(ketimide) complexes $Cp^*_2U[-N{=}CMe(Ar_F)]_2$ [where Ar_F = 2-F-C_6H_4, 3-F-C_6H_4, 4-F-C_6H_4, 2,6-F_2-C_6H_3, 3,5-F_2-C_6H_3, 2,4,6-F_3-C_6H_2, 3,4,5-F_3-C_6H_2, and C_6F_5]. These have been characterized by single-crystal X-ray diffraction, ^{1}H and ^{19}F NMR, cyclic voltammetry, UV–vis-near-IR absorption spectroscopy, and variable-temperature magnetic susceptibility [124].

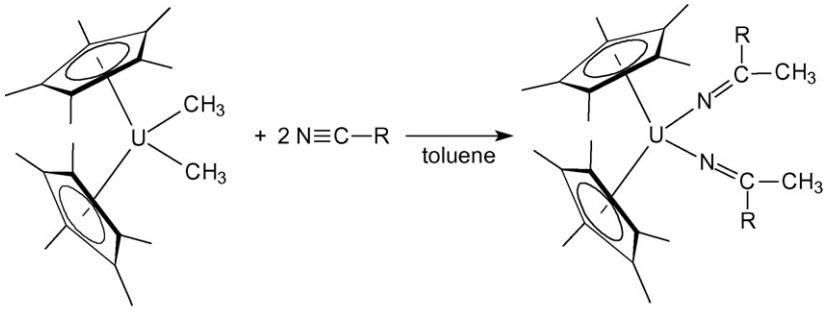

R = 2 - F - C_6H_4, 62 %
3 - F - C_6H_4, 61 %
4 - F - C_6H_4, 40 %
2,6 - F_2 - C_6H_3, 31 %
3,5 - F_2 - C_6H_3, 64 %
2,4,6 - F_3 - C_6H_2, 59 %
3,4,5 - F_3 - C_6H_2, 65 %
C_6F_5, 79 %

Scheme 158.

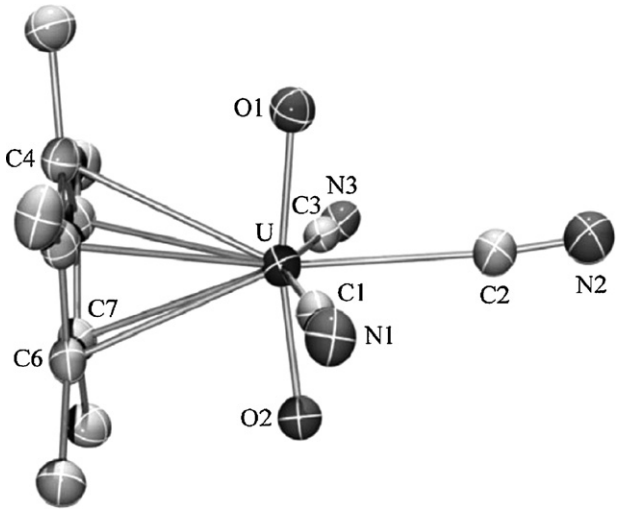

Fig. 33. Molecular structure of the dianion in $[NEt_4]_2[Cp^*UO_2(CN)_3]$ [125].

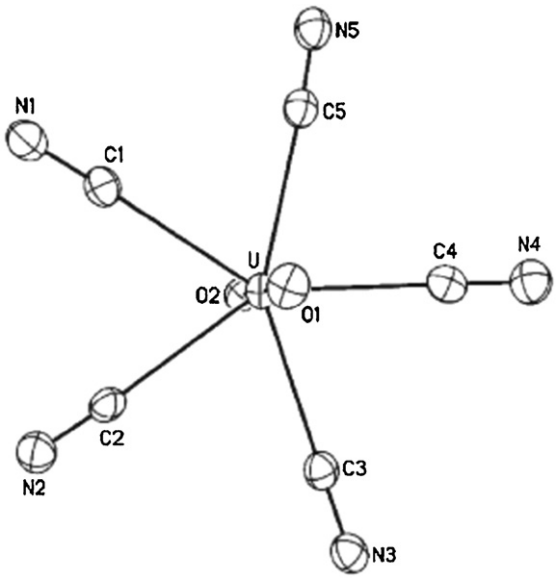

Fig. 34. Molecular structure of the trianion in $[NEt_4]_3[UO_2(CN)_5]$ [126].

Among the major achievements in organoactinide chemistry published in 2007 was the successful preparation and structural characterization of the first cyclopentadienyl complex of uranyl. The U(IV) linear pentacyano metallocene $[NEt_4]_3[Cp^*_2U(CN)_5]$ reacts with 2 molar equivalents of pyridine *N*-oxide in THF or acetonitrile to give the orange U(VI) complex $[NEt_4]_2[Cp^*UO_2(CN)_3]$, the first uranyl species containing the cyclopentadienyl ligand; the crystal structure revealed that the steric effects of the Cp* ligand force the $\{UO_2\}^{2+}$ ion to deviate from linearity (Fig. 33) [125].

Although not an organometallic compound in the strict sense, the synthesis and structural characterization of the first actinyl cyanide complexes should also be mentioned here. As shown in Scheme 159, reaction of $UO_2(OTf)_2$ (OTf = OSO_2CF_3) with 5 molar equivalents of NEt_4CN in acetonitrile led to the formation of the pentacyano uranyl complex $[NEt_4]_3[UO_2(CN)_5]$ which is monomeric in the solid state with the five C-coordinated cyanide ions lying in the equatorial plane perpendicular to the linear $\{UO_2\}$ axis (Fig. 34) [126].

Also reported were bent and linear uranium(IV) metallocenes with terminal and bridging cyanide ligands. Scheme 160 summarizes the reaction sequences employed. Treatment of $Cp^*_2UI_2$ with KCN in THF solution led to the formation of $Cp^*_2U(CN)_2$, which further reacted with NR_4CN to give $[Cp^*_2U(CN)_3][NR_4]$ and $[Cp^*_2U(CN)_5][NR_4]_3$ (R = Et, ^{n}Bu). While the tris(cyanide) $[Cp^*_2U(CN)_3][N^nBu_4]$ adopts the familiar bent sandwich configuration, the pentacyanide $[Cp^*_2U(CN)_5][NEt_4]_3$ is, after the $[Cp^*_2U(NCMe)_5]^{2+}$ cation, the second example of a linear metallocene resulting from complete saturation of the equatorial girdle. Compound $[Cp^*_2U(CN)_3][N^nBu_4]$ was also obtained by oxidation of the trivalent compound $[Cp^*_2U(CN)_3][N^nBu_4]_2$. The rapid and reversible electron transfer between the U(III) and U(IV) complexes was revealed by ^{1}H NMR spectroscopy [127].

The NMR spectra also revealed that $[Cp^*_2U(CN)_5][NEt_4]_3$ is partially dissociated in THF solution into $[Cp^*_2U(CN)_3][NEt_4]$ (Scheme 161), thereby providing the first example of an equilibrating couple of bent and linear metallocenes [$K = 4.24(4) \times 10^{-5}$ at 25 °C, $\Delta H = 199(6)$ kJ mol^{-1}, and $\Delta S = 586(20)$ J mol^{-1} K^{-1}] [127].

The trinuclear compound $[Cp^*_2UCl_2(\mu\text{-}CN)]_2Mg(THF)_4$ and the 2D polymeric complex $[Cp^*_2U(DMF)_3(\mu\text{-}NC)_2(AgI)_2]_n$, which were

$$UO_2(OTf)_2 + 5\ NEt_4CN \xrightarrow[-2\ NEt_4OTf]{\text{acetonitrile}} [NEt_4]_3\,[UO_2(CN)_5]$$

Scheme 159.

$$Cp^*_2UI_2 + 2\ KCN \xrightarrow{THF} Cp^*_2U(CN)_2 + 2\ KI$$

$$Cp^*_2UI_2 + 3\ NR_4CN \xrightarrow{THF} [Cp^*_2U(CN)_3][NR_4] + 2\ NR_4I$$

R = Et, ^{n}Bu

$$Cp^*_2U(OTf)_2 + 5\ NEt_4CN \xrightarrow{MeCN} [Cp^*_2U(CN)_5][NEt_4]_3 + 2\ NEt_4OTf$$

Scheme 160.

obtained during initial attempts on the synthesis of the cyano complexes shown in Scheme 160 and uranium(V) derivatives, exhibit a bent and linear sandwich structure, respectively [127].

Crystals of the U^{IV} cyano complex $[Cp^*_2U(CN)_3][N^nBu_4]\cdot 1.5THF$ were also formed from $Cp^*_2UI_2$ and N^nBu_4CN in THF, while the analytically pure complex $[Cp^*_2U(CN)_3][NEt_4]$ was synthesized in good yield by reaction of $Cp^*_2UI_2$ with NEt_4CN in THF. The U^{III} complex $[Cp^*_2U(CN)_3][N^nBu_4]_2$ was inert towards an excess of cyanide ions, whereas its U^{IV} counterparts were readily transformed into the pentacyanido derivatives $[Cp^*_2U(CN)_5][NR_4]_3$ (R = Me, ^{n}Bu). The orange compound $[Cp^*_2U(CN)_5][NEt_4]_3$ was isolated in 75% yield from $Cp^*_2U(OTf)_2$ and NEt_4CN. Slow diffusion of Et_2O into a MeCN solution of $Cp^*_2UI_2$ and NEt_4CN gave crystals of $[Cp^*_2U(CN)_5][NEt_4]_3\cdot$MeCN. Similarly, in an attempt to synthesize $[Cp^*_2U(CN)_5][N^nBu_4]_3$, brown crystals of the U^V derivative $[Cp^*_2U(CN)_5][N^nBu_4]_2$ were obtained, likely resulting from oxidation of the parent U^{IV} metallocene by adventitious traces of air. The structures of the anions of $[Cp^*_2U(CN)_5]^{3-}$ and $[Cp^*_2U(CN)_5]^{2-}$ are very similar. A view of the anion $[Cp^*_2U(CN)_5]^{2-}$ is shown in Fig. 35. The geometry of the linear metallocene is identical to that of the dication $[Cp^*_2U(NCMe)_5]^{2+}$, with the Cp* rings equidistant from and parallel to the plane defined by the metal center and the five CN

$$[Cp^*_2U(CN)_3][NEt_4] + 2\ NEt_4CN \rightleftharpoons [Cp^*_2U(CN)_5][NEt_4]_3$$

Scheme 161.

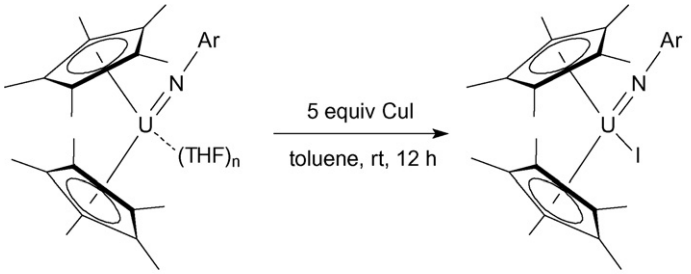

Ar = 2,4,6-^{t}Bu$_3$-C$_6$H$_2$, n = 0 — Ar = 2,4,6-^{t}Bu$_3$-C$_6$H$_2$ 78% Yield
Ar = 2,6-^{i}Pr$_2$-C$_6$H$_3$, n = 1 — Ar = 2,6-^{i}Pr$_2$-C$_6$H$_3$ 81% Yield

Scheme 162.

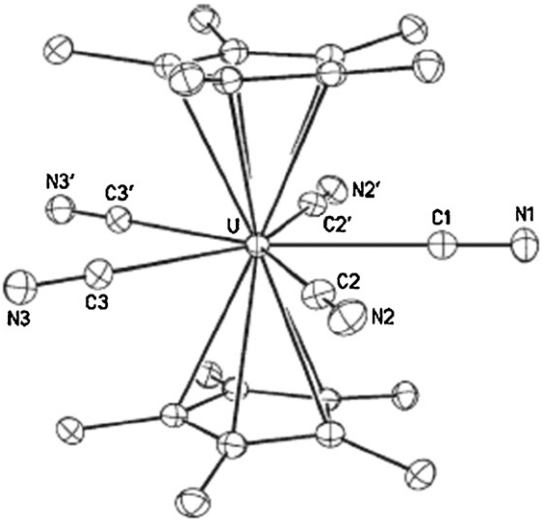

Fig. 35. Molecular structure of the $[Cp^*_2U(CN)_5]^{2-}$ anion [128].

groups. The pentagon of the CN carbon atoms is in a staggered conformation with respect to the eclipsed Cp* rings. As expected from the variation in the radii of the U^{4+} and U^{5+} ions, the mean U–C(Cp*) and U–C(CN) bond lengths in $[Cp^*_2U(CN)_5][N^nBu_4]_2$ are about 0.1 Å smaller than those in $[Cp^*_2U(CN)_5][N^nBu_4]_3$. These results demonstrate that $[Cp^*_2U(CN)_5]^{q-}$ anions are formed with U^{IV}/U^{V} centers but not with U^{III}, thus evidencing that the number of *f*-electrons is prevailing in the stability of linear *versus* bent metallocenes [128].

Surprisingly, facile access to pentavalent uranium metallocenes was found in the one-electron oxidation of uranium(IV) imido complexes with copper(I) salts. Thus reaction of $Cp^*_2U(=N–Ar)(THF)_n$ (Scheme 162) with excess copper(I) iodide in toluene afforded the corresponding U(V) complexes $Cp^*_2U(=N\text{-}2,4,6\text{-}^tBu_3C_6H_2)(I)$ and $Cp^*_2U(=N\text{-}2,6\text{-}^iPr_2\text{-}C_6H_3)(I)$, respectively, as dark brown powders in good isolated yield [129].

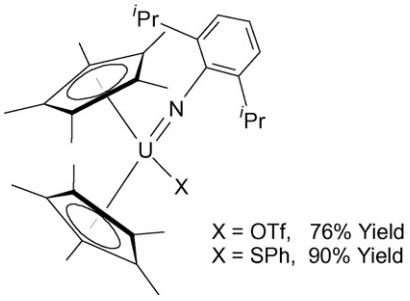

Scheme 163.

This Cu(I)-based oxidation protocol appears to be quite general. Similar reaction of $Cp^*_2U(=N\text{-}2,6\text{-}^iPr_2\text{-}C_6H_3)$ with either CuOTf or CuSPh gives the corresponding U(V) triflate and phenylthiolate complexes, respectively, in good isolated yield (Scheme 163) [129].

The uranium metallocene hydrides $[Cp^*_2U(\mu\text{-}H)]_2$ and $[Cp^*_2U(\mu\text{-}H)H]_2$ were found to effect an eight-electron reduction of 2 equiv. of PhN=NPh to form 2 equiv. of the known U^{6+} bis(imido) complex $Cp^*_2U(=NPh)_2$ with H_2 being a by-product (Scheme 164) [121].

3.3. Actinide cyclooctatetraenyl complexes

Recently developed quasirelativistic energy-consistent 5*f*-in-core pseudopotentials as well as core-polarization potentials corresponding to tetravalent actinides were employed to study the molecular structures, ionic metal-ring binding energies, and Mulliken orbital populations of the actinocenes $An(C_8H_8)_2$ (An = Th–Pu). The results of Hartree–Fock calculations show only small deviations from 5*f*-in-valence calculations, although the 5*f* orbitals contribute to the covalent actinide-ring bonding. For thorocene and uranocene, second-order Møller–Plesset perturbation theory, coupled-cluster theory with single and double excitation operators and a perturbative estimate of triple excitations, and density functional theory yield actinide-ring distances which are in good agreement with the experimental values [130].

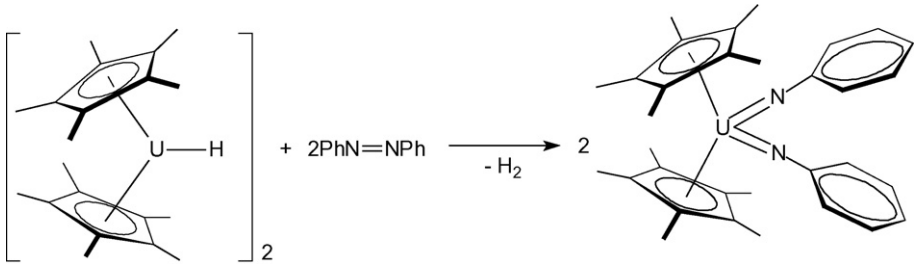

Scheme 164.

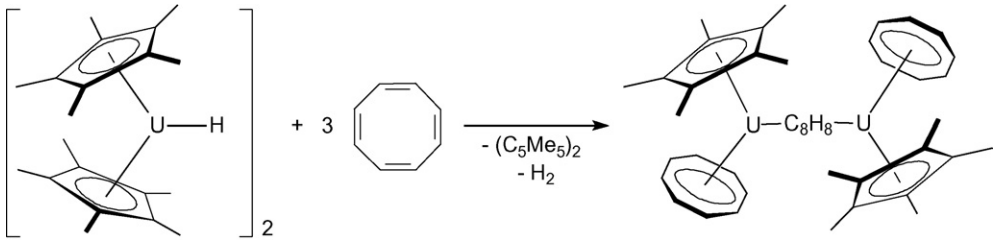

Scheme 165.

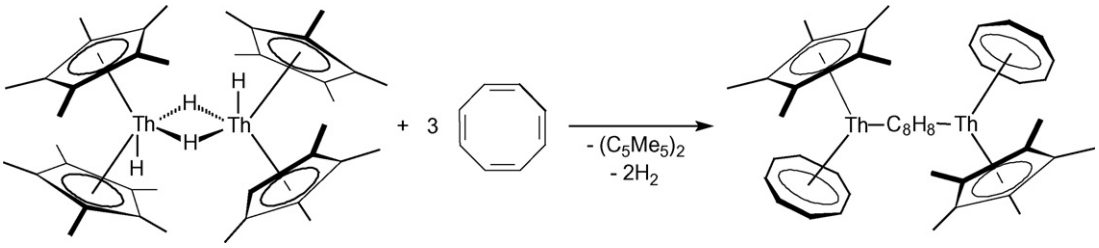

Scheme 166.

The uranium metallocene hydrides $[Cp^*_2U(\mu\text{-}H)]_2$ and $[Cp^*_2U(\mu\text{-}H)H]_2$ were found to effect a six-electron reduction of 3 equiv. of 1,3,5,7-cyclooctatetraene to the known complex $(\mu\text{-}COT)[Cp^*(COT)U]_2$ (Scheme 165) with H_2 being a by-product [121].

Remarkably, the same hydride-based reduction of 1,3,5,7-cyclooctatetraene could also be achieved with the tetravalent thorium metallocene hydride $[Cp^*_2Th(\mu\text{-}H)H]_2$, which reduces 3 equiv. of C_8H_8 to $(\mu\text{-}COT)[Cp^*(COT)Th]_2$ (Scheme 166) with concomitant formation of H_2. This light orange crystalline product was isolated in >80% yield and structurally characterized by X-ray diffraction (Fig. 36) [121].

3.4. Organoactinides in catalysis

A mechanistic study of intramolecular hydroamination/cyclization catalyzed by tetravalent organoactinide complexes has been presented. A series of selectively substituted constrained geometry complexes, (CGC)An(NR_2)Cl and (CGC)An(NMe_2)OAr (CGC = $[Me_2Si(\eta^5\text{-}Me_4C_5)(Bu^tN)]^{2-}$; An = Th, U), was prepared as illustrated in Scheme 167 *via in situ* protodeamination or salt metathesis in high purity and excellent yields and found to be active precatalysts for intramolecular primary and secondary aminoalkyne and aminoalkene hydroamination/cyclization reactions. Substrate reactivity trends, rate laws, and activation parameters for cyclizations mediated by these complexes are virtually identical to those of more conventional (CGC)An(NMe_2)$_2$ (An = Th, U), $[Me_2Si(C_5Me_4)_2]U(CH_2Ph)_2$, and $Cp^*_2An(CH_2SiMe_3)_2$ (An = Th, U) complexes. Together, the data provided strong evidence in these systems for turnover-limiting C-C insertion into an An-N(H)R σ-bond in the transition state. Related complexes $[Me_2Si(C_5Me_4)_2]U(CH_2Ph)(Cl)$ and $Cp^*_2An(CH_2SiMe_3)Cl$ (An = Th, U) were also found to be effective precatalysts for this transformation. Additional arguments supporting M-N(H)R intermediates *versus* M = NR intermediates were presented. Both (CGC)An(NMe_2)$_2$ (An = Th, U) can be quantitatively converted to the neutrally charged, solvent-free dichlorides (CGC)$AnCl_2$ and slightly more soluble diiodides (CGC)AnI_2 with excess Me_3Si-X (X = Cl, I) in non-coordinating solvents [131].

In a closely related study, these constrained geometry organoactinide complexes were found to exhibit broad applicability for the intramolecular hydroamination of diverse C–C unsaturations,

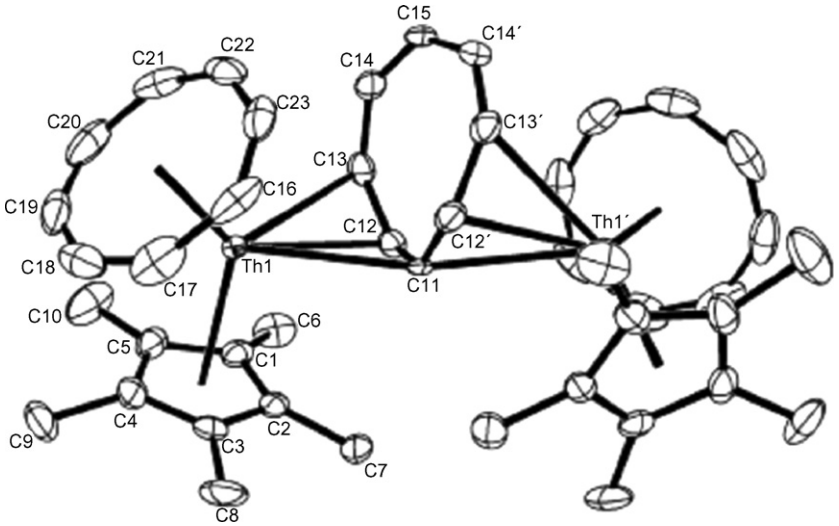

Fig. 36. Molecular structure of $(\mu\text{-}COT)[Cp^*(COT)Th]_2$ [121].

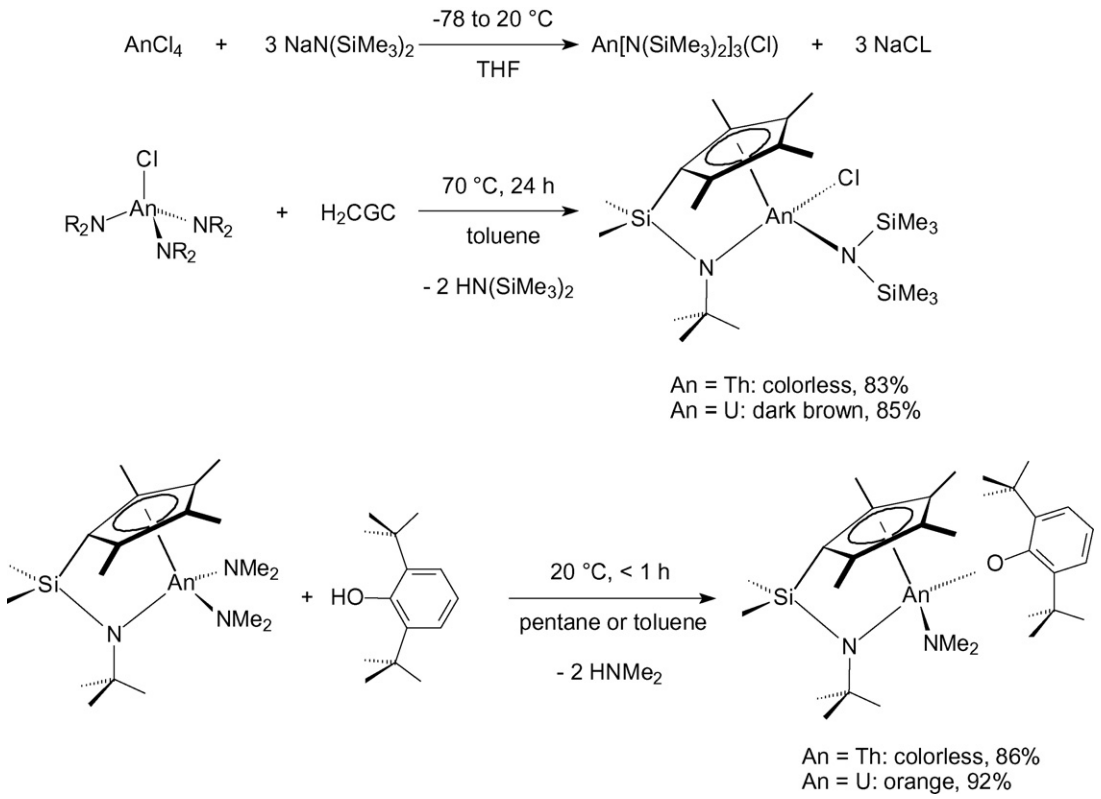

Scheme 167.

including terminal and internal aminoalkenes (primary and secondary amines), aminoalkynes (primary and secondary amines), aminoallenes, and aminodienes. Large turnover frequencies (N_t up to 3000 h^{-1}) and high regioselectivities (≥95%) were observed throughout, along with moderate to high diastereoselectivities (up to 90% *trans* ring closures). With several noteworthy exceptions, reactivity trends track relative 5*f* ionic radii and ancillary ligand coordinative unsaturation. Reactivity patterns and activation parameters were consistent with a reaction pathway proceeding *via* turnover-limiting C=C/C≡C insertion into the An-N σ-bond [132].

References

[1] L. Jiang, Q. Xu, J. Phys. Chem. A 111 (2007) 3271.
[2] L. Jiang, Q. Xu, J. Phys. Chem. A 111 (2007) 3519.
[3] P.F. Weck, T.J.D. Kumar, N. Balakrishnan, J. Chem. Phys. 126 (2007) 094703.
[4] W. Noh, G.S. Girolami, Polyhedron 26 (2007) 3865.
[5] H.-G. Cho, L. Andrews, Organometallics 26 (2007) 633.
[6] H.-G. Cho, L. Andrews, J. Phys. Chem. A 111 (2007) 2480.
[7] X. Li, J. Paldusa, J. Chem. Phys. 126 (2007) 234303.
[8] L. Maron, D. Bourissou, Organometallics 26 (2007) 1100.
[9] L.J. Bowman, K. Izod, W. Clegg, R.W. Harrington, J. Organomet. Chem. 692 (2007) 806.
[10] L.J. Bowman, K. Izod, W. Clegg, R.W. Harrington, Organometallics 26 (2007) 2646.
[11] Y. Luo, M. Nishiura, Z. Hou, J. Organomet. Chem. 692 (2007) 536.
[12] S. Bambirra, D. van Leusen, C.G.J. Tazelaar, A. Meetsma, B. Hessen, Organometallics 26 (2007) 1014.
[13] S. Ge, A. Meetsma, B. Hessen, Organometallics 26 (2007) 5278.
[14] K.D. Conroy, P.G. Hayes, W.E. Piers, M. Parvez, Organometallics 26 (2007) 4464.
[15] M. Rastätter, A. Zulys, P.W. Roesky, Chem. Eur. J. 13 (2007) 3606.
[16] L. Zhang, T. Suzuki, Y. Luo, M. Nishiura, Z. Hou, Angew. Chem. 119 (2007) 1941.
[17] B. Liu, D. Cui, J. Ma, X. Chen, X. Jing, Chem. Eur. J. 13 (2007) 834.
[18] S. Li, W. Miao, T. Tang, D. Cui, X. Chen, X. Jing, J. Organomet. Chem. 692 (2007) 4943.
[19] B. Liu, Y. Yang, D. Cui, T. Tang, X. Chen, X. Jing, Dalton Trans. (2007) 4252.
[20] S.C. Marinescu, T. Agapie, M.W. Day, J.E. Bercaw, Organometallics 26 (2007) 1178.
[21] X. Liu, X. Shang, T. Tang, N. Hu, F. Pei, D. Cui, X. Chen, X. Jing, Organometallics 26 (2007) 2747.
[22] W. Miao, S. Li, D. Cui, B. Huang, J. Organomet. Chem. 692 (2007) 3823.
[23] L. Lukešová, B.D. Ward, S. Bellemin-Laponnaz, H. Wadepohl, L.H. Gade, Organometallics 26 (2007) 4652.
[24] I.S. Edworthy, A.J. Blake, C. Wilson, P.L. Arnold, Organometallics 26 (2007) 3684.
[25] H. Zhou, H. Guo, Y. Yao, L. Zhou, H. Sun, H. Sheng, Y. Zhang, Q. Shen, Inorg. Chem. 46 (2007) 958.
[26] R.E. White, T.P. Hanusa, B.E. Kucera, J. Organomet. Chem. 692 (2007) 3479.
[27] F. Jaroschik, F. Nief, X.-F. Le Goff, L. Ricard, Organometallics 26 (2007) 1123.
[28] F. Jaroschik, F. Nief, X.-F. Le Goff, L. Ricard, Organometallics 26 (2007) 3552.
[29] W. Fan, D.J. Berg, R.H. Mitchell, T.M. Barclay, Organometallics 26 (2007) 4562.
[30] Q. Sun, Q. Wang, P. Jena, B.V. Reddy, M. Marquez, Chem. Mater. 19 (2007) 3074.
[31] Y. Luo, Z. Hou, Organometallics 26 (2007) 2941.
[32] X. Xu, M. Hu, Y. Yao, R. Qi, Y. Zhang, Q. Shen, J. Mol. Struct. 829 (2007) 189.
[33] A.S.P. Frey, M.G. Gardiner, D.N. Stringer, B.F. Yates, Organometallics 26 (2007) 1299.
[34] W. Miao, S. Li, H. Zhang, D. Cui, Y. Wang, B. Huang, J. Organomet. Chem. 692 (2007) 2099.
[35] J. Hitzbleck, K. Beckerle, J. Okuda, J. Organomet. Chem. 692 (2007) 4702.
[36] J. Hitzbleck, J. Okuda, Organometallics 26 (2007) 3227.
[37] W.-X. Zhang, M. Nishiura, Z. Hou, Chem. Eur. J. 13 (2007) 4037.
[38] N. Meyer, P.W. Roesky, Dalton Trans. (2007) 2652.
[39] T. Shima, Z. Hou, J. Am. Chem. Soc. 128 (2006) 8124.
[40] X. Li, J. Baldamus, M. Nishiura, O. Tardif, Z. Hou, Angew. Chem. 118 (2006) 8364.
[41] M.D. Walter, D. Bentz, F. Weber, O. Schmitt, G. Wolmershaeuser, H. Sitzmann, New J. Chem. 31 (2007) 305.
[42] E.L. Werkema, L. Maron, O. Eisenstein, R.A. Andersen, J. Am. Chem. Soc. 129 (2007) 2529.
[43] W.J. Evans, D.B. Rego, J.W. Ziller, A.G. DiPasquale, A.L. Rheingold, Organometallics 26 (2007) 4737.
[44] D.V. Vitanova, F. Hampel, K.C. Hultzsch, J. Organomet. Chem. 692 (2007) 4690.
[45] Z.-X. Zhang, Y.-R. Li, R.-T. Liu, Z.-X. Chen, L.-H. Weng, X.-G. Zhou, Polyhedron 26 (2007) 4986.
[46] L. Ma, J. Zhang, R. Cai, Z. Chen, X. Zhou, Dalton Trans. (2007) 2718.
[47] C. Pi, Z. Zhu, L. Weng, Z. Chen, X. Zhou, Chem. Commun. (2007) 2190.
[48] C. Pi, R. Liu, P. Zheng, Z. Chen, X. Zhou, Inorg. Chem. 46 (2007) 5252.
[49] C. Pi, Z. Zhang, Z. Pang, J. Zhang, J. Luo, Z. Chen, L. Weng, X. Zhou, Organometallics 26 (2007) 1934.
[50] Z. Li-Ying, S. Hong-Ting, Y. Ying-Ming, Z. Yong, S. Qi, J. Organomet. Chem. 692 (2007) 2990.
[51] A.A. Trifonov, I.A. Borovkov, E.A. Fedorova, G.K. Fukin, J. Larionova, N.O. Druzhkov, V.K. Cherkasov, Chem. Eur. J. 13 (2007) 4981.
[52] H.-D. Amberger, H. Reddmann, Z. Anorg. Allg. Chem. 633 (2007) 443.
[53] H.-D. Amberger, H. Reddmann, J. Organomet. Chem. 692 (2007) 5103.
[54] W.J. Evans, T.M. Champagne, J.W. Ziller, Organometallics 26 (2007) 1204.

[55] W.J. Evans, E. Montalvo, S.E. Foster, K.A. Harada, J.W. Ziller, Organometallics 26 (2007) 2904.
[56] K.C. Jantunen, B.L. Scott, J.C. Gordon, J.L. Kiplinger, Organometallics 26 (2007) 2777.
[57] M.T. Gamer, P.W. Roesky, I. Palard, M. Le Hellaye, S.M. Guillaume, Organometallics 26 (2007) 651.
[58] J. Maynadié, J.-C. Berthet, P. Thuéry, M. Ephritikhine, Organometallics 26 (2007) 2623.
[59] M.D. Walter, D.J. Berg, R.A. Andersen, Organometallics 26 (2007) 2296.
[60] C.N. Carlson, C.J. Kuehl, L. Ogallo, D.A. Shultz, J.D. Thompson, M.L. Kirk, R.L. Martin, K.D. John, D.E. Morris, Organometallics 26 (2007) 4234.
[61] C.N. Carlson, B.L. Scott, R.L. Martin, J.D. Thompson, D.E. Morris, K.D. John, Inorg. Chem. 46 (2007) 5013.
[62] K. Vasudevan, A.H. Cowley, Chem. Commun. (2007) 3464.
[63] A. Ashley, G. Balazs, A. Cowley, J. Green, C.H. Booth, D. O'Hare, Chem. Commun. (2007) 1515.
[64] G. Balazs, F. Geoffrey, N. Cloke, J.C. Green, R.M. Harker, A. Harrison, P.B. Hitchcock, C.N. Jardine, R. Walton, Organometallics 26 (2007) 3111.
[65] L.G. Klapshina, I.S. Grigoryev, W.E. Douglas, A.A. Trifonov, I.D. Gudilenkov, V.V. Semenov, B.A. Bushukc, S.B. Bushuk, Chem. Commun. (2007) 1942.
[66] S. Wang, X. Tang, A. Vega, J.-Y. Saillard, S. Zhou, G. Yang, W. Yao, Y. Wie, Organometallics 26 (2007) 1512.
[67] S. Wang, S. Wang, S. Zhou, G. Yang, W. Luo, N. Hu, Z. Zhou, H.-B. Song, J. Organomet. Chem. 692 (2007) 4828.
[68] B. Wang, D. Wang, D. Cui, W. Gao, T. Tang, X. Chen, X. Jing, Organometallics 26 (2007) 3167.
[69] A.-S. Rodrigues, E. Kirillov, C.W. Lehmann, T. Roisnel, B. Vuillemin, A. Razavi, J.-F. Carpentier, Chem. Eur. J. 13 (2007) 5548.
[70] S. Zhou, S. Wang, G. Yang, Q. Li, L. Zhang, Z. Yao, Z. Zhou, H.-B. Song, Organometallics 26 (2007) 3755.
[71] A.A. Trifonov, E.A. Fedorova, I.A. Borovkov, G.K. Fukin, E.V. Baranov, J. Larionova, N.O. Druzhkov, Organometallics 26 (2007) 2488.
[72] Y. Yang, S. Li, D. Cui, X. Chen, X. Jing, Organometallics 26 (2007) 671.
[73] Y. Yang, B. Liu, K. Lv, W. Gao, D. Cui, X. Chen, X. Jing, Organometallics 26 (2007) 4575.
[74] L. Xiang, Q. Wang, H. Song, G. Zi, Organometallics 26 (2007) 5323.
[75] F. Jaroschik, T. Shima, X. Li, K. Mori, L. Ricard, X.-F. Le Goff, F. Nief, Z. Hou, Organometallics 26 (2007) 5654.
[76] J. Wang, C. Zheng, G. Canseco-Melchor, D.J. Hilby, J.A. Maguire, N.S. Hosmane, Organometallics 26 (2007) 577.
[77] K. Miyajima, S. Yabushita, M.B. Knickelbein, A. Nakajima, J. Am. Chem. Soc. 129 (2007) 8473.
[78] P.G. Hayes, W.E. Piers, M. Parvez, Chem. Eur. J. 13 (2007) 2632.
[79] D.U. Rani, D.L.V.K. Dasari, J.F. Nixon, E.D. Jemmis, J. Comput. Chem. 28 (2007) 310.
[80] H. Zhu, E.Y.-X. Chen, Organometallics 26 (2007) 5395.
[81] D. Heitmann, C. Jones, P.C. Junk, K.-A. Lippert, A. Stasch, Dalton Trans. (2007) 187.
[82] T.K. Panda, S. Randoll, C.G. Hrib, P.G. Jones, T. Bannenberg, M. Tamm, Chem. Commun. (2007) 5007.
[83] V. Lorenz, A. Edelmann, S. Blaurock, F. Freise, F.T. Edelmann, Organometallics 26 (2007) 4708.
[84] A. Edelmann, S. Blaurock, V. Lorenz, L. Hilfert, F.T. Edelmann, Angew. Chem. 119 (2007) 6855.
[85] Y. Iiduka, T. Wakahara, K. Nakajima, T. Nakahodo, T. Tsuchiya, Y. Maeda, T. Akasaka, K. Yoza, M.T.H. Liu, N. Mizorogi, S. Nagase, Angew. Chem. 119 (2007) 5658.
[86] T. Kato, J. Mol. Struct. 838 (2007) 84.
[87] M. Zimmermann, K.W. Törnroos, R. Anwander, Angew. Chem. 119 (2007) 3187.
[88] P.L. Arnold, S.T. Liddle, J. McMaster, C. Jones, D.P. Mills, J. Am. Chem. Soc. 129 (2007) 5360.
[89] M. Wiecko, P.W. Roesky, Organometallics 26 (2007) 4846.
[90] T. Chenal, X. Olonde, J.-F. Pelletier, K. Bujadoux, A. Mortreux, Polymer 48 (2007) 1844.
[91] J.-F. Carpentier, E. Kirillov, A.-S. Rodrigues, A. Razavi, Eur. Pat. Appl. 2007, EP 1777240 A1 20070425.
[92] Q. Ban, CN Pat. Appl. 2007, CN 101045739 A 20071003.
[93] J.-F. Carpentier, A.-S. Rodrigues, E. Kirillov, A. Razavi, Eur. Pat. Appl. 2007, EP 1818337 A1 20070815.
[94] S.B. Amin, T.J. Marks, J. Am. Chem. Soc. 129 (2007) 10102.
[95] C. Meermann, K.W. Törnroos, W. Nerdal, R. Anwander, Angew. Chem. 119 (2007) 6628.
[96] J. Thuilliez, C. Boisson, R. Spitz, Pat. Appl. 2007, WO 2007054223.
[97] J. Thuilliez, C. Boisson, R. Spitz, Pat. Appl. 2007, WO 2007054224.
[98] A. Aida, O. Tardif, Jpn. Kokai Tokkyo Koho, 2007, JP 2007063240 A 20070315.
[99] S. Kaita, O. Tardif, PCT Int. Appl. 2007, WO 2007129670 A1 20071115.
[100] P. Zinck, A. Valente, A. Mortreux, M. Visseaux, Polym. Commun. 48 (2007) 4609.
[101] P. Zinck, M. Terrier, A. Mortreux, A. Valente, M. Visseaux, Macromol. Chem. Phys. 208 (2007) 973.
[102] S. Tomasi, H. Weiss, T. Ziegler, Organometallics 26 (2007) 2157.
[103] L. Perrin, O. Eisenstein, L. Maron, New J. Chem. 31 (2007) 549.
[104] W.-J. Juo, T.-H. Lee, W.-C. Liu, S. Ko, S.K. Chittimalla, C.P. Rao, C.-C. Liao, J. Org. Chem. 72 (2007) 7992.
[105] S. Matsunaga, M. Sugita, N. Yamagiwa, S. Handa, A. Yamaguchi, M. Shibasaki, Bull. Chem. Soc. Jpn. 79 (2006) 1906.
[106] J. Päiväsaaril, J. Niinistöl, P. Myllymäkil, C. Dezelah, C.H. Winter, M. Putkonenl, M. Nieminenl, L. Niinistöl, Top. Appl. Phys. 106 (2007) 15.
[107] H.C. Aspinall, Top. Appl. Phys. 106 (2007) 53.
[108] S. Spiga, C. Wiemer, G. Scarel, O. Costa, M. Fanciulli, Top. Appl. Phys. 106 (2007) 203.
[109] D. Eom, S.Y. No, C.S. Hwang, H.J. Kim, J. Electrochem. Soc. 154 (2007) G49.
[110] M. Losurdo, M.M. Giangregorio, G. Bruno, D. Yang, E.A. Irene, A.A. Suvorova, M. Saunders, Appl. Phys. Lett. 91 (2007) 091914.
[111] M.M. Giangregorio, M. Losurdo, A. Sacchetti, P. Capezzuto, G. Bruno, G. Malandrino, I.L. Fragalà, R. Lo Nigro, L. Armelao, D. Barreca, E. Tondello, Appl. Phys. Lett. 91 (2007) 061923.
[112] C.L. Dezelah, P. Myllymäki, J. Päiväsaari, K. Arstila, L. Niinistö, C.H. Winter, J. Mater. Chem. 17 (2007) 1308.
[113] B.O. Roos, R. Lindh, H.-G. Cho, L. Andrews, J. Phys. Chem. A 111 (2007) 6420.
[114] J.T. Lyon, L. Andrews, P.-Å. Malmqvist, B.O. Roos, T. Yang, B.E. Bursten, Inorg. Chem. 46 (2007) 4917.
[115] B.O. Roos, A.C. Borin, L. Gagliardi, Angew. Chem. 119 (2007) 1491.
[116] C.A. Cruz, D.J.H. Emslie, L.E. Harrington, J.F. Britten, C.M. Robertson, Organometallics 2 (2007) 692.
[117] N. Barros, D. Maynau, L. Maron, O. Eisenstein, G. Zi, R.A. Andersen, Organometallics 26 (2007) 5059.
[118] W.J. Evans, K.A. Miller, J.W. Ziller, J. Greaves, Inorg. Chem. 46 (2007) 8008.
[119] W.J. Evans, K.A. Miller, J.W. Ziller, A.G. DiPasquale, K.J. Heroux, A.L. Rheingold, Organometallics 26 (2007) 4287.
[120] W.J. Evans, K.A. Miller, W.R. Hillman, J.W. Ziller, J. Organomet. Chem. 692 (2007) 3649.
[121] W.J. Evans, K.A. Miller, S.A. Kozimor, J.W. Ziller, A.G. DiPasquale, A.L. Rheingold, Organometallics 26 (2007) 3568.
[122] E.J. Schelter, P. Yang, B.L. Scott, R.E. Da Re, K.C. Jantunen, R.L. Martin, P.J. Hay, D.E. Morris, J.L. Kiplinger, J. Am. Chem. Soc. 129 (2007) 5139.
[123] E.J. Schelter, D.E. Morris, B.L. Scott, J.L. Kiplinger, Chem. Commun. (2007) 1029.
[124] E.J. Schelter, P. Yang, B.L. Scott, J.D. Thompson, R.L. Martin, P.J. Hay, D.E. Morris, J.L. Kiplinger, Inorg. Chem. 46 (2007) 7477.
[125] J. Maynadié, J.-C. Berthet, P. Thuéry, M. Ephritikhine, Chem. Commun. (2007) 486.
[126] J.-C. Berthet, P. Thuéry, M. Ephritikhine, Chem. Commun. (2007) 604.
[127] J. Maynadié, J.-C. Berthet, P. Thuéry, M. Ephritikhine, Organometallics 26 (2007) 4585.
[128] J. Maynadié, N. Barros, J.-C. Berthet, P. Thuéry, L. Maron, M. Ephritikhine, Angew. Chem. 119 (2007) 2056.
[129] C.R. Graves, B.L. Scott, D.E. Morris, J.L. Kiplinger, J. Am. Chem. Soc. 129 (2007) 11914.
[130] A. Moritz, M. Dolg, Chem. Phys. 337 (2007) 48.
[131] B.D. Stubbert, T.J. Marks, J. Am. Chem. Soc. 129 (2007) 6149.
[132] B.D. Stubbert, T.J. Marks, J. Am. Chem. Soc. 129 (2007) 4253.